

HARVARD UNIVERSITY
Graduate School of Arts and Sciences



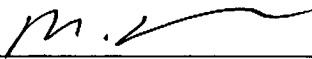
DISSERTATION ACCEPTANCE CERTIFICATE

The undersigned, appointed by the
Division of Medical Sciences
in the subject of Biological and Biomedical Sciences
have examined a dissertation entitled

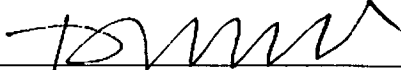
*ZNF335: A Novel Regulator of Stem Cell Proliferation and
Cell Fate
in the Cerebral Cortex*

presented by Yawei Yang

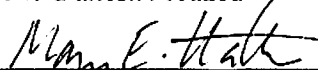
candidate for the degree of Doctor of Philosophy and hereby
certify that it is worthy of acceptance.

Signature:  _____

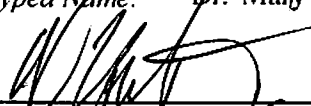
Typed Name: Dr. Mustafa Sahin

Signature:  _____

Typed Name: Dr. Danesh Moazed

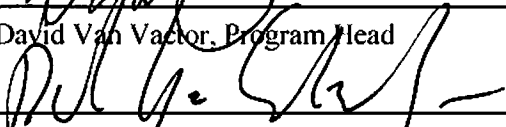
Signature:  _____

Typed Name: Dr. Mary Hatten



Dr. David Van Vactor, Program Head

Date: November 28, 2012



Dr. David Lopes Cardozo, Director of Graduate Studies

**ZNF335: A Novel Regulator of Stem Cell Proliferation and Cell Fate
in the Cerebral Cortex**

A dissertation presented

by

Yawei Yang

to

The Division of Medical Sciences

In partial fulfillment of the requirements

For the degree of

Doctor of Philosophy

In the subject of

Biological and Biomedical Sciences

Harvard University

Cambridge, Massachusetts

November 2012

Copyright © 2012 by Yawei Yang
All Rights Reserved.

Abstract

ZNF335: A Novel Regulator of Stem Cell Proliferation and Cell Fate in the Cerebral Cortex

Though development of the cerebral cortex is of singular importance to human cognition, it remains very poorly understood. Microcephaly, or “small head,” is a neurodevelopmental disorder causing significantly reduced cerebral cortex size, and the disease has proved to be a useful model system for elucidating the steps essential for proper cortical development and cognitive function. Many known microcephaly gene products localize to centrosomes, regulating cell fate and proliferation, however, the elucidation of different microcephaly genes with different functions may shed light on previously unidentified key steps of brain development.

We identify and characterize a nuclear zinc finger protein, *ZNF335/NIF-1*, as a causative gene for severe microcephaly, small somatic size, and neonatal death. *Znf335*-null mice are embryonically lethal and conditional knockout leads to severely reduced cortical size. RNA-interference and postmortem human studies show that *Znf335* is essential for neural progenitor self-renewal, neurogenesis, and neuronal differentiation. *ZNF335* is a component of a vertebrate-specific, trithorax H3K4-methylation complex, directly regulating

REST/NRSF, a master regulator of neural gene expression and cell fate, as well as other essential neural-specific genes. Our results reveal ZNF335 as an essential link between H3K4 complexes and REST/NRSF, and provide the first direct genetic evidence that this pathway regulates human neurogenesis and neuronal differentiation.

Table of Contents

Title	i
Copyright	ii
Abstract	iii-iv
Table of Contents	v
Acknowledgements	vii-xi
Dedication	xii
Chapter 1 – Introduction	1-28
Chapter 2 – Microcephaly gene links Trithorax and REST/NRSF to control neural stem cell proliferation and differentiation	29-87
Chapter 3 – Clinical Information and Experimental Procedures	88-110
Chapter 4 – Discussion	111-121
Appendix	
Global Sequencing Data Analysis and Supplemental Data	122-155
The Cerebrospinal Fluid Provides a Proliferative Niche for Neural Progenitor Cells	157-184

“Biology gives you a brain. Life turns it into a mind”

Jeffrey Eugenides, *Middlesex*.

Acknowledgements

I have had the honor and the great fortune of being surrounded by a wonderful network of friends and colleagues who have together served as a much-needed support structure (and safety net) during this training process of expanding my mind. These people have cheered me on loudly through the good times, and have lifted me up through the worst of times, and together they have propelled me to where I am today. Each thread of this network, and thus in essence each person, was individually essential to the integrity of this support lattice. It is hard to find the words that can adequately convey my deep gratitude for this group of colleagues and friends who have each helped me to grow scientifically or personally during my training, but I will give it a try hoping that they will understand and forgive should my words fail me at the task.

First and foremost, I would like to thank my advisor, Dr. Christopher A. Walsh, who is a mentor, a colleague, and a role model all mixed into one. Before joining the lab, Chris, to me, was not only the epitome of what a great scientist is, but also the example of what was deemed as impossible at the time: a successful *physician*-scientist. As director of the M.D.-Ph.D. program at the time, he not only telephoned me when I was accepted into the program, he also personally welcomed me in on my first day here at Harvard Medical School, and I still remember those first two interactions so vividly in my mind. Seeing him be so “human” and so “normal” and also so reassuring, made my class of 10 anxious incoming M.D.-Ph.D. students feel instantly like we could succeed in the arduous training program that lay ahead of us. Talking to him gave us a renewed reason

of why we wanted to pursue the program in the first place. A year later, he then welcomed me into his lab, and over the years, has constantly and also magically re-instilled that same faith in myself even when I didn't believe it was there. I especially thank him for never wavering to pick me up when I faltered, and for always backing me up when it mattered. I thank him for also believing in me enough to give me the scientific independence to explore science freely while training in his lab. His reassuring faith, his steadfast support, and his constant jewels of wisdom are the fuel behind my scientific achievements and my exponential growth as a scientist. Thus my current work and all of my future work is in part because of him and also indebted to him. I thank him for his patience, his guidance, his wisdom, his constant upbeat personality, and as Barack Obama eloquently puts it: "for having my back."

It was not until I entered the lab, did I realize how hard it was to actually get *into* the lab. Another indicator that Chris is a great advisor comes from the fact that he is able to assemble a group of colleagues who are not only amazing people but also amazing scientists. I have learned so much from each of them individually, and it will be the individual conversations whether early in the morning or late into the evening, whether in the tissue culture room, the mouse room, the microscope room, or the lunch room, and whether serious or light-hearted that I will take with me wherever I go. I will always treasure the friendships and the impactful help that I received because together they served as my second PI. Due to repetitive lab moves, I would like to thank past and present bay members whose sheer proximity made them extremely influential

and helpful in all of my day-to-day lab events. They have been the greatest friends and strongest supporters, and they include: Mauro Zappaterra (the graduate student that I initially rotated with), Ed Gilmore, Byoung-II Bae, Andy Baltus, Maria Lehtinen, Melody Lun, Chiara Manzini, Peter Wang, Kutay Deniz Atabay, Elisabeth Murphy and Dimira Tambunen. I also need to especially thank Andy Baltus for starting this project (and many plants) with me, Gilad Evrony for being my weekend lab friend and for the discussions on life and science, Maria Lehtinen for morning companionship, repeated motivational talks, emails, 5-min lunches, Chiara Manzini for being a great mentor and travel buddy, Byoung-II Bae for always challenging me scientifically and discussing my ideas, and Dilenny Goanzalez, who was a mouse whisperer, miracle worker, mother figure and wonderful friend all in one. Never could I imagine that my thesis training would also bring so much wealth into my life in the form of wonderful relationships. Each member has become a wonderful friend, and I would not leave lab if not for the reassurance that friendships can break the barriers and extend past the walls of the laboratory.

I need to thank especially John Flanagan for being an unwavering mentor from very early on, Michela Fagiolini for all of the advice inside and out of DAC meetings (and the tiramisu recipe), and Lisa Goodrich for her insightful suggestions and enthusiasm on my project. I would also like to thank my thesis committee, Danesh Moazed, Mary E. Hatten, and Mustafa Sahin for passing me (I should note that at the time of writing, I have currently not passed, but I thought

it'd be nice to plan optimistically), but mostly for their time, advice, and invaluable guidance along the way.

The project would not have materialized into the form that it stands today without the miraculous fortune of two wonderful people coming into this project (and into my life). Rebecca Mathew, who is by nature an amazing person, was kind enough to help me, a complete stranger and biochemistry novice, with tedious ChIP-seq experiments. Her wonderful personality combined with her amazing brain capacity has made her the best collaborator, colleague, and friend. I also would like to thank Elisabeth Murphy (Bebe), who came on to the project completely blind without any say in working with me or on the project, but she took the reigns and has deeply impacted the project. She helped to make possible what could only be achieved with 2 pairs of hands, and together, we worked like a storm at an ultrasonic speed for a year and a half, and never once did she complain. She came in not even knowing how to pipette, but over time has blossomed into an amazing scientist, and I secretly hope that I will again have the wonderful fortune of working with her very soon. I am extremely grateful to have both of these great friends (and therapists) come into my life.

The whole of my PhD experience was brightened (and survived) only because of my best friend and favorite collaborator in lab and in life: David Ferrero. Not only is he an amazing scientist--one whom I admired greatly and used as a role model--but he is also a great person who never failed to remind me of all that is beautiful and fun in life *outside* of lab. He has been a wonderful partner and teacher, and, not surprisingly, all of my favorite memories from these

past 4 years include him in it. I thank him for riding the roller coaster of graduate school together, for keeping me sane, and for never allowing me to forget my own accomplishments even for a second. He is an amazing cheerleader and his belief in me never once wavered. I thank him immensely for his love and support and look forward to our continued collaborative adventures beyond grad school.

Finally, I save my biggest thanks for my wonderful family, who was there from the beginning of every challenge, journey, and adventure since the day I was born. They form my strongest and loudest cheerleading team. My parents, as revered physicians, successful scientists, and amazing businessmen, have always been my idols and I use them as examples to lead my own life. Their weekly phone reminders that I can get through anything, and their life lessons on the importance of hard work and perseverance are probably the reasons why I got through my PhD. They gave up a lot for my brother and me, and because of that, everything I do is both because of them and for them. They are truly an inspiration, and their love and support and belief in me is what makes me who I am today. Because of them, I also have my best friend, my older brother Tony. He has been my loudest cheerleader, and also the Yoda of my life, as well as my personal confidant. He is a wonderful role model of an intelligent, caring, loving human being, and I work to make him proud. He gave me the gift of a sister-in-law, Audrey, and gave me the title I am most proud of to date: “aunt Jenny” to my new and perfect niece, Avery. I love them for loving me unconditionally. Thank you to my family for being the solid platform on which I am able to build all of the accomplishments of my life.

To my loving family:
my father, Bill,
my mother, Aiping,
and my brother, Tony,
without whom nothing would be possible.

Chapter 1
Introduction

“As long as our brain is a mystery,
the universe, the reflection of the structure of the brain will also be a mystery.”

–Santiago Ramón y Cajal.

As human beings, even after centuries of scientific advancement, we are still rattled with the complex question of what it is that makes us *human*. What sets us apart from all of the other species both past and present? While philosophers, economists, artists, and scientists may offer differing insights, they converge on the idea that the roots of these “distinctions” may lie within our brain (Baumeister and Leary, 1995; Jablonka et al., 2012; Kahneman, 2011; Pinker, 2011; Prinz, 2012; Trivers, 2011). Movement of the opposable thumb, our upright gait, the use of tools, and the process of communication and generation of philosophical thought stems from the only organ where medical and scientific advancements have not yet made possible removal or transplantation of the organ to be compatible with life (Jablonka et al., 2012; Robbins and Cotran, 1979).

Brain size

So what then makes the brain so special, and what specifically makes the human brain so unique? The human brain is a massive structure made up of 86 billion neurons and 85 billion non-neuronal cells (Azevedo et al., 2009). Throughout the course of mammalian evolution, the cerebral cortex has undergone extensive expansion both radially to create more layers, as well as

tangentially turning the brain from lissencephalic (smooth) to gyrencephalic (folded) (Molnar et al., 2006). While the brain is thought to be the root of our cognitive advancements, the larger size of the human brain still does not live up to our mammalian order. Although listed under *Primata*, or “first rank,” humans are in fact far from advanced in absolute brain size or even in the relative brain size (when compensated for the change in body mass) (Herculano-Houzel, 2012). Given this discrepancy, newer fields of thinking emerged based on the assumption that complexity and cognitive abilities may actually lie in neurons--the processing unit of the brain--thus it is not the size of the brain that matters, but rather the number of neurons and the subsequent connections of those neurons that contribute to our higher brains powers (Kaas, 2000; Ringo, 1991; Roth and Dicke, 2005; Tramo et al., 1998). This increase is not evident when looking at the ratio of neurons to non-neuronal cells, which in humans resemble just a scaled up version of other primates who are thought of as “inferior” (Gabi et al., 2010), but rather the increase is in the sheer count of neurons (Herculano-Houzel, 2012), with an expansion seen specifically in the upper cortical layer neurons in mammals (Marin Padilla, 2004), as well as an increase in the diversity of such neurons (Edlund and Jessell, 1999; Peters and Jones, 1988; Ramon y Cajal, 1995). Due to this, the question now shifts to what creates neurons, and in essence, what is essential for these neurons to develop and to function properly?

Development of the Brain

Early Brain Development

To study neuronal development, one must study brain development as a whole. The brain, housed inside the cranium, functions as an intricate and delicate structure composed of billions of fine-tuned connections which properly receives, processes, and delivers signals to the rest of the body along with the rest of the nervous system. The mammalian cerebral cortex makes up two-thirds of the mass and three-fourths of all the synapses of the nervous system (Rakic, 1988). The brain, along with the rest of the nervous system, starts out more simply as a hollow tube called the neural tube (Rao and Jacobson, 2005). Subsequent patterning and regionalization, defined by FGF, BMP, Wnt, SHH, and other secreted morphogens, help to specify the anterior or rostral end of the neural tube as the telencephalon, and the future cerebral cortex (Jessell and Sanes, 2000; Monuki et al., 2001; Monuki and Walsh, 2001; Rallu et al., 2002; Rash and Grove, 2007; Vaccarino et al., 1999). Further signaling, balanced between the extracellular signal gradients and intracellular molecular signals, continue to subdivide the brain into functional or morphologically distinct regions. Together this signaling balance also guides the developmental programs necessary for progenitor cell maintenance and proliferation, and subsequent neuronal cell fate establishment, differentiation, maturation, and connectivity to form a fully functioning brain.

Cortical Progenitors

The adult cerebral cortex ultimately stems from a finite population of neuroepithelial progenitors that lie within the anterior end of the developing

neural tube. It is the size as well as the rate of expansion of this pool of progenitor cells that help to dictate cortical size (Kornack and Rakic, 1998; Takahashi et al., 1999). The tight control of cortical progenitor cell development also helps to set the proper cytoarchitecture of the cerebral cortex (Hill and Walsh, 2005; Hofman and Falk, 2012).

The complex architecture and growth pattern of the brain can be attributed to the presence of many different types of neural progenitor cells whose individual patterns of proliferation and development help to synchronize brain development and dictate the final makeup of the adult brain (Angevine et al., 2005; Fietz and Huttner, 2011; Kriegstein and Alvarez-Buylla, 2009; Kriegstein et al., 2006). These progenitors not only differ in morphology, but also in gene expression patterns which affect proliferative and differentiation potential. Along with earliest neuroepithelial progenitor cells, the developing neuroepithelium begins to house apical progenitors, called radial glial progenitors, which extend both a basal as well as an apical process from a cell body residing in the ventricular zone (VZ) (Gal et al., 2006; Gotz and Huttner, 2005; Stancik et al., 2010). These progenitors can give rise to identical daughter cells, to neurons, or to another subclass of progenitors. The intermediate progenitor cells (IPC), or basal progenitors, that derive from these apical progenitors (and some from the neuroepithelial progenitors), both lack basal processes and move away from the VZ to reside in the subventricular zone (SVZ). Mammalian evolution has led to the dramatic increase of the SVZ and the IPC progenitors as well as subsequent formation of an additional outer subventricular zone (OSVZ) to house a third

progenitor cell population, called the outer radial glia cells (oRG). It is still debated whether this population of oRGs may directly account for the larger cerebral cortical size as well as the formation of gyri seen in gyrencephalic brains (Fietz et al., 2010; Garcia-Moreno et al., 2012; Hansen et al., 2010; Kelava et al., 2012; Reillo et al., 2011; Shitamukai et al., 2011; Smart et al., 2002; Wang et al., 2011). As the brain grows, the subsequent progenitor population undergoes rapid expansion and finally depletion as it is replaced by an ever-expanding population of neurons that go on to populate and create the laminar structure of the cortex.

Progenitor Cell Development

Progenitor cell division dictates the tempo and progress of brain development as it dictates the number as well as the subtypes of neurons produced. The basic principle of progenitor cell division is that symmetric division give rise to identical daughter cells to replenish the progenitor pool and cause tangential expansion of the cortex, while asymmetric divisions give rise to postmitotic neurons (and later, other cell types of the brain) to cause radial expansion and increased cortical thickness (Chenn and McConnell, 1995; Rakic, 1988; Thornton and Woods, 2009). Neuroepithelial progenitors undergo mainly symmetrical divisions, but the radial glial progenitors undergo mainly symmetric divisions at first, and as development picks up, they then undergo asymmetric divisions to produce one progenitor daughter cell and one early neuronal cell (Haubensak et al., 2004; Noctor et al., 2004; Noctor et al., 2007; Rakic, 1988). Basal progenitors, on the other hand, mainly undergo symmetric divisions to form

two postmitotic neurons (Kriegstein et al., 2006; Martinez-Cerdeno et al., 2006), while the oRGs break the mold and seem to be able to undergo proliferative divisions as well as neurogenic divisions (Fietz et al., 2010; Hansen et al., 2010).

The type of cell division that a progenitor cell undergoes not only affects the size of the progenitor cell pool, but also dictates cell fate. Thus the factors that influence the decision between symmetric and asymmetric division of the progenitors is of great importance. Both intrinsic and extrinsic factors play a role in dictating progenitor cell division. A number of transcription factors such as bHLH transcription factors (Ngn2/Ngn1, Mash1, NeuroD) have been shown to be necessary and sufficient to promote neurogenesis (Bertrand et al., 2002; Schuurmans and Guillemot, 2002). Aside from the transcriptional program, another intrinsic factor is the mitotic spindle, whose orientation sets the plane of division (Bond et al., 2005; Chenn and McConnell, 1995; Lizarraga et al., 2010). In fact, not only does the cleavage plane affect the distribution of a complex of proteins along the apical surface (apical complex), composed of the Par3/Par6/aPKC proteins and their interactors (Kim et al., 2010; Kosodo et al., 2004; Siller and Doe, 2009), but it also affects the distribution of cytoplasmic regulators of cell fate such as the Numb protein, (Rhyu et al., 1994), Notch (Chenn and McConnell, 1995) and Minibrain (Hammerle et al., 2002). Other intrinsic factors include possible differences in the two centrioles that are each separately inherited during division to play a role in dictating the daughter progenitor cell fate vs. the neuronal fate (Wang et al., 2009).

Many extrinsic signals may also play a role in dictating progenitor cell division. In fact, signaling from the pia on the basal surface (Siegenthaler et al., 2009), from the extracellular matrix (Wilsch-Brauninger et al., 2012), or even from the apical surface of the cell may all play a role. Signaling or maintenance of the apical complex affects cell division or even progenitor cell survival (Huttner and Kosodo, 2005; Kim et al., 2010; Kosodo et al., 2004; Lehtinen and Walsh, 2011; Wilsch-Brauninger et al., 2012). Progenitor cells also extend a single cilium into ventricular system filled with the cerebral spinal fluid (CSF) (Lehtinen et al., 2011; Zappaterra et al., 2007). The CSF establishes an external niche through a rich mixture of growth factors and other proteins, and the composition of the CSF as well as signaling of through the cilium both play roles in regulating the progenitor cell maintenance and proliferation (Lehtinen and Walsh, 2011; Lehtinen et al., 2011).

Cortical Neurogenesis

Once asymmetrical division does occur, the newly generated postmitotic neuron migrates along the radial glia to reside in the cerebral cortex. The cerebral cortex is formed in an inside-out manner, where the earliest born neurons reside at the bottom and the newer born neurons reside nearer the top of the cerebral cortex, closer to the pia (Angevine and Sidman, 1961; Bayer and Altman, 1991; Noctor et al., 2004). The molecular makeup, location, morphology, and electrophysiological properties (together summarized as cell identity) of each

subset of neuron differ drastically, and careful characterization of differential cell-specific markers have been performed (Molyneaux et al., 2007).

The asymmetrical divisions from the different subset of progenitor cells lead to sequential waves of neuronal production. At embryonic day 11 (E11), the first wave of postmitotic neurons migrate radially out of the VZ to form the early preplate. Newer neurons then divide the preplate into the superficial marginal zone (MZ) and a subplate that becomes the future cortical plate (CP) (Gupta et al., 2002; Hatten, 1999). The cortical plate can be divided into roughly 6 layers (layers I-VI) (Molyneaux et al., 2007). The newly born postmitotic neurons migrate to their final position either radially along radial glial processes, or tangentially through translocation of the nucleus or along axons in the intermediate zone (Hatten, 1999; Kriegstein and Noctor, 2004). Key lineage tracing and genetic fate mapping studies have revealed that single progenitors cells have the potential to form multiple neuronal subtypes at different times, and that the different subtypes reside in different layers within a restricted radial column, although there is also evidence of wide dispersal of many if not all cell lineages (Luskin et al., 1988; Walsh and Cepko, 1988; Walsh and Cepko, 1992, 1993; Walsh and Reid, 1995).

The intricate control of laminar cytoarchitecture can be studied using genetically engineered mouse mutants such as the *Dcx* mouse or naturally occurring mutants such as the *reeler* mouse, whose loss of the Reelin protein leads to an inversion of the cortical lamination (Gupta et al., 2002; Hatten, 1999). However, whether cell fate dictates migration location, or whether timing of birth

and environment dictate cell fate is still under debate. Cortical progenitor cell studies which have been able to recapitulate the step-wise pattern of development in an in vitro system hints that the cell fate is controlled in a cell-intrinsic manner (Gaspard et al., 2009; Shen et al., 2006). Studies where Notch-mediated inhibition of neurogenesis followed by subsequent adoption of a cell fate matching the now older environment once this inhibition is removed hints away from the idea that cell fate dictated by the number of cell cycles but rather towards the strong roles of environmental influences (Mizutani and Saito, 2005). Early transplantation experiments also add to the argument for the strong influence of cellular environment on cell fate, as well as reveal a progressive restriction of cell fate. Transplantation of deep layer progenitors from a younger brain can adopt a older superficial cell fate if transplanted into an older brain, but the later superficial progenitors seem unable to revert to a younger fate when transplanted into an earlier brain (Desai and McConnell, 2000). This cell fate commitment is dependent on the cell cycle, with progenitor cells in the S-phase able to adopt a new cell fate, while those past S-phase are unable to change their cell fate (McConnell, 1992; McConnell and Kaznowski, 1991). Recent studies, however, have suggested that cell fate reversions might be possible within a tighter time window of development (McConnell, unpublished), or through changing specific molecular programming (Lai et al., 2008; Molyneaux et al., 2005) in order to regain multipotency.

Genetics and Epigenetics of Brain development

Microcephaly

Many complex regulatory steps are needed for the formation of the brain. Human genetics studies have provided key insights into the specific genes essential for brain development (Walsh and Engle, 2010). Microcephaly, or small head, is a clinical disorder that is diagnosed by a smaller than average head circumference, and is frequently accompanied with a decrease in the size of nearly all brain structures (Mochida and Walsh, 2004). Primary microcephaly is frequently characterized by a small head at birth and hints at a genetic or neurodevelopmental disorder affecting progenitor cell number, while secondary microcephaly may be caused by a variety of different genetic or environmental factors and is linked with brain degeneration (Bond and Woods, 2006; Dobyns, 2002; Woods, 2004). Genetic causes of primary microcephaly have provided a wealth of genes involved in neurogenesis, such as *MICROCEPHALIN*, *WDR62*, *NDE1*, *CDK5RAP2*, *CEP152*, *ASPM*, *CENPJ*, and *STIL*. These genes can be categorized broadly as components of the mitotic spindle (Alkuraya et al., 2011; Bakircioglu et al., 2011; Mahmood et al., 2011), and proteins involved in DNA repair (Buck et al., 2006; Matsumoto et al., 2011; O'Driscoll et al., 2006; Renbaum et al., 2009; Shen et al., 2010). Unlike the majority of previously identified microcephaly genes that encode a structural protein, we identify a new microcephaly gene that encodes a zinc finger protein recently identified as a part of a chromatin remodeling complex and regulates brain development through regulation of global patterns of gene expression.

Epigenetics

Many recent studies have now shed light on another level of regulation that goes beyond genetics. Epigenetics is the control of the expression pattern of a gene without actually involving changes in the DNA sequence. DNA methylation, and histone changes can directly alter the expression capability and expression patterns of specific genes (Berger, 2002; Holliday, 2006; Jones and Takai, 2001). There also exists another level of regulation such as recruitment of transcriptional machinery, the alternative splicing of the transcripts, and the stability and turnover of the transcripts via non-coding RNAs (Landry et al., 2003; Qureshi and Mehler, 2012). This does not even begin to unravel other epigenetic and non-epigenetic mechanism that affect the actual protein activity output such as protein modification, protein interaction, degradation, and the role of prions to name a few (Hochstrasser, 1996; Prusiner, 2001).

This global impact makes epigenetics a powerful tool to directly affect evolution, medicine, and large aspects of biology. Epigenetic changes make up a secondary layer of the genetic code that can be passed down from generation to generation in direct response to changes in the environment. These changes can occur much faster--on a multigenerational timescale—and can occur in a reversible format allowing for quick changes in gene expression and fast adaptive responses by an organism (Gilbert and Epel, 2009; Jablonka and Raz, 2009).

Diseases can also present on the backdrop of epigenetics. Genes where single copies are silenced or affected through epigenetic mechanisms make diseases much more penetrant even in the heterozygous state (Jakovcevski and Akbarian, 2012). Also, genes activated or inactivated upon diseases may be due to epigenetic changes adding diagnostic difficulties. Conversely, epigenetic mechanisms can also prove to be extremely important to consider for drug targeting and medical therapies (Egger et al., 2004).

There are now emerging roles of non-coding RNAs, transcription factors, and DNA modifying as well as histone modifying proteins that have been shown to play key roles in regulating development, plasticity and neurological disease (Jakovcevski and Akbarian, 2012; Qureshi and Mehler, 2012). Epigenetics is perfectly suited for the process of development and differentiation as a progenitor cell with the same DNA makeup must change in a way to form the myriad cells within the brain that also contain the same DNA makeup. Focusing on brain development, many examples exist, but we will focus specifically on the effects of histone modification and the roles of associated proteins.

Histone Modification and Brain Development

Within the finite space of the cellular nucleus, DNA is carefully compacted by wrapping around octamers of histone proteins to make a package unit called nucleosomes. This packaging not only helps to condense the DNA material from 1.8 meters into 0.090mm, but the tight windign also affects the accessibility of the DNA to the transcriptional machinery ultimately affecting gene expression

(Peterson and Laniel, 2004). The histone proteins of the nucleosomes have a tail that can undergo posttranslational modifications such as methylation, acetylation, phosphorylation, ubiquitination, sumoylation, citrullination, and ADP-ribosylation. The modification of the histone tails and the modification of the histone cores together make up the histone code, and these modifications affect how tightly or loosely the DNA is wound (Jenuwein and Allis, 2001). Posttranslational modifications can occur on any of the histone tails, and within each tail modification can also occur on a variety of different residues. The combination of the specific modification to the specific residue on the specific histone affects the gene expression in different ways.

Trimethylation of histone 3 lysine 4 (H3K4me3) is one of the most well-studied histone modifications and linked with active transcription. H3K4 trimethylation occurs at the promoter regions of genes as a marker of gene activation or genes primed for activation (Steward et al., 2006). H3K4 trimethylation is performed by histone modification complexes that contains an enzyme aptly named histone methyltransferase. One histone methyltransferase complex, Trithorax/COMPASS, is well-studied from yeast to mammals (Miller et al., 2001; Schuettengruber et al., 2007). TrxG regulates developmental expression of many genes important for patterning, cell proliferation, and stem cell identity by maintaining genes in an active state (Fisher and Fisher, 2011). The TrxG complex activates gene expression through the methylation of Lysine 4 on histone H3 (H3K4) (Papp and Muller, 2006), a marker of actively transcribed genes or genes poised for transcription (Bernstein et al., 2005). SET1

methyltransferases (MLL1, MLL2, and SET1A/B) are the major enzymes carrying out H3K4 methylation, functioning in a multiprotein complex with Ash2L, WDR5, and RbBP5 (Schuettengruber et al., 2011). The complex has been shown to play important roles in progenitor cell development, ES cell development, as well as drosophila development (Bernstein et al., 2006; Fouse et al., 2008; Hanson et al., 1999), but its roles have never been studied in the mammalian system let alone mammalian brain development.

Histone acetylation on histone lysine residues is also a modification linked with gene expression. It increases access by transcriptional proteins by decreasing the interaction of negatively charged DNA with the histone tails (Gray and Ekstrom, 2001). However, most of the well studied epigenetic regulations of brain development have been through gene repression (Huang et al., 1999). A well-studied epigenetic regulator of mammalian brain development is epigenetic regulator of neurogenesis is the repressor element 1 (RE1)-silencing transcription factor (REST)/neuron-restrictive silencer factor (NRSF) (Chong et al., 1995; Schoenherr and Anderson, 1995). REST/NRSF recruits histone modification complexes that contain an enzyme which remove the acetyl residues, also known as histone deacetylases (HDACs), and thus to repress gene expression. REST/NRSF has been shown to be essential for maintaining mammalian progenitors cells in the multipotent, proliferative state through the specific inhibition of neuronal gene expression and ultimately differentiation (Hsieh et al., 2004).

Conclusions

Understanding brain development must stem from a better understanding of the genes within the brain. However, the answer does not lie simply at the DNA code, but rather also at the level of DNA regulation. While a progenitor cell and the differentiated neuron both have the same genetic code, the morphology, localization, and activity of these two cell types become increasingly divergent. To complicate the coordination of brain development even further, the changes in phenotype output from the same genotype input also shifts continuously as development progresses. Through the course of development, a single progenitor must give rise to overlapping waves of neurons each with a unique cellular identity, function, and localization. While signaling from the environment has been shown to contribute to dictating changes in cell development, there are also internal changes in how receptive a cell is to the environmental cues as well as a strong role of cell autonomous regulation in development. The regulation of the dynamic development of the cells within the brain must occur through the regulation of DNA expression levels and timing.

Genetic studies in patients with neurodevelopmental diseases allow us to figure out essential genes of brain development. However, insight into the steps necessary for brain development cannot be gained from the simple identification of the genes, but rather it comes from understanding the mechanism of function of each of these genes. Together, the interplay of forward and reverse genetics as well as the usage of two different model systems provides a powerful paradigm to gain great strides in uncovering the complex steps needed to create such an

intricate and powerful organ. This study is divided into three global parts that allowed for the understanding of gene and function of a new microcephaly gene: *ZNF335*. 1) Obtaining and understanding patient clinical information and phenotype; 2) Understanding the roles of *ZNF335* in the brain and in brain development through studying its mechanism of function; 3) Verifying the essential roles of *ZNF335* brain development through the creation of a conditional knockout mouse and the recapitulation of the human phenotype. In this study, we show that *ZNF335* is essential for progenitor cell proliferation and proper neuronal differentiation, morphology, and fate. *ZNF335* regulates these diverse processes through the regulation of expression of a wide array of genes via association with a histone modification complex. While a global knockout of *Znf335* lead to early embryonic lethality, the brain-specific conditional knockout of *Znf335* leads to the formation of a mouse with the essential loss of all brain structure, mimicking directly the human phenotype. Through this study, we are able to identify a new microcephaly gene with master regulatory roles of brain development.

REFERENCES

Alkuraya, F.S., Cai, X., Emery, C., Mochida, G.H., Al-Dosari, M.S., Felie, J.M., Hill, R.S., Barry, B.J., Partlow, J.N., Gascon, G.G., *et al.* (2011). Human mutations in NDE1 cause extreme microcephaly with lissencephaly [corrected]. *American journal of human genetics* 88, 536-547.

Angevine, J., and Sidman, R. (1961). Autoradiographic study of cell migration during histogenesis of cerebral cortex in the mouse.

Angevine, J.B., Bodian, D., Coulombre, A.J., Edds, M.V., Hamburger, V., Jacobson, M., Lyser, K.M., Prestige, M.C., Sidman, R.L., and Varon, S. (2005). Embryonic vertebrate central nervous system: revised terminology. *The Anatomical Record* 166, 257-261.

Azevedo, F.A.C., Carvalho, L.R.B., Grinberg, L.T., Farfel, J.M., Ferretti, R.E.L., Leite, R.E.P., Lent, R., and Herculano, S. (2009). Equal numbers of neuronal and nonneuronal cells make the human brain an isometrically scaled, primate brain. *The Journal of comparative neurology* 513, 532-541.

Bakircioglu, M., Carvalho, O.P., Khurshid, M., Cox, J.J., Tuysuz, B., Barak, T., Yilmaz, S., Caglayan, O., Dincer, A., Nicholas, A.K., *et al.* (2011). The essential role of centrosomal NDE1 in human cerebral cortex neurogenesis. *American journal of human genetics* 88, 523-535.

Baumeister, R.F., and Leary, M.R. (1995). The need to belong: desire for interpersonal attachments as a fundamental human motivation. *Psychological bulletin* 117, 497.

Bayer, S.A., and Altman, J. (1991). *Neocortical development* (Raven Pr).

Berger, S.L. (2002). Histone modifications in transcriptional regulation. *Current opinion in genetics & development* 12, 142-148.

Bernstein, B.E., Mikkelsen, T.S., Xie, X., Kamal, M., Huebert, D.J., Cuff, J., Fry, B., Meissner, A., Wernig, M., and Plath, K. (2006). A bivalent chromatin structure marks key developmental genes in embryonic stem cells. *Cell* 125, 315-326.

Bertrand, N., Castro, D.S., and Guillemot, F. (2002). Proneural genes and the specification of neural cell types. *Nature Reviews Neuroscience* 3, 517-530.

Bond, J., Roberts, E., Springell, K., Lizarraga, S., Scott, S., Higgins, J., Hampshire, D.J., Morrison, E.E., Leal, G.F., and Silva, E.O. (2005). A centrosomal mechanism involving CDK5RAP2 and CENPJ controls brain size. *Nature genetics* 37, 353-355.

Bond, J., and Woods, C.G. (2006). Cytoskeletal genes regulating brain size. *Current opinion in cell biology* 18, 95-101.

Buck, D., Moshous, D., de Chasseval, R., Ma, Y., le Deist, F., Cavazzana-Calvo, M., Fischer, A., Casanova, J.L., Lieber, M.R., and de Villartay, J.P. (2006). Severe combined immunodeficiency and microcephaly in siblings with hypomorphic mutations in DNA ligase IV. *European journal of immunology* 36, 224-235.

Chenn, A., and McConnell, S.K. (1995). Cleavage orientation and the asymmetric inheritance of Notch1 immunoreactivity in mammalian neurogenesis. *Cell* 82, 631-641.

Chong, J.A., Tapia-Ramirez, J., Kim, S., Toledo-Aral, J.J., Zheng, Y., Boutros, M.C., Altshuler, Y.M., Frohman, M.A., Kraner, S.D., and Mandel, G. (1995). REST: a mammalian silencer protein that restricts sodium channel gene expression to neurons. *Cell* 80, 949-957.

Desai, A.R., and McConnell, S.K. (2000). Progressive restriction in fate potential by neural progenitors during cerebral cortical development. *Development* 127, 2863-2872.

Dobyns, W.B. (2002). Primary microcephaly: new approaches for an old disorder. *American journal of medical genetics* 112, 315-317.

Eklund, T., and Jessell, T.M. (1999). Progression from Extrinsic to Intrinsic Review Signaling in Cell Fate Specification: A View from the Nervous System. *Cell* 96, 211-224.

Egger, G., Liang, G., Aparicio, A., and Jones, P.A. (2004). Epigenetics in human disease and prospects for epigenetic therapy. *Nature* 429, 457-463.

Fietz, S.A., and Huttner, W.B. (2011). Cortical progenitor expansion, self-renewal and neurogenesis, a polarized perspective. *Current opinion in neurobiology* 21, 23-35.

Fietz, S.A., Kelava, I., Vogt, J., Wilsch-Br suninger, M., Stenzel, D., Fish, J.L., Corbeil, D., Riehn, A., Distler, W., and Nitsch, R. (2010). OSVZ progenitors of human and ferret neocortex are epithelial-like and expand by integrin signaling. *Nature neuroscience* 13, 690-699.

Fouse, S.D., Shen, Y., Pellegrini, M., Cole, S., Meissner, A., Van Neste, L., Jaenisch, R., and Fan, G. (2008). Promoter CpG methylation contributes to ES cell gene regulation in parallel with Oct4/Nanog, PcG complex, and histone H3 K4/K27 trimethylation. *Cell stem cell* 2, 160-169.

Gabi, M., Collins, C.E., Wong, P., Torres, L.B., Kaas, J.H., and Herculano-Houzel, S. (2010). Cellular scaling rules for the brains of an extended number of primate species. *Brain, behavior and evolution* 76, 32-44.

Gal, J.S., Morozov, Y.M., Ayoub, A.E., Chatterjee, M., Rakic, P., and Haydar, T.F. (2006). Molecular and morphological heterogeneity of neural precursors in the mouse neocortical proliferative zones. *The Journal of Neuroscience* 26, 1045-1056.

Garcia-Moreno, F., Vasistha, N.A., Trevia, N., Bourne, J.A., and Molnár, Z. (2012). Compartmentalization of cerebral cortical germinal zones in a lissencephalic primate and gyrencephalic rodent. *Cerebral Cortex* 22, 482-492.

Gaspard, N., Gaillard, A., and Vanderhaeghen, P. (2009). Making cortex in a dish: in vitro corticogenesis from embryonic stem cells. *Cell Cycle* 8, 2491-2496.

Gilbert, S.F., and Epel, D. (2009). *Ecological developmental biology: integrating epigenetics, medicine, and evolution* (Sinauer Associates Sunderland, MA).

Gotz, M., and Huttner, W.B. (2005). The cell biology of neurogenesis. *Nature reviews Molecular cell biology* 6, 777-788.

Gray, S.G., and Ekstrom, T.J. (2001). The human histone deacetylase family. *Experimental cell research* 262, 75-83.

Gupta, A., Tsai, L.H., and Wynshaw-Boris, A. (2002). Life is a journey: a genetic look at neocortical development. *Nature Reviews Genetics* 3, 342-355.

Hammerle, B., Vera-Samper, E., Speicher, S., Arencibia, R., Martinez, S., and Tejedor, F. (2002). Mnb/Dyrk1A Is Transiently Expressed and Asymmetrically Segregated in Neural Progenitor Cells at the Transition to Neurogenic Divisions. *Developmental biology* 246, 259-273.

Hansen, D.V., Lui, J.H., Parker, P.R.L., and Kriegstein, A.R. (2010). Neurogenic radial glia in the outer subventricular zone of human neocortex. *Nature* 464, 554-561.

Hanson, R.D., Hess, J.L., Yu, B.D., Ernst, P., Van Lohuizen, M., Berns, A., Van der Lugt, N.M.T., Shashikant, C.S., Ruddle, F.H., and Seto, M. (1999). Mammalian Trithorax and polycomb-group homologues are antagonistic regulators of homeotic development. *Proceedings of the National Academy of Sciences* 96, 14372-14377.

Hatten, M.E. (1999). Central nervous system neuronal migration. *Annual review of neuroscience* 22, 511-539.

Haubensak, W., Attardo, A., Denk, W., and Huttner, W.B. (2004). Neurons arise in the basal neuroepithelium of the early mammalian telencephalon: a major site of neurogenesis. *Proceedings of the National Academy of Sciences of the United States of America* 101, 3196-3201.

Herculano-Houzel, S. (2012). The remarkable, yet not extraordinary, human brain as a scaled-up primate brain and its associated cost. *Proceedings of the National Academy of Sciences* *109*, 10661-10668.

Hill, R.S., and Walsh, C.A. (2005). Molecular insights into human brain evolution. *Nature* *437*, 64-67.

Hochstrasser, M. (1996). Ubiquitin-dependent protein degradation. *Annual review of genetics* *30*, 405-439.

Hofman, M., and Falk, D. (2012). Cerebral cortical development in rodents and primates. *Evolution of the Primate Brain: From Neuron to Behavior* *195*, 45.

Holliday, R. (2006). Epigenetics: a historical overview. *Epigenetics* *1*, 76-80.

Hsieh, J., Nakashima, K., Kuwabara, T., Mejia, E., and Gage, F.H. (2004). Histone deacetylase inhibition-mediated neuronal differentiation of multipotent adult neural progenitor cells. *Proceedings of the National Academy of Sciences of the United States of America* *101*, 16659-16664.

Huang, Y., Myers, S.J., and Dingledine, R. (1999). Transcriptional repression by REST: recruitment of Sin3A and histone deacetylase to neuronal genes. *Nature neuroscience* *2*, 867-872.

Huttner, W.B., and Kosodo, Y. (2005). Symmetric versus asymmetric cell division during neurogenesis in the developing vertebrate central nervous system. *Current opinion in cell biology* *17*, 648-657.

Jablonka, E., Ginsburg, S., and Dor, D. (2012). The co-evolution of language and emotions. *Philosophical Transactions of the Royal Society B: Biological Sciences* *367*, 2152-2159.

Jablonka, E., and Raz, G. (2009). Transgenerational epigenetic inheritance: prevalence, mechanisms, and implications for the study of heredity and evolution. *The Quarterly Review of Biology* *84*, 131-176.

Jakovcevski, M., and Akbarian, S. (2012). Epigenetic mechanisms in neurological disease. *Nature Medicine* *18*, 1194-1204.

Jenuwein, T., and Allis, C.D. (2001). Translating the histone code. *Science Signalling* *293*, 1074.

Jessell, T.M., and Sanes, J.R. (2000). Development: The decade of the developing brain. *Current opinion in neurobiology* *10*, 599-611.

Jones, P.A., and Takai, D. (2001). The role of DNA methylation in mammalian epigenetics. *Science* 293, 1068-1070.

Kaas, J.H. (2000). Why is Brain Size so Important: Design Problems and Solutions as Neocortex Gets Bigger or Smaller. *Brain and Mind* 1, 7-23.

Kahneman, D. (2011). *Thinking, fast and slow* (Farrar, Straus and Giroux).

Kelava, I., Reillo, I., Murayama, A.Y., Kalinka, A.T., Stenzel, D., Tomancak, P., Matsuzaki, F., Lebrand, C., Sasaki, E., and Schwamborn, J.C. (2012). Abundant occurrence of basal radial glia in the subventricular zone of embryonic neocortex of a lissencephalic primate, the common marmoset *Callithrix jacchus*. *Cerebral Cortex* 22, 469-481.

Kim, S., Lehtinen, M.K., Sessa, A., Zappaterra, M.W., Cho, S.H., Gonzalez, D., Boggan, B., Austin, C.A., Wijnholds, J., and Gambello, M.J. (2010). The apical complex couples cell fate and cell survival to cerebral cortical development. *Neuron* 66, 69-84.

Kornack, D.R., and Rakic, P. (1998). Changes in cell-cycle kinetics during the development and evolution of primate neocortex. *Proceedings of the National Academy of Sciences* 95, 1242-1246.

Kosodo, Y., Röpker, K., Haubensak, W., Marzesco, A.M., Corbeil, D., and Huttner, W.B. (2004). Asymmetric distribution of the apical plasma membrane during neurogenic divisions of mammalian neuroepithelial cells. *The EMBO journal* 23, 2314-2324.

Kriegstein, A., and Alvarez-Buylla, A. (2009). The glial nature of embryonic and adult neural stem cells. *Annual review of neuroscience* 32, 149.

Kriegstein, A., Noctor, S., and Martinez-Cerdeño, V. (2006). Patterns of neural stem and progenitor cell division may underlie evolutionary cortical expansion. *Nature Reviews Neuroscience* 7, 883-890.

Kriegstein, A.R., and Noctor, S.C. (2004). Patterns of neuronal migration in the embryonic cortex. *Trends in neurosciences* 27, 392-399.

Lai, T., Jabaudon, D., Molyneaux, B.J., Azim, E., Arlotta, P., Menezes, J.R.L., and Macklis, J.D. (2008). SOX5 controls the sequential generation of distinct corticofugal neuron subtypes. *Neuron* 57, 232-247.

Landry, J.R., Mager, D.L., and Wilhelm, B.T. (2003). Complex controls: the role of alternative promoters in mammalian genomes. *Trends in Genetics* 19, 640-648.

Lehtinen, M.K., and Walsh, C.A. (2011). Neurogenesis at the brain-cerebrospinal fluid interface. *Annual review of cell and developmental biology* 27, 653-679.

Lehtinen, M.K., Zappaterra, M.W., Chen, X., Yang, Y.J., Hill, A.D., Lun, M., Maynard, T., Gonzalez, D., Kim, S., and Ye, P. (2011). The cerebrospinal fluid provides a proliferative niche for neural progenitor cells. *Neuron* 69, 893-905.

Lizarraga, S.B., Margossian, S.P., Harris, M.H., Campagna, D.R., Han, A.P., Blevins, S., Mudbhary, R., Barker, J.E., Walsh, C.A., and Fleming, M.D. (2010). Cdk5rap2 regulates centrosome function and chromosome segregation in neuronal progenitors. *Development* 137, 1907-1917.

Luskin, M.B., Pearlman, A.L., and Sanes, J.R. (1988). Cell lineage in the cerebral cortex of the mouse studied in vivo and in vitro with a recombinant retrovirus. *Neuron* 1, 635-647.

Mahmood, S., Ahmad, W., and Hassan, M.J. (2011). Autosomal Recessive Primary Microcephaly (MCPH): clinical manifestations, genetic heterogeneity and mutation continuum. *Orphanet journal of rare diseases* 6, 39.

Marin Padilla, M. (2004). Ontogenesis of the pyramidal cell of the mammalian neocortex and developmental cytoarchitectonics: a unifying theory. *The Journal of comparative neurology* 321, 223-240.

Martinez-Cerdeno, V., Noctor, S.C., and Kriegstein, A.R. (2006). The role of intermediate progenitor cells in the evolutionary expansion of the cerebral cortex. *Cerebral Cortex* 16, i152-i161.

Matsumoto, Y., Miyamoto, T., Sakamoto, H., Izumi, H., Nakazawa, Y., Ogi, T., Tahara, H., Oku, S., Hiramoto, A., Shiiki, T., *et al.* (2011). Two unrelated patients with MRE11A mutations and Nijmegen breakage syndrome-like severe microcephaly. *DNA Repair (Amst)* 10, 314-321.

McConnell, S.K. (1992). The control of neuronal identity in the developing cerebral cortex. *Current opinion in neurobiology* 2, 23-27.

McConnell, S.K., and Kaznowski, C.E. (1991). Cell Cycle Dependence of Laminar Determination in Developing Neocortex.

Miller, T., Krogan, N.J., Dover, J., Erdjument-Bromage, H., Tempst, P., Johnston, M., Greenblatt, J.F., and Shilatifard, A. (2001). COMPASS: a complex of proteins associated with a trithorax-related SET domain protein. *Proceedings of the National Academy of Sciences* 98, 12902-12907.

Mizutani, K., and Saito, T. (2005). Progenitors resume generating neurons after temporary inhibition of neurogenesis by Notch activation in the mammalian cerebral cortex. *Development* 132, 1295-1304.

Mochida, G.H., and Walsh, C.A. (2004). Genetic basis of developmental malformations of the cerebral cortex. *Archives of neurology* 61, 637.

Molnar, Z., Metin, C., Stoykova, A., Tarabykin, V., Price, D.J., Francis, F., Meyer, G., Dehay, C., and Kennedy, H. (2006). Comparative aspects of cerebral cortical development. *European Journal of Neuroscience* 23, 921-934.

Molyneaux, B.J., Arlotta, P., Hirata, T., Hibi, M., and Macklis, J.D. (2005). Fezl Is Required for the Birth and Specification of Corticospinal Motor Neurons. *Neuron* 47, 817-831.

Molyneaux, B.J., Arlotta, P., Menezes, J.R.L., and Macklis, J.D. (2007). Neuronal subtype specification in the cerebral cortex. *Nature Reviews Neuroscience* 8, 427-437.

Monuki, E.S., Porter, F.D., and Walsh, C.A. (2001). Patterning of the dorsal telencephalon and cerebral cortex by a roof plate-Lhx2 pathway. *Neuron* 32, 591-604.

Monuki, E.S., and Walsh, C.A. (2001). Mechanisms of cerebral cortical patterning in mice and humans. *Nature neuroscience* 4, 1199-1206.

Noctor, S.C., Martinez-Cerdeno, V., Ivic, L., and Kriegstein, A.R. (2004). Cortical neurons arise in symmetric and asymmetric division zones and migrate through specific phases. *Nature neuroscience* 7, 136-144.

Noctor, S.C., Martinez-Cerdeno, V., and Kriegstein, A.R. (2007). Contribution of intermediate progenitor cells to cortical histogenesis. *Archives of neurology* 64, 639.

O'Driscoll, M., Jackson, A.P., and Jeggo, P.A. (2006). Microcephalin: a causal link between impaired damage response signalling and microcephaly. *Cell cycle* 5, 2339-2344.

Peters, A., and Jones, E.G. (1988). *Cerebral Cortex: Development and maturation of cerebral cortex*, Vol 7 (Plenum Pub Corp).

Peterson, C.L., and Laniel, M.A. (2004). Histones and histone modifications. *Current Biology* 14, 546-551.

Pinker, S. (2011). *The better angels of our nature: Why violence has declined* (Penguin Books).

Prinz, J.J. (2012). *Beyond human nature: How culture and experience shape our lives* (Penguin).

Prusiner, S.B. (2001). Neurodegenerative diseases and prions. *New England Journal of Medicine* 344, 1516-1526.

Qureshi, I.A., and Mehler, M.F. (2012). Emerging roles of non-coding RNAs in brain evolution, development, plasticity and disease. *Nature Reviews Neuroscience* 13, 528-541.

Rakic, P. (1988). Specification of cerebral cortical areas. *Science* 241, 170-176.

Rallu, M., Machold, R., Gaiano, N., Corbin, J.G., McMahon, A.P., and Fishell, G. (2002). Dorsoventral patterning is established in the telencephalon of mutants lacking both Gli3 and Hedgehog signaling. *Development* 129, 4963-4974.

Ramon y Cajal, S. (1995). *Histology of the nervous system of man and vertebrates*, Vol 1 (Oxford University Press, New York).

Rao, M.S., and Jacobson, M. (2005). *Developmental neurobiology*, Vol 413 (Kluwer Academic/Plenum Publishers, New York).

Rash, B.G., and Grove, E.A. (2007). Patterning the dorsal telencephalon: a role for sonic hedgehog? *The Journal of Neuroscience* 27, 11595-11603.

Reillo, I., de Juan Romero, C., Garc√a-Cabezas, M.Á., and Borrell, V. (2011). A role for intermediate radial glia in the tangential expansion of the mammalian cerebral cortex. *Cerebral Cortex* 21, 1674-1694.

Renbaum, P., Kellerman, E., Jaron, R., Geiger, D., Segel, R., Lee, M., King, M.C., and Levy-Lahad, E. (2009). Spinal muscular atrophy with pontocerebellar hypoplasia is caused by a mutation in the VRK1 gene. *American journal of human genetics* 85, 281-289.

Rhyu, M.S., Jan, L.Y., and Jan, Y.N. (1994). Asymmetric distribution of numb protein during division of the sensory organ precursor cell confers distinct fates to daughter cells. *Cell* 76, 477-491.

Ringo, J.L. (1991). Neuronal interconnection as a function of brain size. *Brain Behav Evol* 38, 1-6.

Robbins, S.L., and Cotran, R.S. (1979). *Pathologic basis of disease* (Saunders).

Roth, G., and Dicke, U. (2005). Evolution of the brain and intelligence. *Trends in cognitive sciences* 9, 250-257.

Schoenherr, C.J., and Anderson, D.J. (1995). Silencing is golden: negative regulation in the control of neuronal gene transcription. *Curr Opin Neurobiol* 5, 566-571.

Schuettengruber, B., Chourrout, D., Vervoort, M., Leblanc, B., and Cavalli, G. (2007). Genome regulation by polycomb and trithorax proteins. *Cell* 128, 735-745.

Schuurmans, C., and Guillemot, F. (2002). Molecular mechanisms underlying cell fate specification in the developing telencephalon. *Current opinion in neurobiology* 12, 26-34.

Shen, J., Gilmore, E.C., Marshall, C.A., Haddadin, M., Reynolds, J.J., Eyaid, W., Bodell, A., Barry, B., Gleason, D., Allen, K., *et al.* (2010). Mutations in PNKP cause microcephaly, seizures and defects in DNA repair. *Nat Genet* 42, 245-249.

Shen, Q., Wang, Y., Dimos, J.T., Fasano, C.A., Phoenix, T.N., Lemischka, I.R., Ivanova, N.B., Stifani, S., Morrisey, E.E., and Temple, S. (2006). The timing of cortical neurogenesis is encoded within lineages of individual progenitor cells. *Nature neuroscience* 9, 743-751.

Shitamukai, A., Konno, D., and Matsuzaki, F. (2011). Oblique radial glial divisions in the developing mouse neocortex induce self-renewing progenitors outside the germinal zone that resemble primate outer subventricular zone progenitors. *The Journal of Neuroscience* 31, 3683-3695.

Siegenthaler, J.A., Ashique, A.M., Zarbalis, K., Patterson, K.P., Hecht, J.H., Kane, M.A., Folias, A.E., Choe, Y., May, S.R., and Kume, T. (2009). Retinoic acid from the meninges regulates cortical neuron generation. *Cell* 139, 597-609.

Siller, K.H., and Doe, C.Q. (2009). Spindle orientation during asymmetric cell division. *nature cell biology* 11, 365-374.

Smart, I.H.M., Dehay, C., Giroud, P., Berland, M., and Kennedy, H. (2002). Unique morphological features of the proliferative zones and postmitotic compartments of the neural epithelium giving rise to striate and extrastriate cortex in the monkey. *Cerebral Cortex* 12, 37-53.

Stancik, E.K., Navarro-Quiroga, I., Sellke, R., and Haydar, T.F. (2010). Heterogeneity in ventricular zone neural precursors contributes to neuronal fate diversity in the postnatal neocortex. *The Journal of Neuroscience* 30, 7028-7036.

Steward, M.M., Lee, J.S., O'Donovan, A., Wyatt, M., Bernstein, B.E., and Shilatifard, A. (2006). Molecular regulation of H3K4 trimethylation by ASH2L, a shared subunit of MLL complexes. *Nature structural & molecular biology* 13, 852-854.

Takahashi, T., Goto, T., Miyama, S., Nowakowski, R., and Caviness Jr, V. (1999). Sequence of neuron origin and neocortical laminar fate: relation to cell cycle of origin in the developing murine cerebral wall. *The Journal of Neuroscience* 19, 10357-10371.

Thornton, G.K., and Woods, C.G. (2009). Primary microcephaly: do all roads lead to Rome? *Trends in Genetics* 25, 501-510.

Tramo, M.J., Loftus, W., Stukel, T., Green, R., Weaver, J., and Gazzaniga, M. (1998). Brain size, head size, and intelligence quotient in monozygotic twins. *Neurology* 50, 1246-1252.

Trivers, R. (2011). *The folly of fools: the logic of deceit and self-deception in human life* (Basic Books).

Vaccarino, F.M., Schwartz, M.L., Raballo, R., Rhee, J., and Lyn-Cook, R. (1999). 6 Fibroblast Growth Factor Signaling Regulates Growth and Morphogenesis at Multiple Steps during Brain Development. *Current topics in developmental biology* 46, 179-200.

Walsh, C., and Cepko, C. (1988). Clonally related cortical cells show several migration patterns. *Science (New York, NY)* 241, 1342.

Walsh, C., and Cepko, C.L. (1992). Widespread dispersion of neuronal clones across functional regions of the cerebral cortex. *Science (New York, NY)* 255, 434.

Walsh, C., and Cepko, C.L. (1993). Clonal dispersion in proliferative layers of developing cerebral cortex.

Walsh, C., and Reid, C. (1995). Cell lineage and patterns of migration in the developing cortex. *Development of the cerebral cortex*, 21-40.

Walsh, C.A., and Engle, E.C. (2010). Allelic diversity in human developmental neurogenetics: insights into biology and disease. *Neuron* 68, 245-253.

Wang, X., Tsai, J.W., Imai, J.H., Lian, W.N., Vallee, R.B., and Shi, S.H. (2009). Asymmetric centrosome inheritance maintains neural progenitors in the neocortex. *Nature* 461, 947-955.

Wang, X., Tsai, J.W., LaMonica, B., and Kriegstein, A.R. (2011). A new subtype of progenitor cell in the mouse embryonic neocortex. *Nature neuroscience* 14, 555-561.

Wilsch-Brauninger, M., Peters, J., Paridaen, J.T.M.L., and Huttner, W.B. (2012). Basolateral rather than apical primary cilia on neuroepithelial cells committed to delamination. *Development* 139, 95-105.

Woods, C.G. (2004). Human microcephaly. *Current opinion in neurobiology* 14, 112-117.

Zappaterra, M.D., Lisgo, S.N., Lindsay, S., Gygi, S.P., Walsh, C.A., and Ballif, B.A. (2007). A comparative proteomic analysis of human and rat embryonic cerebrospinal fluid. *Journal of proteome research* 6, 3537-3548.

Chapter 2

**Microcephaly gene links Trithorax
and REST/NRSF to control neural stem
cell proliferation and differentiation**

Adapted from a manuscript in Cell (Nov 21, 2012)

**Microcephaly gene links Trithorax and REST/NRSF to control neural stem
cell proliferation and differentiation**

Yawei J. Yang^{1,2,3,4,5,6}, Andrew E. Baltus^{1,2,4}, Rebecca S. Mathew^{4,7}, Elisabeth A. Murphy^{1,8}, Gilad D. Evrony^{1,2,3,4,6}, Dilenny M. Gonzalez^{1,2,4}, Estee P. Wang^{1,2,4,9}, Christine A. Marshall-Walker^{1,4}, Brenda J. Barry^{1,2,4}, Jernej Murn^{7,10}, Antonis Tatarakis⁷, Muktar A. Mahajan¹¹, Herbert H. Samuels¹¹, Yang Shi^{7,10}, Jeffrey A. Golden¹², Muhammad Mahajnah^{13,§}, Ruthie Shenhav^{14,§}, Christopher A. Walsh^{1,2,3,4,*}

¹Division of Genetics, and Manton Center for Orphan Disease Research, Children's Hospital Boston, Boston, MA 02115, USA

²Broad Institute of MIT and Harvard, Cambridge, MA 02142, USA

³Program in Biological and Biomedical Sciences, Harvard Medical School, Boston, MA 02115, USA

⁴Howard Hughes Medical Institute

⁵Harvard-MIT Division of Health Sciences and Technology, Harvard Medical School, Boston, MA 02115, USA and MIT, Cambridge, MA 02142, USA

⁶Harvard MD-PhD MSTP Program, Harvard Medical School, Boston, MA 02115, USA

⁷Department of Cell Biology, Harvard Medical School, Boston, MA 02115, USA

⁸Department of Neuroscience, Northeastern University, Boston, MA 02115, USA

⁹Harvard School of Dental Medicine, Boston, MA 02115, USA; Current Address: Department of Orthodontics, University of Michigan, Ann Arbor, MI 48109, USA

¹⁰Division of Newborn Medicine, Children's Hospital Boston, Boston, MA 02115, USA

¹¹Department of Pharmacology and Medicine, New York University, New York, NY 10016, USA

¹²Department of Pathology, Brigham and Women's Hospital, Boston, MA 02115, USA

¹³Child Development and Pediatric Neurology, Hillel Yaffe Medical Center, Hadera 38100, Israel, The Technion, Israel Institute of Technology, Haifa 32000, Israel.

¹⁴Raphael Recanati Genetics Institute, Rabin Medical Center, Beilinson Campus, Petah Tikva 49100, Israel

§ Authors contributed equally

*Correspondence: christopher.walsh@childrens.harvard.edu

AUTHOR CONTRIBUTIONS

Andrew E. Baltus and Christine A. Marshall-Walker were co-initiators of the project. Marshall-Walker performed initial characterization of patient cell lines, and Baltus helped with the generation of initial knockdown and cloning reagents and maintenance of global Lac-Z reporter cell lines. Estee P. Wang helped with initial genetic sequencing of the family. Rebecca S. Mathew helped with all ChIP-seq and ChIP-qPCR experiments. Elisabeth A. Murphy assisted in characterization of knockdown phenotypes, gene expression analysis, and knockout mouse studies. Gilad D. Evrony helped with all RNA-seq experiments. Dilenny M. Gonzalez performed mouse in utero electroporation experiments. Brenda J. Barry helped with patient data collection and contact with clinicians. Jernej Murn, Yang Shi, Muktar A. Mahajan, and Herbert H. Samuels helped with initial co-IPs in humans. Mathew and Antonis Tatarakis helped with co-IPs in mouse brains. Jeffrey A. Golden performed patient histology. Muhammad Mahajnah and Ruthie Shenhav are the clinicians who saw and referred the patients, and obtained clinical information. Christopher A. Walsh is the corresponding author and oversaw and guided all experimentation.

HIGHLIGHTS

- Mutation in *ZNF335*, an essential brain development gene, leads to severe microcephaly
- *ZNF335* is essential for progenitor maintenance and prevents premature differentiation
- *ZNF335* interacts with a H3K4 methyltransferase complex to regulate gene expression
- *ZNF335* is upstream of REST/NRSF, a master regulator controlling key neuronal genes

INTRODUCTION

Brain development requires carefully regulated yet continuously changing patterns of gene and protein expression. Cerebral cortical neurons are formed from progenitors that at the earliest stages divide mainly symmetrically to expand the progenitor population. At later stages, these apical progenitors divide increasingly in an asymmetrical fashion to produce one progenitor cell and a second, more differentiated cell, either a neuron, or a transit-amplifying progenitor cell that resides in the subventricular zone (Haubensak et al., 2004; Lui et al., 2011). Eventually, symmetrical divisions of progenitors are increasingly replaced by neurogenic cell divisions that produce the neurons of the cerebral cortex in an inside-first, outside last sequence (Fietz and Huttner, 2011; Gotz and Huttner, 2005; Kriegstein and Alvarez-Buylla, 2009). Although much is now understood about the cellular patterns of neurogenesis, the molecular controls of this process remain relatively poorly understood.

Naturally occurring mutations of human cerebral cortical development have provided surprising genetic insights into the process of neurogenesis in vertebrates. Microcephaly reflects small cerebral cortical and other brain structures, and genetic causes of microcephaly have provided a wealth of genes involved in neurogenesis, especially components of the mitotic spindle (Alkuraya et al., 2011; Bakircioglu et al., 2011; Mahmood et al., 2011), and proteins involved in DNA repair (Buck et al., 2006; Matsumoto et al., 2011; O'Driscoll et al., 2006; Renbaum et al., 2009; Shen et al., 2010). However, human microcephaly genes have so far not highlighted the transcriptional pathways that

animal studies have implicated as essential to the process of cerebral cortical neurogenesis (Molyneaux et al., 2007; Sur and Rubenstein, 2005).

A key aspect of the regulation of gene expression during neurogenesis occurs at the level of chromatin structure. Acetylation, methylation, and phosphorylation of histone proteins affect the accessibility of transcriptional proteins to DNA wrapped around nucleosomes (Bannister and Kouzarides, 2011), though their role in brain development and developmental disease remain poorly understood (Clowry et al., 2010; Lessard and Crabtree, 2010; Yoo et al., 2009). The activity, targeting, and regulation of chromatin remodelers to different sites of chromatin contribute to the complex control of gene expression. The Trithorax (trxG) complex maintains developmental expression of many genes important for patterning, cell proliferation, and stem cell identity through a well studied function of maintaining genes in an active state (Dou et al., 2005; Hughes et al., 2004; Ingham, 1985; Petruk et al., 2001; Terranova et al., 2006; Wysocka et al., 2003). While trxG proteins generally promote proliferation, defects of trxG proteins have been linked to altered stem cell fate and cancer (Djabali et al., 1992; Fisher and Fisher, 2011; Martinez et al., 2006; Schuettengruber et al., 2009). The trxG complex activates gene expression through the methylation of Lysine 4 on histone H3 (H3K4) (Beisel et al., 2002; Papp and Muller, 2006), a marker of either actively transcribed genes or genes poised for transcription (Bernstein et al., 2005; Schneider et al., 2004). SET1 methyltransferases (MLL1, MLL2, and SET1A/B) are the major enzymes carrying out H3K4 methylation, functioning in a multiprotein complex that contains essential proteins for global

methylation of H3K4, namely Ash2L, WDR5, and RbBP5 (Cosgrove and Patel, 2010; Dou et al., 2005; Nakamura et al., 2002; Schneider et al., 2005; Steward et al., 2006; Tenney and Shilatifard, 2005; Wang et al., 2010; Yokoyama et al., 2004). While the trxG complex has been implicated in *Drosophila* development (Paro et al., 1998), and while members of the complex have been implicated in vertebrate development and embryonic stem cells (Ang et al., 2011; Bi et al., 2011; Wysocka et al., 2005), the role of the trxG complex has not been studied in neural stem cells or human brain development (Schuettengruber et al., 2011).

Another critical epigenetic regulator of neurogenesis is the repressor element 1 (RE1)-silencing transcription factor (REST)/neuron-restrictive silencer factor (NRSF) (Chong et al., 1995; Schoenherr and Anderson, 1995). REST/NRSF acts as a transcriptional repressor of neuronal differentiation genes through the recruitment of histone deacetylases (HDACs), which place chromatin in a condensed state via the removal of acetyl residues (Ballas et al., 2005; Su et al., 2004). REST/NRSF is expressed in neural stem cell lines and is essential for maintaining progenitor cell fate by inhibiting neuronal specific genes and hence premature neuronal differentiation (Chen et al., 1998; Sun et al., 2005). REST/NRSF has also been suggested to play roles in embryonic stem cells as well as mature cell types (Ballas et al., 2005; Johnson et al., 2008); however, the upstream regulation of REST/NRSF, as well as the interaction of REST/NRSF and TrxG, two central epigenetic regulators of neurogenesis, is completely unknown.

In this study, we identify a new regulator of vertebrate neurogenesis, *ZNF335*, in a family that presents with one of the most severe cases of microcephaly documented. *Znf335* was previously identified as a potential co-regulator (NRC-Interacting Factor 1) of nuclear hormone signaling in HeLa cell lines (Garapaty et al., 2008; Mahajan et al., 2002), and as part of a H3K4 methylation complex, but its functions have never been studied in vivo, let alone the brain. We show that *ZNF335* is essential for normal brain development in human and mouse, and that *ZNF335* interacts with a H3K4 chromatin methyltransferase complex. ChIP-Seq, RNA-Seq and microarray studies reveal that *ZNF335* is essential for expression of a host of brain-specific genes including the master progenitor regulator REST/NRSF, and its target genes. Knockdown of *ZNF335* disrupts progenitor cell proliferation, cell fate, and neuronal differentiation. Together, these data implicate a new type of microcephaly gene that coordinates global transcriptional regulation in brain development, and defines an essential control system for REST/NRSF expression.

RESULTS

A new syndrome of profound microcephaly, neuronal degeneration, and neonatal death

A large consanguineous Arab Israeli pedigree (Fig 1A) presented with seven individuals (two of them identical twins) affected with one of the most severe cases of microcephaly (MCPH) seen to date (head circumference 9 standard deviations below mean), and death by one year of age in all but one case. MRI at 3 months of age compared to an age-matched control (Fig 1C) revealed extreme microcephaly with a severely simplified gyral pattern. The cerebral cortex was even more notably smaller than the skull, with subarachnoid fluid separating the two, an indication of secondary shrinkage of the brain relative to skull usually reflecting degeneration (Barkovich, 2007). Histopathology of Patient 5 at 7 months of age revealed a thinned cerebral cortex with only about 20% of the cortex showing the normal six cortical layers, and neuronal disorganization (Fig 1B). The few neurons that were present demonstrated little apparent polarity or dendritic maturation. Layer I, a normally cell-sparse layer containing many neuronal processes, was severely reduced in thickness, potentially reflecting defects in process outgrowth and/or defects of Layer I Cajal-Retzius cells. Layers II-VI, normally neuron-rich, showed sparse neurons of abnormally small size, suggesting incomplete neuronal differentiation. Well-differentiated pyramidal neurons, normally the most abundant neuron in the cortex, were also almost completely unidentifiable either because of aberrant

Figure 1

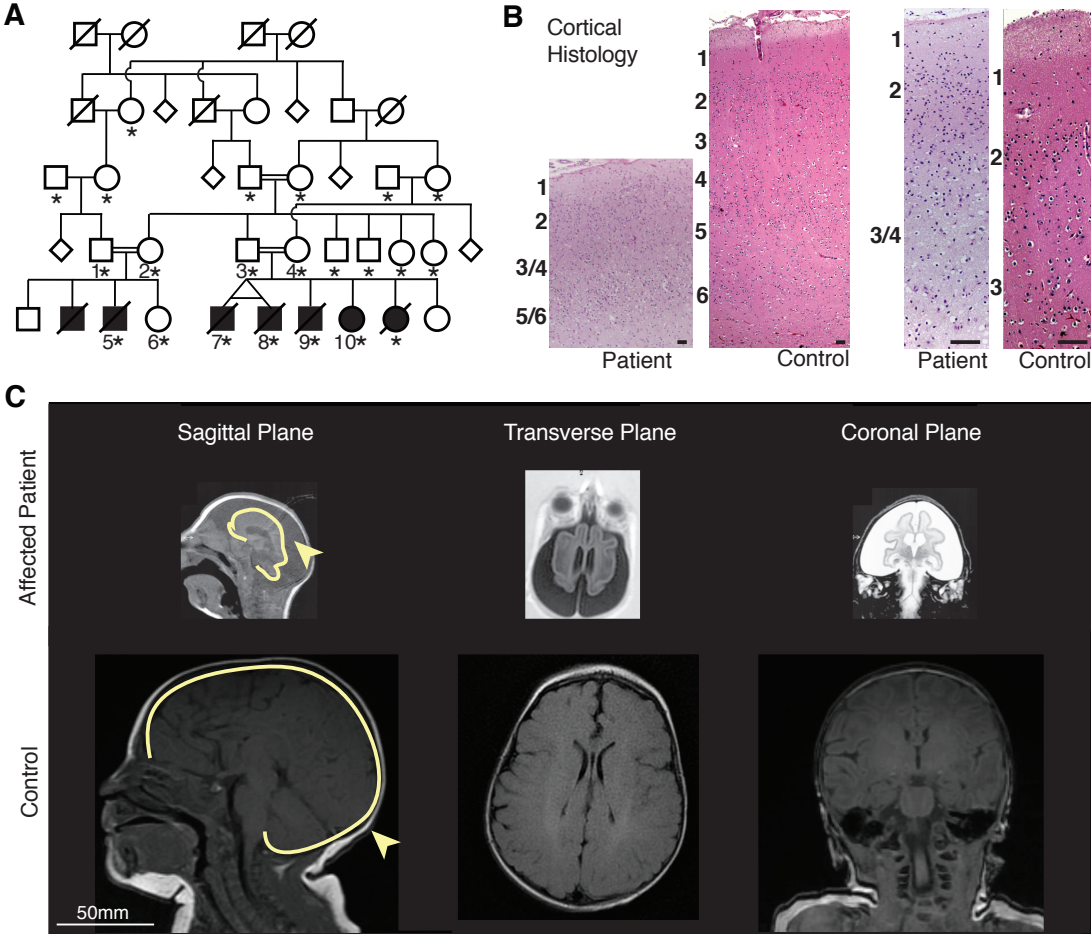


Figure 1 (Continued). A new syndrome of severe microcephaly and neuronal degeneration

(A) Pedigree of family with severe microcephaly. Double lines: consanguineous marriages. Black shading: known affected. Diagonal line: deceased at time of publication. Asterisk (*): sequence analysis was completed on the individual.

(B) Cortical histology of patient vs. age-matched controls at 10X (left panels) and 40X (right panels) magnification. Patients show decreased cortical thickness and abnormal cortical layers. Scale: 300 μ m.

(C) MRI of patient vs. age-matched controls show decreased brain size including cerebellum and brain stem, increased extraaxial space, and enlarged ventricles. Whole brains are outlined in yellow, showing separation of brain from skull.

differentiation, or severely reduced numbers (Fig 1B).

The cerebellum showed severely reduced external as well as internal granule cell layers (EGL, IGL)--which normally contain granule precursors and granule cells at this age (Fig 2D)--suggesting widespread loss of these cell types as well. There were few Purkinje cells, and increased numbers of eosinophilic, gemistocytic astrocytes in the Purkinje cell layer (PCL) consistent with a degenerative process. Calbindin immunoreactivity (Fig 2D) highlighted the severely reduced number, and abnormal localization and orientation of the rare remaining Purkinje cells (Fig 2D). A few mature granule cells persisted in the EGL, from which they normally have migrated into the IGL (Fig 2E, Top), suggesting defective migration. There is also a strikingly cell-sparse IGL, normally the location of countless mature granule cells, the most abundant neuronal type in the entire brain (Fig 2E, Bottom), suggesting profound defects in generation and/or survival. These post-mortem histological studies suggest that the responsible gene has essential roles in normal neurogenesis, neuronal migration, neuronal polarity, as well as neuronal survival. The small birth weight (1.3 kg, <5% of normal for Patient 7), birth length (51 cm, <2% of normal for Patient 8) and other somatic features (Supplementary Clinical Information) indicate that somatic size was affected, as well as brain size, though there were no specific clinical manifestations in other organs (Supplemental Clinical Information).

Figure 2

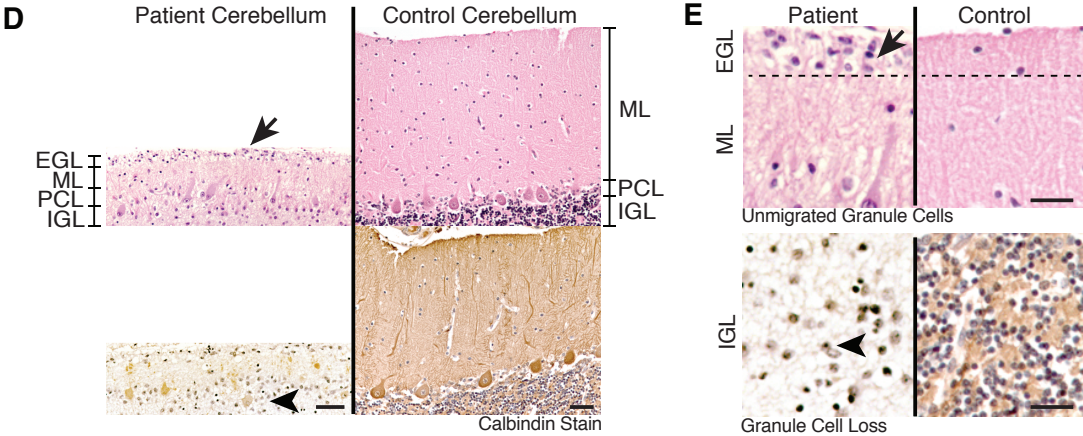


Figure 2 (Continued). A new syndrome of severe microcephaly and neuronal degeneration

(D) Cerebellar histology. Calbindin-stained sections of patients vs. age-matched controls. Patients have persistent external granule cell layer (EGL), decreased molecular layer (ML), abnormal Purkinje cell layer (PCL), and decreased internal granule cell layer (IGL). Scale: 100 μ m.

(E) Patients have unmigrated EGL cells above a thinner molecular layer (top panels, arrow). Patients have severely reduced granule cell density compared to control (bottom panels, arrowhead). Scale: 50 μ m.

See also Supplemental Experimental Procedures.

A splice donor/missense mutation of *ZNF335/NIF1* causes severe microcephaly

The genetic mutation was identified by conventional linkage mapping and gene sequencing, and was confirmed and further characterized using mRNA-transcriptome sequencing. Mapping using single nucleotide polymorphism (SNP) arrays, followed by fine mapping, identified a single, ~2Mb interval that was homozygous and identical-by-descent in all affected pedigree members (Fig 3A), and in none of the unaffected individuals (multipoint logarithm of odds (LOD) = 4.54). Sequence analysis of the 40 genes in the minimal linked region showed only one homozygous nonsynonymous change not already identified in dbSNP: a G to A transition at position 3332 of the coding sequence of the *ZNF335* (Zinc Finger Protein 335) gene, also known as *NIF-1*. All affected individuals were homozygous for this mutation, all parents were heterozygous, and an unaffected sibling was wild type consistent with an autosomal recessive mode of inheritance (Fig 3A). This change was absent from 100 Middle Eastern control patients, 200 sequenced unaffected Arabic control exomes and 2500 European control exomes (NHLBI GO Exome Sequencing Project), confirming it is not a rare benign change. This c.3332g>a mutation results in a predicted change of Arg (CGC) at amino acid position 1111 of the *ZNF335* protein to His (CAC) (Fig 3B). Moreover, the c.3332g>a transition is located at the final position of the splice donor site of exon 20, and a G at this position is highly conserved in mammalian splice donor sites (Cartegni et al., 2002)

Northern blot analysis of RNA and high throughput mRNA-sequencing from

Figure 3

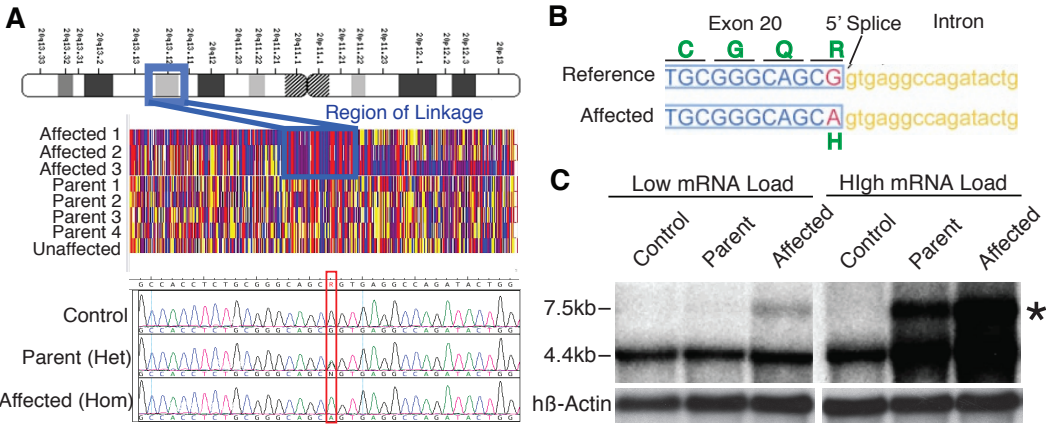


Figure 3 (Continued). Severe microcephaly reflects a splicing/missense mutation *ZNF335*

(A) Patients show linkage at chromosome 20q13.12. Sequencing shows a c.3332g>a mutation in gene *ZNF335*. Upper panel: schematic of chromosome 20. Middle panel: single nucleotide polymorphism genotyping. Each column represents a SNP, and the red and blue indicate homozygosity, whereas yellow shows heterozygosity. A large region (boxed) shows mainly red and blue SNPs in affected patients with heterozygosity in parents. Bottom panel: representative sequencing data.

(B) Mutation is at 5' Splice site of *ZNF335* and leads to R1111>H missense mutation.

(C) Northern blot shows production of a new larger transcript (*) in heterozygous parents and homozygous patients.

lymphocyte cell lines derived from an affected patient (Patient10) and a heterozygous parent (Patient4) confirmed that this mutation disrupted normal splicing. Whereas a cell line from an unrelated individual showed a normal 5Kb transcript (Fig 3C), both affected patient and heterozygous carriers showed a larger transcript, which was absent in the control, suggesting that the c.3332g>a mutation produces a larger transcript with intron retention. Some normally-sized transcripts in homozygous mutant lymphocytes suggests that some normally-spliced RNA (albeit encoding a R1111H mutation) may still be formed. To determine the identity of the larger mutant transcript, and to systematically rule out any other possible mutations in the coding portion of the entire genome, we performed mRNA-sequencing of cytoplasmic RNA. mRNA-sequencing verified the *ZNF335* mutation, and also revealed the production of abnormal *ZNF335* transcripts that show inclusion of both the introns (introns 19, 20) flanking the mutation-containing exon (Fig 4D, S1A). An unbiased genome-wide search across all 354,244 Refseq-annotated introns for differentially transcribed introns showed that the retained long intron of *ZNF335* was significantly higher than in control cells (p-value of 1.57×10^{-31}). The inclusion of introns 19 and 20 (Fig 4D, S1A) account for the increased size of the mutant transcript, which was verified with RT-PCR, and confirms that RNA-Sequencing is a useful tool for unbiased identification of patient mutations and splice mutants (data not published).

Western blot analysis of homozygous patient cell line showed severely reduced *ZNF335* protein levels at the previously reported size of ~190kD (Fig 4F). The inclusion of introns 19 and 20 leads to a premature stop codon that

Figure 4

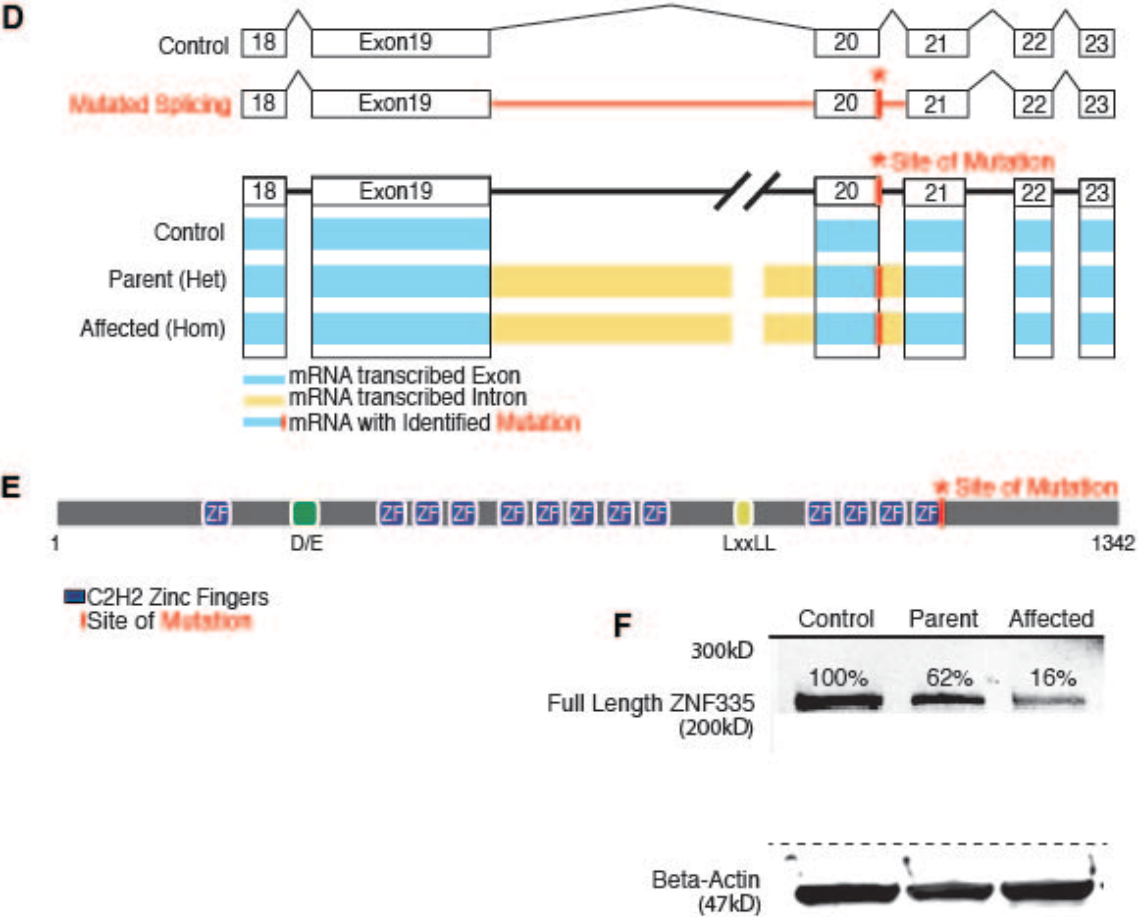


Figure 4 (Continued). Severe microcephaly reflects a splicing/missense mutation *ZNF335*

(D) Schematic of exons and intronic splicing for a control and the predicted problems with intronic splicing in a patient with a c.3332g>a mutation. Schematic of RNA-sequencing data shows detection of reads within exons (blue), and within introns (yellow) upstream and downstream of the mutation-containing exon. Incomplete splicing is present in heterozygous parents and homozygous patients but not in control cells. RNA-sequencing data also detected the base change mutation (*).

(E) Predicted structure of *ZNF335*. Mutation lies in the last zinc finger motif.

(F) Western blot of patient lymphoblast cell lines show heterozygous parents and homozygous patients produce a reduced amount of full length *ZNF335* protein, and no evidence of larger or degraded protein products.

See also Fig S1.

could cause transcript degradation (Isken and Maquat, 2007). Yet, a small amount ($\approx 16\%$ of control levels) of full-length, R1111H-mutated protein is still formed, suggesting that some transcript might have escaped incomplete splicing. No larger protein or degraded protein products were detected in the heterozygous parent or affected patient. Evolutionary analysis of available Znf335 orthologues indicates that the Arginine at position 1111 falls in the 13th zinc-finger domain (Fig 4E), and this Arginine is absolutely conserved in all known Znf335 sequences (Fig S1B). Interestingly, no clear *ZNF335* orthologue can be identified outside of vertebrates. These results are all consistent with the hypothesis that the identified mutation in *ZNF335* is the causative mutation in this family.

ZNF335 is essential for early embryonic mouse development

In order to confirm that Znf335 is essential in early brain development, we examined mice with engineered null Znf335 mutations and observed that homozygous loss of Znf335 leads to early embryonic lethality as early as embryonic day 7.5 (E7.5), (Fig 5A, S2C). The essential requirement of Znf335 in early embryonic development suggests that the human *ZNF335* mutation could be hypomorphic, since the human mutation results in some stable protein, albeit carrying a missense mutation. Examination of 100 individuals with varying degrees of MCPH—though none as severe—showed no other patients with homozygous *ZNF335* mutations or deletions, suggesting that null *ZNF335* mutations in humans may also be lethal prenatally. In summary, our data

suggest that *ZNF335* encodes a gene essential for normal human brain development and mouse development, and prompted us to examine its function in more detail.

The pattern and timing of *ZNF335* expression are consistent with roles in neurogenesis, as well as potentially in other processes. Northern analysis from adult (Fig S2A) and embryonic (Fig S2B) human tissues revealed widespread expression of *ZNF335*, including during embryonic brain development. Western blot analyses of wild type (WT) mouse brain tissue show that *Znf335* is expressed throughout cortical development with expression peaking at the height of neurogenesis from E13-E15 (Fig 5C). Similarly, *Znf335* is also expressed at the peak of hippocampal development and cerebellar development (Fig 5C, Fig S2D). To localize the expression of *Znf335* in specific cell populations, heterozygous genetrapp mice containing a B-galactosidase fusion reporter gene were stained histochemically. *Znf335-lacZ* was expressed in the developing forebrain and midbrain of E8.5 embryos (Fig 5B, 5D). Immunofluorescence analysis using antisera raised against *Znf335* confirmed expression in the ventricular zone (VZ), subventricular zone (SVZ), as well as at lower levels in the developing cortical plate, but showed low or undetectable expression in NeuN-labeled neurons of the cortical plate at E12.5 and E14.5 (Fig 5D). At P20 and P30, *Znf335* expression returns at low levels in the adult cerebral cortex possibly linked with neuronal maturation (Fig 5C, 5D, 5F, and data not shown). Higher magnification showed *Znf335* immunoreactivity in nuclei of progenitor cells where it co-localizes with DAPI-stained DNA (Fig 5E), but is largely or completely

Figure 5

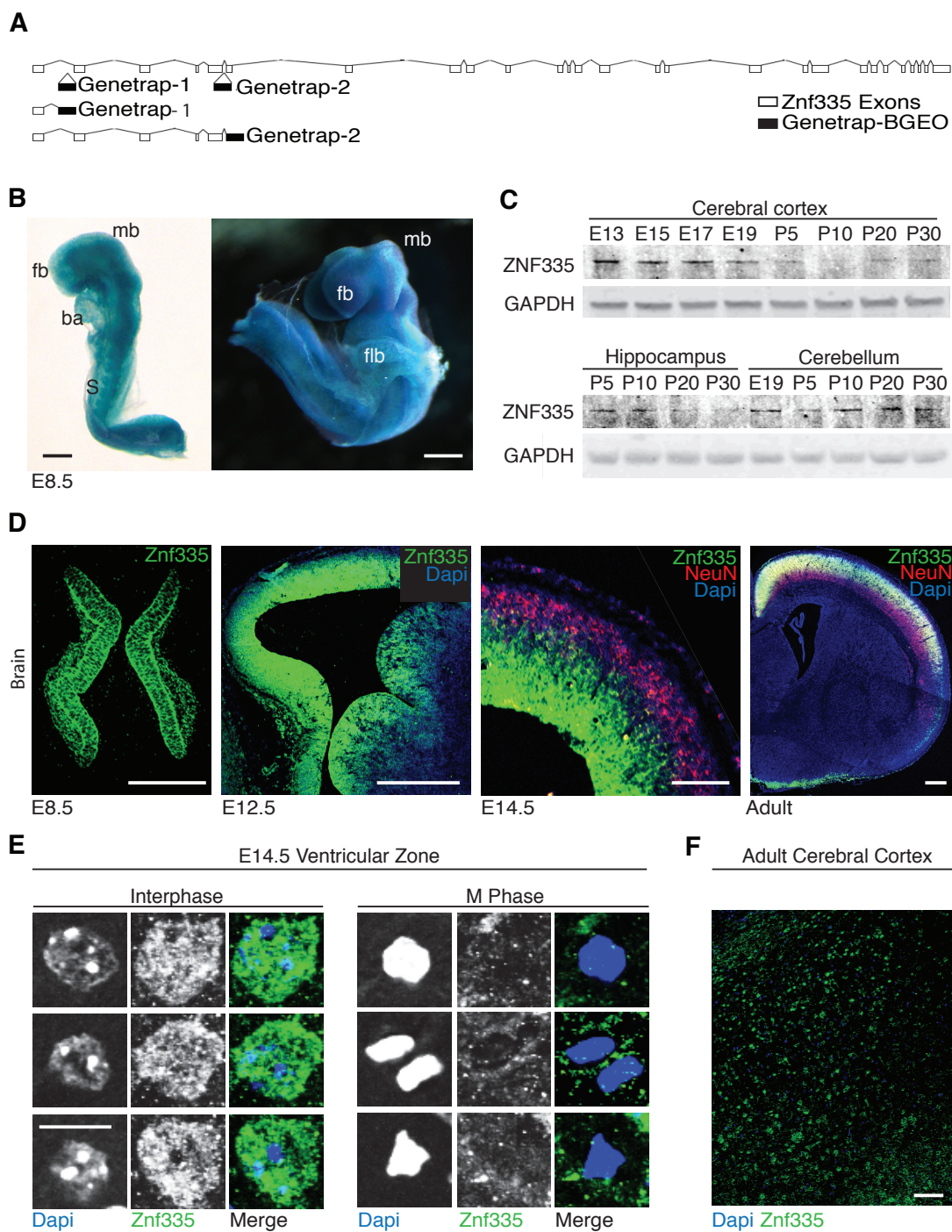


Figure 5 (Continued). Znf335 is essential for mouse development and is expressed in nuclei of progenitor cells.

(A) Location of genetrapp insertion of two genetrapp mice leading to early truncation of protein to mimic a null allele.

(B) Znf335 is expressed at E8.5 in developing forebrain (fb), midbrain (mb), somites (S), Branchial arch (ba), Forelimb bud (flb). Scale: 300 μ m.

(C) Western blot analysis of Znf335 protein expression throughout brain development. In the cortex, expression is highest at E13.5 before tapering off and returns slightly postnatally.

(D) Immunohistochemistry shows Znf335 expression in progenitor cells at E8.5 and in the ventricular zone of developing cortex and not in NeuN+ neurons at E12.5 and E14.5. Protein is also expressed throughout cortical plate later in development. Scale: 50, 50, 50, 400 μ m.

(E) Znf335 localizes to the nucleus, and colocalizes with euchromatin of progenitor cells in the ventricular zone of developing mouse brain, while Znf335 is excluded from heterochromatic foci. This colocalization disappears in cells in the M-Phase of the cell cycle. Scale: 10 μ m.

(F) Sparse expression of Znf335 in adult cerebral cortex. Scale: 100 μ m.

See also Fig S2.

absent in heterochromatic foci. This expression pattern is consistent with roles of *Znf335* in the progenitor cells prenatally and with possible roles in gene expression.

ZNF335 regulates neural progenitor self renewal and neurogenesis

The expression of *Znf335* in progenitor cells along with the severely reduced brain size of patients hint at a role of *Znf35* in regulating proliferation. In addition, lymphoblast cells lines from patients show decreased growth rate (Fig 6A) and the p.Arg1111His mutation in ZNF335 leads to decreased interaction with Ki-67, a component of a chromatin complex expressed in virtually all proliferating cells, and required for growth and survival (Fig S3A) (Garapaty et al., 2009). To assess roles of *Znf335* in progenitor proliferation directly, we selectively removed *Znf335* from cerebral cortical progenitor cells by electroporating GFP expressing plasmids that express either an shRNA against *Znf335* (shRNA-ZNF335, Fig S3B-C), or an shRNA containing silent mutations, making it unable to target *Znf335* (UT-Control). Electroporation was performed into neural progenitor cells of E9.5 and E12.5 cerebral cortices, which are made up of a high proportion of progenitor cells. Targeted cells were selected upon dissociation using Fluorescent Activated Cell Sorting (FACS) 24 hours post electroporation, and the formation of proliferating reaggregate spheres was used to assess progenitor cell proliferation. Knockdown of ZNF335 in both E9.5 and E12.5 progenitor populations led to a decrease in reaggregate sphere formation (Fig 6B), confirming the important role of *Znf335* in progenitor cell proliferation

Figure 6

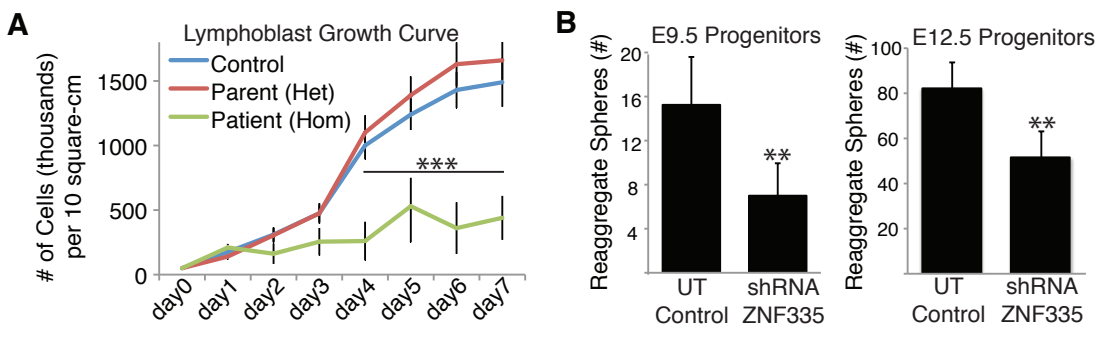


Figure 6 (Continued). Znf335 is essential for progenitor cell proliferation and cell cycle maintenance.

(A) Growth curves of lymphoblast cell lines derived from heterozygous parent, homozygous patient and control shows decreased growth rate in cells from patient with low levels of mutated ZNF335.

(B) Knockdown of Znf335 leads to decreased formation of progenitor cell reagggregates in E9.5 and E12.5 progenitor cell cultures showing decreased proliferation upon knockdown of Znf335. E9.5: UT-Control, 15.25 +/- 4.3; ShRNA-ZNF335, 7.1 +/-2.9, T-test, p=0.0032, n=6; E12.5 UT-Control, 82.2 +/- 11.5; ShRNA-ZNF335, 51.6 +/- 11.6, Data are represented as mean +/-SD. T-Test, p=0.001; n=6 rounds of FACS sorting. Each sort is from pooled embryos from 3 different dams with roughly half of their embryos electroporated with either shRNA-Znf335 or UT-control constructs.

and self-renewal.

In utero electroporation into developing cortices allowed targeting of cortical progenitor cells along the ventricular zone and follow-up studies in the native 5D architecture of the brain. 48 hours post electroporation, fewer Znf335-deficient cells were observed in the VZ—an area where most progenitor cells localize in the developing cortex—compared to controls (Fig 7C, 7E). This phenotype could be rescued by WT Znf335 but not by Mutated Znf335, containing the c.3332g>a mutation (Fig 7C, 7E, S3D). Bromodeoxyuridine (BrdU) pulse labeling experiments showed that this decrease was most likely due to the fact that fewer progenitor cells were still undergoing DNA synthesis even 24 hours post knockdown compared to the UT controls (Fig 7F). A BrdU/Ki67 co-labeling experiment was performed to mark progenitor cells that either remained in the cell cycle (P Fraction), or exited the cell cycle (Q Fraction). By 48 hours post knockdown, a greater proportion of targeted progenitor cells exited the cell cycle as compared to UT-Control and wildtype (WT) unelectroporated controls (Fig 7D, 7G). Taken together, these data show that Znf335 is important for self-renewal of progenitor cells by keeping progenitors in the cell cycle and preventing premature cell cycle exit.

We confirmed the premature exit of Znf335-deficient cells from the cell cycle by allowing the electroporated mice to develop until adulthood. A higher proportion of Znf335-deficient neurons were present in deeper layers of the cortex (Fig 7H, 7I), consistent with early cell cycle exit, and fewer Znf335 deficient neurons occupied more superficial layers, usually the location of later

Figure 7

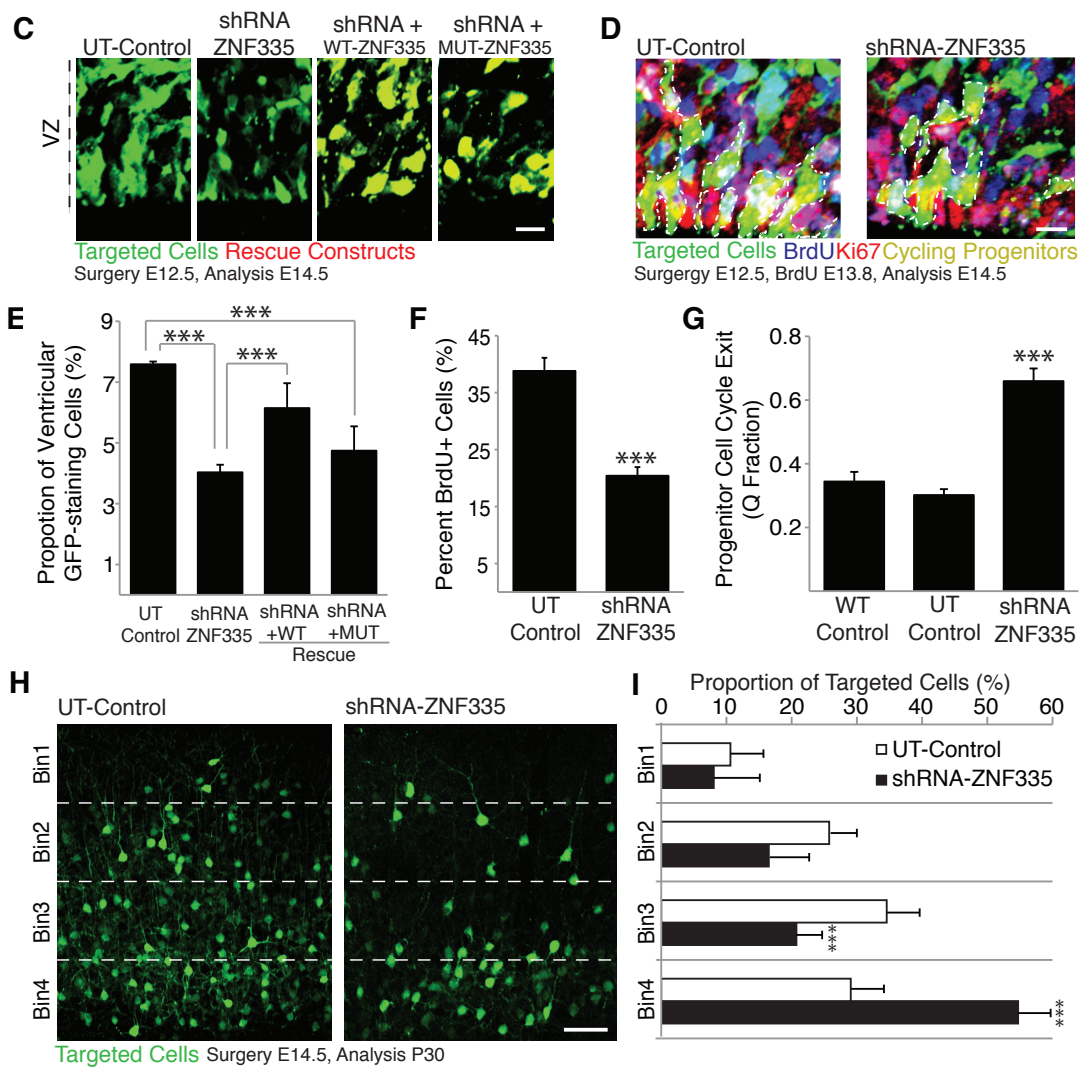


Figure 7 (Continued). Znf335 is essential for progenitor cell proliferation and cell cycle maintenance.

(C) shRNA-ZNF335 knockdown leads to fewer cells present within the ventricular zone when compared to UT-Control. WT-ZNF335 rescues the number of progenitors but MUT-ZNF335 does not. Scale: 10 μ m.

(D) shRNA-ZNF335 knockdown leads to fewer cycling progenitors in the ventricular zone as compared to the UT-Control. Scale: 10 μ m.

(E) Quantification of 7C. Knockdown of Znf335 leads to fewer percentage of targeted cells present within 250 μ m² of the ventricular zone as compared to UT-Control. WT-ZNF335 rescues the amount of GFP-staining cells in the VZ while MUT does not. UT-Control: 7.59 +/- 0.09; ShRNA-ZNF335: 4.0 +/- 0.25; shRNA+WT: 6.27 +/- 0.7; shRNA+MUT: 4.74 +/- 0.8, mean+/-SD, T-test, P=0.0001; n=12 means of different electroporated litters.

(F) Knockdown of Znf335 leads to fewer cells that are BrdU positive 48hours post knockdown within 50 μ m² of the ventricular zone as compared to UT-Control. UT-Control: 38.8 +/- 2.9; shRNA-ZNF335: 20.4 +/- 1.7, mean +/-SEM, T-test, P=0.0001; n=12 electroporated brains that were analyzed using serial sections).

(G) Knockdown of Znf335 leads to increased cell cycle exit (decreased BrdU+/Ki67+ cells out of total BrdU+ cells) as compared to UT-Control. (WT-Control: 0.34 +/- 0.03; UT-Control: 0.30 +/- 0.02; ShRNA-ZNF335: .66 +/- 0.04, mean+/-SD, ANOVA, P<0.0001; n=12 electroporated brains that were analyzed used serial sections).

(H) Knockdown of Znf335 leads to more targeted cells in the lower layers of the mouse cortex and fewer targeted cells in upper layers of the mouse cortex, indicating more premature neurogenesis upon knockdown of Znf335. Earlier born neurons reside in deeper layers vs. later born neurons that reside in the upper layers. Scale: 50 μ m.

(I) Cortex was divided into equal-sized bins and counted for proportion of targeted cells present in that bin. *UT-Control*: Bin1: 10.6 +/- 4.9; Bin2: 25.8 +/- 3.7; Bin3: 34.6 +/- 5.2; Bin 4: 29.1 +/- 4.8; *shRNA-ZNF335*: Bin1: 8.1 +/- 7.1; Bin2: 16.5 +/- 6.1; Bin3: 20.7 +/- 3.6; Bin4: 54.7 +/- 5.1. mean+/-SD, T-test; Bin3:P=0.0003, Bin4:P=0.0001; n=12 electroporated brains. Only matching sections between conditions were compared.

See also Fig S3.

born neurons. ZNF335-deficient neurons also exhibited abnormal cell fates. While the majority of the control neurons were Cux1-positive and FoxP1-negative (markers of Layers II-IV and layers III-V, respectively), knockdown neurons instead took on the identity of the lower layer, earlier born neurons (Cux1-negative, FoxP1-positive) (Fig 8A, 8C). These data indicate that Znf335 deficiency leads to premature cell cycle exit and premature neuronal fate determination. Premature neuronal generation leads to a depletion of dividing cells and is consistent with our patient phenotype of the severely reduced cortical size and abnormal cortical layering.

ZNF335 also regulates neuronal morphogenesis and dendrite outgrowth

Further analysis of Znf335-deficient neurons demonstrates abnormal neuronal morphology reminiscent of the patient histology (Fig 1B, 2D). Knockdown cells analyzed at P0 showed abnormal cell orientation and radial glia (Fig 8B-a,b). By P6 and P8, knockdown neurons showed smaller cell bodies and lacked normal vertical apical dendritic process (Fig 8B-c-f). By P16, the dendritic outgrowth of knockdown cells was disorganized, abnormally oriented (Fig 8B-g,h), and only 25% of cells exhibited the stereotypical orientation perpendicular to the pial surface versus 95% in the controls (Fig 8D). By adulthood, knockdown neurons showed disorganized dendritic branching, abnormal dendritic orientation, and signs of dendritic breakdown (Fig 8B-i-n). WT-Znf335 but not Mut-Znf335 rescued the orientation phenotype, confirming the specificity of this phenotype, as well as confirming that the p.H1111R mutation is deficient but

Figure 8

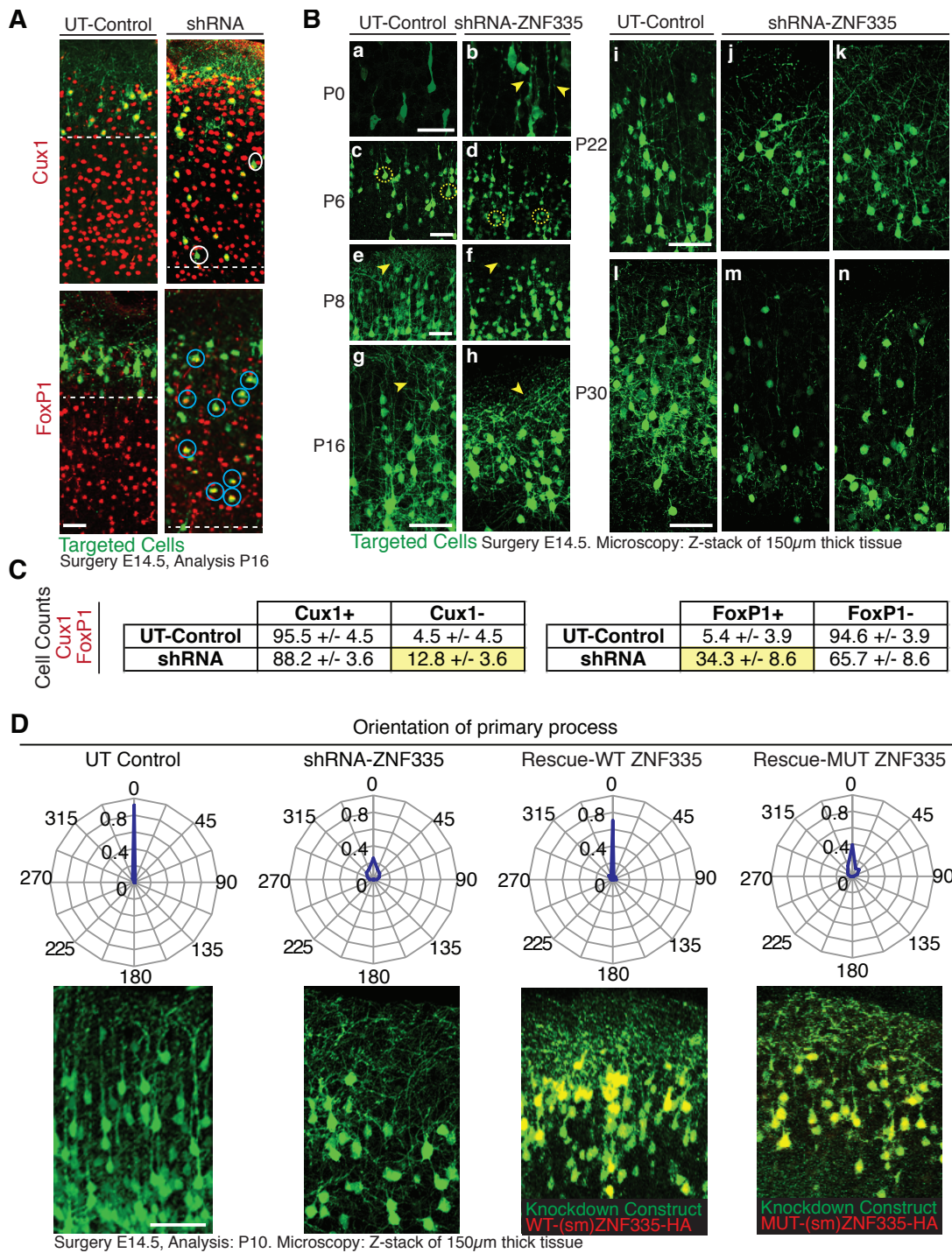


Figure 8 (Continued). Znf335 deficiency leads to decreased cell size, and abnormal dendritic shape and orientation.

al dendritic shape and orientation.

(A) Knockdown of ZNF335 leads to reduction of cells in the cortical plate and production of Cux1-negative (white circles) and FoxP1-positive (blue circles) cells showing a change in cell fate. Dashed line represents end of zone containing GFP-positive cells. Scale: 50 μ m.

(B) Knockdown and control cells were targeted at E14.5 and analyzed at P0 (a,b), P6 (c,d) to show abnormal radial glia (P0, arrowhead) and abnormal cell body shape and size (P6, dashed circle). There is abnormal dendritic arborization (arrowhead) and orientation in knockdown cells at P8 (e,f), P16 (g,h), P22 (i,j,k), and P30 (l,m,n). Scale: 50 μ m.

(C) Analysis of 8A. Knockdown showed production of more Cux1-negative cells as compared to Control, and production of more FoxP1-positive cells as compared to Control.

(D). Knockdown cells show abnormal orientation based on orientation of their basal dendritic process which is normally perpendicular to the pial surface of the brain. WT-ZNF335 rescues the orientation but MUT-ZNF335 does not. Scale: 50 μ m. 0.92 of total UT-Control cells have apical process orientated perpendicular to pial surface (0 $^{\circ}$), 0.03 at 22.5 $^{\circ}$, and 0.04 at 337.5 $^{\circ}$. shRNA-ZNF335 knockdown cells have only 0.25 of total cells oriented at 0 $^{\circ}$, 0.13 at 22.5 $^{\circ}$, 0.11 at 45 $^{\circ}$, 0.08 at 67.5 $^{\circ}$, 0.04 at 90 $^{\circ}$, 0.04 at 270 $^{\circ}$, 0.08 at 292.5 $^{\circ}$, 0.12 at 315 $^{\circ}$, and 0.13 at 337.5 $^{\circ}$. WT-ZNF335 rescue of shRNA-ZNF335 knockdown have 0.7 cells at 0 $^{\circ}$, 0.03 at 22.5 $^{\circ}$, 0.05 at 45 $^{\circ}$, 0.3 at 67.5 $^{\circ}$, 0.04 at 90 $^{\circ}$, 0.02 at 270 $^{\circ}$, 0.03 at 292.5 $^{\circ}$, 0.07 at 315 $^{\circ}$, and 0.05 at 337.5 $^{\circ}$. MUT-ZNF335 rescue of shRNA-ZNF335 knockdown have 0.4 cells at 0 $^{\circ}$, 0.1 at 22.5 $^{\circ}$, 0.11 at 45 $^{\circ}$, 0.06 at 67.5 $^{\circ}$, 0.01 at 90 $^{\circ}$, 0.03 at 270 $^{\circ}$, 0.06 at 292.5 $^{\circ}$, 0.08 at 315 $^{\circ}$, and 0.14 at 337.5 $^{\circ}$. Data presented as proportion of total cells oriented in +/-11.25 $^{\circ}$ of radial direction n=6 electroporated brains. Only matching sections were analyzed between different conditions.

See also Fig S4.

likely hypomorphic (Fig 8D). These phenotypes are reminiscent of the sparse neurons with reduced dendrites and abnormal orientation seen in patient histology studies. Microarray analysis of such neurons with decreased ZNF-335 expression showed decreased expression levels of genes important for brain development, such as neuron-specific transcription factors, dendritic branching and pruning genes, cell cycle and specific signaling factors, and neuronal specific microtubule binding partners (Fig S4), all of which could account for the neuronal and patient phenotypes.

ZNF335 interacts with a chromatin remodeling complex

In order to elucidate how loss of *ZNF335* could have such broad roles, we identified candidate interacting protein partners by complex purification. Immunoprecipitations (IPs) were performed on FLAG-tagged ZNF335 in stable HeLAS3 cell lines as well as on endogenous E14.5 developing mouse brain lysates. Experiments utilizing IP followed by mass spectrometry (MS) and western verification revealed that ZNF335 pulled down members of a human H3K4 methyltransferase complex such as MLL, SETD1A, CFP1, ASH2, RbBP5, and WDR5 (Fig 9A, Table S1, and online data), (Garapaty et al., 2009; Schuettengruber et al., 2011). Together, these proteins form a complex analogous to that of the Trx complex in *Drosophila*, or the complex COMPASS (Complex Proteins Associated with Set1) in *Saccharomyces cerevisiae*—two complexes shown to be required for activation of specific patterns of gene expression (Schuettengruber et al., 2011). Knockdown of members of this

methyltransferase complex have been shown to cause stunted embryonic development and death, while WDR5 expression has been shown to activate self-renewal genes in embryonic stem cells (Ang et al., 2011). The interaction of ZNF335 with a H3K4 methyltransferase complex presents an avenue that would allow ZNF335 to regulate a large number of genes, consistent with the widespread effects of loss of ZNF335 in brain and other tissues.

ZNF335 regulates histone methylation and expression of specific genes

Chromatin IP followed by deep sequencing (ChIP-Seq) identified ZNF335-bound promoters representing possible ZNF335-regulated genes. ChIP-Seq was performed on developing mouse E14.5 lateral telencephalon with two separate antisera and two biological replicates. Znf335 peaks overlapped with the promoter region (Fig 9B-C) of a variety of genes; for example, genes that play roles in cell proliferation, somatic development, cell death, neuronal maturation, and signaling pathways, among others (Fig S5, Table S3). Since ZNF335 interacts in a methyltransferase complex, we looked at the methylation patterns of these ZNF335-bound promoters (Shen, 2012), and the peaks of ZNF335-binding overlapped with the H3K4trimethylation (H3K4me3) peaks (Fig S5A). Similarly, in patients with decreased levels of ZNF335, H3K4me3 marks at the promoters of Znf335 bound genes were also decreased, while control H3K27me3 marks were not changed (Fig S5B). Finally, since H3K4me3 is linked with gene expression, RNA-seq data from the parents and patients who have low H3K4me3 marks also showed decrease levels of gene expression of these

Figure 9

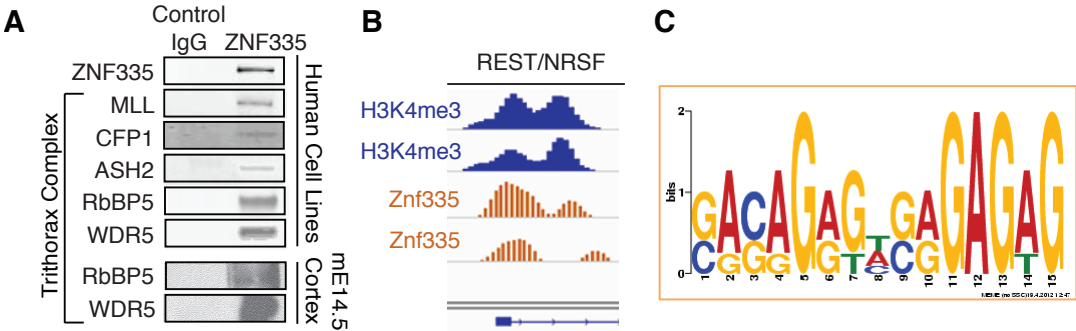


Figure 9 (Continued). Znf335 interacts with trithorax complex proteins and is upstream of many neuronal differentiation genes including REST/NRSF.

(A) Blots show co-immunoprecipitation of Znf335 with members of the trithorax complex in human cell lines and mouse E14.5 cortex indicating an interaction of Znf335 with the histone methyltransferase complex.

(B) Znf335 binds to promoter region of *REST/NRSF*, and overlaps peaks of H3K4me3 binding.

(C) Promoter Binding consensus motif for Znf335 with GAGAG motif that is predicted for C2H2 zinc fingers (Omichinski et al., 1997).

ZNF335 target genes (Table S2, S3). Together, these data hint at a role of ZNF335 in a methyltransferase complex that is important for the H3K4trimethylation and ultimately the expression levels of a large variety of genes. GeneGO analysis performed on the genes identified through ChIP-Seq, microarrays, and RNA-seq data from patients showed that the genes affected by Znf335 were involved in a variety of pathways important for both somatic development as well as brain development (Table S4-7).

ZNF335 is upstream of NRSF/REST

Interestingly, we observed Znf335 bound to the promoter region of the known progenitor cell master regulator *REST/NRSF* (Fig 9B). A direct relationship between ZNF335 and expression of REST/NRSF is suggested by decreased Trx complex binding and decreased H3K4me3 marks at the REST/NRSF promoter (Fig 10D-E), as well as decreased mRNA levels of *REST/NRSF* in heterozygous parents and *ZNF335*-mutant patient cell lines (Fig 10F). Decreased *REST/NRSF* expression was also seen upon ZNF335 knockdown of HeLA and Hek293 cells (Fig 10G), supporting a close, potentially direct, relationship. Conversely, expression of a dominant-negative REST (*DN-REST*)--which contains the DNA binding domain only (Chong et al., 1995; Schoenherr and Anderson, 1995)--as well as overexpression of *REST/NRSF*, did not significantly alter *ZNF335* expression (Fig 10H). Rescue experiments also showed that the premature cell cycle exit and premature migrating neurons seen in the absence of ZNF335 could be rescued by REST, but not by DN-REST,

Figure 10

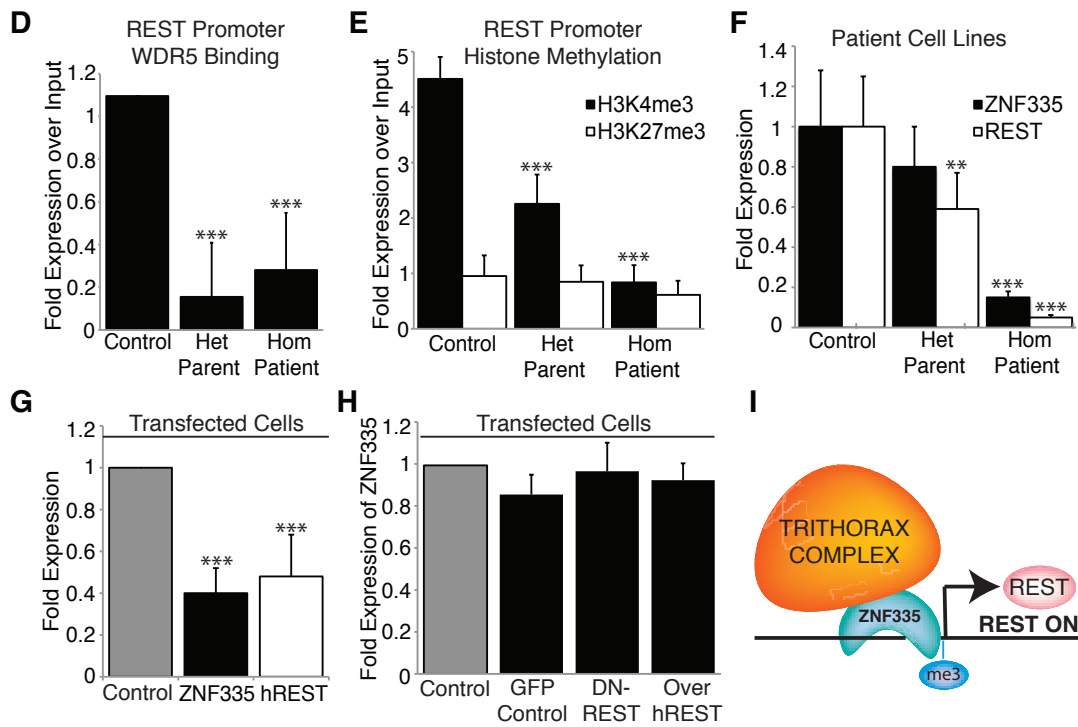


Figure 10 (Continued). Znf335 interacts with trithorax complex proteins and is upstream of many neuronal differentiation genes including REST/NRSF.

(D) Decreased binding of trithorax complex proteins such as WDR5 to the *REST* promoter under low levels of Znf335. WDR5: Control: 1.09 +/- 0, Het Parent: 0.16 +/- 0.25, Hom Patient: 0.28 +/- 0.27; chromatin was obtained and compiled from 3 different growth cultures. Two IPs were performed for each pooled set of chromatin isolated from lymphoblast cell lines, and qPCR was run in triplicates in comparison to input. All qPCR runs were normalized to GAPDH.

(E) Decreased H3K4 trimethylation (marker of gene activation) of the *REST* promoter under low levels of Znf335, but no changes in H3K27 trimethylation. H3K4me3: Control: 4.5 +/- 0.39, Het Parent: 2.25 +/- 0.53, Hom Patient: 0.84 +/- 0.3; H3K27me3: Control: 0.95 +/- 0.37; Het Parent: 0.85 +/- 0.29; Hom Patient: 0.6, +/- 0.25; chromatin was obtained and compiled from 3 different growth cultures. Two IPs were performed for each pooled set of chromatin isolated from lymphoblast cell lines, and qPCR was run in triplicates in comparison to input. All qPCR runs were normalized to GAPDH.

(F) qPCR measurement show lower levels of properly spliced *ZNF335* expression and *hREST* expression in het parents and hom patients as compared to controls. *ZNF335* analysis was done with primers specific to only the properly spliced mRNA. Incomplete splice forms would not have been picked up with primer pairs (Exon19F, Exon 20R, Exon21R): Control: 1 +/- 0.28, Het Parent: 0.80 +/- 0.21, Hom Patient: 0.15 +/- 0.03; *hREST*: Control: 1 +/- 0.25; Het Parent: 0.59 +/- 0.18; Hom Patient: 0.05, +/- 0.01; Mean+/-SD, T-test compared to control, homozygous patients $p < 0.001$; $n = 9$ qPCR readouts from 3 different growth cultures. RNA was extracted from lymphoblast cell lines. All qPCR runs were normalized to *NMYC* and GAPDH.

(G) Decreased levels of *hREST* expression is seen upon direct knockdown of *ZNF335*. Control: 1, *ZNF335*: 0.41 +/- 0.12, $P = 0.0001$; *hREST*: 0.48 +/- 0.20, $P = 0.0001$; Mean+/-SD, T-test; $n = 6$ individual transfections of HeLa cell lines. All qPCR runs were normalized to GAPDH.

(H) Conversely, *ZNF335* expression is not significantly changed upon expression of Dominant-Negative REST, or overexpression of *hREST*. GFP Control: 0.85 +/- 0.09; DN-REST: 0.97 +/- 0.14; Over-*hREST*: 0.92 +/- 0.08; Mean+/-SD, T-test, non-significant; $n = 3$ sets of transfections of HeLa cell lines. Similar results also seen with Hek293 cells lines (data not published). All qPCR runs were normalized to GAPDH.

(I) Schematic of Znf335 interacting with the trithorax complex to trimethylate H3K4 at the promoter of *REST* to turn on *REST* expression.

Figure 11

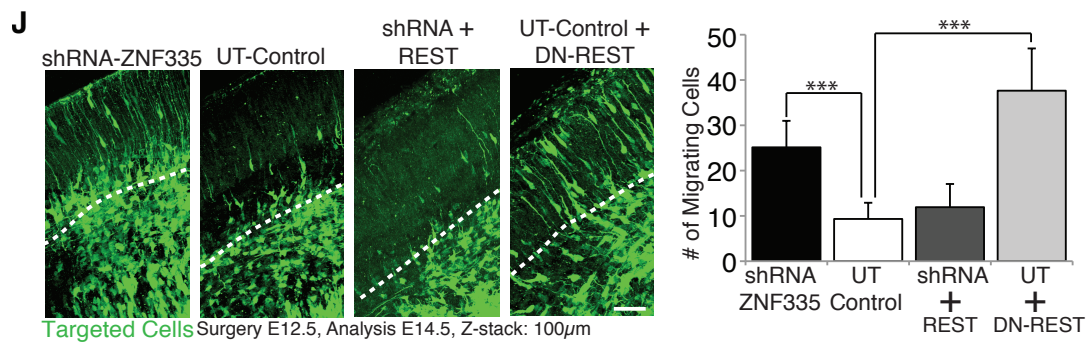


Figure 11 (Continued). Znf335 interacts with trithorax complex proteins and is upstream of many neuronal differentiation genes including REST/NRSF.

(J) Knockdown of Znf335 leads to premature cell cycle exit and neuronal migration in cortical plate. Addition of REST rescues the phenotype and recapitulates control while addition of dominant-negative REST mimics Znf335 knockdown phenotype. Dashed line represents bottom of cortical plate. Scale: 50 μ m. UT-Control: 9.32 +/- 3.57; shRNA-ZNF335: 25.6 +/- 8.34; shRNA+REST rescue 11.92 +/- 5.1; UT+DN-REST rescue: 37.6 +/- 0.3. UT-shRNA P=0.0001, UT-DNREST rescue P=0.0001; Mean+/-SD, T-test; n=3 different electroporation litters, and analysis from each litter was pooled.

See also Fig S5 and Tables S1-S7.

which caused a phenotype similar to ZNF335 deficiency (Fig 11J). These data, along with the promoter binding of REST/NRSF by Znf335, suggests direct regulation of REST/NRSF expression by Znf335 (Fig 10I), and may provide an avenue for abnormal neurogenesis secondary to abnormal REST regulation.

ZNF335 is essential for neuronal production and brain formation

Further analysis of Znf335-knockdown neurons showed stereotypical neuronal morphology (small cell bodies, dendrites, axons), but with a surprising loss of immunoreactivity for *D11Bwg0517e/Fox3*, or Neuronal nuclei (*NeuN*), an ubiquitous marker of all differentiated neurons (Dredge and Jensen, 2011) (Fig 12A, 12B, S6A), suggesting an apparent state of incomplete neuronal differentiation. This failure to express mature neuronal markers could reflect the abnormal premature neurogenesis caused by early progenitor cell cycle exit (Fig 7D), or—perhaps more likely—could reflect direct requirements for Znf335 in controlling gene expression in postmitotic neurons or in neuronal maturation and activity. The altered morphology (Fig 8B), and the arrested development (Fig 12A) exhibited by Znf335 knockdown neurons is reminiscent of the altered neuronal phenotype, altered cortical layers and decreased cortical size phenotype seen in patients (Fig 1B, 1C).

Similar to Znf335-deficient cortical neurons, Znf335 knockdown cerebellar granule cells showed abnormal cell migration, morphology, and differentiation. Znf335-deficient cerebellar granule cells also showed migration arrest with decreased migration into the IGL (Fig S6B-D) recapitulating the human

Figure 12

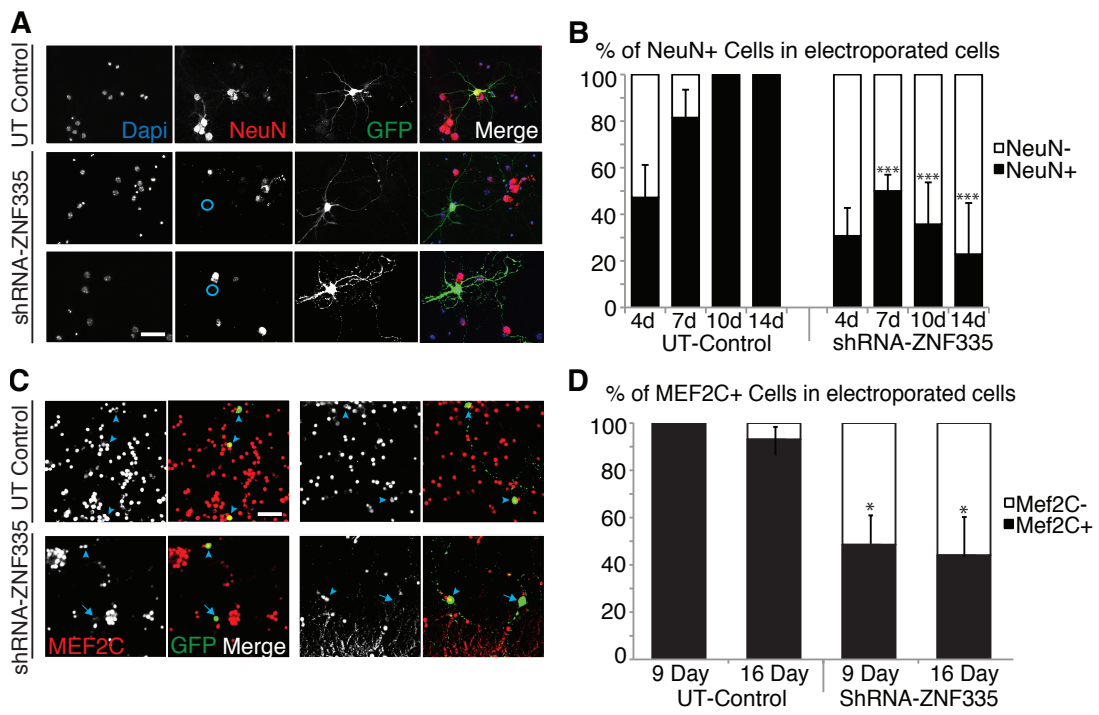


Figure 12 (Continued). Znf335 is essential for neuronal differentiation and brain development.

(A) Knockdown of Znf335 leads to presence of NeuN⁻ cells (blue circles) that nonetheless have neuronal morphology in 14 day culture systems. NeuN is a marker of differentiated neurons. Scale: 20 μ m.

(B) Quantification of NeuN⁺ and NeuN⁻ cells upon knockdown of Znf335 in short and long term culture shows decreased production of NeuN⁺ cells over long term culture. Control NeuN⁺: 4day: 48.2 \pm 14.1; 7day: 81.5 \pm 12.1; 10day: 100 \pm 0.9; 14day: 100 \pm 1.5; shRNA-ZNF335 NeuN⁺: 4day: 30.7 \pm 12.3; 7day: 50.0 \pm 7.0; 10day: 35.7 \pm 18.1; 14day: 22.9 \pm 19.1); Mean \pm SD, T-test, 7,10,14day: P<0.0001; n=12 separate cortical neuron cultures from 12 litters.

(C) Knockdown of Znf335 leads to Mef2C⁻ cells (arrows), while UT Control shows Mef2C⁺ cells (arrowhead). Scale: 20 μ m.

(D) Quantification of Mef2C⁺ and Mef2C⁻ cells shows decreased production of Mef2C⁺ cells upon knockdown of Znf335 in short and long term cultures. Control Mef2C⁺: 9day: 100 \pm 0.8; 16day: 93.0 \pm 8.2; shRNA-ZNF335 Mef2C⁺: 9day: 48.5 \pm 12.1; 16day: 44.0 \pm 15.2); Mean \pm SD, T-test, 9Day:P=0.0018, 16day:P=0.008; n=3 separate granule cell cultures from 3 different litters.

phenotype (Fig 2D, 2E). *Znf335*-deficient granule cells also showed decreased *Mef2C* expression even after long-term culture (Fig 12C, 12D), and long-term *Znf335* knockdown in cortical neurons also lead to decreased *Mef2C* transcript expression, again suggesting an arrest of normal transcriptional patterns. A decrease in *Mef2C* has been implicated in cell death (Mao et al., 1999), and our findings that knockdown of *Znf335* also led to increased cell death (Fig 12D) might suggest that this effect is mediated through *Mef2c*.

Finally, to confirm the essential role of *Znf335* in cerebral cortical neurogenesis, we created a brain-specific, conditional knockout of *Znf335* to bypass the embryonic lethality of a global knockout (Fig 5A). *Emx1-Cre* mediated removal of *Znf335* (*Znf335* CKO) (Fig S7) produced a brain with an essentially absent cortex lacking all cortical neurons at sites of *Emx1* expression (Fig 13E, 13F) (Gorski et al., 2002). The lack of cortical plate and cortical neurons is in accordance with the essential role of *Znf335* in progenitor cells and postmitotic neurons. The small brain phenotype of the *Znf335* CKO further confirms that *Znf335* is responsible for the severe phenotype seen in our patients, and verifies *Znf335* as a new microcephaly gene essential for brain structure formation and development.

Figure 13

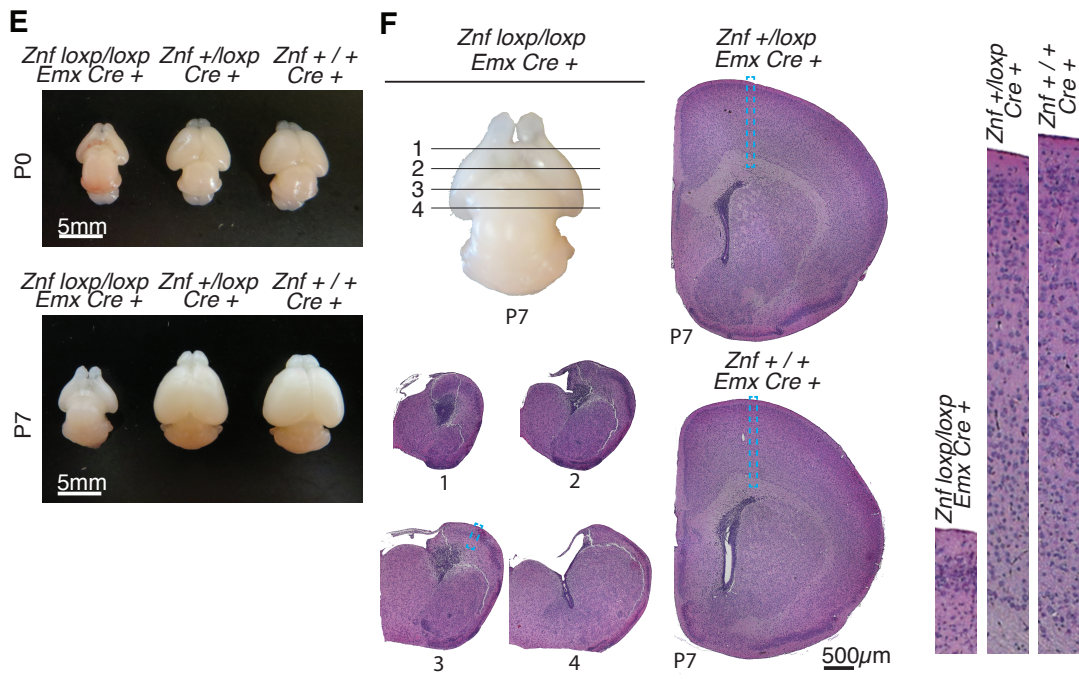


Figure 13 (Continued). Znf335 is essential for neuronal differentiation and brain development.

(E) Znf335 CKO (*Znflox/lox;Emx1Cre+*) shows decreased formation of cerebral cortex in all areas where *Emx1-Cre* is expressed, and a small lateral cortex in areas where *Emx1-cre* is reduced or turned on later at both P0 and P7. (F) H&E stain of coronal brain sections of ZnfCKO (*Znflox/lox;Emx1Cre+*), ZnfHet (*Znf+/lox;Emx1Cre+*), and ZnfWT (*Znf+/+;Emx1Cre+*) shows that ZnfCKO lack all cortical structure and cortical neurons. The loss of cortical brain structure leads to the formation of a small brain with a thin sheath of tissue and enlarged ventricles. Blue dashed boxed represent enlarged cortical sections (Right panels).

See also Fig S6 and S7.

CONCLUSIONS

Here we identify *ZNF335/NIF1* as a central regulator of mammalian neurogenesis and neuronal differentiation. *ZNF335* was identified in a large Arab-Israeli family with 7 of 10 kids affected with severe microcephaly. The affected patient presented with severely reduced brain structure as well as aberrant cortical and cerebellar architecture and histology. The mutation identified was a c.3332g>a transition at an intron exon junction leading to incomplete splicing and the creation of a larger transcript. While most of the transcripts are degraded, some transcript is made into protein although with a R1111H missense mutation.

Global knockout of *ZNF335* leads to embryonic lethality due to the global roles of *ZNF335* in development. In the brain, *ZNF335* is expressed in the progenitor population of the developing brain and seems to localize to the nucleus hinting at a role in gene regulation. *ZNF335* is important for proper cell proliferation and knockdown of *ZNF335* leads to decreased progenitors cells and increased progenitor cell cycle exit leading to premature neurogenesis. The neurons formed exhibit abnormal morphology, orientation and branching patterns. The neurons also exhibit abnormal cell fate and incomplete neuronal differentiation.

Biochemistry studies showed that *ZNF335* interacts with members of a histone H3K4 methyltransferase complex, the Trithorax complex. ChIP-sequencing analysis shows that *ZNF335* binds to the promoter regions of a larger number of genes important for growth and development. The binding

pattern of ZNF335 overlapped with the H3K4me3 marks of those genes. Correspondingly, ZNF335 expression is also important for the H3K4me3 levels of the promoters of these genes, and ZNF335 is essential for gene expression.

One of the genes that ZNF335 regulates is *REST/NRSF*, a known master regulator of brain development. ZNF335 binds to the promoter of *REST/NRSF* and is also essential for H3K4 trimethylation levels of *REST/NRSF*. Knockdown of *REST/NRSF* recapitulates the ZNF335 knockdown phenotype, while addition of *REST/NRSF* rescues the ZNF335 knockdown phenotype.

The brain specific conditional knockout of ZNF335 bypasses the embryonic lethality of the global ZNF335 knockout. The conditional knockout of the ZNF335 leads to the essential loss of all cortical structure and recapitulates the human phenotype. We show that ZNF335 is an essential gene of brain development and proves to be a new type of microcephaly gene that is responsible for proper gene activation.

ACKNOWLEDGMENTS

We thank D. Moazed, M.E. Hatten, B. Ren, D.M. Ferrero, and members of the Walsh laboratory for helpful discussions; L. Shechtman for tissue, N. Dwyer for early mapping, G. Mandel for DN-REST construct, E.E. Govek for help with cerebellar slices, K.S. Krishnamoorthy for control MRIs, D.J. Tischfield, L.B. Hills, K.D. Atabay, P.P. Wang, D.G. Tierney, and J.M. Felie for technical assistance. This work was supported by a Stuart H.Q. & Victoria Quan Fellowship (Y.J.Y.); a NIH MSTP grant T32GM007753 (Y.J.Y. and G.D.E.); a NIH T32 HD007466 (A.E.B.); The Damon Runyon Cancer Research Foundation DRG-2042-10 (R.S.M.); HHMI Medical Research Fellows Program (E.P.W.); RO1 DK16636 (H.H.S.); NIH grants (GM058012, GM071004, and CA118487) (Y.S.); grants from the NINDS (RO1 NS032457 and R01 NS35129), and the Manton Center for Orphan Disease Research (C.A.W.). C.A.W. is an Investigator of the Howard Hughes Medical Institute. The content is solely the responsibility of the authors and does not necessarily represent the official views of the NINDS or the NIH.

REFERENCES

Adams, N.C., Tomoda, T., Cooper, M., Dietz, G., and Hatten, M.E. (2002). Mice that lack astrotactin have slowed neuronal migration. *Development* 129, 965-972.

Alkuraya, F.S., Cai, X., Emery, C., Mochida, G.H., Al-Dosari, M.S., Felie, J.M., Hill, R.S., Barry, B.J., Partlow, J.N., Gascon, G.G., *et al.* (2011). Human mutations in NDE1 cause extreme microcephaly with lissencephaly [corrected]. *American journal of human genetics* 88, 536-547.

Ang, Y.S., Tsai, S.Y., Lee, D.F., Monk, J., Su, J., Ratnakumar, K., Ding, J., Ge, Y., Darr, H., Chang, B., *et al.* (2011). Wdr5 mediates self-renewal and reprogramming via the embryonic stem cell core transcriptional network. *Cell* 145, 183-197.

Bakircioglu, M., Carvalho, O.P., Khurshid, M., Cox, J.J., Tuysuz, B., Barak, T., Yilmaz, S., Caglayan, O., Dincer, A., Nicholas, A.K., *et al.* (2011). The essential role of centrosomal NDE1 in human cerebral cortex neurogenesis. *American journal of human genetics* 88, 523-535.

Ballas, N., Grunseich, C., Lu, D.D., Speh, J.C., and Mandel, G. (2005). REST and its corepressors mediate plasticity of neuronal gene chromatin throughout neurogenesis. *Cell* 121, 645-657.

Bannister, A.J., and Kouzarides, T. (2011). Regulation of chromatin by histone modifications. *Cell research* 21, 381-395.

Barkovich, A.J., Moore, K.R., Jones, B.V., Vezina, G., Koch, B.L., Raybaud, C., Grant, P.E., Blaser, S.I., Hedlund, G.L., Illner, A. (2007). *Diagnostic Imaging: Pediatric Neuroradiology*, 1st edn (Salt Lake City, Utah, Amirsys- Elsevier).

Beisel, C., Imhof, A., Greene, J., Kremmer, E., and Sauer, F. (2002). Histone methylation by the Drosophila epigenetic transcriptional regulator Ash1. *Nature* 419, 857-862.

Bernstein, B.E., Kamal, M., Lindblad-Toh, K., Bekiranov, S., Bailey, D.K., Huebert, D.J., McMahon, S., Karlsson, E.K., Kulbokas, E.J., 3rd, Gingeras, T.R., *et al.* (2005). Genomic maps and comparative analysis of histone modifications in human and mouse. *Cell* 120, 169-181.

Bettencourt-Dias, M., Hildebrandt, F., Pellman, D., Woods, G., and Godinho, S.A. (2011). Centrosomes and cilia in human disease. *Trends in genetics : TIG* 27, 307-315.

Bi, Y., Lv, Z., Wang, Y., Hai, T., Huo, R., Zhou, Z., Zhou, Q., and Sha, J. (2011). WDR82, a key epigenetics-related factor, plays a crucial role in normal early embryonic development in mice. *Biol Reprod* 84, 756-764.

Bruce, A.W., Donaldson, I.J., Wood, I.C., Yerbury, S.A., Sadowski, M.I., Chapman, M., Gottgens, B., and Buckley, N.J. (2004). Genome-wide analysis of repressor element 1 silencing transcription factor/neuron-restrictive silencing factor (REST/NRSF) target genes. *Proc Natl Acad Sci U S A* 101, 10458-10463.

Buck, D., Moshous, D., de Chasseval, R., Ma, Y., le Deist, F., Cavazzana-Calvo, M., Fischer, A., Casanova, J.L., Lieber, M.R., and de Villartay, J.P. (2006). Severe combined immunodeficiency and microcephaly in siblings with hypomorphic mutations in DNA ligase IV. *European journal of immunology* 36, 224-235.

Cartegni, L., Chew, S.L., and Krainer, A.R. (2002). Listening to silence and understanding nonsense: exonic mutations that affect splicing. *Nat Rev Genet* 3, 285-298.

Chae, T.H., Kim, S., Marz, K.E., Hanson, P.I., and Walsh, C.A. (2004). The *hyh* mutation uncovers roles for alpha Snap in apical protein localization and control of neural cell fate. *Nat Genet* 36, 264-270.

Chen, Z.F., Paquette, A.J., and Anderson, D.J. (1998). NRSF/REST is required in vivo for repression of multiple neuronal target genes during embryogenesis. *Nat Genet* 20, 136-142.

Chong, J.A., Tapia-Ramirez, J., Kim, S., Toledo-Aral, J.J., Zheng, Y., Boutros, M.C., Altshuler, Y.M., Frohman, M.A., Kraner, S.D., and Mandel, G. (1995). REST: a mammalian silencer protein that restricts sodium channel gene expression to neurons. *Cell* 80, 949-957.

Clowry, G., Molnar, Z., and Rakic, P. (2010). Renewed focus on the developing human neocortex. *Journal of anatomy* 217, 276-288.

Cosgrove, M.S., and Patel, A. (2010). Mixed lineage leukemia: a structure-function perspective of the MLL1 protein. *Febs J* 277, 1832-1842.

Djabali, M., Selleri, L., Parry, P., Bower, M., Young, B.D., and Evans, G.A. (1992). A trithorax-like gene is interrupted by chromosome 11q23 translocations in acute leukaemias. *Nat Genet* 2, 113-118.

Dou, Y., Milne, T.A., Tackett, A.J., Smith, E.R., Fukuda, A., Wysocka, J., Allis, C.D., Chait, B.T., Hess, J.L., and Roeder, R.G. (2005). Physical association and coordinate function of the H3 K4 methyltransferase MLL1 and the H4 K16 acetyltransferase MOF. *Cell* 121, 873-885.

Dredge, B.K., and Jensen, K.B. (2011). NeuN/Rbfox3 nuclear and cytoplasmic isoforms differentially regulate alternative splicing and nonsense-mediated decay of Rbfox2. *PLoS One* 6, e21585.

Feng, Y., and Walsh, C.A. (2004). Mitotic spindle regulation by Nde1 controls cerebral cortical size. *Neuron* 44, 279-293.

Fietz, S.A., and Huttner, W.B. (2011). Cortical progenitor expansion, self-renewal and neurogenesis—a polarized perspective. *Curr Opin Neurobiol* 21, 23-35.

Fisher, C.L., and Fisher, A.G. (2011). Chromatin states in pluripotent, differentiated, and reprogrammed cells. *Curr Opin Genet Dev* 21, 140-146.

Garapaty, S., Mahajan, M.A., and Samuels, H.H. (2008). Components of the CCR4-NOT complex function as nuclear hormone receptor coactivators via association with the NRC-interacting Factor NIF-1. *J Biol Chem* 283, 6806-6816.

Garapaty, S., Xu, C.F., Trojer, P., Mahajan, M.A., Neubert, T.A., and Samuels, H.H. (2009). Identification and characterization of a novel nuclear protein complex involved in nuclear hormone receptor-mediated gene regulation. *J Biol Chem* 284, 7542-7552.

Glaser, S., Lubitz, S., Loveland, K.L., Ohbo, K., Robb, L., Schwenk, F., Seibler, J., Roellig, D., Kranz, A., Anastassiadis, K., *et al.* (2009). The histone 3 lysine 4 methyltransferase, Mll2, is only required briefly in development and spermatogenesis. *Epigenetics Chromatin* 2, 5.

Gotz, M., and Huttner, W.B. (2005). The cell biology of neurogenesis. *Nat Rev Mol Cell Biol* 6, 777-788.

Greenway, D.J., Street, M., Jeffries, A., and Buckley, N.J. (2007). RE1 Silencing transcription factor maintains a repressive chromatin environment in embryonic hippocampal neural stem cells. *Stem Cells* 25, 354-363.

Haubensak, W., Attardo, A., Denk, W., and Huttner, W.B. (2004). Neurons arise in the basal neuroepithelium of the early mammalian telencephalon: a major site of neurogenesis. *Proc Natl Acad Sci U S A* 101, 3196-3201.

Hoyer, J., Ekici, A.B., Endeke, S., Popp, B., Zweier, C., Wiesener, A., Wohlleber, E., Dufke, A., Rossier, E., Petsch, C., *et al.* (2012). Haploinsufficiency of ARID1B, a member of the SWI/SNF-a chromatin-remodeling complex, is a frequent cause of intellectual disability. *Am J Hum Genet* 90, 565-572.

Hughes, C.M., Rozenblatt-Rosen, O., Milne, T.A., Copeland, T.D., Levine, S.S., Lee, J.C., Hayes, D.N., Shanmugam, K.S., Bhattacharjee, A., Biondi, C.A., *et al.*

(2004). Menin associates with a trithorax family histone methyltransferase complex and with the *hoxc8* locus. *Mol Cell* *13*, 587-597.

Ingham, P.W. (1985). A clonal analysis of the requirement for the trithorax gene in the diversification of segments in *Drosophila*. *Journal of embryology and experimental morphology* *89*, 349-365.

Johnson, R., Teh, C.H., Kunarso, G., Wong, K.Y., Srinivasan, G., Cooper, M.L., Volta, M., Chan, S.S., Lipovich, L., Pollard, S.M., *et al.* (2008). REST regulates distinct transcriptional networks in embryonic and neural stem cells. *PLoS Biol* *6*, e256.

Kim, S., Lehtinen, M.K., Sessa, A., Zappaterra, M.W., Cho, S.H., Gonzalez, D., Boggan, B., Austin, C.A., Wijnholds, J., Gambello, M.J., *et al.* (2010). The apical complex couples cell fate and cell survival to cerebral cortical development. *Neuron* *66*, 69-84.

Kriegstein, A., and Alvarez-Buylla, A. (2009). The glial nature of embryonic and adult neural stem cells. *Annual review of neuroscience* *32*, 149-184.

Lessard, J.A., and Crabtree, G.R. (2010). Chromatin regulatory mechanisms in pluripotency. *Annual review of cell and developmental biology* *26*, 503-532.

Lizarraga, S.B., Margossian, S.P., Harris, M.H., Campagna, D.R., Han, A.P., Blevins, S., Mudbhary, R., Barker, J.E., Walsh, C.A., and Fleming, M.D. (2010). *Cdk5rap2* regulates centrosome function and chromosome segregation in neuronal progenitors. *Development* *137*, 1907-1917.

Lui, J.H., Hansen, D.V., and Kriegstein, A.R. (2011). Development and evolution of the human neocortex. *Cell* *146*, 18-36.

Mahajan, M.A., Murray, A., and Samuels, H.H. (2002). NRC-interacting factor 1 is a novel cotransducer that interacts with and regulates the activity of the nuclear hormone receptor coactivator NRC. *Mol Cell Biol* *22*, 6883-6894.

Mahmood, S., Ahmad, W., and Hassan, M.J. (2011). Autosomal Recessive Primary Microcephaly (MCPH): clinical manifestations, genetic heterogeneity and mutation continuum. *Orphanet journal of rare diseases* *6*, 39.

Mao, Z., Bonni, A., Xia, F., Nadal-Vicens, M., and Greenberg, M.E. (1999). Neuronal activity-dependent cell survival mediated by transcription factor MEF2. *Science* *286*, 785-790.

Martinez, A.M., Colomb, S., Dejardin, J., Bantignies, F., and Cavalli, G. (2006). Polycomb group-dependent Cyclin A repression in *Drosophila*. *Genes Dev* *20*, 501-513.

Matsumoto, Y., Miyamoto, T., Sakamoto, H., Izumi, H., Nakazawa, Y., Ogi, T., Tahara, H., Oku, S., Hiramoto, A., Shiiki, T., *et al.* (2011). Two unrelated patients with MRE11A mutations and Nijmegen breakage syndrome-like severe microcephaly. *DNA Repair (Amst)* 10, 314-321.

Miller, T., Krogan, N.J., Dover, J., Erdjument-Bromage, H., Tempst, P., Johnston, M., Greenblatt, J.F., and Shilatifard, A. (2001). COMPASS: a complex of proteins associated with a trithorax-related SET domain protein. *Proc Natl Acad Sci U S A* 98, 12902-12907.

Molyneaux, B.J., Arlotta, P., Menezes, J.R., and Macklis, J.D. (2007). Neuronal subtype specification in the cerebral cortex. *Nat Rev Neurosci* 8, 427-437.

Morrison, M.E., and Mason, C.A. (1998). Granule neuron regulation of Purkinje cell development: striking a balance between neurotrophin and glutamate signaling. *J Neurosci* 18, 3563-3573.

Nagata, I., Ono, K., Kawana, A., and Kimura-Kuroda, J. (2006). Aligned neurite bundles of granule cells regulate orientation of Purkinje cell dendrites by perpendicular contact guidance in two-dimensional and three-dimensional mouse cerebellar cultures. *J Comp Neurol* 499, 274-289.

Nakamura, T., Mori, T., Tada, S., Krajewski, W., Rozovskaia, T., Wassell, R., Dubois, G., Mazo, A., Croce, C.M., and Canaani, E. (2002). ALL-1 is a histone methyltransferase that assembles a supercomplex of proteins involved in transcriptional regulation. *Mol Cell* 10, 1119-1128.

O'Driscoll, M., Jackson, A.P., and Jeggo, P.A. (2006). Microcephalin: a causal link between impaired damage response signalling and microcephaly. *Cell cycle* 5, 2339-2344.

O'Driscoll, M., and Jeggo, P.A. (2008). The role of the DNA damage response pathways in brain development and microcephaly: insight from human disorders. *DNA Repair (Amst)* 7, 1039-1050.

Papp, B., and Muller, J. (2006). Histone trimethylation and the maintenance of transcriptional ON and OFF states by trxG and PcG proteins. *Genes Dev* 20, 2041-2054.

Paro, R., Strutt, H., and Cavalli, G. (1998). Heritable chromatin states induced by the Polycomb and trithorax group genes. *Novartis Found Symp* 214, 51-61; discussion 61-56, 104-113.

Petruk, S., Sedkov, Y., Smith, S., Tillib, S., Kraevski, V., Nakamura, T., Canaani, E., Croce, C.M., and Mazo, A. (2001). Trithorax and dCBP acting in a complex to maintain expression of a homeotic gene. *Science* 294, 1331-1334.

Renbaum, P., Kellerman, E., Jaron, R., Geiger, D., Segel, R., Lee, M., King, M.C., and Levy-Lahad, E. (2009). Spinal muscular atrophy with pontocerebellar hypoplasia is caused by a mutation in the VRK1 gene. *American journal of human genetics* 85, 281-289.

Schneider, J., Dover, J., Johnston, M., and Shilatifard, A. (2004). Global proteomic analysis of *S. cerevisiae* (GPS) to identify proteins required for histone modifications. *Methods Enzymol* 377, 227-234.

Schneider, J., Wood, A., Lee, J.S., Schuster, R., Dueker, J., Maguire, C., Swanson, S.K., Florens, L., Washburn, M.P., and Shilatifard, A. (2005). Molecular regulation of histone H3 trimethylation by COMPASS and the regulation of gene expression. *Mol Cell* 19, 849-856.

Schoenherr, C.J., and Anderson, D.J. (1995). Silencing is golden: negative regulation in the control of neuronal gene transcription. *Curr Opin Neurobiol* 5, 566-571.

Schuettengruber, B., Chourrout, D., Vervoort, M., Leblanc, B., and Cavalli, G. (2007). Genome regulation by polycomb and trithorax proteins. *Cell* 128, 735-745.

Schuettengruber, B., Ganapathi, M., Leblanc, B., Portoso, M., Jaschek, R., Tolhuis, B., van Lohuizen, M., Tanay, A., and Cavalli, G. (2009). Functional anatomy of polycomb and trithorax chromatin landscapes in *Drosophila* embryos. *PLoS Biol* 7, e13.

Schuettengruber, B., Martinez, A.M., Iovino, N., and Cavalli, G. (2011). Trithorax group proteins: switching genes on and keeping them active. *Nat Rev Mol Cell Biol* 12, 799-814.

Sheen, V.L., Ganesh, V.S., Topcu, M., Sebire, G., Bodell, A., Hill, R.S., Grant, P.E., Shugart, Y.Y., Imitola, J., Houry, S.J., *et al.* (2004). Mutations in ARFGEF2 implicate vesicle trafficking in neural progenitor proliferation and migration in the human cerebral cortex. *Nat Genet* 36, 69-76.

Shen, J., Gilmore, E.C., Marshall, C.A., Haddadin, M., Reynolds, J.J., Eyaid, W., Bodell, A., Barry, B., Gleason, D., Allen, K., *et al.* (2010). Mutations in PNKP cause microcephaly, seizures and defects in DNA repair. *Nat Genet* 42, 245-249.

Shen, Y., Yue, F., McCleary, D.F., Ye, Z., Edsall, L., Wagner, U., Dixon, J., Lee, L., Lobanenkov, V., Ren, B. (2012). A draft map of cis-regulatory sequences in the mouse genome. *Nature*.

Smeyne, R.J., Chu, T., Lewin, A., Bian, F., Sanlioglu, S., Kunsch, C., Lira, S.A., and Oberdick, J. (1995). Local control of granule cell generation by cerebellar Purkinje cells. *Mol Cell Neurosci* 6, 230-251.

Steward, M.M., Lee, J.S., O'Donovan, A., Wyatt, M., Bernstein, B.E., and Shilatifard, A. (2006). Molecular regulation of H3K4 trimethylation by ASH2L, a shared subunit of MLL complexes. *Nat Struct Mol Biol* 13, 852-854.

Su, X., Kameoka, S., Lentz, S., and Majumder, S. (2004). Activation of REST/NRSF target genes in neural stem cells is sufficient to cause neuronal differentiation. *Mol Cell Biol* 24, 8018-8025.

Sun, Y.M., Greenway, D.J., Johnson, R., Street, M., Belyaev, N.D., Deuchars, J., Bee, T., Wilde, S., and Buckley, N.J. (2005). Distinct profiles of REST interactions with its target genes at different stages of neuronal development. *Mol Biol Cell* 16, 5630-5638.

Sur, M., and Rubenstein, J.L. (2005). Patterning and plasticity of the cerebral cortex. *Science* 310, 805-810.

Tenney, K., and Shilatifard, A. (2005). A COMPASS in the voyage of defining the role of trithorax/MLL-containing complexes: linking leukemogenesis to covalent modifications of chromatin. *J Cell Biochem* 95, 429-436.

Terranova, R., Agherbi, H., Boned, A., Meresse, S., and Djabali, M. (2006). Histone and DNA methylation defects at Hox genes in mice expressing a SET domain-truncated form of Mll. *Proc Natl Acad Sci U S A* 103, 6629-6634.

Wang, Y.Y., Liu, L.J., Zhong, B., Liu, T.T., Li, Y., Yang, Y., Ran, Y., Li, S., Tien, P., and Shu, H.B. (2010). WDR5 is essential for assembly of the VISA-associated signaling complex and virus-triggered IRF3 and NF-kappaB activation. *Proc Natl Acad Sci U S A* 107, 815-820.

Wysocka, J., Myers, M.P., Laherty, C.D., Eisenman, R.N., and Herr, W. (2003). Human Sin3 deacetylase and trithorax-related Set1/Ash2 histone H3-K4 methyltransferase are tethered together selectively by the cell-proliferation factor HCF-1. *Genes Dev* 17, 896-911.

Wysocka, J., Swigut, T., Milne, T.A., Dou, Y., Zhang, X., Burlingame, A.L., Roeder, R.G., Brivanlou, A.H., and Allis, C.D. (2005). WDR5 associates with histone H3 methylated at K4 and is essential for H3 K4 methylation and vertebrate development. *Cell* 121, 859-872.

Yokoyama, A., Wang, Z., Wysocka, J., Sanyal, M., Aufiero, D.J., Kitabayashi, I., Herr, W., and Cleary, M.L. (2004). Leukemia proto-oncoprotein MLL forms a SET1-like histone methyltransferase complex with menin to regulate Hox gene expression. *Mol Cell Biol* 24, 5639-5649.

Yoo, A.S., Staahl, B.T., Chen, L., and Crabtree, G.R. (2009). MicroRNA-mediated switching of chromatin-remodelling complexes in neural development. *Nature* 460, 642-646.

Zheng, J.N., Ma, T.X., Cao, J.Y., Sun, X.Q., Chen, J.C., Li, W., Wen, R.M., Sun, Y.F., and Pei, D.S. (2006). Knockdown of Ki-67 by small interfering RNA leads to inhibition of proliferation and induction of apoptosis in human renal carcinoma cells. *Life Sci* 78, 724-729.

Chapter 3
Clinical Information and Experimental Procedures

CLINICAL INFORMATION

The overall pedigree is one of a family of Israeli Arab ancestry with multiple loops of consanguinity, consisting of two main nuclear branches.

Nuclear family A: This family includes parents who are first cousins of Israeli Arab ancestry and multiple affected children. They first came to attention with the birth of male twin infants, Patients 7 & 8. Prenatal ultrasound examination at 28 weeks gestation revealed microcephaly in both feti and the twins were delivered by cesarean section at 35 weeks for intra uterine growth restriction.

At birth both children were noted to have severe microcephaly, dysmorphic facial features including prominent nasal bridge, arthrogryposis, choanal atresia and bilateral cataracts. Postnatal renal ultrasound was normal. Birth weight for patient 7 was 1395 grams and he was hospitalized at 8 weeks old with hypothermia. Sepsis work up was negative but he died at 3 months old. The second twin's birth weight was 1700 grams and he was hospitalized at 2 months old with pneumonia and hypothermia. By age 3 months his head circumference was 27.5 cm (-9.0 Standard Deviations) and length was 51 cm (-4.3 Standard Deviations). Physical exam revealed the slow sloping forehead, micrognathia, prominent helices, bilateral simian creases, flexion contractures of both hands with overriding fingers, dorsiflexion of both feet with overriding toes and increased tone and spasticity. MRI of the brain revealed obvious microcephaly with a cortex with normal thickness, very few sulci and no observable basal ganglia, absence of the corpus callosum, enlarged ventricles, lack of olfactory

sulci, markedly reduced white matter volume, delayed myelination and hypoplastic cerebellar hemispheres, vermis and brainstem. This family also had another son and two daughters with similar features. All died by age 18 months old with the exception of a female, who was still living at age 5 years old with severe psychomotor retardation and dysmorphisms.

Nuclear family B: This family is related to the previous family (A) as the father of Family A is siblings with the mother of Family B. Also, the mother of Family A is first cousin once removed to the father of Family B. The parents in this nuclear family B are related as first cousins once removed. This nuclear family includes two affected males with similar clinical features to the previously described children and there are also two unaffected siblings, a male and a female. The first affected male died at 2.5 months old. The second affected male, patient 5, had negative genetic workup including a karyotype and FISH for 17p13.3 (Miller-Dieker syndrome). Post-mortem Histology: Lissencephalic cortex with reduced white matter and abnormal lamination lacking the normal six layers. Grey-white matter boundary is preserved but signs of cell degeneration, abnormal cell orientation, and gliosis. Cerebellum showed severely reduced molecular layer external granule layer, molecular layer, and internal granule layer. Bergmann glia was present in the purkinje cell layer, and there were few purkinje cells, with abnormal polarity, and cell-sparse internal granule layer.

Patient Studies

Peripheral blood samples were collected from patients and unaffected family members and mapping was performed using single nucleotide polymorphism (SNP) arrays and microsatellite markers to narrow down the boundaries of shared homozygosity. All coding exons were sequenced in the area of homozygosity on chromosome 20q13.2 to reveal the only homozygous coding mutation in the gene *ZNF335*. All human studies were reviewed and approved by the institutional review board of the Children's Hospital, Boston, the Beth Israel Deaconess Medical Center and local institutions.

Genome-wide linkage scans: We collected peripheral blood samples from the affected children and their parents and grandparents after obtaining written informed consent according to the protocols approved by the participating institutions. All human studies were reviewed and approved by the institutional review board of the Children's Hospital, Boston, the Beth Israel Deaconess Medical Center and the local institutions. A total of 22 individuals (indicated with an asterisk in Figure 1A) were genotyped via Affymetrix 10K Xba121, Affymetrix 250K Nsp, Affymetrix 250 Sty, and Affymetrix 5.0. One block of homozygosity on chromosome 20q13.12 emerged as being shared by all affected individuals (shaded in in Figure 1A). To refine the region of homozygosity, samples underwent a microsatellite genome-wide linkage screen using ~400 markers in the ABI linkage mapping set MD v2.5 at ~10cM average density (Applied Biosystems). Fine mapping was done using polymorphic microsatellite markers from the ABI linkage mapping set HD v2.5 at a 5cM average density (Applied

Biosystems) and additional microsatellite markers identified using the UCSC Human Genome Browser. The candidate interval was defined by markers D20S838-6 and D20S197-12 giving an interval of a 2MB locus. Singlepoint and multipoint LOD scores were calculated using Allegro, assuming a recessive mode of disease inheritance, full penetrance and a disease allele frequency of 0.0001. The LOD score is 4.538 ($P < 0.0001$).

DNA sequence analysis: Sequence analysis of the coding exons of the 40 protein-coding RefSeq genes in the linked interval (Fig 2A) revealed a candidate mutation in *ZNF335* (*Zinc Finger Protein 335* also known as *NIF1*, *NRC Interacting Factor 1*. Location 20q13.12, MIM 610825, NM 022095). The change was a c.3332g>a. All affected children were homozygous for this change and the parents, who were obligate carriers, were all heterozygous.

Sequencing of ZNF335 in controls: Coding *ZNF335* exons and at least 50 basepairs of flanking sequence were PCR amplified and submitted for Sanger capillary electrophoresis (Polymorphic DNA Technologies) in accordance with standard methods. Samples included 100 neurologically normal patients. We also reviewed whole exome sequencing for 200 unaffected Arabic control patients and 2500 European control patients.

EXPERIMENTAL PROCEDURES

Animals

Timed pregnant CD1, and Swiss Webster dams (Charles River Laboratories and Taconic). Genetrap 1 and 2 (AY0030 and XG241) (The Genetrap Consortium). Ex-Utero and In-Utero electroporations were performed on timed pregnant E9.5-E14.5 embryos. All animal experimentation was carried out under protocols approved by the IACUCs of Harvard Medical School and Children's Hospital Boston.

Culture Systems

Primary cortical neurons were isolated from E14.5 mouse cells and dissociated by the Papain Dissociation System (Worthington Biochem. Corp). Cells were grown on Poly-L-Ornithine coated plates (Sigma) in Neurobasal (Gibco) with 0.6% glucose, B27 (Gibco), N2 (Gibco), 1mM Penicillin, Streptomycin, L-glutamine, and transfected 1hr post plating. Primary granule neurons were isolated from P5 mouse pups and grown on Poly-L-Ornithine coated cover slips in Basal Medium, Eagle (Gibco), with 10% Calf Serum (Hyclone), 1mM penicillin, streptomycin, L-glutamine; 25mM KCl. Neurons were transfected 2 days post plating with calcium phosphate. All experiments were analyzed in a double blind manner using an unpaired T-test.

Immunostaining

Paraffin sections (5µM) of brains were dehydrated and subjected to antigen retrieval with Antigen Unmasking Solution (Vector), followed by blocking (PBS/5% serum), permeabilization (0.04% Tween20), and antibody incubation. Alternatively, cryosections (8µm-16µm) and vibratome sections (50µm-200µm) were permeabilized (0.04% Tween20, 0.1% Triton X100), blocked, and incubated with antibodies (24h-48h). For the migration assays, slices were immunostained with rabbit anti-GFP antibody (Invitrogen) and mouse anti-Calbindin antibody (Swant). All samples were counterstained with Hoechst 33258 (Sigma). All images were taken with Zeiss 510. For morphology analysis and images of thick sections (>16µm), Z-stack images were obtained using Zeiss 510. Sections were morphologically matched before comparing experimental to control conditions. Data analysis was performed through a double-blind method using ImageJ Software.

Antibodies:

Znf335/Nif1 (797, 798A, IHC specific, 2000, Bethyl); BrdU (250, AbD Serotec); Ki67 (250, Abnova); Vimentin 4A4 (500, Assay Designs); GLAST (250, Chemicon); NeuN (4000, Millipore); FLAG (500, Sigma); GFP (500, Abcam); ASH2 (500, Bethyl Laboratories); MLL/HRX (1000, Millipore); RbBP5 (500, Bethyl Laboratories); SETD1A (200, Novus Biologicals); CGBP (200 Gene Tex); MATR3 (Aviva Systems Biology); WDR5 (200 Milipore); FoxP1 (500 Abcam); Cux1/CDP (500 Santa Cruz).

X-gal Staining

Embryos and adult animals were perfused with 4% PFA and brains were sectioned (50um) then stained with 1g/L X-Gal (Invitrogen).

FACS Sort

Tissues and cells were dissociated using either the Papain Dissociation System (Worthington Biochem Corp) or Neurocult (Stem Cell). Dissociated cells were sorted for GFP using FACSVantage under lowest sustainable pressure. Cells were only used if re-sort verification of >95% pure GFP-positive population was obtained.

Microarray

RNA was isolated with RNeasy Mini Kit (Qiagen), and processed with the Microarray Core Facility (DFCI) using Mouse 430.2 microarray chips. Gene expression was analyzed using DChip Software. All of the raw microarray data were deposited to NCBI's Gene Expression Omnibus (<http://www.ncbi.nlm.nih.gov/geo/>) under deposition number GSE36386.

Neurospheres

E19.5 and E12.5 mouse cortex was dissected in sterile HBSS and dissociated by the papain Dissociation System (Worthington Biochem Corp). Suspension cultures were transfected with either Lipofectamine 2000 (Invitrogen) or Calcium

Phosphate (Clontech). 24hrs post, cells were dissociated using Neurocult (Stemcell) and FACS sort was used to isolate and plate only GFP-positive (transfected) cells and cells were plated at 56K/cm².

In Utero Electroporations

Plasmid DNA suspended at 1ug/ul in ddH₂O was stained with DNA Loading Dye (Invitrogen) and microinjected into the lateral ventricle of developing embryos by eye or using ultrasound guidance (Olson et al., 2006). Moms were allowed to recover and embryos were harvested at different stages. All animal surgical experiment was carried out under protocols approved by the IACUCs of Harvard Medical School, and Children's Hospital Boston. For cell cycle analysis 70 ug BrdU/g body weight was administered via an intraperitoneal injection at 32 hours post electroporation and animals were examined at 48 hours post electroporation. Analysis were done on serial 5-16um paraffin sections and only analyzed between sections in matching brain regions and well as matching medial to lateral orientation of cells between knockdown and control. Rescues were performed by co-electroporating the expression constructs at the same time at the knockdown and control constructs while keeping the amount of shRNA-ZNF335 and UT-Control constructs equal to non-rescue experiments.

Cerebellar Slices

For ex vivo cerebellar electroporations, P8 cerebella were dissected, soaked in endotoxin free plasmid DNA suspended at 2 µg/µl in complete Hanks Balance

Salt Solution (HBSS), transferred to a CUY520-P5 Platinum Block Petridish Electrode (Protech International) and electroporated with an ECM 830 square wave electroporator (BTX Genetronics) at 80 V, 5 pulses, 50 ms pulse, and 500 ms interval. Electroporated cerebella were embedded in 3% low melting point agarose in HBSS, and 250 μ m coronal or sagittal cerebellar slices were prepared using a VT1000S Vibratome (Leica Microsystems). Slices were transferred to Millicell tissue culture inserts (Millipore) and cultured in Basal Medium Eagle supplemented with 2 mM L- glutamine, 0.5% glucose, 1x ITS (Sigma), and 50 U/ml Penicillin-Streptomycin, at the air-medium interface. In experiments where proliferation was assayed, 25 μ M EdU was added to the culture medium at 24 hours in culture. Slices were fixed after 48 hours and 72 hours in culture using ice-cold 4% paraformaldehyde/4% sucrose/1x PBS for two hours.

Northern Blot

Mouse probes were generated from mouse *Zfp335* cDNA (Clone ID 6848450, Open Biosystems) to contain a 960-bp sequence corresponding to nucleotide position 2,227–3,231 of the cDNA or a 560-bp sequence corresponding to nucleotide position 3,922-4,475 of the cDNA. Human probes were generated from human *ZNF335* cDNA (Clone ID 5285131, Open Biosystems) to contain a 446-bp sequence corresponding to nucleotide position 2,073-2,519 of the cDNA or a 584-bp sequence corresponding to nucleotide position 2,587-3,171 of the cDNA. Probes were generated using pCRII (Invitrogen), Northern blots were done with RNA extracted from human patient lymphocytes or using Mouse

Embryo MTN Blot (Clontech), Human 12-Lane MTN Blot (Clontech), and Human Fetal MTN Blot II (Clontech).

Western Blot

Bands were either detected with Pico-ECL or Femto-ECL detection kits (Invitrogen), or with the Odyssey Infrared Imaging System (Li-Cor Biosciences). Quantitation was achieved with Odyssey Infrared Imaging System (Li-Cor Biosciences).

CO-IP/Mass Spectrometry

HeLaS3 Co-IP: Protein complex of NIF1 was isolated and purified as described previously (Ogawa et al., 2002). Briefly, nuclear extract was prepared from 10L of HeLa S3 cells stably expressing Flag-NIF1 fusion protein. NIF1 complex was purified using anti-Flag M2 mAb-conjugated agarose beads (Sigma) in a buffer containing 20 mM Tris-HCl, pH 7.9, 100mM KCl, 5 mM MgCl₂, 10% glycerol, 1 mM phenylmethylsulphonyl fluoride (PMSF), 0.1% Nonidet P40, and 10 mM 2-mercaptoethanol.

Mouse E14.5 Co-IP: Nuclear lysates of mouse E14.5 brains from 20 litters were pooled for analysis following the published methods (Chen et al., 2009). IP material was separated by 4–12% gradient SDS–polyacrylamide-gel electrophoresis (SDS–PAGE) and stained with Coomassie blue. Protein bands were excised and analyzed by mass spectrometry at the Harvard Medical School Taplin Biological Mass Spectrometry Facility.

RNA-Sequencing Analysis

EBV-transformed lymphoblastoid cell lines from Het Parents (LIS-4411), Homozygous Patients (LIS-4421), and 7 unrelated individuals were cultured in RPMI-1640 media supplemented with 10% FBS and penicillin-streptomycin. Approximately 80 million cells from each cell line were fractionated with Cell Fractionation Buffer (PARIS kit, Ambion) to separate cytoplasmic and nuclear lysates. RNA was purified from the lysates with the mirVana PARIS kit (Ambion). RNA was DNase treated (Qiagen) and cleaned-up (RNeasy, Qiagen). Cytoplasmic and nuclear RNA yields and integrity were confirmed on a NanoDrop spectrophotometer (Thermo Scientific) and RNA 6000 Bioanalyzer (Agilent). Separation of cytoplasmic from nuclear RNA was confirmed by electrophoresis (unspliced rRNA visible only in nuclear fraction, data not shown), and by qPCR for U1 snRNA enrichment in the nuclear fraction (data not shown).

PolyA-tailed mRNA from cytoplasmic RNA fractions was purified with two rounds of polyA-selection: a first purification with Poly(A)Purist MAG (Life technologies), and a second purification with the Oligotex mRNA kit (Qiagen). Absence of rRNA following polyA(pA)-selection was confirmed by RNA 6000 Bioanalyzer. About 200-400ng of pA-cytoplasmic RNA was fragmented using RNaseIII as specified in the SOLiD Whole Transcriptome Analysis Kit (Applied Biosystems). Initial sequencing of Het Parent (LIS-4411), Homozygous Patient (LIS-4421) and 3 unrelated controls revealed a strong bias in the protocol's enzymatic

fragmentation, leading to reduced library diversity. In a subsequent experiment we employed an alternative more random RNA heat-fragmentation method. pA-cytoplasmic RNA from homozygous patient (LIS-4421) and 7 unrelated controls was heat fragmented by incubation with 1ul RNase III reaction buffer (SOLiD, Applied Biosystems) in a 10ul volume for 10 mins. at 95°C to obtain a more random fragmentation. Heat-fragmented RNA was end-repaired with 1ul T4 PNK (10U/ul) and 1ul ATP (10mM) in a 12ul volume, incubated for 30 mins. at 37°C. The RNA was cleaned-up with the RiboMinus Concentration Module (Invitrogen).

Fragmentation by both methods was confirmed with the RNA 6000 Bioanalyzer chip. Barcoded sequencing libraries preserving strand-information were prepared with the SOLiD Whole Transcriptome Analysis Kit (Applied Biosystems). RNaseIII-fragmented and heat-fragmented libraries were sequenced to an average depth of 56 million and 70 million reads per sample, respectively, on the SOLiD version 3 Plus sequencing system.

Sequencing reads were spectrally corrected using the SOLiD Accuracy Enhancer Tool (Applied Biosystems) and mapped with standard settings using Bioscope software v1.3 (Applied Biosystems) to the human genome reference (hg19) and splice-junctions obtained from the UCSC Genes annotation track (Kent et al., 2002). All differential gene and intron expression analyses were performed with sequencing data from the heat-fragmented libraries. The number of uniquely mapped reads per gene and per-intron were counted using htseq-count (Anders,

2007) and the RefSeq gene and intron annotations. Differential gene and intron expression analysis were performed with DESeq (Anders and Huber, 2010).

Consensus Sequence Motif Analysis

Consensus sequencing binding motif was achieved using the Meme and Dreme softwares (meme.ncbr.net) and our ChIP-Seq data sets. Promoter sequences with Znf335-binding peaks were utilized to generate the binding motif, and analyzed over controls using promoter sequences of genes that did not exhibit Znf335-binding.

ChIP-Sequencing Analysis

Embryonic cerebellum tissue was isolated from mouse embryos at E14.5. Cross-linking, chromatin isolation, sonication and immunoprecipitation using two distinct rabbit polyclonal antibody raised against Znf335/Nif1 were performed as previously described (Barrera et al., 2008; Renthall et al., 2009; Tsankova et al., 2004). Sequencing libraries were generated from 1-10 ng of ChIP DNA by adaptor ligation, gel-purification and 18 cycles of PCR, according to standard Illumina protocols (<http://www.illumina.com/support/documentation.ilmn>). Gel-purified amplified ChIP DNA and control DNA between 175 and 400 bp were sequenced on the Illumina Genome Analyzer II platform according to the manufacturer's specifications by ELIM Biopharmaceuticals (<http://www.elimbio.com/>) to generate 36-bp reads.

ChIP-seq Data Analysis: Sequence reads were aligned to the mouse reference genome (mm9) using Bowtie (Langmead et al., 2009). Only reads which mapped uniquely to the genome were retained. Table 1 CHIP shows a summary of the alignment and mapping statistics. The peak calling program MACS (Zhang et al., 2008) was used to identify peaks with the mapped reads. Table 2 MACS shows the parameters used when running MACS (mainly default parameters). Enriched intervals were identified by comparison of the mean fragment count in 1-kb windows against a sample-specific expected distribution obtained by sequencing the control DNA. Enriched intervals, or peaks, were normalized based on the total number of reads per ChIP-seq library (reads per million) and mapped to their corresponding genomic position using custom Python scripts.

All of the raw ChIP-seq data were deposited to NCBI's Gene Expression Omnibus (<http://www.ncbi.nlm.nih.gov/geo/>) with the deposition number GSE36386 for genome-wide maps of *Znf335* localization in embryonic cerebellum tissue at E14.5.

Table 1 CHIP. Summary of ChIP-seq and mapping results:

Tissue	Total Reads	Alignable to Mouse	Unique unambiguously aligned	Peaks Genome-Wide (p-value<0.05)
E14.5 cerebellum 797 IP	19,990,327	12,686,545 (63.46%)	9,269,198 (46.37%)	329
E14.5 cerebellum 798a IP	23,444,810	13,833,985 (59.01%)	9,938,918 (42.39%)	307
Input DNA	20,809,489	20,169,768 (96.93%)	15,099,608 (72.56%)	N/A

This table shows a summary of the alignment statistics obtained from Bowtie (ref). Default parameters were used except when generating alignment files for unique, unambiguously aligned reads, in this case the mismatch variable (-m) was set to 1.

Table 2 MACS. MACS program parameters:

Name	Value	Description
mfold	12	threshold for high quality peaks when determining <i>d</i>
gsize	1.87E9	effective genome size
tsize	36	tag length
bw	250	bandwidth (length of sheared fragments)
p-value	0.05	p-value to determine significant peaks

This table shows the parameters that were used when running MACS. Default parameters were used for all other values.

Ontological, pathway and network analysis: Ontological analysis used Gene Ontology (GO) categories to determine processes or functional categories that were represented in both ChIP data sets or commonly expressed in the short and long-term microarray data sets, as described previously (Ashburner et al., 2000) using the GeneGo functional annotation module of Metacore (http://www.genego.com/genego_lp.php). This analysis determined the number of genes in a category present in the i) ChIP-seq, ii) microarray or iii) RNA-seq data and the number of chromatin-binding or expression changes that would be part of that category by random chance given the number of commonly expressed genes. Statistical significance of each process or category was established by p-value (p-value<0.01). Only the processes or categories which passed this threshold were grouped by common function and are represented for each genome-wide data set (Fig. 6D).

ChIP-qPCR

Analysis were done on human lymphoblast cell lines harvested on the exponential growth stage. ChIP-qPCR was performed following published methods (Kim et al., 2010), 3ug of antibodies were used for each ChIP. Antibodies used were: H3K4me3 (Millipore), H3K27me3 (Millipore), WDR5 (Abcam), MLL (Millipore).

ChIP-qPCR Promoter Primer Sequences

AIMP1,

Forward: TTAGTGCACCAGACGCTGCATTC,

Reverse: TATGTCCTTTCGTGGCCAGTTTGG.

Rbbp5,

Forward: TTCTACCTCACCTACATGTTCCCG,

Reverse: CTCCGAAGACTTTCGGCCTTAGAA.

Caprin1,

Forward: AACGATTTGCCTGAAGGACCCTA

Reverse: ACTTAGCCAGCCAGCAGC.

Pes1,

Forward: CCTGGACTTGTACAGGCATCTCAT

Reverse: TTCTTCTTCTCAAGGCCTCCCATC.

Pdap1,

Forward: AACACATACCGGAAGCTCCT,

Reverse: AGCGGCTCTGGAATTCTATACAGG.

Hspa9,

Forward: CGCAATTTATCCCGTGTGACCTTG,

Reverse: AGCATGATGGTTGGAGAAAGCCTG

Taf9,

Forward: TCATCGAAAGCCAGGTAACCAGTG,

Reverse: AGGATGTTTCGGAAGCAACATGGTC.

Suds3,

Forward: AACTGCTAGGCAGACGG,

Reverse: TCTCCAGCTCTTCATCCTCCT.

Dand5,

Forward: GGAACCCAGCTGGTCTGAATTTAC,

Reverse: AAGCAGGCACAGAAGAGTGGATAG.

REST/NRSF,

Forward: TGCTGTGATTACCTGGTCGGTGAA,

Reverse: TCTTCGAGCTCTTGCCTTTGTCCT.

Gene Expression Validation

hREST

F&R: Mm0083268_m1 (Taqman);

GAPDH-F: 5'CCAAGGTCATCCATGACAAC;

GAPDH-R: 5'GGCCATCCACAGTCTTCTG;

ZNF335-F: 5'GTCTGTCACACAGGCTCAAC;

ZNF335-R: 5'GCACTGGTCTCGTCTGTACCAA;

ZNF-Exon19F: GCTGAGATGGAGAGTCACAAG

ZNF-Exon20R; CTGCACTGGCTACACTGG;

ZNF-Exon21R; TGGATGTGGAAGTTGAGGTG

shRNA constructs

shRNA-ZNF335:

CAGCAGCTTCCTCAACAAAGTTCAAGAGACTTTCTTGAGGAAGCTGCTC

UT-CONTROL:

CTGCTGCATCGTCTACTAAGTTCAAGAGACTTAGTAGACGATGCAGCAG

Znf335 CKO mouse generation

Design: In mouse, the *ZNF335* gene is called *Zfp335* for Zinc finger Protein **335**. A Loxp (L83) site and a FNFL (Frt-Neo-Frt-Loxp) cassette were engineered to flank promoter and exon1/2 (2kb) of the *Zfp335* allele to generate “L83/FNFL” *Zfp335* allele on a **Bacterial Artificial Chromosome (BAC)**. A gene targeting vector was constructed by retrieving the 2kb short homology arm (5' to L83), the floxed sequence containing promoter and exon1/2, the FNFL cassette, and the 5kb long homology arm (end of FNFL to 3') into a plasmid vector carrying a DTA (Diphtheria Toxin Alpha chain) negative selection marker. The FNFL cassette conferred G418 resistance during gene targeting in PTL1 (129B6 hybrid) ES cells and the DTA cassette provided an autonomous negative selection to reduce the random integration event. Several targeted ES cells were identified. These targeted ES cells were injected into C57BL/6 blastocysts to generate chimeric mice. Male chimeras should be bred to homozygous ACTB(FIpe/FIpe) females (in C57BL/6 background, Jackson labs) to transmit the floxed ZFP335 allele (**L83/FL146 allele** with neo cassette removed by Fpe recombinase) Mice carrying floxed ZFP335 allele were crossed to Emx1-Cre mice (in C57BL/6 mice, Jackson labs) to generate ZFP335 conditional knockout study. The mice are maintained on a mixed C57/Bl6 and 129B6 background.

For histological analysis, brains were perfused with PBS and then followed by 4% PFA before paraffin embedding and sectioning.

SUPPLEMENTAL REFERENCES

Adams, N.C., Tomoda, T., Cooper, M., Dietz, G., and Hatten, M.E. (2002). Mice that lack astrotactin have slowed neuronal migration. *Development* *129*, 965-972.

Anders, S. (2007). HTSeq: Analysing high-throughput sequencing data with Python (Free Software Foundation, Inc.).

Anders, S., and Huber, W. (2010). Differential expression analysis for sequence count data. *Genome Biol* *11*, R106.

Ashburner, M., Ball, C.A., Blake, J.A., Botstein, D., Butler, H., Cherry, J.M., Davis, A.P., Dolinski, K., Dwight, S.S., Eppig, J.T., *et al.* (2000). Gene ontology: tool for the unification of biology. The Gene Ontology Consortium. *Nat Genet* *25*, 25-29.

Barrera, L.O., Li, Z., Smith, A.D., Arden, K.C., Cavenee, W.K., Zhang, M.Q., Green, R.D., and Ren, B. (2008). Genome-wide mapping and analysis of active promoters in mouse embryonic stem cells and adult organs. *Genome Res* *18*, 46-59.

Chen, C., Jin, J., James, D.A., Adams-Cioaba, M.A., Park, J.G., Guo, Y., Tenaglia, E., Xu, C., Gish, G., Min, J., *et al.* (2009). Mouse Piwi interactome identifies binding mechanism of Tdrkh Tudor domain to arginine methylated Miwi. *Proc Natl Acad Sci U S A* *106*, 20336-20341.

Kent, W.J., Sugnet, C.W., Furey, T.S., Roskin, K.M., Pringle, T.H., Zahler, A.M., and Haussler, D. (2002). The human genome browser at UCSC. *Genome Res* *12*, 996-1006.

Kim, T.K., Hemberg, M., Gray, J.M., Costa, A.M., Bear, D.M., Wu, J., Harmin, D.A., Laptewicz, M., Barbara-Haley, K., Kuersten, S., *et al.* (2010). Widespread transcription at neuronal activity-regulated enhancers. *Nature* *465*, 182-187.

Langmead, B., Trapnell, C., Pop, M., and Salzberg, S.L. (2009). Ultrafast and memory-efficient alignment of short DNA sequences to the human genome. *Genome Biol* *10*, R25.

Morrison, M.E., and Mason, C.A. (1998). Granule neuron regulation of Purkinje cell development: striking a balance between neurotrophin and glutamate signaling. *J Neurosci* *18*, 3563-3573.

Nagata, I., Ono, K., Kawana, A., and Kimura-Kuroda, J. (2006). Aligned neurite bundles of granule cells regulate orientation of Purkinje cell dendrites by

perpendicular contact guidance in two-dimensional and three-dimensional mouse cerebellar cultures. *J Comp Neurol* 499, 274-289.

Ogawa, H., Ishiguro, K., Gaubatz, S., Livingston, D.M., and Nakatani, Y. (2002). A complex with chromatin modifiers that occupies E2F- and Myc-responsive genes in G0 cells. *Science* 296, 1132-1136.

Olson, E.C., Kim, S., and Walsh, C.A. (2006). Impaired neuronal positioning and dendritogenesis in the neocortex after cell-autonomous Dab1 suppression. *J Neurosci* 26, 1767-1775.

Renthal, W., Kumar, A., Xiao, G., Wilkinson, M., Covington, H.E., 3rd, Maze, I., Sikder, D., Robison, A.J., LaPlant, Q., Dietz, D.M., *et al.* (2009). Genome-wide analysis of chromatin regulation by cocaine reveals a role for sirtuins. *Neuron* 62, 335-348.

Shen, Y., Yue, F., McCleary, D.F., Ye, Z., Edsall, L., Wagner, U., Dixon, J., Lee, L., Lobanenko, V., Ren, B. (2012). A draft map of cis-regulatory sequences in the mouse genome. *Nature*.

Smeyne, R.J., Chu, T., Lewin, A., Bian, F., Sanlioglu, S., Kunsch, C., Lira, S.A., and Oberdick, J. (1995). Local control of granule cell generation by cerebellar Purkinje cells. *Mol Cell Neurosci* 6, 230-251.

Tsankova, N.M., Kumar, A., and Nestler, E.J. (2004). Histone modifications at gene promoter regions in rat hippocampus after acute and chronic electroconvulsive seizures. *J Neurosci* 24, 5603-5610.

Zhang, Y., Liu, T., Meyer, C.A., Eeckhoute, J., Johnson, D.S., Bernstein, B.E., Nusbaum, C., Myers, R.M., Brown, M., Li, W., *et al.* (2008). Model-based analysis of ChIP-Seq (MACS). *Genome Biol* 9, R137.

Chapter 4
Discussion

Summary

This dissertation research has aimed to elucidate an essential gene and its mechanisms of action in regulating brain development. The research paradigm used in this project provides a useful avenue for shedding light on and understanding key regulatory steps of mammalian development. In this chapter, I will consider the implications of these findings and describe future directions.

We use human genetics to identify genes that are essential for brain development. Although a very useful technique for searching for causative genes, it is not possible to find all mutations such as non-coding mutations, or genes of complex traits due to gene-gene and gene-environment interactions, genetic heterogeneity, low penetrance, and limited statistical power. Since this technology is also biased towards finding recessive alleles, it is also possible that we may be missing some of the key master regulators of brain development, where a null mutation would unanimously lead to embryonic lethality. New technologies such as whole exome and whole genome sequencing are now available for a more comprehensive search of disease genes as well as genes of complex traits; however, obstacles in data analyses for such large datasets still remain (Bilguvar et al., 2010; Choi et al., 2009; Lupski et al., 2010; Ng and Kirkness, 2010; Pan et al., 2008).

In this study we identify *ZNF335/NIF1* as a central regulator of mammalian neurogenesis and neuronal differentiation. A splice donor/missense mutation of *ZNF335* results in an extremely small brain in humans, and genetic ablation leads to early embryonic lethality in mice, while *Emx1-Cre* driven knockout leads

to virtual absence of cortical structure. Loss of Znf335 causes premature cell cycle exit of progenitors, precociously depleting the progenitor pool. ZNF335 is a part of a H3K4 methyltransferase complex and associates with the promoters of many key developmental genes to affect H3K4me3 as well as expression levels of target genes. A critical downstream target of ZNF335 is REST/NRSF (master regulator of neurogenesis) representing a pathway critical for this neurogenetic function. Beyond its effects on progenitor cell proliferation, ZNF335 also has essential effects on cell fate and cell morphology (and ultimately survival).

Mutation

The mutation can affect protein function through two ways: 1) either via the production of a mutated protein containing a missense mutation, or 2) via the decrease in overall expression levels of the protein (even if mutated). Despite the profound phenotype of *ZNF335* mutation in humans, the mutation we describe is almost certainly hypomorphic. While overexpression of the wildtype protein can rescue Znf335 deficiency, overexpression of the human mutation can only partially rescue Znf335 deficiency. Also, conditional ablation of Znf335 in mouse cortex results in loss of essentially the entire cortex. Thus, null mutations in ZNF335 in humans are presumably embryonically lethal as in mice, illustrating the utility of unusual, partial loss-of-function mutations in humans to elucidate essential early embryonic functions of such genes.

We still cannot be sure how the mutation directly affects protein function since the mutation is near the C-terminus of the protein but also at the last zinc

finger. The mutation might easily affect the binding of ZNF335 specific DNA targets but also the mutation might affect the protein's interactions with other binding partners that may be needed for regulating DNA expression. In vitro DNA binding experiments such as electrophoretic mobility shift assays or protein binding microarrays between the WT and MUT proteins can help to better verify the sites of DNA binding obtained through the ChIP-seq experiments as well as to study the effects of the mutation on gene target binding (Geertz and Maerkl, 2010). In vitro binding assays and in vivo Co-IPs can study the effects of the mutation on protein-protein interactions.

Complex Interaction

This study provides direct insight into the function of TrxG complex proteins in embryonic neurogenesis. The interaction of Znf335 with proteins of the H3K4 methyltransferase complex suggests roles for Znf335 in the regulation, targeting, or stability of the complex. Epigenetic regulation causes programming of gene expression, and specific histone methylation can further orchestrate gene regulation in a cell type and tissue dependent manner. Mutations in neural specific chromatin regulatory complexes, nBAF, have been shown to affect proliferation and are linked with microcephaly (Hoyer et al., 2012), and Polycomb gene repressing complexes have been studied in the development of the nervous system; however, very little is known about the role of activating complexes, especially the TrxG complex, on brain development, let alone mammalian brain development. This interaction provides a potential role for the

broad effects of the *ZNF335* mutation on human patients, the large number of genes and developmental processes altered by *Znf335* knockdown, as well as the embryonic lethality in *Znf335*-null mice, especially since knockouts of other histone methyltransferases are also lethal embryonically (Glaser et al., 2009).

These studies do not rule out the possibility that ZNF335 may interact with proteins other than members of the TrxG complex. ZNF335 may only interact with the TrxG complex at a specific time point or in a specific population of cells, and ZNF335 may thus regulate gene expression in a dynamic fashion. For development to occur, genes must be both turned on as well as turned off. Genes that are important for progenitor cells must be turned off for proper neuronal differentiation and genes important for neuronal cells must not be turned on until time of differentiation. For this transition, ZNF335 may play an important role in bringing different complexes to a specific subpopulation of genes. ZNF335 could either interact with another activating complex with different activating dynamics, ZNF335 could switch to interact with an inhibitory complex, or ZNF335 itself can also be regulated and decreased over time.

Further analyses of the changing interaction patterns of ZNF335 with other proteins can be accomplished through Co-IP experiments utilizing different populations of cells. Co-IP experiments performed on separated populations of cells (such as progenitors vs. neurons) might help to elucidate cell type specific complex proteins. At the same time, co-IP studies using human control as well as the patient cell lines can elucidate any effects of the mutation on these interactions.

Gene Regulation

Loss of Znf335 alters expression levels of many key genes--including *DLX* *homeobox* genes (early brain development), *Neurogenin*, *Nfib*, *Olig1*, *Math1*, *REST/NRSF*, *Co-REST 2* (neurogenesis)--among many other genes important for dendritic branching, cell adhesion, and signaling. Changes in these genes could explain phenotypes seen in the patients and correlate with abnormal neurogenesis evident in mouse models and account for the virtual absence of cortical neurons in the Znf335 CKO. Genes whose expression changes upon *Znf335* deficiency could be primary targets of Znf335, or secondary targets of other regulatory genes downstream of Znf335 such as REST/NRSF revealing Znf335 as a critical regulator of gene expression essential for proper neuronal development.

In order to better study the effects of mutated ZNF335 on gene regulation, ChIP-seq experiments looking at ZNF335 binding either in stable cell lines (expressing the WT-ZNF335 vs the MUT-ZNF335), or in patient cell lines (control vs. patient cell lines) can help to distinguish any binding differences. At the same time ChIP-seq for H3K4me3 marks in the patient cell lines vs. the control cell lines would prove to be a useful way of assaying global changes in H3K4me3 marks and gene regulation upon *ZNF335* mutation. These global sequencing data sets will prove powerful when cross-referenced with changes in transcript expression using the RNA-seq data sets to identify genes not only directly targeted but also regulated by ZNF335.

Neuronal Function

Znf335 also regulates differentiation and gene transcription in postmitotic neurons. Znf335 deficiency blocks normal expression of 'canonical' neuronal marker genes such as NeuN and Mef2C, which could be either a secondary effect of premature and improper neurogenesis or may hint at a role of Znf335 in regulating cell identity, survival, and activity of mature neurons. ZNF335 regulates a variety of non-REST/NRSF targets that are important for the final stages of neuronal differentiation, such as genes regulating dendritic branching, and ion channels, which may suggest roles of ZNF335 in other neuron specific transcriptional complexes.

The regulation of so many neuronal genes helps to confirm that ZNF335 must play a role in differentiated neurons. ZNF335 expression does return at low levels by postnatal day 20-30 in the adult cerebral cortex where mature neurons reside. This re-expression in differentiated neurons hints at the fact that ZNF335 must play a different role than just activating genes in progenitor cells, and thus it must do so through the interactions with different complexes. The effects of ZNF335 knockdown on neuronal morphology and dendritic branching hint at the fact that ZNF335 is essential for neuronal activity. Electrophysiological studies on the control and knockdown neurons may help to identify the essential roles of ZNF335 in differentiated neurons. Pathological findings also suggest neurodegeneration in the patients, thus ZNF335 might play an important role in regulating neuronal survival.

Regulation of ZNF335

If ZNF335 is so important for proper progenitor cell development, then it must be regulated in some way. First point of regulation is that ZNF335 must be kept on and expressed at adequate amounts in order to ensure progenitor cell proliferation and survival. RNA-seq analysis showed that the heterozygous parents actually produced a higher amount of the transcript seeming as if an autoregulatory mechanism was in play to stimulate the amount of ZNF335 production should it fall below threshold. To understand autoregulation, we must first study the dosage effects of ZNF335 on brain development, as well as to carefully track the effects that decreasing levels of ZNF335 has on *ZNF335* transcript levels using the heterozygous parent cell lines and the heterozygous mouse model system. Autoregulation of ZNF335 may occur through a completely independent mechanism distinct from the TrxG complex. Conversely, there must also be control systems set in place such that overstimulation and thus overexpression of ZNF335 does not occur.

On the other end of the development spectrum, just like the genes that ZNF335 controls, ZNF335 itself must also be turned off in order to prevent constitutive progenitor cell proliferation and the disease state. In fact, we know that ZNF335 expression decreases as the progenitor population decreases throughout the course of embryonic brain development. However, the decrease in ZNF335 expression might be due to transcriptional regulation, alternative splicing, or protein degradation. ZNF335 itself might control genes that later play

a role in inhibiting its own expression.

Conditional Knockout

The generation of the conditional knockout mouse is a useful model system. Not only does the mouse bypass many laborious in vitro experiments, but it also helps to overcome the embryonic lethality of the global knockout. The conditional knockout recapitulates the patient phenotype and helps to reconfirm the essential roles of ZNF335 in brain development. The conditional knockout mouse provides the ability to not only study the dosage effects of ZNF335 in the heterozygous animals, but it also allows for careful analysis of the functions of ZNF335 in different cell systems through the use of different cre-driver lines. The conditional knockout mouse model provides a useful tool for further studies in both biochemistry as well as animal behavior.

Conclusions

Identifying and understanding the function of specific disease genes can help us to gain a better understanding of brain development and ultimately contribute to medical advancements. Genetic causes of microcephaly continue to grow in diversity, and include proteins involved in vesicle trafficking, mitotic spindle organization, and DNA repair (Thornton and Woods, 2009). With each gene, we have gained a better understanding of the specific steps that govern normal brain development, and teased out the independent needs of distinct subpopulations in the brain. Premature neuronal fate specification, with

consequent loss of progenitor cells, could be a frequent cellular mechanism resulting in microcephaly (Lehtinen and Walsh, 2011). *ZNF335* deficiency causes additional feature of neuronal degeneration, making it strikingly different, and more severe, than other microcephaly syndromes, which are typically compatible with postnatal survival and in many cases some intellectual function. Thus our data reveal *ZNF335* as a unique type of microcephaly gene, and provides evidence of a new upstream regulator of the balance between progenitor cell division and differentiation. Studies of the roles of *ZNF335* not only highlighted a new type of gene that regulates brain development, but studies in its function also helped to shed light on large cohorts of genes that act in unison as essential players in normal brain development. A deepening understanding of these complex steps can help to guide future therapeutic interventions as we bridge the fundamental gap between the lab bench and the bedside.

REFERENCES

Bilguvar, K., Ozturk, A.K., Louvi, A., Kwan, K.Y., Choi, M., Tatli, B., Yalnizoglu, D., Tuysuz, B., Caglayan, A.O., and Gokben, S. (2010). Whole-exome sequencing identifies recessive WDR62 mutations in severe brain malformations. *Nature* *467*, 207-210.

Choi, M., Scholl, U.I., Ji, W., Liu, T., Tikhonova, I.R., Zumbo, P., Nayir, A., Bakkalofülu, A., $\sqrt{\text{ñizen}}$, S., and Sanjad, S. (2009). Genetic diagnosis by whole exome capture and massively parallel DNA sequencing. *Proceedings of the National Academy of Sciences* *106*, 19096-19101.

Geertz, M., and Maerkl, S.J. (2010). Experimental strategies for studying transcription factor,ÄiDNA binding specificities. *Briefings in functional genomics* *9*, 362-373.

Glaser, S., Lubitz, S., Loveland, K.L., Ohbo, K., Robb, L., Schwenk, F., Seibler, J., Roellig, D., Kranz, A., Anastassiadis, K., *et al.* (2009). The histone 3 lysine 4 methyltransferase, Mll2, is only required briefly in development and spermatogenesis. *Epigenetics Chromatin* *2*, 5.

Hoyer, J., Ekici, A.B., Endeke, S., Popp, B., Zweier, C., Wiesener, A., Wohlleber, E., Dufke, A., Rossier, E., Petsch, C., *et al.* (2012). Haploinsufficiency of ARID1B, a member of the SWI/SNF-a chromatin-remodeling complex, is a frequent cause of intellectual disability. *Am J Hum Genet* *90*, 565-572.

Lehtinen, M.K., and Walsh, C.A. (2011). Neurogenesis at the brain-cerebrospinal fluid interface. *Annual review of cell and developmental biology* *27*, 653-679.

Lupski, J.R., Reid, J.G., Gonzaga-Jauregui, C., Rio Deiros, D., Chen, D.C.Y., Nazareth, L., Bainbridge, M., Dinh, H., Jing, C., and Wheeler, D.A. (2010). Whole-genome sequencing in a patient with Charcot,ÄiMarie,ÄiTooth neuropathy. *New England Journal of Medicine* *362*, 1181-1191.

Ng, P.C., and Kirkness, E.F. (2010). Whole genome sequencing. *Methods in Molecular Biology* *628*, 215-226.

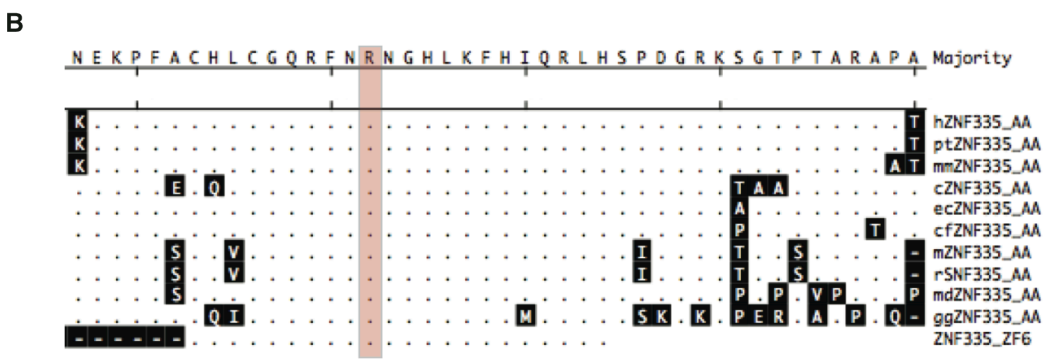
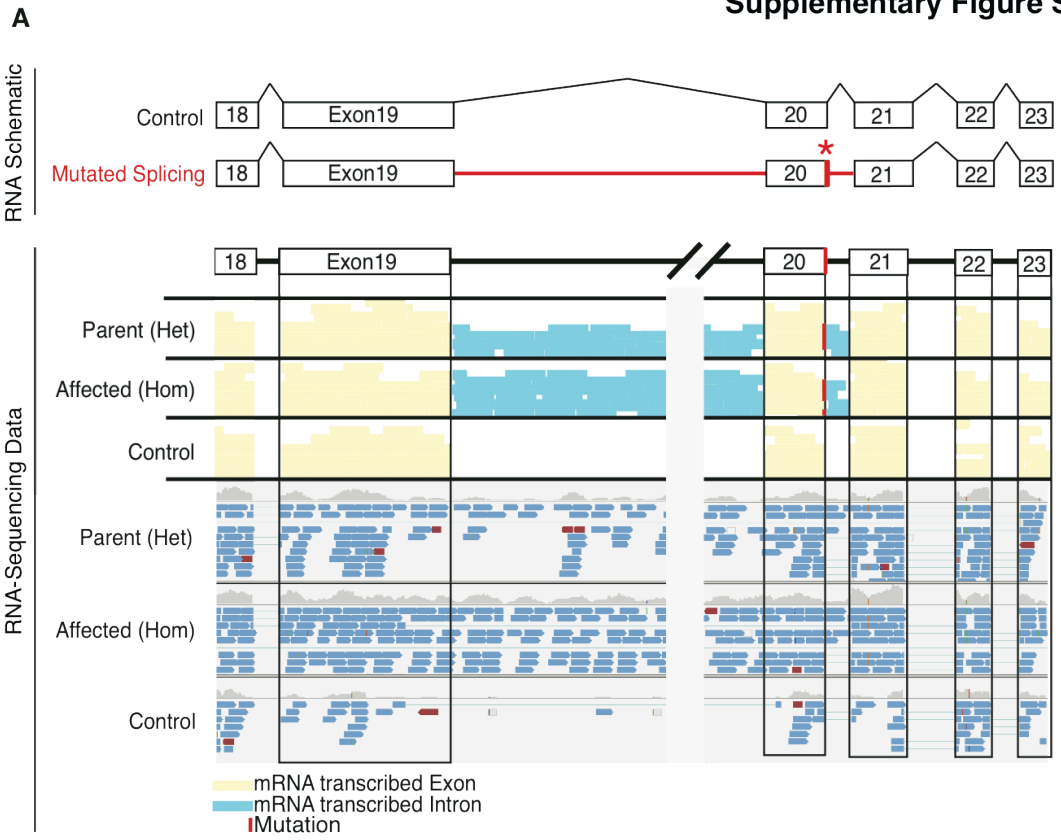
Pan, Q., Shai, O., Lee, L.J., Frey, B.J., and Blencowe, B.J. (2008). Deep surveying of alternative splicing complexity in the human transcriptome by high-throughput sequencing. *Nature genetics* *40*, 1413-1415.

Thornton, G.K., and Woods, C.G. (2009). Primary microcephaly: do all roads lead to Rome? *Trends Genet* *25*, 501-510.

APPENDIX

Global Sequencing Data Analysis and Supplemental Data

Supplementary Figure S1

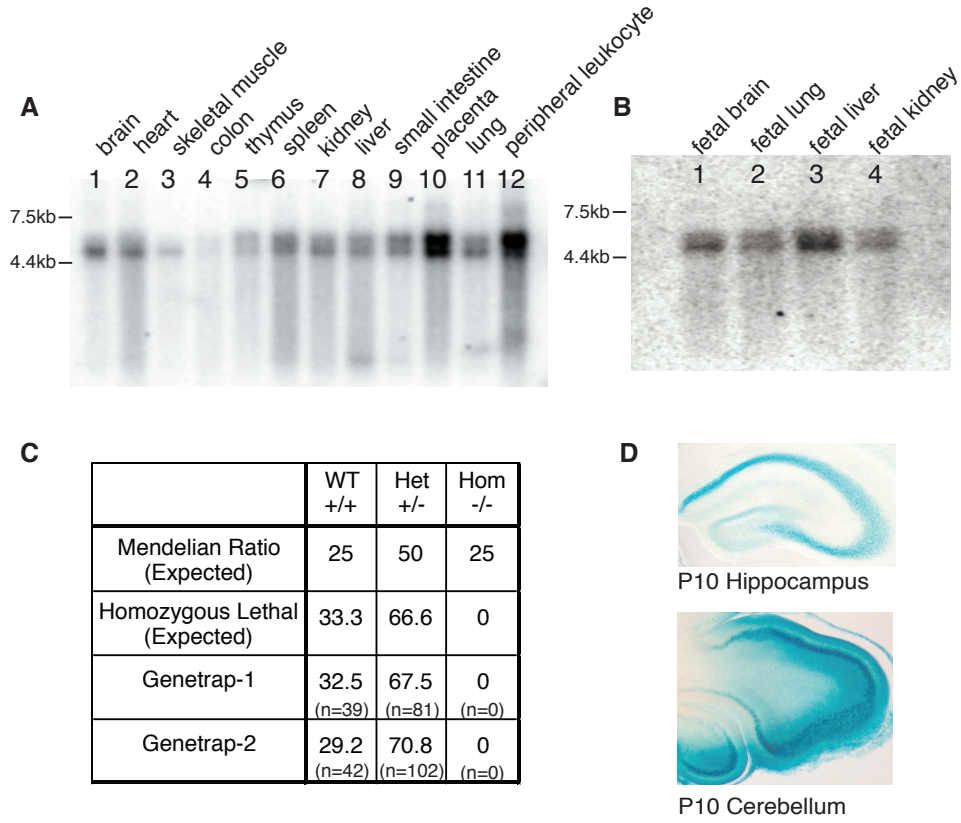


Supplemental Figure S1 (Continued), related to Figures 3-4, *Znf335* RNA-seq data and *Znf335* amino acid conservation.

(A) RNA-seq schematic of the data along with the raw reads picked up by RNA-seq showing the presence of the intron both before and after exon 20 containing the mutation (red). With an unbiased genome-wide search across all 354,244 Refseq-annotated introns for differentially transcribed introns in our patients compared to 7 control cell lines, the retained long intron of *ZNF335* is ranked as the 4th most significant differentially transcribed intron with an adjusted p-value of 1.57×10^{-31} . Many of the other top entries are included in the following chart. Many of the top entries are not really included introns, but rather true differentially expressed genes in patient, but in which there is an intron annotation that overlaps an alternative isoform's exon, thus making it a false positive.

(B) Analysis of the amino acid conservation of the arginine R 1111 in *Znf335* across a variety of different species. Top to bottom: human, chimp, macaque, cow, horse, dog, mouse, rat, opossum, chicken, zebrafish. *ZNF335* is highly divergent in zebrafish and not detectable outside of vertebrates.

Supplementary Figure S2



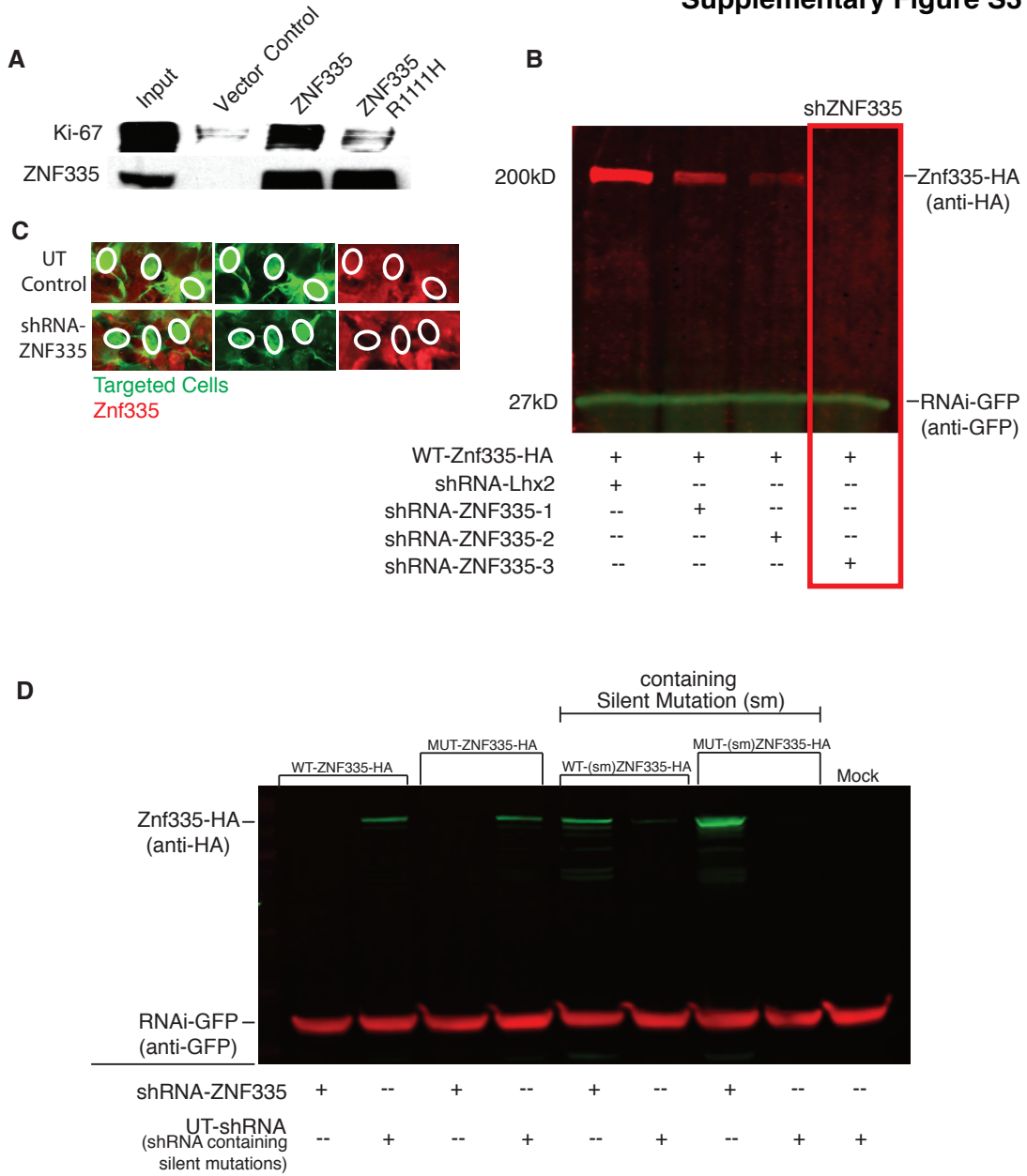
Supplemental Figure S2 (Continued), related to Figure 5, Znf335 is expressed in a variety of tissues and is essential for mouse development.

(A, B) Northern blot analysis of *Znf335* expression in a variety of adult (A) and embryonic (B) organ systems shows that *Znf335* is ubiquitously expressed and might play more roles than just brain development.

(C) Genotype segregation, as confirmed by PCR, of litters from *Znf335*^{Genetrap/+} and *Znf335*^{Genetrap/+} crosses show a complete absence of homozygous *genetrap* mice in both strains as early as E7.5 showing that *Znf335* is essential for mouse development and possibly implantation. n represents number of individual pups analyzed and found to contain that specific genotype.

(D) LacZ staining of developing hippocampus and developing cerebellum from a P10 *Znf335*^{Genetrap/+} shows that *Znf335* is expressed in the developing hippocampus and developing cerebellum.

Supplementary Figure S3



Supplemental Figure S3 (Continued), related to Figures 6-7, Knockdown efficiency of shRNAs targeted against Znf335 and characterization of knockdown-resistant rescue constructs.

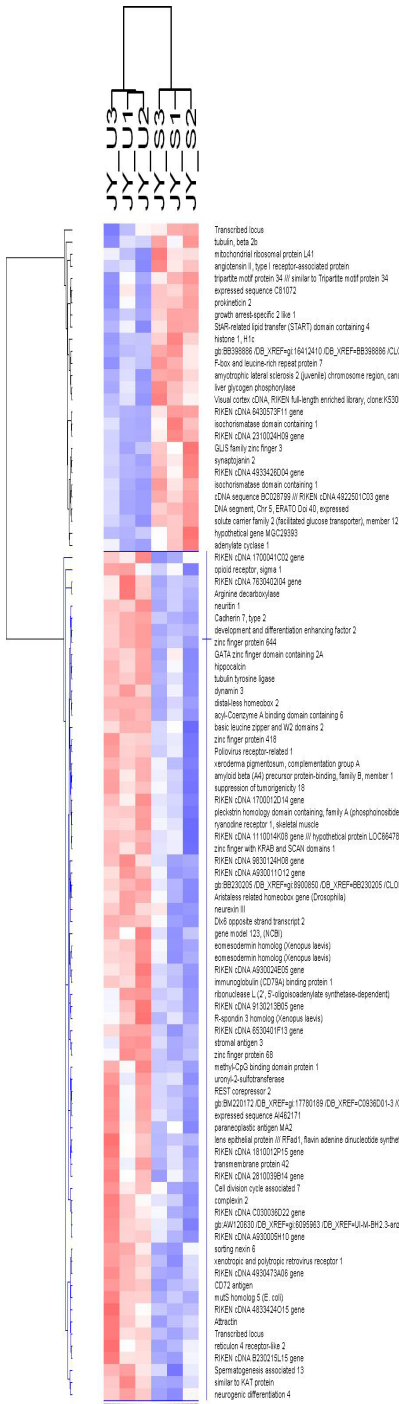
(A) ZNF335 interacts with Ki67, a marker of proliferation. The mutations R1111H leads to a decrease of ZNF335 interaction with Ki67. The antibody is MIB1, which is a mouse monoclonal. It identifies two forms ~350kDa and 395 kDa in Western blotting. Ki-67 is a highly phosphorylated protein and as a result in some cells is detected in Western blotting as a broad band.

(B) Three different knockdown constructs were designed and shRNA that we utilized knockdown up to 95% of protein after 24 hours.

(C) IHC analysis of cells 48 hours electroporation with shRNA-ZNF335 shows the lack of ZNF335 protein expression in comparison to control.

(D) The expression constructs containing the silent mutation (sm) prevent the rescue constructs from being targeted by the shRNA-ZNF335. Co-transfections of shRNA-ZNF335 along with the rescue constructs (sm) allows for knockdown of endogenous ZNF335 and expression of the (sm) rescue construct at the same time.

Supplementary Figure S4



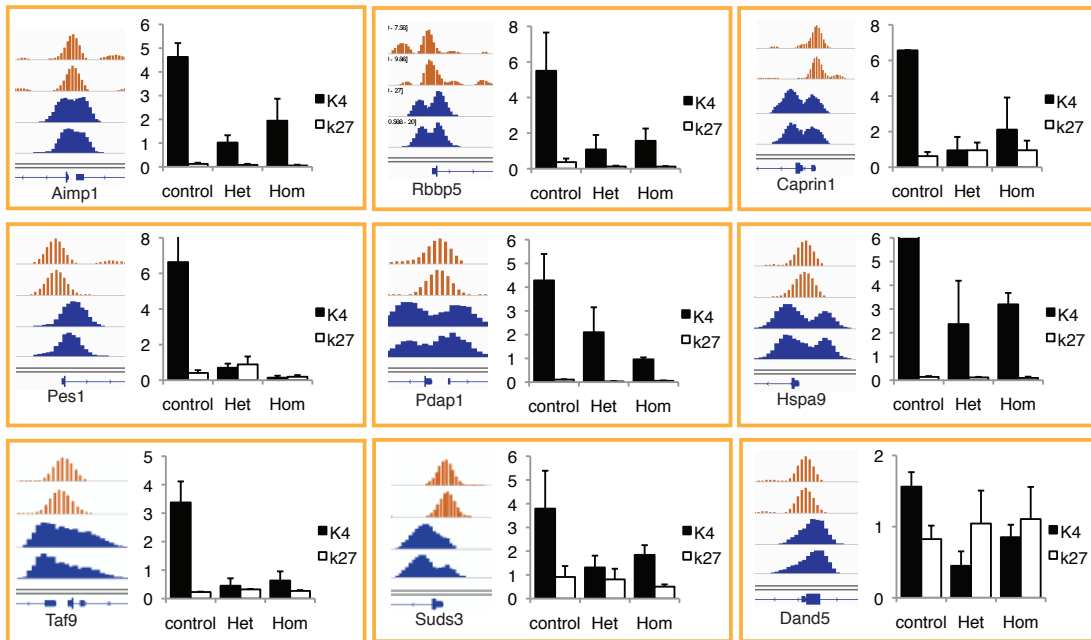
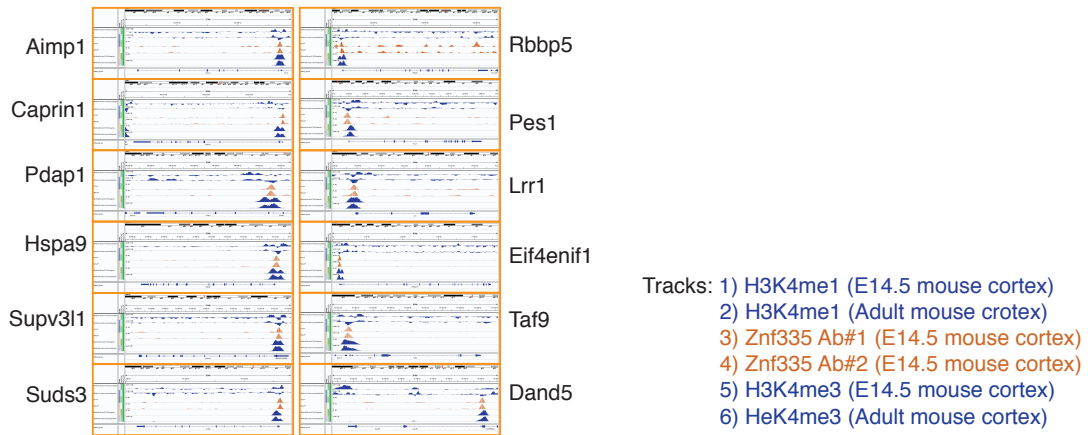
Notable Gene Changes

INCREASE	DECREASE
Brain Development	Brain Development
snail homolog-early TF (neural tube)	distal-less homeobox 2 (DLX2)-forebrain development DLX4-Craniofacial development DLX6
Hormone Signaling	Neuron Development
growth hormone receptor NRF2-thyroid hormone	neurogenin-TF for neurons Nuclear factor I/B-Transcription factor olig transcription factor 1 Math1-granule neurons REST corepressor 2-neuronal differentiation
Microtubule/Actin	Dendrites
Dynein light chain MAP7 synaptotagmin 2-binds actin in dendrites	Neuritin-Neurite arborization/activity Tubulin tyrosin ligase-neurite outgrowth Disabled homolog 1-Regulate Reelin (neurogenesis, dendrites)
Vesicle	Cell Adhesion
Synaptotagmin-vesicle traffic syntaxin binding protein 3A-SNARE Intersectin 2-Clathrin Endocytosis	NCAM1-Cell adhesion Cadherin-Cell adhesion Neurexin III-receptor adhesion
Activity	Gene Regulation
annexin A11-calcium binding protein chloride intracellular channel 5	WDR61-transcription regulation through SKI/PAF (Histone) MeCP1-binds methylated DNA
Signaling	Vesicle
SKI like-inhibit TGFB BMP5-TGFB family	synaptic nuclear envelope Complexin 2-regulate SNARE/VAMP dynamitin-clathrin coated cell membrane DDEF2-golgi plasma in brain
OTHER	Activity
Histone H1C	Hippocalcin-Neuronal calcium sensor Sodium channel, Type IV, beta-voltage gated
	Cell Cycle
	CDC7
	Signaling
	IGFBP1 Secreted frizzled related protein 1-Wnt signaling sorting nexin 6-TGFB family
	OTHER
	Amyloid beta (APP)

Supplemental Figure S4 (Continued), related to Figure 8, Microarray Analysis of changes in gene expression upon long-term knockdown of Znf335.

Cells electroporated with shRNA-ZNF335 vs. UT-Control at E14.5 were allowed to mature until embryos were P0 and the dissociated. GFP-positive (targeted cells) were selected for using FACS analysis and RNA from the two cell populations were utilized for microarray analysis. Knockdown of Znf335 for four days led to changes in expression of genes important for neuronal differentiation and activity. S1-3 (shRNA knockdown cells), U1-U3 (UT control cells) as summarized in the tables next to the heat map of changes in gene expression. Red=increase in expression, Blue=decrease in expression. Genes presented show a greater than 1.5 fold change with a P value of equal or less than 0.05. Microarray data is available online. Please see supplemental materials & methods.

Supplementary Figure S5



Supplemental Figure S5 (Continued), related to Figures 9-11, ChIP-Seq binding of Znf335 and Changes in histone modifications in the absence of Znf335.

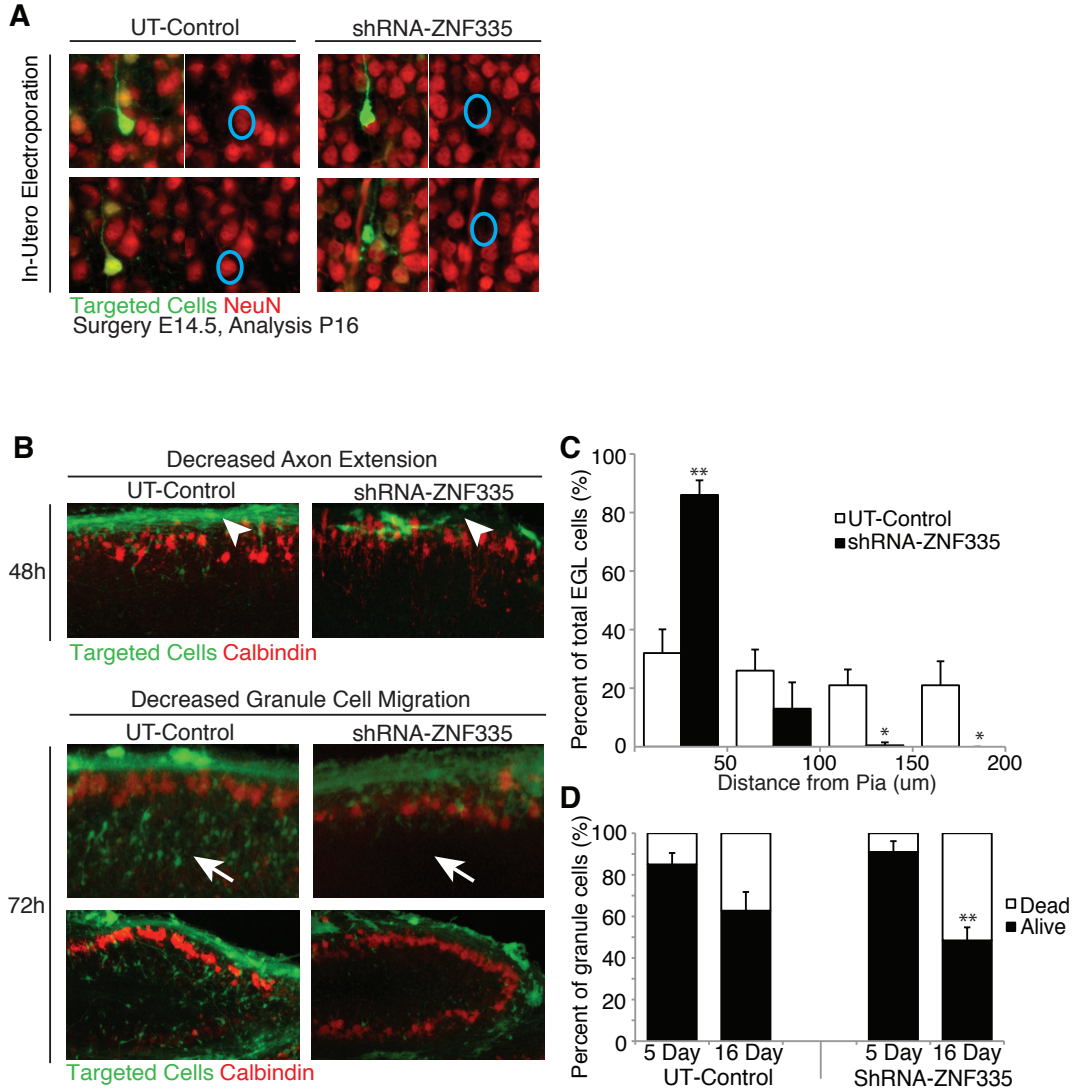
(A) Znf335 bound to promoter regions of a variety of different genes, and this binding overlapped with the H3K4me3 binding sites but not the H3K4me1 binding sites. ChIP-Sequencing peaks show that the Znf335 complex binds to promoter regions of several genes important in brain development such as *Aimp1*, *Caprin1*, *Pdap1*, *Hspa9*, *Supv3l1*, *Suds3*, *Rbbp5*, *Pes1*, *Lrr1*, *Eif4enif1*, *Taf9*, *Dand5*. Top two tracks (blue) show H3K4me1 peaks at these promoters (Shen, 2012), Middle two tracks (orange) per gene is from ChIP-Seq data with two different antisera raised against Znf335. Bottom two tracks (blue) show H3K4me3 peaks at these promoters (Shen, 2012). The Znf335-bound peaks overlap with H3K4me3 peaks of these promoters, but not with the H3K4me1 peaks. See also Table S3.

(B) Close up analysis of the overlap of the peaks for Znf335 binding (orange) and H3K4me3 (blue) peaks at the promoter region of representative genes. ChIP-qPCR Analysis of changes in H3K4me3 levels (black bars) vs. the control H3K27me3 levels (white bars) show that there is a decrease in the levels of H3k4me3 levels in the heterozygous parents and homozygous patients while there is no change in H3K27me3. (AIMP1: K4: Control: 4.63 +/- 0.58, Het Parent: 1.02 +/- 0.3, Hom Patient: 1.94 +/- 0.93; K27: Control: 0.12 +/- 0.05, Het Parent: 0.08 +/- 0.04, Hom Patient: 0.05 +/- 0.03. Rbbp5: K4: Control: 5.5 +/- 2.15, Het Parent: 1.08 +/- 0.81, Hom Patient: 1.57 +/- 0.69; K27: Control: 0.37 +/- 0.2, Het

Supplemental Figure S5 (Continued), related to Figures 9-11, ChIP-Seq binding of Znf335 and Changes in histone modifications in the absence of Znf335.

Parent: 0.12 +/- 0.05, Hom Patient: 0.12 +/- 0.03. Caprin1: K4: Control: 6.56 +/- 0.01, Het Parent: 0.95 +/- 0.75, Hom Patient: 2.11 +/- 1.8; K27: Control: 0.62 +/- 0.23, Het Parent: 0.95 +/- 0.43, Hom Patient: 0.95 +/- 0.54. Pes1: K4: Control: 6.63 +/- 2.54, Het Parent: 0.7 +/- 0.23, Hom Patient: 0.14 +/- 0.11; K27: Control: 0.41 +/- 0.16, Het Parent: 0.89 +/- 0.45, Hom Patient: 0.19 +/- 0.09. Pdap1: K4: Control: 4.28 +/- 1.11, Het Parent: 2.1 +/- 1.05, Hom Patient: 0.96 +/- 0.08; K27: Control: 0.11 +/- 0.02, Het Parent: 0.03 +/- 0.02, Hom Patient: 0.05 +/- 0.02. Hspa9: K4: Control: 6.2 +/- 0.78, Het Parent: 2.36 +/- 1.8, Hom Patient: 3.2 +/- 0.5; K27: Control: 0.14 +/- 0.04, Het Parent: 0.12 +/- 0.02, Hom Patient: 0.1 +/- 0.05. Taf9: K4: Control: 3.38 +/- 0.73, Het Parent: 0.45 +/- 0.26, Hom Patient: 0.63 +/- 0.32; K27: Control: 0.23 +/- 0.01, Het Parent: 0.32 +/- 0.02, Hom Patient: 0.27 +/- 0.03. Suds3: K4: Control: 3.79 +/- 1.6, Het Parent: 1.31 +/- 0.49, Hom Patient: 1.84 +/- 0.41; K27: Control: 0.91 +/- 0.46, Het Parent: 0.81 +/- 0.45, Hom Patient: 0.50 +/- 0.09. Dand5: K4: Control: 1.56 +/- 0.2, Het Parent: 0.45 +/- 0.2, Hom Patient: 0.85 +/- 0.18; K27: Control: 0.83 +/- 0.19, Het Parent: 1.04 +/- 0.46, Hom Patient: 1.1 +/- 0.45. All numbers were normalized to input and compared to GAPDH control. IP DNA was pooled from two separate IPs from pooled chromatin from 3 cell lines. qPCR analysis was done using triplicates.

Supplementary Figure S6



Supplemental Figure S6 (Continued), related to Figures 12-13, Incomplete neuronal differentiation and granule cell migration upon Znf335 knockdown.

(A) Similar to cortical cultures (Fig 7A, 7B), knockdown of Znf335 in vivo through in utero electroporations also causes a lack of NeuN expression hinting at a state of incomplete neuronal differentiation.

(B) To assess the affects of knockdown of ZNF335 on migration, we selectively removed *Znf335* from granule cell progenitors using shRNA-ZNF335 and UT-Control, and then prepared cerebellar slice cultures. At 48hrs post electroporation, developing knockdown granule cells exhibited delayed axon extension, sending out shortened filopodia-like extensions, although these axons extended by 72hrs. Abnormal axonal extension (upper panel, arrowhead) and delayed migration of granule neurons (lower panels, arrows) past the Purkinje cell layer (Calbindin-stained) upon knockdown of Znf335 at 48hours and 72hours post electroporation, respectively.

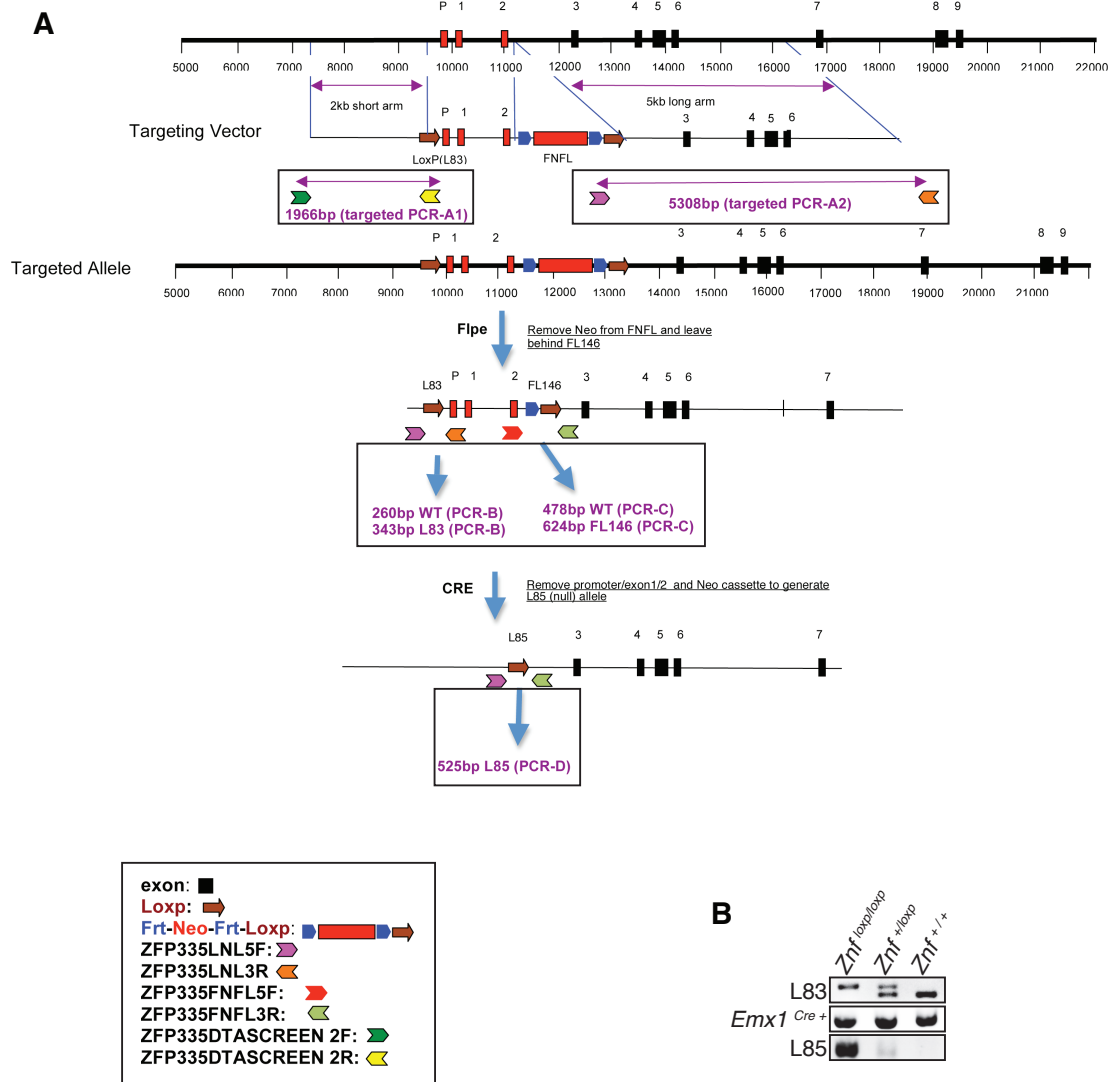
(C) By 72hrs post knockdown, granule cells that would normally have migrated past the Purkinje cell layer into the IGL were retarded in their migration. Not only did fewer cells migrate, they also migrated a shorter distance past the Purkinje cells. Since proper migration and interaction with Purkinje cells strongly influence the survival of granule cells (Morrison and Mason, 1998; Smeyne et al., 1995), the roles of Znf335 in regulating proliferation, migration, and differentiation of

Supplemental Figure S6 (Continued), related to Figures 12-13, Incomplete neuronal differentiation and granule cell migration upon Znf335 knockdown.

granule cells provide a likely cause for the cell sparse granule cell layer (GCL) seen in the patients (Fig 2D). Granule cells, in turn, also regulate Purkinje cell orientation (Adams et al., 2002; Morrison and Mason, 1998; Nagata et al., 2006), thus the decreased number of granule cells present in the patients, and also seen in our explant experiments, could be one of the reasons for the poorly oriented Purkinje cells present in the patients (Fig 2D). Distance of granule cell migration past the purkinje cell layer. (UT-Control: 50um: 33.5+/-5.6; 100um: 26.2+/-8.3; 150um: 22.8+/-4.1; 200um: 23.1+/-8.1; shRNA-ZNF335: 50um: 84.2+/-7.3; 100um: 18.5+/-4.3; 150um: 2.4+/-1.8; 200um: 0.8+/-0.4); Mean+/-SD, T-test, Pvalues: 50um=0.0007; 100um:0.2268; 150um:0.0014; 200um:0.0089; n=3 separate experiments using 3 pups each.

(D) Granule Cell Survival Assay (UT-Control Alive: 5day:85.0+/-5.5; 16day:64.0+/-9.2; shRNA-ZNF335: 5day:91.0+/-5.2; 16day: 47.1+/-6.1). Mean+/-SD, T-test, Pvalues: 5dayP=0.0302; 16dayP=0.0008; n=9 separate experiments using 3 pups each.

Supplementary Figure S7



**Supplemental Figure S7 (Continued), related to Figures 12-13, Znf335
Conditional Knockout**

(A) The creation of the Znf335-floxed allele containing two loxp sites flanking the Promoter, Exon1, and Exon2 of *Znf335* essentially bypassing the initiation of *Znf335* transcript expression. No other putative promoters were found through the genome browser or while looking at H3K4me3 peaks or PolIII peaks as a marker of gene promoter. **See supplemental Materials & Methods.**

(B) Analysis and verification of the *Znf^{loxp/loxp}:Emx1^{Cre+}*, *Znf^{loxp/+}:Emx1^{Cre+}*, and *Znf^{+/+}:Emx1^{Cre+}* mouse genotype. L83 products were from tail genomic DNA and L85 products were from DNA of developing forebrain tissue, where *Cre* is expressed.

Supplementary Table S1

HeLAS3 Co-IP/Mass Spec
Methyltransferase Complex <i>SETD1</i> WDR5 RbBP5 Ash2
Inhibitor of Deactylase p30 DBC-1
Bind specific chromatin regions TRIM28
Transcription Activator Host cell factor C1 (HCF-1)
mRNA Splicing DDX5 DDX48 Matrin 3 DDX21
Transcription Factor YY1
OTHERS Ki67 Histone 2A EMSY

mouse E14.5 cortex Co-IP/Mass Spec
Methyltransferase Complex WDR5 Matrin 3 SETD1a
Bind specific chromatin regions TRIM28
mRNA Splicing DDX5 Matrin 3 DDX5 DDX21
OTHERS Ki67 Histone 2A

Supplemental Table S1 (Continued), related to Figures 9-11, ZNF335 Complex. Mass spectrometry of purified complex of ZNF335-Interacting proteins from Human Cell Lines. Compiled data from our studies and from (Garapaty et al., 2009) (Left panel). Mass spectrometry of purified Znf335-Interacting proteins from nuclear lysates of developing brains from mouse E14.5 embryos. Compiled data from our studies (right panel). Additional sheets in excel include mass spectrometry peptide results from HeLaS3 Control, HeLaS3 ZNF335, E14.5m Control, and E14.5m ZNF335 samples.

Supplementary Table S2

Total Genes		
399		
H3K4 at Promoter	Both ZNF & H3K4 at Promoter	
332 (83.21%)	245 (61.40%)	

Genes Containing RNA-Sequencing Reads		
279 (69.92%)		
H3K4 at Promoter	Both ZNF & H3K4 at Promoter	
258 (92.47%)	196 (70.25%)	

RNA-Seq Patient Data					
Homozygous			Heterozygous		
Decrease	Comparable	Increased	Decrease	Comparable	Increased
230 (82.44%)	13 (4.66%)	36 (12.90%)	205 (73.47%)	22 (7.89%)	52 (18.64%)
Average Change compared to control 0.6287			Average Change compared to control 0.6273		

Supplemental Table S2 (Continued), related to Figures 9-11, CHIP-seq data analysis with H3K4me3 binding and gene expression levels.

A total of 399 genes were picked up by both CHIP-seq using two distinct Znf335 antisera. 83.21% of the genes had a peak at the H3K4 promoter while 61.40% had a peak that overlapped for Znf335 and H3K4. Of all the genes detected, 69.92% of genes also had data for transcript expression levels in the heterozygous parents and homozygous patients as compared to the controls. The group of genes that were bound to by Znf335 collectively showed a 0.6287 fold in expression in the homozygous patients and 0.6273 in the heterozygous parents as compared to the controls. As a whole, this pool of genes which are putative Znf335 targets are significantly decreased in expression as compared to the global average of changes in all gene expression which normalized out to only 1.04, indicating roughly no change.

Supplementary Table S3

Name	Binding At Promoter			RNA-Seq Normalized Data			Ratio of Expression to Control	
	797	798	H3K4	Hom	Het	Control	Hom/Control	Het/Control
	1 1700012A03Rik	N/A	N/A	NO H3K4ME3 PEAK				
2 1700057K13Rik	N/A	N/A	NO H3K4ME3 PEAK					
3 2310015B20Rik	N/A	N/A	NO H3K4ME3 PEAK					
4 7420461P10Rik	N/A	N/A	NO H3K4ME3 PEAK					
5 B3gnt6	N/A	N/A	NO H3K4ME3 PEAK	0	0	0		
6 Cib4	N/A	N/A	NO H3K4ME3 PEAK	0	0	0		
7 Gm10220	N/A	N/A	NO H3K4ME3 PEAK					
8 Gm10754	N/A	N/A	NO H3K4ME3 PEAK					
9 Gm14047	N/A	N/A	NO H3K4ME3 PEAK					
10 Gm7550	N/A	N/A	NO H3K4ME3 PEAK					
11 Hmx3	N/A	N/A	NO H3K4ME3 PEAK	1.6337	0.9013	3.4539	0.47301996	0.26095719
12 Il34	N/A	N/A	NO H3K4ME3 PEAK	0	0	0.1014	0	0
13 Insig2	N/A	N/A	NO H3K4ME3 PEAK	6.1755	5.9212	14.289	0.43217442	0.41437999
14 Itin1	N/A	N/A	NO H3K4ME3 PEAK	0.135	0	0.1526	0.88458816	0
15 Mir138-1	N/A	N/A	NO H3K4ME3 PEAK	0	0	0		
16 Olfr161	N/A	N/A	NO H3K4ME3 PEAK					
17 Pkhd1	N/A	N/A	NO H3K4ME3 PEAK	0.2456	0.2504	0.1996	1.23075304	1.25476884
18 Prg4	N/A	N/A	NO H3K4ME3 PEAK	0.0632	0	0		
19 Rassf8	N/A	N/A	NO H3K4ME3 PEAK	0.0544	0	0		
20 Siglec15	N/A	N/A	NO H3K4ME3 PEAK	0.318	0.1286	3.557	0.08939159	0.03616485
21 Tubb2a-ps2	N/A	N/A	NO H3K4ME3 PEAK	15.271	50.941	43.104	0.35429195	1.18182303
22 Vmn1r2	N/A	N/A	NO H3K4ME3 PEAK					
23 1700044K03Rik	N/A	N/A	NO H3K4ME3 PEAK					
24 4922501L14Rik	N/A	N/A	NO H3K4ME3 PEAK					
25 4930525F21Rik	N/A	N/A	NO H3K4ME3 PEAK					
26 AA986860	N/A	N/A	NO H3K4ME3 PEAK					
27 Acacb	N/A	N/A	NO H3K4ME3 PEAK	0.069	0.1465	0.2742	0.25162147	0.53443729
28 Adcy10	N/A	N/A	NO H3K4ME3 PEAK	0.1765	0.1429	0.2859	0.617613	0.49973238
29 Amn	N/A	N/A	NO H3K4ME3 PEAK	0.2049	1.3678	0.1158	1.76917498	11.8098692
30 Ankar	N/A	N/A	NO H3K4ME3 PEAK	0.289	0.3507	0.36	0.80270223	0.9742416
31 Cyp2b19	N/A	N/A	NO H3K4ME3 PEAK					
32 Gjd4	N/A	N/A	NO H3K4ME3 PEAK	0	0	0		
33 Gm10466	N/A	N/A	NO H3K4ME3 PEAK					
34 Gm13034	N/A	N/A	NO H3K4ME3 PEAK					
35 Gm14496	N/A	N/A	NO H3K4ME3 PEAK					
36 Gm1821	N/A	N/A	NO H3K4ME3 PEAK					
37 Gm5458	N/A	N/A	NO H3K4ME3 PEAK					
38 Gm6194	N/A	N/A	NO H3K4ME3 PEAK					
39 Gm765	N/A	N/A	NO H3K4ME3 PEAK					
40 Gtdc1	N/A	N/A	NO H3K4ME3 PEAK	7.875	6.324	17.604	0.44733924	0.35923654
41 Izumo1	N/A	N/A	NO H3K4ME3 PEAK	0	0	0		
42 Mir101c	N/A	N/A	NO H3K4ME3 PEAK	0	0	0		
43 Mir128-2	N/A	N/A	NO H3K4ME3 PEAK	0	0	0		
44 Mir17	N/A	N/A	NO H3K4ME3 PEAK	0	0	0		
45 Mir3059	N/A	N/A	NO H3K4ME3 PEAK					
46 Mir3108	N/A	N/A	NO H3K4ME3 PEAK					
47 Nav2	N/A	N/A	NO H3K4ME3 PEAK	0.6524	1.0733	1.4084	0.46321137	0.76209377
48 Nt5c1b	N/A	N/A	NO H3K4ME3 PEAK	0	0	0.1234	0	0
49 Pgk2	N/A	N/A	NO H3K4ME3 PEAK	0	0	0		
50 Pglyrp4	N/A	N/A	NO H3K4ME3 PEAK	0.9572	1.7955	1.7346	0.55185576	1.03512625
51 Phc1	N/A	N/A	NO H3K4ME3 PEAK	2.4654	5.2365	4.4908	0.54899228	1.16604577
52 Ptprd	N/A	N/A	NO H3K4ME3 PEAK	0.1104	0.1532	0.1427	0.7740136	1.07362114
53 Rgs18	N/A	N/A	NO H3K4ME3 PEAK	0	0	0		
54 Rini	N/A	N/A	NO H3K4ME3 PEAK	11.99	10.186	12.493	0.95969743	0.8153526
55 Kpri1	N/A	N/A	NO H3K4ME3 PEAK					
56 Speer7-ps1	N/A	N/A	NO H3K4ME3 PEAK					
57 Tex16	N/A	N/A	NO H3K4ME3 PEAK					
58 Tgif2lx2	N/A	N/A	NO H3K4ME3 PEAK					
59 Tmem30c	N/A	N/A	NO H3K4ME3 PEAK	0	0	0		
60 Ttc36	N/A	N/A	NO H3K4ME3 PEAK	0	0	0		
61 Ttr	N/A	N/A	NO H3K4ME3 PEAK	0	0	0		
62 Tylms-ps	N/A	N/A	NO H3K4ME3 PEAK					
63 Tyrp1	N/A	N/A	NO H3K4ME3 PEAK	0	0	0.049	0	0
64 Ugt1a5	N/A	N/A	NO H3K4ME3 PEAK	0	0	0		
65 Vmn1r238	N/A	N/A	NO H3K4ME3 PEAK					
66 Whsc1l1	N/A	N/A	NO H3K4ME3 PEAK	14.512	13.156	20.755	0.69919201	0.63388276
67 Zfp541	N/A	N/A	NO H3K4ME3 PEAK	0.0344	0	0.2725	0.12637004	0
68 1600021P15Rik	N	N	H3K4 Peak					
69 1700003E16Rik	N	N	H3K4 Peak					
70 1700012B15Rik	N	N	H3K4 Peak					
71 1700034H14Rik	N	N	H3K4 Peak					
72 2210408I21Rik	N	N	H3K4 Peak					
73 2810405K02Rik	N	N	H3K4 Peak					
74 2810429I04Rik	N	N	H3K4 Peak					
75 6330578E17Rik	N	N	H3K4 Peak					
76 Anxa3	N	N	H3K4 Peak	3.1548	1.9145	19.939	0.15822454	0.09601876
77 Arhgap15	N	N	H3K4 Peak	52.324	54.261	70.018	0.7473014	0.77496008
78 Arhgap5	N	N	H3K4 Peak	0.6311	0.5241	1.2204	0.5171456	0.42945273
79 Armc4	N	N	H3K4 Peak	0.4466	0.0542	0.1972	2.26458716	0.2748537
80 Arv1	N	N	H3K4 Peak	21.195	19.829	25.348	0.83615541	0.78227696
81 Asrgl1	N	N	H3K4 Peak	0.9232	2.0809	5.9984	0.15390428	0.3469036
82 Atf7ip	N	N	H3K4 Peak	5.6125	5.0674	9.169	0.61212061	0.55266926
83 Atp6v1h	N	N	H3K4 Peak	39.415	39.296	42.269	0.93248023	0.9296531
84 Atp7a	N	N	H3K4 Peak	1.0712	1.4826	2.3794	0.45019102	0.62308827
85 Atxn7	N	N	H3K4 Peak	1.3688	1.6078	1.9717	0.69423495	0.81541403
86 Avpr1a	N	N	H3K4 Peak	0	0	0		
87 Bbx	N	N	H3K4 Peak	4.4279	4.0905	5.492	0.80624727	0.74480335
88 Bcl2	N	N	H3K4 Peak	0.8108	1.163	1.9721	0.41114638	0.58974099
89 Cbr3	N	N	H3K4 Peak	0	0.3482	1.1351	0	0.30675165
90 Cdh2	N	N	H3K4 Peak	0.5844	0.4877	0.9033	0.64702509	0.53989133
91 Cdk5rap2	N	N	H3K4 Peak	17.18	17.682	30.866	0.55660778	0.5728652
92 Cdk8	N	N	H3K4 Peak	23.264	26.375	21.169	1.09898058	1.24594687
93 Chn1	N	N	H3K4 Peak	1.9603	0.3037	7.9564	0.24637931	0.03817416
94 Chordc1	N	N	H3K4 Peak	34.41	26.145	29.858	1.15248095	0.87566609
95 Chrd1	N	N	H3K4 Peak	0.0778	0.0944	0.044	1.76917811	2.14275488
96 Clic5	N	N	H3K4 Peak	0.0267	0.0648	0.0603	0.44229437	1.07362625
97 Col12a1	N	N	H3K4 Peak	0.3168	0.3177	0.5597	0.56614676	0.56763339
98 Crtc3	N	N	H3K4 Peak	3.4549	4.9795	7.5737	0.45617635	0.65747427
99 D0H4S114	N	N	H3K4 Peak					
100 Dapk1	N	N	H3K4 Peak	12.25	11.966	21.954	0.55797481	0.54504293

Supplementary Table S3 (Continued)

101	Dfna5	N	N	H3K4 Peak	96.475	96.994	177.77	0.54268782	0.54561067
102	Dlg2	N	N	H3K4 Peak	0.119	0.2406	0.3513	0.33863929	0.68501265
103	Dmrt2	N	N	H3K4 Peak	0	0.5937	0.0602	0	9.86418295
104	Dnahc11	N	N	H3K4 Peak					
105	Dock2	N	N	H3K4 Peak	72.732	61.633	115.94	0.62729939	0.53157904
106	Dsel	N	N	H3K4 Peak	0	0	0		
107	Eif5a	N	N	H3K4 Peak	876.32	895.71	775.78	1.12959602	1.15458893
108	Epha6	N	N	H3K4 Peak	0.0434	0.1053	0.3065	0.14153657	0.34356821
109	Fam196b	N	N	H3K4 Peak	0	0	0		
110	Fam19a4	N	N	H3K4 Peak	0.0715	0.0867	0		
111	Fstl5	N	N	H3K4 Peak	0	0.0802	0.0875	0	0.91617962
112	Fzd8	N	N	H3K4 Peak	0	0	0		
113	Gaint11	N	N	H3K4 Peak	3.8677	7.0413	6.9868	0.55356642	1.00779752
114	Gda	N	N	H3K4 Peak	1.0282	0.3209	0.2325	4.42291643	1.38037615
115	Gk5	N	N	H3K4 Peak	1.4607	1.8438	2.1931	0.6660587	0.84073302
116	Hsf1	N	N	H3K4 Peak	39.952	49.12	48.1	0.83061052	1.02120799
117	Igsf10	N	N	H3K4 Peak	0	0.0226	0		
118	Ipo11	N	N	H3K4 Peak	19.827	15.492	18.619	1.06489712	0.83203983
119	Kcnv1	N	N	H3K4 Peak	0	0.1983	0.3848	0	0.51535187
120	Kctd16	N	N	H3K4 Peak	0	0.0374	0.1044	0	0.35787648
121	Lhfp14	N	N	H3K4 Peak	0	0	0		
122	Luzp2	N	N	H3K4 Peak	0	0.1841	0.1344	0	1.37002894
123	Ly6c2	N	N	H3K4 Peak					
124	Ndurf3	N	N	H3K4 Peak	59.368	61.286	69.252	0.85727653	0.88496233
125	Negr1	N	N	H3K4 Peak	0	0.0342	0.0623	0	0.54801124
126	Nfz	N	N	H3K4 Peak	5.6585	6.677	5.946	0.95165625	1.12294398
127	Nnat	N	N	H3K4 Peak	0	0	0.7574	0	0
128	Nppc	N	N	H3K4 Peak	0	0	0		
129	Ntm	N	N	H3K4 Peak	0	0	0.0529	0	0
130	Parl	N	N	H3K4 Peak	102.58	104.07	114.81	0.89344134	0.90642801
131	Pik3cg	N	N	H3K4 Peak	3.1434	2.3395	2.6714	1.17669585	0.87576038
132	Pixdc2	N	N	H3K4 Peak	0.4305	0.2239	3.693	0.11655993	0.06062958
133	Poc5	N	N	H3K4 Peak	8.7101	6.54	19.296	0.45138784	0.33892476
134	Poir3b	N	N	H3K4 Peak	5.5249	4.6667	5.6634	0.97554641	0.82401499
135	Ppp2r2b	N	N	H3K4 Peak	0	0	0		
136	Pthlh	N	N	H3K4 Peak	0	0	18.747		
137	Rab28	N	N	H3K4 Peak	6.9583	7.697	18.747	0.37116674	0.41056963
138	Scn2b	N	N	H3K4 Peak	0.0324	0	0.0286	1.13229519	0
139	Sepsecs	N	N	H3K4 Peak	2.7127	1.9892	2.3958	1.13227314	0.83027381
140	Sic24a2	N	N	H3K4 Peak	0	0	0		
141	Sic2a8	N	N	H3K4 Peak	1.2061	1.2809	1.92	0.62819792	0.66714063
142	Sic4a10	N	N	H3K4 Peak	0.0838	0.1695	0.444	0.18871565	0.38174108
143	Smarca2	N	N	H3K4 Peak	66.177	128.35	75.277	0.87911113	1.70502701
144	Snord88c	N	N	H3K4 Peak	0	0	0		
145	Spock3	N	N	H3K4 Peak	0	0	0.0591	0	0
146	Tmem169	N	N	H3K4 Peak	0.0922	0.1119	0.0521	1.76917644	2.14726199
147	Tmem38b	N	N	H3K4 Peak	7.069	6.2482	6.7752	1.04335973	0.92221756
148	Trpc4	N	N	H3K4 Peak	0	0	0		
149	Ttl17	N	N	H3K4 Peak	0	0	0		
150	Usp39	N	N	H3K4 Peak	25.418	19.895	20.231	1.25640113	0.98338672
151	Vps13c	N	N	H3K4 Peak	7.792	9.3246	11.761	0.6625135	0.79281712
152	Yars	N	N	H3K4 Peak	58.8	62.111	82.786	0.71026709	0.75026303
153	Zfp770	N	N	H3K4 Peak	1.0248	0.995	1.655	0.61921134	0.60122964
154	Znhit1	N	N	H3K4 Peak	14.355	27.518	17.679	0.81197819	1.55653664
155	Adk	N	VERY SMALL	H3K4 Peak	51.409	47.796	57.311	0.89701279	0.83397254
156	Ankyf1	N	VERY SMALL	H3K4 Peak	4.3491	3.7947	5.8587	0.74232002	0.64769217
157	Asxl3	N	VERY SMALL	H3K4 Peak	0	0	0		
158	Basp1	N	VERY SMALL	H3K4 Peak	7.7226	15.298	10.813	0.71421939	1.41485479
159	Col8a1	N		H3K4 Peak	0	0	0		
160	Entpd6	N	VERY SMALL	H3K4 Peak	10.742	11.846	14.689	0.73127561	0.80643185
161	Lrig2	N	VERY SMALL	H3K4 Peak	1.5097	1.9288	2.1558	0.70030151	0.89468875
162	Mpdz	N	VERY SMALL	H3K4 Peak	0.0858	0.1041	0.0727	1.1794508	1.42149807
163	Pou4f1	N	VERY SMALL	H3K4 Peak	0	0	0		
164	Prkab2	N	VERY SMALL	H3K4 Peak	0.5883	0.7497	0.7014	0.83873713	1.06887619
165	Rtel1	N	VERY SMALL	H3K4 Peak	6.7094	8.1015	7.4679	0.89843116	1.08483732
166	Rwdd3	N	VERY SMALL	H3K4 Peak	4.2623	8.3084	14.601	0.29192099	0.56903526
167	Vwc2l	N	VERY SMALL	H3K4 Peak	0	0	0		
168	Inhba	N	Y	H3K4 Peak	0	0	0		
169	Manf	N	Y	H3K4 Peak	151.36	137.31	206.25	0.73386053	0.66576808
170	Mdm2	N	Y	H3K4 Peak	5.112	6.073	7.2504	0.70507022	0.83761656
171	Polr3k	N	Y	H3K4 Peak	22.456	23.965	25.939	0.86572136	0.92391648
172	Ptprz1	N	Y	H3K4 Peak	0.0782	0.0475	0.0433	1.80608001	1.09602234
173	Pxmp3	N	Y	H3K4 Peak					
174	Pxmp3	N	Y	H3K4 Peak					
175	Spink10	N	Y	H3K4 Peak					
176	Zfp330	N	Y	H3K4 Peak					
177	Bcl6	VERY SMALL	N	H3K4 Peak	0.0436	0	0.0483	0.90303757	0
178	Gaint9	VERY SMALL	N	H3K4 Peak	0	0.0727	0		
179	Ifngr2	VERY SMALL	N	H3K4 Peak	28.154	33.56	53.423	0.52698916	0.62818658
180	Pik3c2a	VERY SMALL	N	H3K4 Peak	4.8116	4.6485	7.2234	0.66610599	0.64352936
181	Rnf216	VERY SMALL	N	H3K4 Peak	12.789	15.991	14.027	0.91174562	1.14004919
182	Samd14	VERY SMALL	N	H3K4 Peak	0.1716	0	0.682	0.25162128	0
183	Sorcs1	VERY SMALL	N	H3K4 Peak	0.0877	0.0266	0.0972	0.90303876	0.27400565
184	Sulf1	VERY SMALL	N	H3K4 Peak	0.0837	0.1016	0.0986	0.84922076	1.030703
185	Trim7	VERY SMALL	N	H3K4 Peak	0.2651	0.0643	0.4696	0.56439963	0.13700253
186	Wdpcp	VERY SMALL	N	H3K4 Peak					
187	Adamts3	Y	N	H3K4 Peak	0.0274	0.0333	0.0968	0.28307348	0.34356732
188	Bod1	Y	N	H3K4 Peak	9.485	7.2075	7.8547	1.2075519	0.91759849
189	Ccdc68	Y	N	H3K4 Peak	0.3474	0.2811	0.4702	0.73885093	0.59782962
190	D10Wsu52e	Y	N	H3K4 Peak					
191	Galr1	Y	N	H3K4 Peak	0	0	0		
192	Itpk1	Y	N	H3K4 Peak	6.3389	11.196	7.91	0.80137218	1.41539465
193	Lmo1	Y	N	H3K4 Peak	0	0	0		
194	Mill2	Y	N	H3K4 Peak					
195	Naa20	Y	N	H3K4 Peak	29.419	27.991	21.673	1.35739234	1.29148576
196	Nkain2	Y	N	H3K4 Peak	0	0	0		
197	Ptn	Y	N	H3K4 Peak	12.35	15.7	13.388	0.92246215	1.17262834
198	Spock1	Y	N	H3K4 Peak	0	0	0.0292	0	0
199	St3gal5	Y	N	H3K4 Peak	2.2099	2.8447	1.409	1.56844055	2.01899273
200	Zadhz	Y	N	H3K4 Peak	0.5225	0.5989	0.6429	0.81273584	0.93161873

Supplementary Table S3 (Continued)

201	I500016L03Rik	VERY SMALL	VERY SMALL	H3K4 Peak					
202	Akr1b3	VERY SMALL	VERY SMALL	H3K4 Peak					
203	Bach1	VERY SMALL	VERY SMALL	H3K4 Peak	0.8571	0.6712	2.4693	0.34711764	0.2718049
204	Csda	VERY SMALL	VERY SMALL	H3K4 Peak	89.615	93.564	82.593	1.08501578	1.13283224
205	Dhd1	VERY SMALL	VERY SMALL	H3K4 Peak	3.4214	4.1077	4.2825	0.79893052	0.95919859
206	E130203B14Rik	VERY SMALL	VERY SMALL	H3K4 Peak					
207	Garnl3	VERY SMALL	VERY SMALL	H3K4 Peak	0.3414	0.4661	2.2236	0.15353196	0.20963459
208	Gata6	VERY SMALL	VERY SMALL	H3K4 Peak	0	0	0.5242	0	0
209	Gtf2ird1	VERY SMALL	VERY SMALL	H3K4 Peak	3.0272	5.2004	1.3925	2.17397611	3.73458337
210	Jarid2	VERY SMALL	VERY SMALL	H3K4 Peak	3.2978	2.489	3.3285	0.99075868	0.74776553
211	Khdrbs2	VERY SMALL	VERY SMALL	H3K4 Peak	5.8257	7.4073	11.638	0.50059463	0.63650526
212	Lrrc4c	VERY SMALL	VERY SMALL	H3K4 Peak	0	0	0		
213	Mtx2	VERY SMALL	VERY SMALL	H3K4 Peak	71.039	62.993	132.12	0.53770654	0.47680581
214	Ntrk2	VERY SMALL	VERY SMALL	H3K4 Peak	3.3535	0.5349	6.3634	0.52699963	0.08406439
215	P4ha2	VERY SMALL	VERY SMALL	H3K4 Peak	6.6386	15.512	11.503	0.57713908	1.34858206
216	Ptprr	VERY SMALL	VERY SMALL	H3K4 Peak	0.0914	0	0.1033	0.88459216	0
217	Rpp21	VERY SMALL	VERY SMALL	H3K4 Peak	59.588	77.885	55.496	1.07373504	1.40343989
218	Slco3a1	VERY SMALL	VERY SMALL	H3K4 Peak	0	0	0.0276	0	0
219	Tbx3	VERY SMALL	VERY SMALL	H3K4 Peak	0	0	0		
220	Tcf4	VERY SMALL	VERY SMALL	H3K4 Peak	7.4472	3.9501	11.752	0.63370973	0.33612638
221	Tle3	VERY SMALL	VERY SMALL	H3K4 Peak	14.123	14.2	21.088	0.6697269	0.67335935
222	Tmem117	VERY SMALL	VERY SMALL	H3K4 Peak	0.9463	2.2971	1.8339	0.51602085	1.25259289
223	Irpc7	VERY SMALL	VERY SMALL	H3K4 Peak	0	0	0.048	0	0
224	Tspan12	VERY SMALL	VERY SMALL	H3K4 Peak	2.2396	3.8509	3.1318	0.71513325	1.22961064
225	Ttc7b	VERY SMALL	VERY SMALL	H3K4 Peak	0	0.1691	0.2872	0	0.58897293
226	Wbscr17	VERY SMALL	VERY SMALL	H3K4 Peak	0	0	0		
227	Xytl1	VERY SMALL	VERY SMALL	H3K4 Peak	0.4784	0.6636	0.5676	0.84283696	1.16908853
228	4930473A06Rik	Y	Y	H3K4 Peak					
229	Ctsc	VERY SMALL	Y	H3K4 Peak	47.399	40.614	67.028	0.70714776	0.60591842
230	Dcl1	VERY SMALL	Y	H3K4 Peak	0.0499	0.1212	0		
231	Fam19a5	VERY SMALL	Y	H3K4 Peak	0	0	0		
232	Mxd1	VERY SMALL	Y	H3K4 Peak	0.1713	0.5892	0.6133	0.27934432	0.96061283
233	Rpn1	VERY SMALL	Y	H3K4 Peak	95.19	108.67	120.78	0.78811734	0.89971105
234	Syt10	VERY SMALL	Y	H3K4 Peak	0	0	0		
235	2510009E07Rik	Y	VERY SMALL	H3K4 Peak					
236	Axin2	Y	VERY SMALL	H3K4 Peak	0	0.0457	0.2087	0	0.21920458
237	Bambi	Y	VERY SMALL	H3K4 Peak	0.0925	0	0		
238	Dbdd2	Y	VERY SMALL	H3K4 Peak	0	0.1263	0		
239	Dpy19l1	Y	VERY SMALL	H3K4 Peak	3.2788	1.4326	4.3435	0.75486354	0.32982544
240	Foxo1	Y	VERY SMALL	H3K4 Peak	0.2502	0.8098	0.9235	0.27091199	0.87681655
241	Kdm3b	Y	VERY SMALL	H3K4 Peak	9.0374	10.258	8.8706	1.01880139	1.15643551
242	Kin	Y	VERY SMALL	H3K4 Peak	18.998	21.737	36.217	0.52455228	0.60019162
243	Malt1	Y	VERY SMALL	H3K4 Peak	10.816	11.934	18.572	0.58237267	0.64256985
244	Npr3	Y	VERY SMALL	H3K4 Peak	0	0.0732	0		
245	Rab14	Y	VERY SMALL	H3K4 Peak	11.772	11.936	10.978	1.07235314	1.08729197
246	Rps17	Y	VERY SMALL	H3K4 Peak	11854	13495	16019	0.73998077	0.84245156
247	Sesn3	Y	VERY SMALL	H3K4 Peak	6.1814	7.5024	3.8116	1.62174479	1.96831498
248	Sorcs3	Y	VERY SMALL	H3K4 Peak	0.0554	0.1345	0.1227	0.45152041	1.09602379
249	St6galnac2	Y	VERY SMALL	H3K4 Peak	0.1516	0.092	0		
250	Tgfa	Y	VERY SMALL	H3K4 Peak	0	0	0		
251	Ttc14	Y	VERY SMALL	H3K4 Peak	2.5325	1.9413	2.2366	1.13229574	0.86795912
252	Wgr7b	Y	VERY SMALL	H3K4 Peak	56.074	49.74	60.691	0.92392143	0.81955209
253	1110032F04Rik	Y	Y	H3K4 Peak					
254	2510012J08Rik	Y	Y	H3K4 Peak					
255	3000002C10Rik	Y	Y	H3K4 Peak					
256	4921530L18Rik	Y	Y	H3K4 Peak					
257	Actr10	Y	Y	H3K4 Peak	14.769	26.728	29.664	0.49785936	0.90103155
258	Aimp1	Y	Y	H3K4 Peak	32.46	31.949	41.569	0.7808781	0.76856848
259	Akr1c14	Y	Y	H3K4 Peak					
260	Alkbh5	Y	Y	H3K4 Peak	7.8525	13.253	11.924	0.65857257	1.11146895
261	Anapc1	Y	Y	H3K4 Peak	70.757	67.285	61.698	1.14682672	1.09055089
262	Ankle2	Y	Y	H3K4 Peak	17.068	19.76	26.009	0.656219	0.75972163
263	Ankrd28	Y	Y	H3K4 Peak	9.8727	8.7063	17.01	0.58041753	0.51184449
264	Arhgap11a	Y	Y	H3K4 Peak	11.617	12.824	21.523	0.53975356	0.59583879
265	Arnt2	Y	Y	H3K4 Peak	0.0486	0.059	0.0215	2.26459635	2.74854525
266	Atp5l	Y	Y	H3K4 Peak	36.581	38.553	42.131	0.86827483	0.91507896
267	Atpbd4	Y	Y	H3K4 Peak	2.6809	4.3113	5.6232	0.47675599	0.76669921
268	BC018507	Y	Y	H3K4 Peak					
269	Bckdha	Y	Y	H3K4 Peak	21.22	26.956	25.391	0.83575482	1.06163674
270	Caprin1	Y	Y	H3K4 Peak	83.628	100	91.491	0.91405403	1.09303408
271	Ccdc103	Y	Y	H3K4 Peak	0.635	1.079	1.2921	0.49143817	0.83503982
272	Ccdc43	Y	Y	H3K4 Peak	7.0878	8.693	6.0312	1.17518765	1.44134242
273	Ccdc58	Y	Y	H3K4 Peak	51.097	56.624	40.839	1.25119801	1.38653287
274	Cct4	Y	Y	H3K4 Peak	413.07	345.56	318.16	1.29828107	1.08611309
275	Cdc73	Y	Y	H3K4 Peak	6.6072	7.2694	12.813	0.51566222	0.56734566
276	Cdkn2a	Y	Y	H3K4 Peak	4.7271	12.275	6.5866	0.71768482	1.86365976
277	Cog4	Y	Y	H3K4 Peak	62.46	62.979	71.248	0.87665444	0.88393607
278	Cox5a	Y	Y	H3K4 Peak	1073	1128.3	1896.9	0.56564783	0.59477369
279	Cox7a2l	Y	Y	H3K4 Peak	21.745	30.386	38.409	0.56614708	0.7911094
280	D11Wsu99e	Y	Y	H3K4 Peak					
281	Dand5	Y	Y	H3K4 Peak	0.01	0.02	0.1	0.1	0.2
282	Ddx39b	Y	Y	H3K4 Peak					
283	Dgkz	Y	Y	H3K4 Peak	6.6756	14.925	20.491	0.32578033	0.7283712
284	Dhx15	Y	Y	H3K4 Peak	131.42	107.24	142.09	0.92489971	0.75469773
285	Dync1l12	Y	Y	H3K4 Peak	8.3509	11.118	10.527	0.79330274	1.05615245
286	Eif2s3x	Y	Y	H3K4 Peak					
287	Eif4eni1	Y	Y	H3K4 Peak	16.076	15.589	18.369	0.87520007	0.84864933
288	Eif4h	Y	Y	H3K4 Peak	113.46	121.44	135.21	0.83917372	0.89815691
289	Fam58b	Y	Y	H3K4 Peak	0	0	0		
290	Farsb	Y	Y	H3K4 Peak	106.51	112.97	114.07	0.93372374	0.99037416
291	Fgfbp3	Y	Y	H3K4 Peak	0	0	0.2067	0	0
292	G530011O06Rik	Y	Y	H3K4 Peak					
293	Golga5	Y	Y	H3K4 Peak	16.001	15.001	33.495	0.47771011	0.44784296
294	Gorab	Y	Y	H3K4 Peak	1.5415	1.7961	3.4155	0.45132031	0.5258572
295	Gtf3c4	Y	Y	H3K4 Peak	6.9748	5.9608	7.9781	0.87424215	0.74714437
296	Habp4	Y	Y	H3K4 Peak	6.587	10.588	14.021	0.46980607	0.75513348
297	Hadha	Y	Y	H3K4 Peak	105.78	164.91	182.63	0.57920933	0.90299513
298	Hs2st1	Y	Y	H3K4 Peak	5.2636	5.7582	8.672	0.60696404	0.66399715
299	Hspa9	Y	Y	H3K4 Peak	375.49	390.63	349.75	1.07358071	1.11686281
300	Il1rap1	Y	Y	H3K4 Peak	0	0	0.0659	0	0

Supplementary Table S3 (Continued)

301	Ipo13	Y	Y	H3K4 Peak	8.5559	10.096	12.069	0.70891706	0.83651504
302	Irgq	Y	Y	H3K4 Peak	0	0	0.0547	0	0
303	Large	Y	Y	H3K4 Peak	1.0252	9.5395	6.6014	0.15529911	1.44507142
304	Lgr4	Y	Y	H3K4 Peak	0.4256	0.4059	1.1545	0.3686531	0.35155565
305	Lnep	Y	Y	H3K4 Peak	6.8159	6.54	9.9905	0.68223481	0.65462054
306	Lrr1	Y	Y	H3K4 Peak					
307	Lymr4	Y	Y	H3K4 Peak	7.4261	4.0859	8.832	0.84081349	0.46262524
308	Mapkapk5	Y	Y	H3K4 Peak	25.412	19.042	23.202	1.00903798	0.84094112
309	Mcp1	Y	Y	H3K4 Peak	4.3968	4.7207	7.2168	0.60925235	0.65413107
310	Mier3	Y	Y	H3K4 Peak	1.0121	2.2334	2.6815	0.37743378	0.83289018
311	Mir181a-1	Y	Y	H3K4 Peak	0	0	0		
312	Mrp11	Y	Y	H3K4 Peak	44.467	46.506	44.946	0.9893427	1.0347041
313	Mrps5	Y	Y	H3K4 Peak	59.349	67.836	110.26	0.53827387	0.61524787
314	Mrps7	Y	Y	H3K4 Peak	29.197	24.491	25.841	1.12988862	0.94776437
315	Mrto4	Y	Y	H3K4 Peak	74.177	64.051	74.371	0.99739951	0.86124068
316	Mthfs	Y	Y	H3K4 Peak	9.3619	9.1775	9.9728	0.93874621	0.92025185
317	Nbea	Y	Y	H3K4 Peak	0.6599	0.4527	0.4378	1.50707683	1.03386192
318	Ncn	Y	Y	H3K4 Peak	22.092	23.753	20.442	1.08071775	1.16198341
319	Ndufa10	Y	Y	H3K4 Peak	34.499	38.641	32.668	1.05602968	1.18283724
320	Ndufa4	Y	Y	H3K4 Peak	194.79	188.19	250.47	0.77767974	0.75134147
321	Neur1b	Y	Y	H3K4 Peak	0	0	0		
322	Nhirc3	Y	Y	H3K4 Peak	0.2697	1.7456	2.2356	0.12062551	0.78081793
323	Nr2f2	Y	Y	H3K4 Peak	0	0.0758	0.2481	0	0.30539342
324	Nsun2	Y	Y	H3K4 Peak	76.965	79.519	87.692	0.87767641	0.90679537
325	Nup205	Y	Y	H3K4 Peak	31.157	32.076	58.779	0.54708857	0.54571221
326	Nup85	Y	Y	H3K4 Peak	56.323	50.934	63.397	0.85841726	0.80341941
327	Nup98	Y	Y	H3K4 Peak	27.725	29.347	24.243	1.14365974	1.21054586
328	Papd4	Y	Y	H3K4 Peak	16.028	16.046	24.466	0.65511336	0.65585724
329	Pcbp2	Y	Y	H3K4 Peak	2.1465	1.8725	5.5094	0.38960725	0.33987244
330	Pcbp1	Y	Y	H3K4 Peak	0	0	0		
331	Pdap1	Y	Y	H3K4 Peak	50.739	49.883	44.994	1.12768204	1.10865942
332	Pdia6	Y	Y	H3K4 Peak	202.2	224.04	304.1	0.6649063	0.73671749
333	Pes1	Y	Y	H3K4 Peak	101.1	107.74	75.843	1.3330626	1.42055868
334	Pi4kb	Y	Y	H3K4 Peak	12.684	13.498	16.285	0.77887355	0.82886495
335	Pin4	Y	Y	H3K4 Peak	6.2612	5.6693	10.015	0.62517998	0.56607523
336	Plekht2	Y	Y	H3K4 Peak	0.9146	1.6324	1.966	0.46520242	0.83031786
337	Pno1	Y	Y	H3K4 Peak	20.887	19.282	19.647	1.06312066	0.9814369
338	Poir2e	Y	Y	H3K4 Peak	43.802	48.974	58.859	0.74417976	0.83205883
339	Poir3f	Y	Y	H3K4 Peak	8.6684	9.5317	11.516	0.75271576	0.82768125
340	Ppp1r15b	Y	Y	H3K4 Peak	2.147	1.2479	1.9485	1.10185679	0.64040913
341	Psmc1	Y	Y	H3K4 Peak	109.24	93.045	103.14	1.05936091	0.90234011
342	Psmc12	Y	Y	H3K4 Peak	71.19	69.274	76.967	0.92495706	0.90005262
343	Psmg2	Y	Y	H3K4 Peak	155.7	198.41	298.3	0.52197117	0.66512906
344	Rabggtb	Y	Y	H3K4 Peak	71.439	72.989	73.407	0.97319204	0.99429485
345	Rabl2	Y	Y	H3K4 Peak	8.0124	10.706	10.647	0.75256227	1.00556036
346	Rbbp5	Y	Y	H3K4 Peak	10.451	11.85	14.691	0.71137628	0.80663803
347	REST/NRSF	Y	Y	H3K4 Peak	0.6526	0.9504	1.364	0.47843533	0.69681376
348	Rexo1	Y	Y	H3K4 Peak	5.3624	6.0012	5.861	0.91492066	1.02391401
349	Rpl21	Y	Y	H3K4 Peak	0.2818	0.3421	0.3121	0.90303893	1.09602222
350	Rpl35a	Y	Y	H3K4 Peak	1034.7	1043	1297.2	0.7976318	0.80401483
351	Rpl7	Y	Y	H3K4 Peak	3881.7	3891.2	4654.5	0.8339657	0.8360175
352	Rps10	Y	Y	H3K4 Peak	4180.6	3280.6	4240.5	0.98588135	0.77362758
353	Rps12	Y	Y	H3K4 Peak	2177.7	1945.6	2869.8	0.75883169	0.67797183
354	Rps23	Y	Y	H3K4 Peak	2034.9	1986.7	2679.6	0.75940529	0.74141759
355	Rps24	Y	Y	H3K4 Peak	486.53	461.62	538.77	0.90303786	0.85680081
356	Rps27a	Y	Y	H3K4 Peak	1583.2	1536.7	1667.8	0.94924543	0.9213529
357	Rrbp1	Y	Y	H3K4 Peak	17.541	17.563	11.841	1.48181611	1.48324028
358	Ruf2	Y	Y	H3K4 Peak	1.158	0.9029	3.5039	0.3362340	0.2576759
359	Sart3	Y	Y	H3K4 Peak	38.911	32.031	47.99	0.8108089	0.66743974
360	Sec61b	Y	Y	H3K4 Peak	271.06	287.99	225.04	1.20447203	1.27971099
361	SEP15	Y	Y	H3K4 Peak					
362	Shisa2	Y	Y	H3K4 Peak	0	0	0		
363	Skp1a	Y	Y	H3K4 Peak					
364	Sic16a12	Y	Y	H3K4 Peak	0	0	0		
365	Sic22a23	Y	Y	H3K4 Peak	0.1039	0.3782	0.3164	0.32837788	1.19565863
366	Sic35b1	Y	Y	H3K4 Peak	42.097	54.032	65.33	0.64437931	0.82706107
367	Sic39a10	Y	Y	H3K4 Peak	0.891	0.6488	1.2422	0.71723608	0.52230684
368	Smc2	Y	Y	H3K4 Peak	15.93	14.821	20.801	0.76585178	0.71253095
369	Smox	Y	Y	H3K4 Peak	0.073	0.0886	0.4515	0.16175654	0.19632444
370	Spcs1	Y	Y	H3K4 Peak	75.783	89.835	107.46	0.70520835	0.83596992
371	Ssb	Y	Y	H3K4 Peak	219.03	189.12	240.25	0.91165489	0.78718923
372	Stam2	Y	Y	H3K4 Peak	6.6592	6.0108	11.54	0.57705699	0.5208676
373	Stk39	Y	Y	H3K4 Peak	0.2436	0.7096	0.5163	0.47179002	1.37426938
374	Sudg1	Y	Y	H3K4 Peak	58.9	77.467	104.04	0.56614762	0.74460817
375	Suds3	Y	Y	H3K4 Peak	5.3981	7.2477	12.783	0.42230002	0.56700489
376	Supv3l1	Y	Y	H3K4 Peak	22.373	21.833	19.388	1.15395526	1.12609797
377	Taf9	Y	Y	H3K4 Peak	114.56	119.18	118.65	0.96556985	1.00450078
378	Tcf7l1	Y	Y	H3K4 Peak	0.0578	0.0701	0.3199	0.18060791	0.21920452
379	Tm9sf1	Y	Y	H3K4 Peak	2.4218	3.1777	2.9718	0.81493583	1.06928844
380	Tmem48	Y	Y	H3K4 Peak	29.489	34.708	45.839	0.6433162	0.75716199
381	Tomm20	Y	Y	H3K4 Peak	21.583	19.446	34.893	0.61853735	0.55730409
382	Trap1	Y	Y	H3K4 Peak	206.89	200.26	180.1	1.14876015	1.11193657
383	Tsn	Y	Y	H3K4 Peak	15.31	13.752	13.584	1.12707142	1.01235304
384	Ttc8	Y	Y	H3K4 Peak	0.6517	1.5819	2.0847	0.3125897	0.75878295
385	Txnrd2	Y	Y	H3K4 Peak	2.1117	8.2803	13.198	0.15999803	0.62738349
386	Tysnd1	Y	Y	H3K4 Peak	4.8248	4.1246	3.9026	1.2363034	1.05687732
387	Ufm1	Y	Y	H3K4 Peak	10.242	9.3042	17.956	0.57037441	0.51816096
388	Upf2	Y	Y	H3K4 Peak	12.216	11.157	20.404	0.59870714	0.54680631
389	Usp1	Y	Y	H3K4 Peak	7.5727	7.225	9.5517	0.79280904	0.75640932
390	Vars	Y	Y	H3K4 Peak	49.69	89.177	66.26	0.74951548	1.34589567
391	Vdac2	Y	Y	H3K4 Peak	192.01	208.44	215.25	0.90036717	0.97742581
392	Vps26b	Y	Y	H3K4 Peak	3.2172	4.3796	3.4895	0.92196326	1.25508452
393	Vtilb	Y	Y	H3K4 Peak	31.639	52.655	53.218	0.59451872	0.98942453
394	Vwf	Y	Y	H3K4 Peak	0.0361	0.2411	0.2711	0.13321113	0.88923354
395	Wdr92	Y	Y	H3K4 Peak	5.6156	5.1765	13.246	0.42393952	0.39078762
396	Zfp365	Y	Y	H3K4 Peak	0.6065	0.3221	0.4617	1.31351083	0.69746702
397	Zfp777	Y	Y	H3K4 Peak	0.3635	1.5755	1.955	0.18591918	0.80589977
398	Zkscan2	Y	Y	H3K4 Peak	0.291	0.2173	0.1384	2.10283703	1.57060065
399	Zrand2	Y	Y	H3K4 Peak	76.13	75.963	121.08	0.62877177	0.62739331

Supplemental Table S3 (Continued), related to Figures 9-11, Znf335 ChIP-Seq analyzed with H3K4me3 peaks and changes in gene expression. Genes that are bound to by Znf335 from two separate antisera are listed in the table with annotations of whether or not Znf335 was bound to the promoter region of the gene or instead throughout the body. Presence or absence of a H3K4me3 peak for these same genes in the mouse developing E14.5 brain were also noted. RNA-seq normalized expression data are listed from controls, heterozygous parents, or homozygous patients. The data is from two separate RNA-seq experiments with a total of 7 controls. The ratios of gene expression in comparison to the controls are in the last two columns showing downregulated more than 10% (green), no change within 10% of control (yellow), or upregulated greater than 10% genes (red). The majority of the genes that are bound to by Znf335 show decreased expression in the homozygous patients that have decreased Znf335 expression. There are many genes showing the expected, intermediate result in het parents compared to homozygous patients, and others seemingly showing as severe decreases in hets as in homozygotes.

Supplementary Table S4

GeneGo CHIP-Seq Pathway Analysis

#	Maps	pValue	Ratio	enrichment	
1	Development_WNT signaling pathway. Part 1. Degradation of beta-	9.336E-05	3	19	4.03
2	PGE2 pathways in cancer	1.289E-04	4	55	3.89
3	Oxidative stress_Role of ASK1 under oxidative stress	5.485E-04	3	34	3.26
4	Cell adhesion_Tight junctions	6.502E-04	3	36	3.19
5	Apoptosis and survival_HTR1A signaling	1.704E-03	3	50	2.77
6	Cytoskeleton remodeling_TGF, WNT and cytoskeletal remodeling	1.866E-03	4	111	2.73
7	Development_WNT signaling pathway. Part 2	2.016E-03	3	53	2.70
8	Development_Regulation of epithelial-to-mesenchymal transition (E	3.458E-03	3	64	2.46
9	Protein folding_Membrane trafficking and signal transduction of G-a	3.626E-03	2	19	2.44
10	Apoptosis and survival_Beta-2 adrenergic receptor anti-apoptotic ac	5.301E-03	2	23	2.28
11	Development_Glucocorticoid receptor signaling	5.765E-03	2	24	2.24
12	Apoptosis and survival_p53-dependent apoptosis	8.353E-03	2	29	2.08
13	Proteolysis_Putative SUMO-1 pathway	8.353E-03	2	29	2.08
14	DNA damage_ATM/ATR regulation of G1/S checkpoint	1.011E-02	2	32	2.00
15	Autophagy_Autophagy	1.011E-02	2	32	2.00
16	Immune response_IL-7 signaling in T lymphocytes	1.408E-02	2	38	1.85
17	Apoptosis and survival_APRIL and BAFF signaling	1.479E-02	2	39	1.83
18	Transcription_P53 signaling pathway	1.479E-02	2	39	1.83
19	Translation_Non-genomic (rapid) action of Androgen Receptor	1.553E-02	2	40	1.81
20	Development_Role of Activin A in cell differentiation and proliferation	1.553E-02	2	40	1.81
21	Apoptosis and survival_Anti-apoptotic TNFs/NF-kB/Bcl-2 pathway	1.627E-02	2	41	1.79
22	Apoptosis and survival_Apoptotic TNF-family pathways	1.704E-02	2	42	1.77
23	Signal transduction_AKT signaling	1.781E-02	2	43	1.75
24	Cell adhesion_Ephrin signaling	1.941E-02	2	45	1.71
25	Neurophysiological process_Receptor-mediated axon growth repuls	1.941E-02	2	45	1.71
26	Mechanisms of CFTR activation by S-nitrosoglutathione (normal an	2.023E-02	2	46	1.69
27	Signal transduction_PTEN pathway	2.023E-02	2	46	1.69
28	Development_WNT5A signaling	2.023E-02	2	46	1.69
29	ATP/ITP metabolism	2.025E-02	3	122	1.69
30	Some pathways of EMT in cancer cells	2.455E-02	2	51	1.61
31	G-protein signaling_Proinsulin C-peptide signaling	2.546E-02	2	52	1.59
32	Muscle contraction_ACM regulation of smooth muscle contraction	2.922E-02	2	56	1.53
33	Muscle contraction_Regulation of eNOS activity in endothelial cells	3.735E-02	2	64	1.43
34	Cell adhesion_Role of CDK5 in cell adhesion	4.226E-02	1	9	1.37
35	Muscle contraction_GPCRs in the regulation of smooth muscle tone	5.958E-02	2	83	1.22
36	CFTR folding and maturation (norm and CF)	6.497E-02	1	14	1.19
37	GTP-XTP metabolism	6.868E-02	2	90	1.16
38	DNA damage_Role of SUMO in p53 regulation	7.835E-02	1	17	1.11
39	Cell adhesion_Chemokines and adhesion	8.242E-02	2	100	1.08
40	Transcription_Assembly of RNA Polymerase II preinitiation complex	8.277E-02	1	18	1.08
41	Cytoskeleton remodeling_Cytoskeleton remodeling	8.526E-02	2	102	1.07
42	Development_Alpha-1 adrenergic receptors signaling via cAMP	8.717E-02	1	19	1.06
43	Cytoskeleton remodeling_Role of Activin A in cytoskeleton remodeli	9.154E-02	1	20	1.04
44	CTP/UTP metabolism	9.397E-02	2	108	1.03
45	Cell cycle_Chromosome condensation in prometaphase	9.590E-02	1	21	1.02
46	Transcription_Role of heterochromatin protein 1 (HP1) family in tran	1.002E-01	1	22	1.00
47	Proteolysis_Putative ubiquitin pathway	1.045E-01	1	23	0.98
48	Immune response_IL-15 signaling via JAK-STAT cascade	1.045E-01	1	23	0.98
49	Cell adhesion_Endothelial cell contacts by non-junctional mechanis	1.088E-01	1	24	0.96
50	Translation_Opioid receptors in regulation of translation	1.088E-01	1	24	0.96

Supplemental Table S4 (Continued), related to Figure 9-11, Znf335 ChIP-Seq Pathways. GeneGo pathway analysis of all genes that Znf335 was bound to in developing mouse E14.5 lateral telencephalon.

Supplementary Table S5

GeneGo Microarray Pathway Analysis

#	Maps	Ratio	pValue
1	Cytoskeleton remodeling_TGF, WNT and cytoskeletal remodeling	52	1.863E-13
2	Cytoskeleton remodeling_Cytoskeleton remodeling	43	1.496E-09
3	Development_Role of HDAC and calcium/calmodulin-dependent kin	28	4.155E-09
4	Some pathways of EMT in cancer cells	27	4.337E-09
5	Signal transduction_Activation of PKC via G-Protein coupled recept	27	7.575E-09
6	Development_WNT signaling pathway. Part 2	27	1.297E-08
7	Cell adhesion_Histamine H1 receptor signaling in the interruption of	24	2.617E-08
8	Transport_Clathrin-coated vesicle cycle	31	1.107E-07
9	Signal transduction_PKA signaling	25	1.197E-07
10	Cell adhesion_Integrin-mediated cell adhesion and migration	24	1.327E-07
11	Protein folding and maturation_POMC processing	18	1.335E-07
12	Development_IGF-1 receptor signaling	25	1.937E-07
13	Immune response_Gastrin in inflammatory response	30	1.985E-07
14	Immune response_Innate immune response to RNA viral infection	17	2.358E-07
15	Development_Hedgehog signaling	23	2.426E-07
16	Immune response_Function of MEF2 in T lymphocytes	24	3.533E-07
17	Development_PIP3 signaling in cardiac myocytes	23	3.993E-07
18	Immune response_CD40 signaling	28	6.372E-07
19	Development_S1P1 receptor signaling via beta-arrestin	18	9.554E-07
20	Development_Melanocyte development and pigmentation	23	1.022E-06
21	Cell adhesion_Chemokines and adhesion	37	1.087E-06
22	Signal transduction_AKT signaling	21	1.335E-06
23	Neurophysiological process_Corticoliberin signaling via CRHR1	23	1.591E-06
24	Immune response_IFN gamma signaling pathway	24	2.036E-06
25	Transcription_Androgen Receptor nuclear signaling	21	3.390E-06
26	Cell adhesion_ECM remodeling	23	3.675E-06
27	G-protein signaling_Regulation of p38 and JNK signaling mediated	19	4.472E-06
28	Signal transduction_PTEN pathway	21	5.249E-06
29	Blood coagulation_GPCRs in platelet aggregation	28	5.264E-06
30	Immune response_IFN alpha/beta signaling pathway	14	5.501E-06
31	Development_Glucocorticoid receptor signaling	14	5.501E-06
32	Development_Mu-type opioid receptor signaling via Beta-arrestin	14	5.501E-06
33	Development_GM-CSF signaling	22	6.628E-06
34	Cardiac Hypertrophy_NF-AT signaling in Cardiac Hypertrophy	26	8.374E-06
35	Development_WNT signaling pathway. Part 1. Degradation of beta-	12	8.413E-06
36	G-protein signaling_RhoA regulation pathway	17	9.173E-06
37	Signal transduction_cAMP signaling	18	1.312E-05
38	G-protein signaling_Proinsulin C-peptide signaling	22	1.430E-05
39	Development_Angiopietin - Tie2 signaling	17	1.504E-05
40	Cytoskeleton remodeling_Regulation of actin cytoskeleton by Rho G	13	1.925E-05
41	Development_Regulation of epithelial-to-mesenchymal transition (E	25	2.026E-05
42	Cell cycle_Influence of Ras and Rho proteins on G1/S Transition	22	2.058E-05
43	Development_TGF-beta-dependent induction of EMT via RhoA, PI3	20	2.153E-05
44	Development_VEGF signaling and activation	19	2.614E-05
45	Translation_Non-genomic (rapid) action of Androgen Receptor	18	3.147E-05
46	Cytoskeleton remodeling_Role of PKA in cytoskeleton reorganisatio	18	3.147E-05
47	Regulation of lipid metabolism_Insulin signaling:generic cascades	20	3.156E-05
48	Development_TGF-beta-dependent induction of EMT via MAPK	20	3.156E-05
49	Apoptosis and survival_Anti-apoptotic TNFs/NF-kB/IAP pathway	14	3.388E-05
50	Development_Gastrin in cell growth and proliferation	24	3.524E-05

Supplemental Table S5 (Continued), related to Figure 9-11, Pathway analysis of Znf335 knockdown microarray data. GeneGo pathway analysis of all genes that were altered upon knockdown of Znf335 in the E14.5 mouse lateral telencephalon.

Supplementary Table S6

GeneGo RNA-Seq Pathway Analysis

#	Maps	Ratio	min(pValue)
1	Development_Delta- and kappa-type opioid receptors signaling via	5	1.008E-04
2	Apoptosis and survival_Endoplasmic reticulum stress response patt	7	1.172E-04
3	Proteolysis_Role of Parkin in the Ubiquitin-Proteasomal Pathway	5	1.251E-04
4	Cytoskeleton remodeling_Neurofilaments	5	1.755E-03
5	Development_Angiotensin signaling via beta-Arrestin	4	1.755E-03
6	Translation_Regulation of translation initiation	4	2.355E-03
7	Regulation of lipid metabolism_Stimulation of Arachidonic acid prod	5	2.367E-03
8	Cell adhesion_Gap junctions	4	3.500E-03
9	Development_Glucocorticoid receptor signaling	3	3.541E-03
10	Regulation of degradation of deltaF508 CFTR in CF	2	4.472E-03
11	Development_WNT signaling pathway. Part 2	5	5.142E-03
12	Cytoskeleton remodeling_Keratin filaments	4	6.817E-03
13	Cardiac Hypertrophy_Ca(2+)-dependent NF-AT signaling in Cardiac	6	7.010E-03
14	Mechanisms of CFTR activation by S-nitrosoglutathione (normal an	3	1.262E-02
15	Development_Hedgehog signaling	4	1.604E-02
16	Chemotaxis_Leukocyte chemotaxis	5	2.132E-02
17	Apoptosis and survival_Role of IAP-proteins in apoptosis	3	2.738E-02
18	Cell cycle_Role of Nek in cell cycle regulation	3	2.975E-02
19	Immune response_IL-22 signaling pathway	3	3.223E-02
20	Development_S1P1 receptor signaling via beta-arrestin	3	3.223E-02
21	Oxidative stress_Role of ASK1 under oxidative stress	3	3.481E-02
22	Chemotaxis_CXCR4 signaling pathway	4	3.481E-02
23	Immune response_Antigen presentation by MHC class II	1	4.392E-02
24	Cardiac Hypertrophy_NF-AT signaling in Cardiac Hypertrophy	5	4.893E-02
25	CFTR folding and maturation (norm and CF)	1	5.106E-02
26	Apoptosis and survival_Apoptotic TNF-family pathways	3	5.912E-02
27	Cytoskeleton remodeling_TGF, WNT and cytoskeletal remodeling	4	6.410E-02
28	Regulation of degradation of wt-CFTR	1	6.518E-02
29	Transcription_Assembly of RNA Polymerase II preinitiation complex	2	6.518E-02
30	Immune response_MIF - the neuroendocrine-macrophage connect	3	7.359E-02
31	Immune response_ICOS pathway in T-helper cell	3	7.359E-02
32	Atherosclerosis_Role of ZNF202 in regulation of expression of gene	1	7.563E-02
33	Neurophysiological process_Dopamine D2 receptor signaling in CN	3	7.743E-02
34	Transcription_Role of heterochromatin protein 1 (HP1) family in tran	2	7.850E-02
35	Cytoskeleton remodeling_ESR1 action on cytoskeleton remodeling	2	7.909E-02
36	Immune response_IL-12 signaling pathway	3	8.254E-02
37	Proteolysis_Putative ubiquitin pathway	2	8.254E-02
38	Immune response_MIF-JAB1 signaling	2	8.597E-02
39	Glycolysis and gluconeogenesis p.3 / Human version	2	8.597E-02
40	Glycolysis and gluconeogenesis p.3	2	8.597E-02
41	Development_Signaling of Beta-adrenergic receptors via Beta-arres	2	9.280E-02
42	Immune response_NFAT in immune response	3	9.365E-02
43	Transcription_Role of Akt in hypoxia induced HIF1 activation	1	9.620E-02
44	Immune response_T cell receptor signaling pathway	3	9.790E-02
45	Cell adhesion_ECM remodeling	3	9.790E-02
46	Cell cycle_Transition and termination of DNA replication	2	9.959E-02
47	Apoptosis and survival_nAChR in apoptosis inhibition and cell cycle	2	1.030E-01
48	Development_Osteopontin signaling in osteoclasts	2	1.063E-01
49	Cytoskeleton remodeling_RalA regulation pathway	2	1.063E-01
50	Immune response_Th17 cell differentiation	2	1.097E-01

Supplemental Table S6 (Continued), related to Figures 9-11, Pathway analysis of RNA-Seq data from patients vs. controls. GeneGo pathway analysis of all genes that were altered from the RNA-sequencing datasets of the homozygous patients, heterozygous parents, vs. controls.

Supplementary Table S7

GeneGo COMBINED Pathway and Processes Analysis

#	Maps	min(pValue)	Ratio	
1	Cytoskeleton remodeling_TGF, WNT and cytoskeletal remodeling	1.835E-06	19	111
2	Cytoskeleton remodeling_Cytoskeleton remodeling	4.405E-06	17	102
3	Proteolysis_Role of Parkin in the Ubiquitin-Proteasomal Pathway	1.221E-04	7	24
4	Development_WNT signaling pathway, Part 2	4.979E-04	11	53
5	Cell adhesion_Chemokines and adhesion	5.550E-04	13	100
6	PGE2 pathways in cancer	5.917E-04	11	55
7	Development_Angiotensin signaling via beta-Arrestin	1.722E-03	9	25
8	Cytoskeleton remodeling_FAK signaling	2.109E-03	10	57
9	Immune response_TREM1 signaling pathway	2.519E-03	10	59
10	Regulation of lipid metabolism_Stimulation of Arachidonic acid production by ACM receptors	2.932E-03	10	72
11	Development_Glucocorticoid receptor signaling	4.095E-03	6	24
12	Oxidative stress_Role of ASK1 under oxidative stress	8.604E-03	6	34
13	Immune response_Immunological synapse formation	1.230E-02	8	59
14	Immune response_MIF-JAB1 signaling	1.806E-02	6	24
15	Immune response_HSP60 and HSP70/TLR signaling pathway	1.969E-02	7	54
16	Immune response_IL-22 signaling pathway	3.180E-02	6	33
17	Immune response_T cell receptor signaling pathway	3.350E-02	8	52
18	CFTR folding and maturation (norm and CF)	5.484E-02	2	14
19	Transcription_Assembly of RNA Polymerase II preinitiation complex on TATA-less promoters	6.997E-02	3	18
20	Immune response_ICOS pathway in T-helper cell	7.269E-02	6	46
21	Apoptosis and survival_Apoptotic TNF-family pathways	9.674E-02	6	42
22	Cell cycle_Transition and termination of DNA replication	1.068E-01	5	28
#	Processes	min(pValue)	Ratio	
1	cellular process	2.943E-14	1269	15610
2	negative regulation of cellular process	5.087E-11	374	3413
3	cellular localization	7.578E-11	253	1960
4	establishment of localization in cell	9.274E-11	230	1711
5	regulation of cell communication	2.811E-10	222	1835
6	negative regulation of biological process	3.840E-10	397	3756
7	localization	7.281E-10	503	4755
8	positive regulation of biological process	3.319E-09	435	4208
9	regulation of multicellular organismal process	3.506E-08	262	2323
10	regulation of response to stimulus	5.942E-08	315	2853
11	regulation of signal transduction	3.503E-07	243	2131
12	regulation of developmental process	1.637E-06	199	1846
13	nervous system development	2.001E-06	240	2298

Supplemental Table S7 (Continued), related to Figures 9-11, Pathway analysis of data from Microarray, ChIP-Seq, and RNA-Seq combined.
GeneGo pathway analysis of all genes that were altered from all datasets combined.

APPENDIX

The Cerebrospinal Fluid Provides a Proliferative Niche for Neural Progenitor Cells

The Cerebrospinal Fluid Provides a Proliferative Niche for Neural Progenitor Cells

Maria K. Lehtinen,^{1,2,9} Mauro W. Zappaterra,^{1,2,3,9} Xi Chen,^{1,2,4} Yawei J. Yang,^{1,2,3,4} Anthony D. Hill,^{1,2} Melody Lun,^{1,2,6} Thomas Maynard,⁵ Dilenny Gonzalez,^{1,2} Seonhee Kim,⁸ Ping Ye,⁷ A. Joseph D'Ercole,⁷ Eric T. Wong,⁶ Anthony S. LaMantia,⁵ and Christopher A. Walsh^{1,2,3,*}

¹Division of Genetics, Howard Hughes Medical Institute, and Manton Center for Orphan Disease Research, Children's Hospital Boston, Boston, MA 02115, USA

²Broad Institute of MIT and Harvard, Cambridge, MA 02142, USA

³Program in Biological and Biomedical Sciences, Harvard Medical School, Boston, MA 02115, USA

⁴Harvard-MIT Division of Health Sciences and Technology, Harvard Medical School, Boston, MA 02115, USA

⁵Department of Pharmacology and Physiology, The George Washington Institute for Neuroscience, The George Washington University School of Medicine, Washington, DC 20037, USA

⁶Brain Tumor Center & Neuro-Oncology Unit, and Division of Signal Transduction, Beth Israel Deaconess Medical Center, Boston, MA 02215, USA

⁷Department of Pediatrics, The University of North Carolina at Chapel Hill, Chapel Hill, NC 27599, USA

⁸Pediatric Research Center, Department of Pediatrics, University of Texas Health Science Center at Houston, MSE411, 6431 Fannin Street, Houston, TX 77030, USA

⁹These authors contributed equally to this work

*Correspondence: christopher.walsh@childrens.harvard.edu

DOI 10.1016/j.neuron.2011.01.023

SUMMARY

Cortical development depends on the active integration of cell-autonomous and extrinsic cues, but the coordination of these processes is poorly understood. Here, we show that the apical complex protein Pals1 and Pten have opposing roles in localizing the Igf1R to the apical, ventricular domain of cerebral cortical progenitor cells. We found that the cerebrospinal fluid (CSF), which contacts this apical domain, has an age-dependent effect on proliferation, much of which is attributable to Igf2, but that CSF contains other signaling activities as well. CSF samples from patients with glioblastoma multiforme show elevated Igf2 and stimulate stem cell proliferation in an Igf2-dependent manner. Together, our findings demonstrate that the apical complex couples intrinsic and extrinsic signaling, enabling progenitors to sense and respond appropriately to diffusible CSF-borne signals distributed widely throughout the brain. The temporal control of CSF composition may have critical relevance to normal development and neuro-pathological conditions.

INTRODUCTION

Neural development involves a dynamic interplay between cell autonomous and diffusible extracellular signals that regulate symmetric and asymmetric division of progenitor cells (Johansson et al., 2010). In mammalian neural progenitors, homologs of *C. elegans* and *Drosophila* polarity proteins,

including Par3 (partitioning defective protein 3) and Pals1 (protein associated with Lin 7), assemble as apical complexes that play essential roles in regulating self-renewal and cell fate (Margolis and Borg, 2005). The unequal distribution of apical surface components during mitosis is a key determinant of daughter cell fate in *C. elegans* and *Drosophila* (Fishell and Kriegstein, 2003; Kemphues, 2000; Siller and Doe, 2009; Wodarz, 2005). Recently, mammalian Par3 was shown to promote asymmetric cell division by specifying differential Notch signaling in radial glial daughter cells (Bultje et al., 2009), suggesting that the inheritance of the apical complex guides progenitor responses to proliferative signals as well.

Secreted signals can act at a distance to guide decisions governing progenitor proliferation and cell fate (Johansson et al., 2010), but little is known of how secreted signals interact with cell-autonomous ones. Insulin-like growth factor 1 (Igf1) promotes progenitor proliferation (Hodge et al., 2004; Popken et al., 2004). Insulin/Igf1 signaling is regulated by E-catenin in keratinocytes (Vasioukhin et al., 2001) and β -catenin in oligodendrocyte progenitors (Ye et al., 2010), suggesting that cell polarity proteins govern cellular responses to extrinsic cues.

Direct interactions between Par3 and Pten (phosphatase and tensin homolog) (Feng et al., 2008; Pinal et al., 2006; von Stein et al., 2005; Wu et al., 2007) suggest that the apical complex interacts with growth factor signaling pathways. Indeed, disrupting the apical complex via *Pals1* leads to attenuated pS6 signaling, premature cell cycle exit, and rapid cell death, resulting in the absence of nearly the entire cerebral cortex (Kim et al., 2010). In turn, *Pals1*-deficiency can be partially rescued by concomitant activation of mTOR (mammalian target of rapamycin) (Kim et al., 2010), a downstream effector of growth factor signaling. Growth factor signaling, in particular via the type 1 Igf receptor (Igf1R), mediates powerful, age-dependent effects on the development and maintenance of many organ systems

including the brain through the regulation of progenitor cell division (Baker et al., 1993; Hodge et al., 2004; Liu et al., 2009; Popken et al., 2004; Randhawa and Cohen, 2005). Nevertheless, the mechanisms coordinating the availability of Igf ligands to cortical progenitor cells have remained unclear.

Though vascular sources of secreted proliferative signals are well characterized (Palmer et al., 2000; Shen et al., 2004, 2008; Tavazoie et al., 2008), the apical surfaces of early cortical precursors and their primary cilia do not approximate blood vessels but instead directly contact the cerebrospinal fluid (CSF) (Fuchs and Schwark, 2004; Kim et al., 2010), suggesting that secreted factors may interact with progenitor cells at this interface. The CSF proteome shows a complex and dynamic pattern of protein expression (Dziegielewska et al., 1981; Parada et al., 2005; Zappaterra et al., 2007), suggesting important roles beyond provision of a fluid cushion for the central nervous system and maintenance of extracellular ionic balance. The CSF has recently been implicated in carrying secreted proteins in several contexts, including Fgf2 to midbrain progenitors (Martin et al., 2006), Sonic hedgehog to cerebellar progenitors (Huang et al., 2010) and Slit guidance of neuroblasts in adult brain (Sawamoto et al., 2006). Regulation of cerebral cortical progenitor cells by growth factors distributed in the lateral ventricular CSF would provide potentially global control over cerebral cortical neurogenesis, but this hypothesis has not been examined.

Here, we show that the apical complex couples autonomous regulation of progenitor proliferation to CSF-borne signals in the developing cerebral cortex. *Pals1* and *Pten* interact genetically to regulate cerebral cortical size and progenitor proliferation and have opposing roles in localizing the Igf1R to the apical domain of cortical progenitors. Apically localized Igf1Rs respond to CSF-borne Igf ligands, particularly Igf2, and CSF regulates cortical progenitor proliferation in an Igf2-dependent fashion. Finally, CSF Igf2 concentration is elevated in patients with malignant glioblastoma, suggesting that CSF proteins may regulate CNS tumorigenesis. Our findings suggest that the apical complex couples autonomous and extrinsic signaling in cerebral cortical progenitors, enabling these cells to respond appropriately to diffusible CSF-borne signals that regulate cortical neural stem cells during development and disease.

RESULTS

Genetic Interactions of *Pals1* and *Pten* at the Apical Surface Region

Since *Pals1* loss disrupts growth factor signaling and cortical development (Kim et al., 2010), we looked for potential interactions of *Pals1* with other regulators of growth factor signaling and found genetic interactions between *Pals1* and *Pten* (Groszer et al., 2001). Cerebral cortex-specific deletion of *Pals1* was achieved by crossing mice with a conditional *Pals1* allele (*Pals1^{loxP/loxP}*) (Kim et al., 2010) with mice carrying *Emx1*-promoter-driven Cre recombinase (*Emx1Cre^{+/-}*) (Gorski et al., 2002). *Pals1^{loxP/loxP}/Emx1Cre^{+/-}* mice lacked nearly the entire cortical structure due to premature cell cycle exit and cell death (Kim et al., 2010), with heterozygotes having an intermediate phenotype (Figure 1A). In contrast, *Pten* deficiency, obtained by crossing *Pten^{loxP/loxP}* mice (Groszer et al., 2001) with either

Emx1Cre^{+/-} or *NestinCre^{+/-}* mice, resulted in cortical hyperplasia arising from excessive and extended proliferation of apical progenitors (Figure 1A; see Figures S1A–S1E available online; Groszer et al., 2001). While the broadest groupings of cells were preserved in *Pten* mutants, the cortical plate was disorganized across its entire radial extent (Figures S1A–S1C). No phenotypic abnormalities were observed in either heterozygous *Pten^{loxP/loxP}/NestinCre^{+/-}* mice or in *Pten^{loxP/loxP}/NestinCre^{-/-}* littermate controls (Figure S1A and data not shown). Conditional deletion of *Pten* in the *Pals1^{loxP/+}/Emx1Cre^{+/-}* mice resulted in an almost normal cortical size (Figure 1A). Histological analyses of *Pals1^{loxP/+}/Emx1Cre^{+/-}* mice or *Pten^{loxP/+}/Pals1^{loxP/+}/Emx1Cre^{+/-}* mice revealed a severely disrupted laminar organization of the dorsomedial cortex (Figure 1B; Kim et al., 2010). Double mutants showed a relatively normal organization of the marginal zone (Figure 1B), consistent with a genetic interaction between the apical complex and *Pten*. The expression of apical complex components, especially *Cdc42*, were abnormal in *Pten* cortex (Figure S1F and data not shown). The proportion of proliferative progenitor cells marked by Ki67-positive staining cells was greater in the double mutant cortex compared to conditional *Pals1* heterozygotes (Figure 1C) and brain size was also more normal by embryonic day (E) 14.5 (Figures S1G and S1H). Proportions of early-born neurons marked by *Tbr1* and *Ctip2* were also more normal in the *Pten^{loxP/loxP}/Pals1^{loxP/+}/Emx1Cre^{+/-}* mice than in either *Pals1* or *Pten* mutants alone (Figure 1D and data not shown). However, cells in the double mutant brain appeared irregular in size and lamination (Figure 1D), a finding consistent with roles for *Pten* in the regulation of cell size and polarity (Figure S1C; Chalhouh et al., 2009; Groszer et al., 2001) and with a role for *Pten* downstream of the apical complex.

The genetic interaction between *Pals1* and *Pten* and the decreased proliferation of progenitors and prominent cell death in *Pals1* mutants (Kim et al., 2010) prompted us to test whether the apical complex interacts with Igf signaling, since Igfs play a prominent role in cell cycle kinetics of cortical progenitors, cell survival, and brain size (Hodge et al., 2004; Liu et al., 2009; Popken et al., 2004; Schubert et al., 2003). The Igf1R, which binds both Igf1 and Igf2, mediates the proliferative response to Igf signaling (Weber et al., 1992). Surprisingly, Igf1R was enriched in cortical progenitors at the apical, ventricular surface, interdigitating with β -catenin (Figures 2A–2D), suggesting the apical region as the likely site for binding of Igf1R ligand. Apical Igf1R expression was strikingly decreased in *Pals1^{loxP/loxP}/Emx1Cre^{+/-}* mice (Figure 2E). By contrast in the absence of *Pten*, Igf1R immunoreactivity demonstrated a considerable basolateral spread in clusters of radial glia (Figure 2F and data not shown). Analyses of downstream signaling events, using a specific antibody against the phosphorylated form of Rsk substrate S6 ribosomal protein (phospho-S6rp), revealed an apical pattern of activity within control brains (Figure 2G). In contrast in *Pten* mutants, phospho-S6rp showed a broad distribution across the cortical tissue, with many robust phospho-S6rp-positive cells extending basally away from the lateral ventricle (Figure 2G). While the majority of cells positive for Igf1R were clearly apical progenitors, some upregulation of Igf1R in basal progenitors is possible. Though we cannot rule

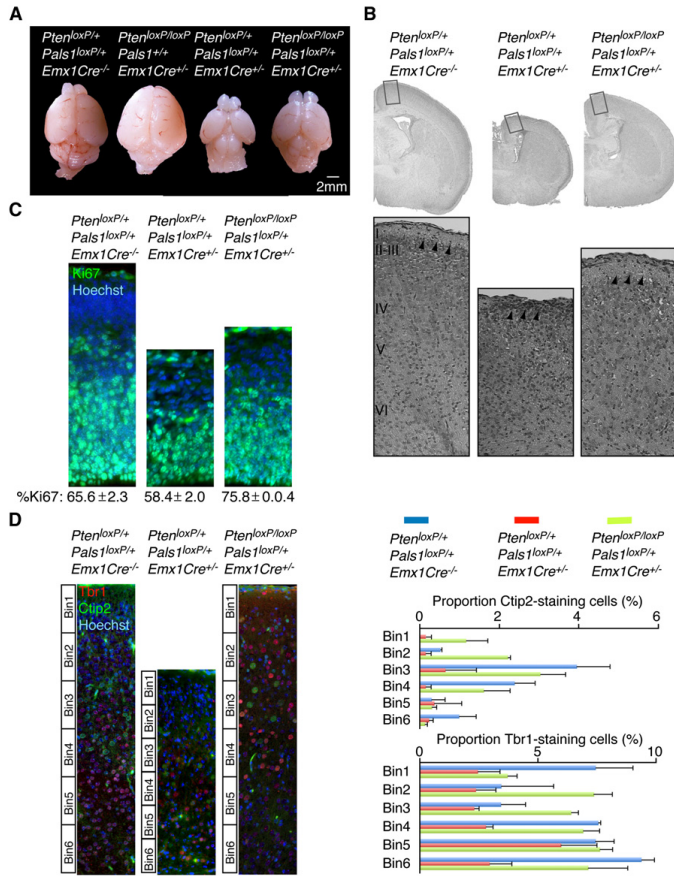


Figure 1. The Apical Complex and *Pten* Modulate Brain Size

(A) Conditional *Pten* deletion (*Pten^{loxP/loxP}/Pals1^{loxP/+}/Emx1Cre^{+/-}*) resulted in hyperplasia and an enlarged cerebral cortex. Ablation of *Pten* in *Pten^{loxP/loxP}/Pals1^{loxP/+}/Emx1Cre^{+/-}* mice largely restored the small brain phenotype of *Pten^{loxP/+}/Pals1^{loxP/+}/Emx1Cre^{+/-}* neonates.

(B) H&E staining of *Pten^{loxP/+}/Pals1^{loxP/+}/Emx1Cre^{-/-}*, *Pten^{loxP/+}/Pals1^{loxP/+}/Emx1Cre^{+/-}*, and *Pten^{loxP/loxP}/Pals1^{loxP/+}/Emx1Cre^{+/-}* neonates. Arrowheads point to marginal zone.

(C) The proportion of Ki67-positive staining progenitors was restored in the E14.5 *Pten^{loxP/loxP}/Pals1^{loxP/+}/Emx1Cre^{-/-}* cortex compared to *Pten^{loxP/+}/Pals1^{loxP/+}/Emx1Cre^{-/-}* (percent Ki67-positive staining cells \pm SEM; *Pten^{loxP/+}/Pals1^{loxP/+}/Emx1Cre^{-/-}*, 65.6 ± 2.3 ; *Pten^{loxP/+}/Pals1^{loxP/+}/Emx1Cre^{+/-}*, 58.4 ± 2.0 ; *Pten^{loxP/loxP}/Pals1^{loxP/+}/Emx1Cre^{+/-}*, 75.8 ± 0.4 ; ANOVA, $p < 0.01$, $n = 3$).

(D) Left panels: representative images of Ctip2-positive and Tbr1-positive staining neurons analyzed in *Pten^{loxP/+}/Pals1^{loxP/+}/Emx1Cre^{-/-}*, *Pten^{loxP/+}/Pals1^{loxP/+}/Emx1Cre^{+/-}*, and *Pten^{loxP/loxP}/Pals1^{loxP/+}/Emx1Cre^{+/-}* neonates. Right panels: the cortical plate was subdivided into six equal bins and Ctip2 and Tbr1 positive cells quantified per bin are expressed as percent of total cells per bin. *Pten* deletion in the *Pten^{loxP/loxP}/Pals1^{loxP/+}/Emx1Cre^{+/-}* mice restored the proportions of early-born cells marked by Tbr1 and Ctip2 (percent positive staining cells/total: *Pten^{loxP/+}/Pals1^{loxP/+}/Emx1Cre^{-/-}* Ctip2 = 8.13 ± 2.0 , Tbr1 = 38.7 ± 2.4 ; *Pten^{loxP/+}/Pals1^{loxP/+}/Emx1Cre^{+/-}* Ctip2 = 1.6 ± 1.2 , Tbr1 = 18.8 ± 3.1 ; *Pten^{loxP/loxP}/Pals1^{loxP/+}/Emx1Cre^{+/-}* Ctip2 = 8.5 ± 1.6 , Tbr1 = 39.1 ± 2.6 ; ANOVA, $p < 0.05$, $n = 3$). See also Figure S1.

out that *Pals1* and *Pten* could function independently to regulate Igf signaling and cortical growth, we interpret our data to suggest that within the cortical ventricular zone, *Pals1* and *Pten* spatially restrict IgfR expression and Igf signaling to the apical membrane domain.

Loss and gain of Igf signaling in mutant mice produced phenotypes similar to those seen when apical complex signaling is disrupted. Mice with Igf1R deficiency limited to neural precursors (*Igf1R^{loxP/loxP}/NestinCre^{+/-}*) were microcephalic (Figure 2H–2J; Kappeler et al., 2008; Liu et al., 2009) and had a reduced frequency of phospho-Histone H3 (PH3, a marker of cell division) proliferative progenitors in the ventricular zone (PH3-positive cells/100 μ m VZ \pm SEM at E16.5: control, 2.9 ± 0.3 ; *Igf1R^{loxP/loxP}/NestinCre^{+/-}*, 1.7 ± 0.1 ; unpaired t test, $p < 0.01$; $n = 4$ and $n = 3$, respectively). We did not observe differences in progenitor cell survival at the ventricular zone in these mice as assessed by cleaved caspase 3 (CC3) immunoreactivity (data not shown). Conversely, mice with increased Igf activity

(Igf1 expressed from the human GFAP promoter) were macrocephalic (data not shown) (Ye et al., 2004) and had increased proliferative progenitors at the ventricular surface (PH3-positive cells/100 μ m VZ \pm SEM at E18.5: control, 0.9 ± 0.08 ; *Igf1_Tg*, 1.2 ± 0.07 ; unpaired t test, $p < 0.05$, $n = 3$ and $n = 4$, respectively). Together with published work demonstrating that *Insulin receptor substrate 2* (*Irs2*) deletion leads to microcephaly (Schubert et al., 2003), these data suggest that Igf signaling in cortical progenitors, facilitated at the apical surface via *Pals1* and an intact apical complex, regulates cortical development.

CSF-Borne Igf Signaling

The normal apical localization of the Igf1R, and the fact that we did not observe *Igf1* or *Igf2* mRNA in neural progenitor cells by in situ hybridization (Figures 3A, 3B, and data not shown; Ayer-Lievre et al., 1991), suggested that progenitor cells may be exposed to Igfs derived from the lateral ventricle CSF. We confirmed the presence of Igf2 in an unbiased tandem mass

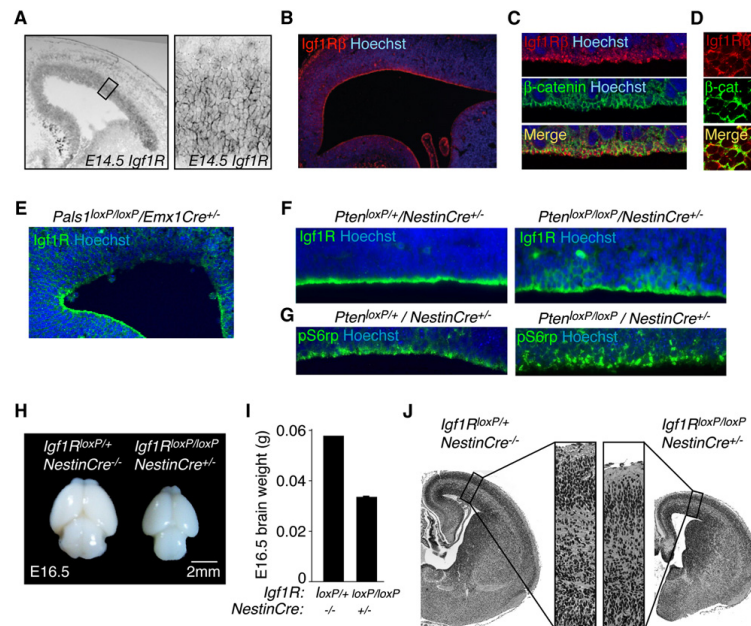


Figure 2. Igf1R Expression in Cortical Progenitor Cells

(A) Left panel: *Igf1R* in situ hybridization at E14.5 mouse. Right panel: high-magnification image of area denoted in left panel.
 (B) Igf1R enriched along the ventricular surface of E17 rat cortex.
 (C) Confocal images of Igf1Rβ and β-catenin immunostaining in rat E17 ventricular zone.
 (D) En face view of the mouse E16.5 ventricular zone immunostained with Igf1Rβ and β-catenin.
 (E) Ventricular Igf1R expression was disrupted in E12.5 *Pals1^{loxP/loxP}/Emx1Cre^{+/+}* controls.
 (F) Left panel: Igf1R expression was enriched along the apical, ventricular zone of E14.5 *Pten^{loxP/loxP}/NestinCre^{+/-}* controls. Right panel: Igf1R expression expanded basolaterally in *Pten^{loxP/loxP}/NestinCre^{+/-}* radial glia.
 (G) Left panel: pS6rp activity along the ventricular progenitors of E14.5 *Pten^{loxP/loxP}/NestinCre^{+/-}* controls. Right panel: pS6rp localization extended basolaterally in *Pten^{loxP/loxP}/NestinCre^{+/-}* radial glia. See also Figure S1.
 (H) *Igf1R* deficiency in NestinCre expressing cells diminished brain size at E16.5.
 (I) Brain weights of *Igf1R^{loxP/loxP}/NestinCre^{+/-}* and controls at E16.5 (brain weight (g) ± SEM: *Igf1R^{loxP/loxP}/NestinCre^{+/-}*: 0.06; *Igf1R^{loxP/loxP}/NestinCre^{+/-}*: 0.03 ± 0.001; n = 2 [+/-], n = 3 [-/-]).
 (J) H&E staining of brains shown in (H).

spectrometry (LC-MS/MS) analysis of CSF (Table S1; Binoux et al., 1986) and detected Igf1 in CSF by ELISA (E14 CSF [Igf1], 72.2 ng/ml, n = 2; E17 CSF [Igf1], 69.6 ng/ml; adult CSF [Igf1], 68.8 ng/ml, n = 3). Igf1 expression in the CSF remained stable across the ages sampled (see above). In contrast, expression of Igf2 in rat CSF was temporally dynamic; it peaked during periods of neurogenesis and declined in adulthood (Figure 3C). High levels of *Igf2* mRNA expression by the choroid plexus suggested this as a source of CSF Igf2 (Figure 3B), and quantitative PCR revealed that rat choroid plexus expressed 10.7-fold more Igf2 than its cortical counterpart at E17 (data not shown). We confirmed that Igf2 mRNA was also expressed in vascular endothelial cells, and leptomeninges in the rat embryo at E14 and E17 as well as pericytes at E17 (Figures 3A, 3B, and data not shown; Bondy et al., 1992; Dugas et al., 2008; Stylianopoulou et al., 1988), suggesting that extrachori-

dal sources of Igf2 may contribute to CSF-Igf2 content as well. Immunogold labeling revealed Igf2 binding to progenitors along the apical, ventricular surface (Figure 3D). Moreover, Igf2 binding to progenitors was highly enriched along primary cilia (Figure 3E), which extend directly into the ventricular space (Figure 3F; Cohen et al., 1988). We did not observe enriched Igf2 binding beyond the apical surface of ventricular zone progenitor cells (data not shown). Thus, the robust expression of Igf2 by the choroid plexus and the apical binding of Igf2 to progenitors along the ventricular zone strongly suggest that the CSF distributes choroid plexus secreted Igf2 to cortical progenitor cells.

Purified rat E17 CSF directly stimulated Igf1R mediated signaling activity, reflected by Igf1Rβ phosphorylation as well as phosphorylation of Akt and MAPK (Figure 3G), two downstream targets of Igf signaling as well as other growth factors that may be present in CSF. Igf2 treatment by itself induced Igf

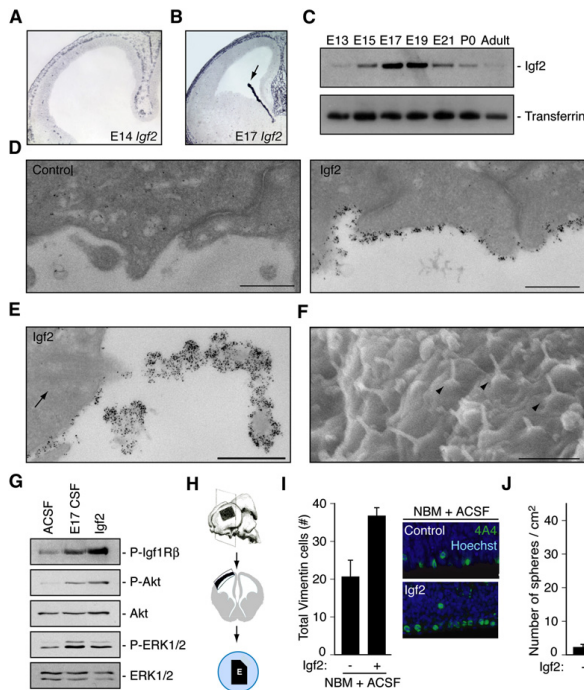


Figure 3. Igf2 Is Expressed in Cerebrospinal Fluid and Stimulates Progenitor Proliferation

(A and B) *Igf2* in situ hybridization of rat E14 and E17 cortex. Arrow points to choroid plexus.

(C) Transient *Igf2* expression in rat CSF.

(D) Immunogold labeling of endogenous *Igf2* in E17 rat brain. Left panel: no primary control. Right panel: *Igf2* binding to ventricular surface of cortical progenitors. Scale bar represents 500 nm.

(E) *Igf2* binding to primary cilium of cortical progenitor cell. Arrow points to ciliary basal body. Scale bar represents 500 nm.

(F) Scanning EM of mouse ventricular surface at E12.5. Arrowheads point to primary cilia projecting into the ventricular space. Scale bar represents 2 μ m.

(G) Lysates of cortical cells deprived of growth factors for 6 hr and treated with ACSF, E17 CSF, or *Igf2* for 5 min were immunoblotted with antibodies to P-Igf1R, P-Akt, Akt, P-ERK1/2, and ERK1/2.

(H) Schematic of cortical explant dissections: explant placed on membrane with ventricular side down contacting CSF and notch making medial-caudal side.

(I) Left panel: E16 explants cultured with NBM plus 20% ACSF (control) or with supplemental *Igf2* immunostained with anti-Vimentin 4A4 and Hoechst represented as mean \pm SEM (*Igf2* mean, 36.7 ± 2.1 ; control mean, 20.4 ± 4.46 ; $n = 8$; Mann-Whitney; $p < 0.005$). Vimentin 4A4-positive cells increased in explants cultured with *Igf2* compared to control. Right panels: representative images of explants quantified in left panels.

(J) Single cells dissociated from primary neurospheres cultured in control media or control media containing *Igf2* (20 ng/ml). *Igf2* stimulated secondary sphere formation after 10 DIV (*Igf2* mean, 39.3 ± 4.1 ; control mean, 2.2 ± 0.75 ; $n = 3$; t test; $p < 0.005$). See also Table S1.

signaling similar to embryonic CSF (Figure 3G). *Igf2* binding to progenitors, the localization of the *Igf1R*, its phosphorylation, as well as the phosphorylation of its downstream targets Akt and MAPK in response to CSF, strongly suggest that the CSF is a primary source of *Igf* ligands for cerebral cortical neuroepithelial cells, although additional sources cannot be completely excluded.

We next tested whether *Igf2* supports progenitor proliferation in a cerebral cortical explant system. In this system, rat embryonic cortex dissected from the lateral pallium is placed on polycarbonate membranes and floated on defined media (Figure 3H). We found that *Igf2* added to neurobasal medium (NBM) with 20% artificial CSF (ACSF) stimulated the proliferation of progenitor cells marked by phospho-Vimentin 4A4 in rat cortical explants (Figure 3I; Noctor et al., 2002). In addition, *Igf2* treatment alone maintained GLAST-positive neurospheres, an *in vitro* model of neural stem cells, even in the absence of *Fgf2* (fibroblast growth factor 2) and *Egf* (epidermal growth factor) (Figure 3J; Vescovi et al., 1993). Finally, pharmacologic activation of the signaling pathway with insulin demonstrated that activation of *Igf* signaling by ligands other than *Igf2* is sufficient to stimulate proliferation (PH3-positive cells/100 μ m VZ \pm SEM in E16 rat explant: control mean, 5.6 ± 0.7 ; insulin (10 μ g/ml) mean, 11.2 ± 0.4 ; Mann-Whitney, $p < 0.05$; $n = 6$). Therefore, *Igf* signaling modulates proliferation of isolated

cortical precursors or those maintained in their pallial environment *in vitro*.

CSF Promotes Proliferation of Progenitor Cells in an Age-Dependent Manner

Since the CSF is a complex fluid containing many factors including *Igf* binding proteins that may modulate *Igf2* bioavailability and signaling (Figures 4A and 4B; Table S1; Clemmons, 1997; Zappaterra et al., 2007), we tested whether native CSF alone could support cortical tissue growth. We used a heterochronic “mix-and-match” approach for exposing cortical tissue to CSF collected at different ages. E16 rat cortical explants with intact meninges and vasculature cultured with 100% E17 rat CSF for 24 hr, without any additional exogenous media or factors, retained remarkable tissue architecture, cell viability, and proliferation, approximating *in vivo* E17 rat cortex (Figure 4C). In contrast, E16 explants cultured with 100% artificial CSF failed to thrive, had decreased mitotic activity, disorganized neuronal morphology, and increased cell death (Figures 4C, S2A, and S2B). Filtration analysis of E17 CSF showed that the sizes of CSF factors that support stem cells likely range from 10 kDa–100 kDa, suggesting that they are proteins (Table S2 and data not shown). Thus, the embryonic CSF proteome provides essential growth and survival factors for the developing cortex.

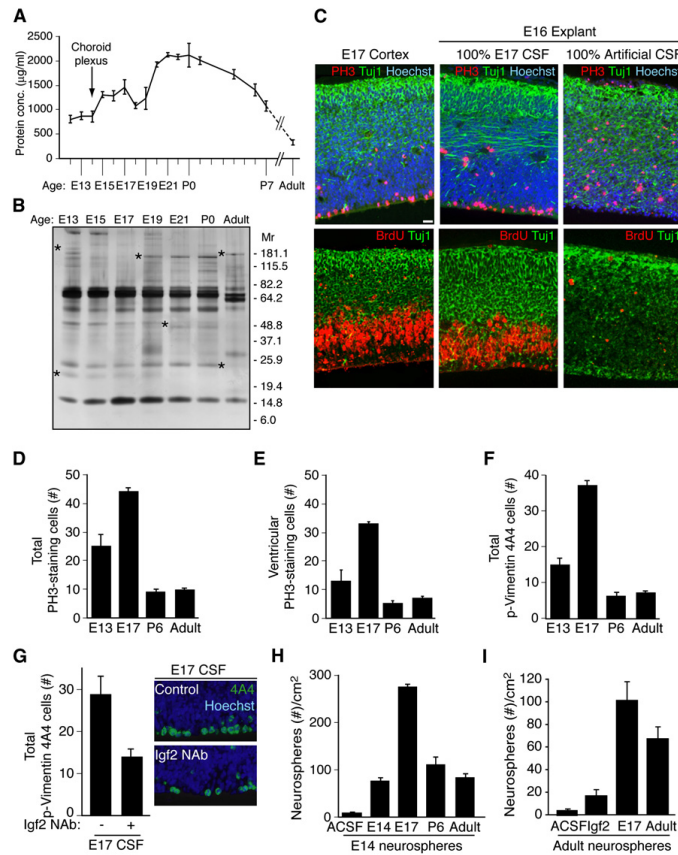


Figure 4. Embryonic CSF Supports Cortical Explant Viability and Stimulates Proliferation of Neural Progenitor Cells

(A) Total CSF protein concentration over the course of rat development.

(B) Silver stain of embryonic rat CSF revealed a dynamic fluid with numerous changes in protein composition over time. Asterisks indicate proteins with varying CSF expression during development.

(C) E17 rat cortex and E16 explants grown for 24 hr in 100% embryonic E17 CSF or 100% artificial CSF, respectively. Upper panels: anti-PH3 (red), and anti-Tuj1 (green), Hoechst (blue) immunostaining. Lower panels: anti-BrdU (red) and anti-Tuj1 (green) immunostaining. Explants cultured in 100% E17 CSF in vitro maintained tissue histology similar to embryo in vivo. Survival and proliferation of explants cultured with E17 CSF indicated by immunoreactivity for PH3 along the ventricular surface, BrdU incorporation in the ventricular zone, and Tuj1-positive-staining neurons in the developing cortical plate.

(D) E16 explants cultured in 100% E13, E17, P6, or adult CSF for 24 hr were immunostained with anti-PH3 (see Figure S2C). Quantification of total PH3-positive-staining cells per 400 µm explant showed that proliferating cells increased in explants cultured with E17 CSF compared to E13, P6, or adult CSF. Immuno-positive cells are represented as mean ± SEM (E17 mean, 44.1 ± 1.43; E13 mean, 25 ± 4.2; P6 mean, 9.2 ± 0.8; adult mean, 9.6 ± 0.9, n = 4; Kruskal-Wallis; p < 0.005).

(E) Quantification of ventricular PH3-staining cells in explants (D). PH3-positive cells along the ventricle were significantly increased in explants cultured with E17 CSF compared to E13, P6, or adult CSF (E17 mean, 32.3 ± 0.79; E13 mean, 12.8 ± 3.9; P6 mean, 4.9 ± 1.0; adult mean, 6.9 ± 0.73; n = 4; Kruskal-Wallis; p < 0.01).

(F) E16 explants (D) immunostained with anti-Vimentin 4A4 (see Figure S2C) were quantified. Vimentin 4A4-positive cells were significantly increased in explants cultured with E17 CSF compared to E13, P6, or adult CSF (E17 mean, 37.1 ± 1.4; E13 mean, 14.9 ± 1.9; P6 mean, 6.1 ± 1.05; adult mean, 7.3 ± 0.6; n = 4; Kruskal-Wallis; p < 0.005).

(G) Left panel: E16 explants cultured in control E17 CSF or E17 CSF with Igf2 neutralizing antibody (Igf2 NAb), immunostained with anti-Vimentin 4A4 and Hoechst (E17 control mean, 28.8 ± 4.3; E17 Igf2 NAb mean, 13.9 ± 2.0; n = 4; Mann-Whitney; p < 0.05). Vimentin 4A4-positive cells decreased in explants cultured with E17 CSF plus Igf2 NAb compared to control. Right panels: representative images of explants quantified in left panels.

(H) Primary neurospheres derived from E14 cortex were grown in 20% artificial (A), E14, E17, P6, or adult CSF for 10 days in vitro (DIV). E17 CSF generated the most spheres/cm² (E17 mean, 274 ± 8.0; E14 mean, 77 ± 7.0; P6 mean, 110 ± 17.5; adult mean, 81 ± 8.8; n = 3; ANOVA; p < 0.005). See also Figure S2.

(I) Neurospheres derived from adult rat SVZ were cultured in artificial (A)CSF, Igf2 (20 ng/ml), E17 CSF, or adult rat CSF for 10DIV. Igf2, E17 CSF, and adult CSF supported the growth and maintenance of adult neurospheres (ACSF, 4.76 ± 0.67; Igf2, 17.3 ± 3.2; E17 CSF, 101.7 ± 15.8; adult CSF, 67.8 ± 12.6; Kruskal-Wallis, Igf2 versus E17 CSF, p < 0.05; E17 CSF versus adult CSF, N.S.; n = 3).

See also Figure S2 and Tables S2 and S3.

By comparing rat CSF from several ages, we determined that the effects of CSF on survival and proliferation are strikingly age dependent and mimicked the temporal profile of CSF-Igf2 expression (Figure 3C). E17 CSF (near the middle of neurogenesis) maintained the healthiest explants and produced the maximal increase in the frequency of PH3-labeled proliferating cells in E16 cortical explants compared to explants cultured with E13 (early in neurogenesis), P6, or adult CSF (Figures 4D, 4E, S2C, and data not shown). Many mitotic cells were identified

as proliferating neuroepithelial progenitor cells by their immunoreactivity for phospho-Vimentin (4A4; Figures 4F and S2C). In contrast, no differences were seen in Tbr2-positive basal progenitors, which do not contact the CSF directly (data not shown). Together, these data suggest that age-dependent differences in CSF signals are both supportive and instructive for neuroepithelial precursor proliferation in the developing cortex. The CSF effects may be specific to neuroepithelial progenitors, which contact the ventricle through the apical

complex, without affecting the intermediate progenitors of the SVZ.

We tested directly whether CSF-borne Igf2 was necessary to explain the effects of age-specific CSF on rat cortical explants. The frequency of proliferating cells declined in explants grown in E17 CSF in the presence of Igf2 neutralizing antibodies (Igf2 Nab; Figure 4G). Igf2 neutralization with Igf2 NAb did not interfere with Igf1 levels in CSF compared to control as assayed by ELISA (data not shown). While Igf signaling is known to promote neuronal survival (Popken et al., 2004), we did not observe differences in ventricular progenitor cell survival in these explant experiments (data not shown), suggesting that Igf actions on neural cell survival likely depends on the cell type, developmental stage, and microenvironment. These data confirm the important role for CSF borne Igf2 in regulating cerebral cortical progenitor cells but do not rule out roles of other CSF borne factors as well.

CSF Influence on Isolated Neural Stem Cells Requires Igf Signaling

Neural stem cells cultured as neurospheres confirmed the age-dependent capacity of CSF to maintain neural stem cells (Reynolds and Weiss, 1996) and provided additional evidence suggesting that Igf2-mediated signaling is an essential determinant of CSF activity on neural stem cells. CSF from any age supported the proliferation and maintenance of isolated cortical stem cells cultured as primary or secondary neurospheres (Figure 4H and data not shown; Vescovi et al., 1993). However, E17 CSF was maximally effective in generating increased numbers of neurospheres, larger neurospheres, and maintained neurospheres even in long-term cultures for up to 44 days in vitro (Figures 4H, S2D–S2G, and data not shown). Neurospheres grown in CSF retained responsiveness to Fgf2 and Egf, indicating that the CSF maintains stem cells in an uncommitted fate (Figure S2H). CSF generated neurospheres from adult SVZ precursors as well (Figure 4I). Consistent with these observations and our explant studies, the Igf1R inhibitor picropodophyllin blocked the formation of spheres in the presence of E17 CSF (data not shown). Our data suggest that the choroid plexus is the most prominent source of Igf2 in CSF (Figures 3 and S3A). Accordingly, media conditioned with E17 choroid plexus provided enhanced support for neurosphere formation compared to media conditioned with embryonic cortex, adult choroid plexus, or adult brain (Table S3), demonstrating that one or more factors actively secreted from the embryonic choroid plexus, including potentially Igf2, is sufficient for stem cell growth and maintenance. Thus, distinct factors secreted by the choroid plexus into the embryonic CSF, including Igf2, confer E17 CSF with an age-associated advantage to stimulate and maintain neural stem cell proliferation, and Igf signaling is likely one pathway that promotes this process.

Genetic Inactivation of Igf Signaling Impairs Brain Development

Mouse explant experiments confirmed a requirement for Igf signaling in the proliferation of progenitor cells. Mouse embryonic CSF supported the survival and proliferation of mouse cortical progenitors (C57BL/6 explants: 20% ACSF in NBM

mean, 7.4 ± 0.2 ; 20% E16.5 CSF in NBM mean, 14.1 ± 1.4 ; Mann-Whitney; $p < 0.01$; $n = 3$), and purified Igf2 in 20% ACSF in NBM stimulated cortical progenitor proliferation (Figure 5A). When the *Igf1R* was genetically inactivated in cortical progenitors (*Igf1R^{oxP/oxP}/NestinCre^{+/+}*) (Liu et al., 2009), wild-type CSF no longer stimulated cortical progenitor proliferation (ACSF, 17.6 ± 2.9 ; E16.5 CSF, 16.4 ± 3.0 ; Mann-Whitney; N.S.; $n = 3$). Importantly, CSF obtained from *Igf2^{-/-}* mice failed to stimulate progenitor proliferation in wild-type explants compared to control (Figure 5B), suggesting that Igf2 in its native CSF environment stimulates proliferation of progenitor cells during cerebral cortical development.

As expected for the roles we have shown for Igf2 in regulating proliferation, we found that *Igf2*-deficiency reduced brain size (Figure 5C). *Igf2^{-/-}* brain weight decreased by 24% at P8 compared to controls (Figure 5D). Accordingly, the overall cortical perimeter and surface area were reduced in *Igf2^{-/-}* brains compared to controls as well (Figures 5E–5G). Profound defects in somatic size couple to brain size (Purves, 1988). As previously reported (DeChiara et al., 1991; Baker et al., 1993), *Igf2^{-/-}* body weight was reduced compared to control (mean body weight (g) at P8: *Igf2^{+/+}*, 5.6 ± 0.01 ; *Igf2^{-/-}*, 2.8 ± 0.1 ; Mann-Whitney; $p < 0.0001$; $n = 11$), suggesting that Igf2 may be a secreted factor that scales brain size to body size. Consistent with the mouse CSF Igf2 expression pattern that is significantly increased during later embryonic development (Figure S3B), blunting Igf2 expression markedly reduced the proliferating progenitor cells at E16.5 compared to controls (PH3-positive cells/100 μm^2 VZ \pm SEM at E16.5: *Igf2^{+/+}*, 2.5 ± 0.3 ; *Igf2^{-/-}*, 1.7 ± 0.1 ; Mann-Whitney; $p < 0.05$; $n = 5$). NeuN- and late-born Cux1-staining neurons were reduced in *Igf2^{-/-}* mice (Figure 5H and data not shown), confirming that Igf2 contributes to cortical progenitor proliferation and to late stages of neurogenesis. Taken together, our genetic experiments support a model in which the apical complex localizes Igf signaling in progenitors by ensuring the apical, ventricular localization of the Igf1R. In this manner, the apical complex couples cell autonomous and extracellular signals to the regulation of cortical development.

Glioblastoma CSF Expresses High Igf2

Our data, together with recent findings implicating Igf signaling in the maintenance of adult neural stem cells (Llorens-Martín et al., 2010), raised the possibility that abnormalities of the CSF may be relevant to conditions showing abnormal proliferation, including in glioblastoma multiforme (GBM), a malignant astrocytic brain tumor. Igf-PI3K-Akt signaling has been implicated as a key regulator of gliomagenesis (Louis, 2006; Soroceanu et al., 2007), and mutations in *PTEN* are commonly found in patients with GBM (Louis, 2006). We analyzed Igf2 concentration in a panel of 56 human GBM patient CSF samples collected from 21 individuals representing the full range of disease progression and 8 disease-free controls and found that CSF from GBM patients contained significantly more Igf2 than CSF from disease-free controls (Igf2 concentration expressed as mean \pm SEM for GBM patients, 340.4 ± 12.9 ng/ml; $n = 56$; disease-free controls, 222.9 ± 41.5 ng/ml; $n = 8$; Mann-Whitney, $p < 0.01$). Three GBM samples containing the highest Igf2 concentrations (605.8 ng/ml,

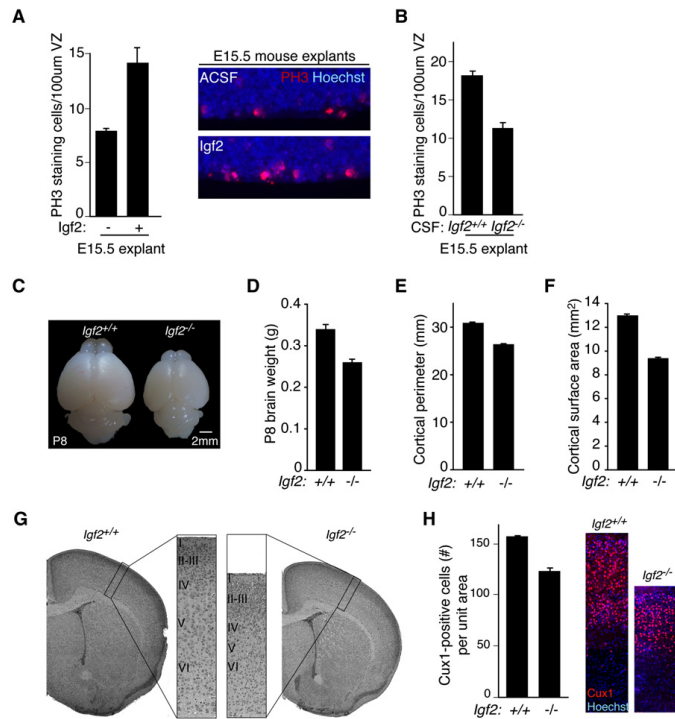


Figure 5. CSF Igf2 Regulates Progenitor Proliferation and Brain Size

(A) Left panels: E15.5 C57BL/6 explants cultured in NBM supplemented with 20% ACSF or ACSF/Igf2. Igf2 stimulated the proliferation of PH3-positive cortical progenitor cells (C57BL/6 explants: ACSF mean, 7.4 ± 0.2 ; Igf2 mean, 11.2 ± 0.3 ; Mann-Whitney, $p < 0.05$; $n = 3$). Right panels: representative images of explants quantified in left panels.

(B) E15.5 C57BL/6 explants cultured in NBM supplemented with 20% E16.5 wild-type or *Igf2*^{-/-} CSF. *Igf2*-deficient CSF failed to stimulate progenitor cell proliferation compared to control (*Igf2*^{+/+}, 17.9 ± 0.8 ; *Igf2*^{-/-} CSF, 11.4 ± 1.0 ; Mann-Whitney; $p < 0.06$; $n = 3$ and $n = 4$, respectively).

(C) Representative images of P8 *Igf2*^{-/-} and control brains.

(D) *Igf2* deficiency reduced P8 brain weight (*Igf2*^{+/+}, $0.34 \text{ g} \pm 0.008$; *Igf2*^{-/-}, $0.26 \text{ g} \pm 0.004$; Mann-Whitney, $p < 0.0001$, $n = 11$).

(E) *Igf2* deficiency reduced P8 cortical perimeter (*Igf2*^{+/+}, $30.9 \text{ mm} \pm 0.01$; *Igf2*^{-/-}, $26.4 \text{ mm} \pm 0.1$; Mann-Whitney, $p < 0.0001$, $n = 11$).

(F) *Igf2* deficiency reduced P8 cortical surface area (*Igf2*^{+/+}, $13.0 \text{ mm}^2 \pm 0.1$; *Igf2*^{-/-}, $9.4 \text{ mm}^2 \pm 0.1$; Mann-Whitney, $p < 0.0001$, $n = 11$).

(G) H&E staining of *Igf2*^{-/-} and control brains at P8.

(H) Left panels: *Igf2*^{-/-} brains have reduced numbers of upper layer neurons marked by Cux1 (total Cux1-positive staining cells in equally sized cortical columns expressed as mean \pm SEM: *Igf2*^{+/+}, 157 ± 1.5 ; *Igf2*^{-/-}, 131.3 ± 3.3 ; t test, $p < 0.005$, $n = 3$). Right panels: representative images of *Igf2*^{-/-} and control brains quantified in left panels.

See also Figure S3.

502.8 ng/ml, and 468.7 ng/ml) came from patients with advanced disease (Figure 6A and Table 1). By contrast, the three patients with the lowest levels of Igf2 (142.1 ng/ml, 145.4 ng/ml, and 153.9 ng/ml) all had early or stable glioma (Figure 6A and Table 1). Similar to rodent ventricular CSF, human lumbar CSF stimulated cortical progenitor cell proliferation in our explant assay, with CSF from GBM patients causing greater proliferation than CSF from disease-free controls (Figure 6B). Moreover, human GBM patient CSF neutralized with Igf2 antibodies failed to stimulate the proliferation of progenitor cells (Figure 6B; Igf2 concentration following NAb absorption, GBM1(PBS): 605.8 ng/ml; GBM1 (NAb), 45.6 ng/ml; GBM2(PBS), 502.8 ng/ml; GBM2(NAb), 218.3 ng/ml; GBM3(PBS), 468.7 ng/ml; GBM3(NAb), 248.8 ng/ml). Taken together, these data suggest that beyond embryonic brain development, CSF-Igf2, in particular, is a potential mediator of GBM pathology and that the CSF mechanisms that normally regulate neural stem cells are misregulated in GBM.

CSF-Mediated Long-Range Distribution of Additional Secreted Factors

Whereas our studies suggest an important role for Igf2 in controlling proliferation in late stages of neurogenesis and potentially

postnatally, they do not rule out the presence of other secreted factors that may act at long ranges via the CSF, and so we performed functional screening tests for several other families of factors. The CSF contained Wnt signaling activity (Zhou et al., 2006), based upon phosphorylation of LRP6, a Wnt coreceptor in response to CSF exposure (Figure 7A). Several Wnt ligands were expressed along the ventricular surface and in the choroid plexus (Figure 7B and data not shown; Grove et al., 1998). Frizzled (Fz) receptors, which bind LRP6 to transduce Wnt signals, showed enhanced expression in ventricular progenitors (Figure 7B and data not shown; Zhou et al., 2006), suggesting that CSF may distribute Wnts to precursors throughout the ventricular surface. Additional signaling activities that influence cortical development were also found in the CSF, with responsive cells seen broadly in the ventricular zone. There were dynamic levels of bone morphogenetic protein (Bmp) activity in the CSF during different stages of cortical development (Figure 7C). Using a luciferase-based assay in which overall Bmp activity can be quantified between 0.1 and 100 ng/ml (data not shown), we found that Bmp activity in the CSF decreased during embryogenesis and peaked in adulthood (Figure 7C). CSF-borne Bmp activity may be responsible for stimulating progenitors widely throughout the cortical ventricular zone in vivo, based on

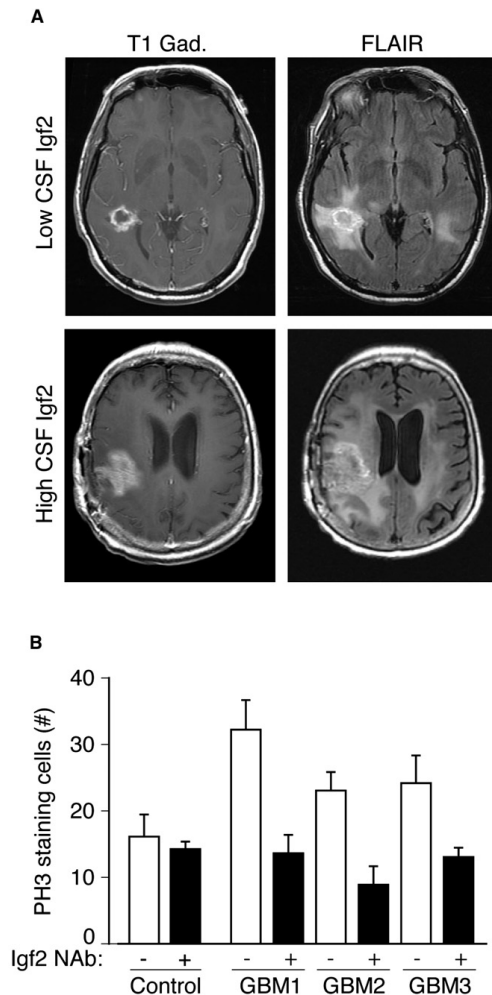


Figure 6. Glioblastoma CSF Igf2 Supports Progenitor Proliferation

(A) MRI scans from subjects with low and high CSF Igf2 levels. Gadolinium-enhanced T1-weighted (T1-Gad) MRI sequence delineated the contrast-enhanced portion of the tumor where tumor angiogenesis developed. Fluid attenuation inversion recovery (FLAIR) images included area of nonvascularized and invasive tumor (Macdonald et al., 1990).

(B) Twenty percent human GBM CSF in NBM stimulated PH3-positive proliferating cells compared to an average of three disease-free control CSFs in E16 rat explants (control = 16.0 ± 4.1 [n = 3]; GBM1 = 32.3 ± 4.3 [n = 4]; GBM2 = 23.0 ± 2.8 [n = 5]; GBM3 = 23.4 ± 3.8 [n = 4]; Mann-Whitney, $p < 0.05$). Igf2(NAb) inhibited GBM CSF-stimulated progenitor proliferation (GBM1 = 13.5 ± 2.9 [n = 4]; GBM2 = 9.0 ± 2.7 [n = 4]; GBM3 = 13.0 ± 1.5 [n = 3]; Mann-Whitney, $p < 0.05$). CSF Igf2 concentration before and after Igf2 NAb absorption: GBM1(PBS) = 605.8 ng/ml; GBM1(NAb) = 45.6 ng/ml; GBM2(PBS) = 502.8 ng/ml; GBM2(NAb) = 218.3 ng/ml; GBM3(PBS) = 468.7 ng/ml; GBM3(NAb) = 248.8 ng/ml).

widespread labeling for nuclear phospho-SMAD1/5/8 (Figure 7D) in the absence of any known Bmp ligands localizing to the ventricular zone (Shimogori et al., 2004), whereas Bmps 2, 4, 5, and 7 are expressed in embryonic and adult choroid plexus (Figure 7E; Hébert et al., 2002; Shimogori et al., 2004). Moreover, growth and differentiation factors 3 and 8 (GDF3 and GDF8), both members of the TGF- β superfamily of proteins that can influence Bmp signaling (Levine and Brivanlou, 2006) were found in our MS analyses of CSF (data not shown), though we do not consider our MS analysis to have recovered all potential smaller ligands in the CSF. Retinoic acid (RA) (Haskell and LaMantia, 2005; Siegenthaler et al., 2009) activity in CSF also varied over the course of cortical development (Figure 7F). A luciferase-based assay that quantifies RA activity ranging between 10^{-9} and 10^{-6} M (data not shown) revealed that RA activity in CSF peaked early and decreased in adulthood (Figure 7F). In parallel, RA responsive cortical progenitors localized to the developing ventricular zone (Figure 7G). Similar to Wnts and Bmps, RA is most likely released into CSF since RA synthetic and catabolic enzymes were expressed in the choroid plexus (Figure 7H) and meninges (data not shown). Thus, CSF shows bioavailability of a wide range of activities known to regulate neurogenesis, patterning, and neuronal survival in the cerebral cortex and throughout the CNS.

DISCUSSION

We show that the CSF plays an essential, active role in distributing signals in the central nervous system. The key findings of our study are (1) the apical complex is essential for the apical localization of Igf1R; (2) *Pten* deficiency in the *Pals1* background results in an almost normally sized brain; (3) CSF Igf2 binds to the apical domain of cortical progenitor cells, stimulating their proliferation in an age-dependent manner; (4) Igf2 is upregulated in GBM patient CSF, contributing to the range of proliferative activities of GBM patient CSF; and (5) the CSF provides an adaptive library of secreted factors throughout life. The dynamic regulation of several potent modulators of neural stem cells reinforces the central relationship between local signaling at the apical surface via ligands delivered by the CSF during cortical neurogenesis.

Asymmetric Growth Factor-Based Signaling

It has been suggested that asymmetry of signaling at the apical versus basolateral aspect of cortical progenitors regulates progenitor progress through the cell cycle (Bultje et al., 2009; Sun et al., 2005). The basolateral expansion of the Igf1R signaling domain we report in *Pten* mutants suggests potential links between asymmetric growth factor signaling and proliferation. Although asymmetric localization of the Egfr in cortical progenitors has previously been reported (Sun et al., 2005), the ventricular enrichment of the Igf1R was not known and raises the possibility that the apical enrichment of the Igf1R along with other apical proteins confers a differential responsiveness to mitogenic signals, akin to Notch signaling (Bultje et al., 2009). Since Igfs are potent mitogens for cortical progenitors (Hodge et al., 2004; Popken et al., 2004), one model might suggest that inheritance of the apical complex promotes progenitor fate by differentially concentrating Igf1R and its

Table 1. Clinical Presentation of GBM Patients with Lowest and Highest CSF Igf2 Concentrations

	Patient	[Igf2] ng/ml	Clinical Presentation		Life Span
			Tumor size: T1-Gad (cm ²)	Tumor size: FLAIR (cm ²)	
Low CSF Igf2	L1	142.1	7.14	6.46	Stable disease at follow-up; 3 weeks post-CSF collection
	L2	145.4	8.50	54.12	Stable disease at follow-up; 3 weeks post-CSF collection
	L3	153.9	5.94	20.5	Stable disease at follow-up; 5 weeks post-CSF collection
High CSF Igf2	H1	605.8	47.31	102.83	Deceased at 1 week post-CSF collection
	H2	502.8	13.69	53.90	Deceased at 52 weeks post-CSF collection
	H3	468.7	23.94	36.48	Deceased at 30 weeks post-CSF collection

Patients with the lowest CSF Igf2 concentrations (L1–L3) had early or stable GBM disease state, while patients with the highest CSF Igf2 concentrations (H1–H3) had advanced disease and aggressive tumor progression at time of CSF collection. Tumor size was determined by Macdonald's criteria, where T1-Gad MRI sequence delineated the contrast-enhanced portion of tumor, and FLAIR images include areas of nonvascularized and invasive tumor (Macdonald et al., 1990). High-CSF Igf2 patients had larger T1-Gad tumor sizes compared to low-CSF Igf2 patients (Mann-Whitney; $p < 0.05$; $n=3$).

downstream signaling proteins into cells that retain their perikarya or at least a process (likely a cilium) in the ventricular zone, causing these cells to remain in the cycling pool. The presence of proliferation-inducing factors in the CSF suggests that withdrawal of the progenitor's apical ventricular process may be an important step in neuronal differentiation (Cappello et al., 2006), by insulating progenitor cells from proliferative signals in CSF, with vascular niches potentially supplying sources of secreted factors for stem cells at other stages (Palmer et al., 2000; Shen et al., 2004, 2008; Tavazoie et al., 2008).

Our data provides a new perspective on the production and provision of Igf ligands, which are known to regulate stem cell populations in the brain and other proliferative epithelia (Bendall et al., 2007; Hodge et al., 2004; Liu et al., 2009; Popken et al., 2004; Ye et al., 2004; Zhang and Lodish, 2004). In the E17 rat brain, the choroid plexus was the strongest source of Igf2, though we cannot discount a contribution by the vasculature or other cellular sources of Igf2 that may percolate into the CSF. Indeed, both pericytes and endothelial cells express Igf2 (Dugas et al., 2008), and Igfs from vascular tissue may have local effects beyond apically mediated Igf1R signaling shown here. Thus, locally derived Igf2 may play distinct roles at different developmental time points and in different cellular contexts, and Igf signaling may also be influenced by CSF Igf1 and insulin. Although Igf2 availability decreased in adult CSF (Figures 3C and S3B), *Igf2* continued to be expressed in adult choroid plexus (data not shown) and maintained adult neurospheres (Figure 4I), suggesting that low levels of CSF Igf2 contribute to the maintenance of adult neural stem cells. The aberrant increase in Igf2 in advanced GBM patients reinforces the hypothesis that Igf signaling has an influence on proliferation of cortical precursors. Our identification of *Igf2* regulation of neurogenesis and brain size complements a literature in which Igf signaling is well known to influence body and brain size (Baker et al., 1993; DeChiara et al., 1991; Purves, 1988), raising the intriguing possibility that Igf2 represents a secreted factor that may scale brain size to body size.

Fluid-Based Signaling in the CNS and Beyond

The activity of growth promoting factors in the CSF and their action on progenitors across the apical surface may be a model for other epithelia including lung, gut, and vascular endothelia

that develop in relation to extracellular fluids (Bendall et al., 2007; Scadden, 2006). Extracellular fluid apparently regulates the microenvironment of hematopoietic stem cells, where Igf signaling regulates progenitor proliferation (Orkin and Zon, 2008; Zhang and Lodish, 2004). The differential capacity of Igf signaling to confer a proliferative advantage to stem cells may be regulated in part by Igf's interactions with binding proteins or other secreted factors in the environment (Clemmons, 1997). Our experiments focused on the age-associated effects of CSF on survival and proliferation across the cortical ventricular zone. However, the distribution of CSF resident proteins, as well as the flow of the CSF, may also influence ciliary orientation and maturing ependymal cell polarity (Mirzadeh et al., 2010), which create activity gradients as has been shown for Slit (Sawamoto et al., 2006).

If a major component of the stem cell niche reflects secreted factors acting at long distances from their sources, modulation of the proteomic composition of extracellular fluids may also provide unexpected ways to regulate stem cell behavior in health and disease. For example, while Igf2 activity peaked in embryonic CSF, some CSF-borne Igf persisted in adulthood (Figures 3, S3B, and data not shown). Igf2 and Igf1 in adult CSF may contribute to the retention of neural stem cell properties in the adult SVZ (Doetsch et al., 1999). Importantly, the regulation of CSF growth factors may also extend to pathologic states. Igf2 and other diffusible growth factors that drive neural progenitor proliferation during development are upregulated in some GBM patients (Louis, 2006; Soroceanu et al., 2007), and GBM patients have elevated Igf2 levels in their CSF. CSF A β_{1-42} and phosphorylated Tau levels were recently shown to assist in Alzheimer's disease diagnosis (De Meyer et al., 2010). Thus, modulation of the proteomic composition of extracellular fluids together with the integration of cell autonomous determinants of self-renewal by the apical complex may ultimately provide unexpected ways to regulate stem cell behavior in health and disease.

EXPERIMENTAL PROCEDURES

Animals

Time pregnant Sprague-Dawley, C57BL/6, and Swiss Webster dams were purchased from Charles River Laboratories and Taconic. *Pals1^{loxP/loxP}/NestinCre^{+/+}*, *Pals1^{loxP/loxP}/Emx1Cre^{+/+}*, *Igf1R^{loxP/loxP}/NestinCre^{+/+}*, and

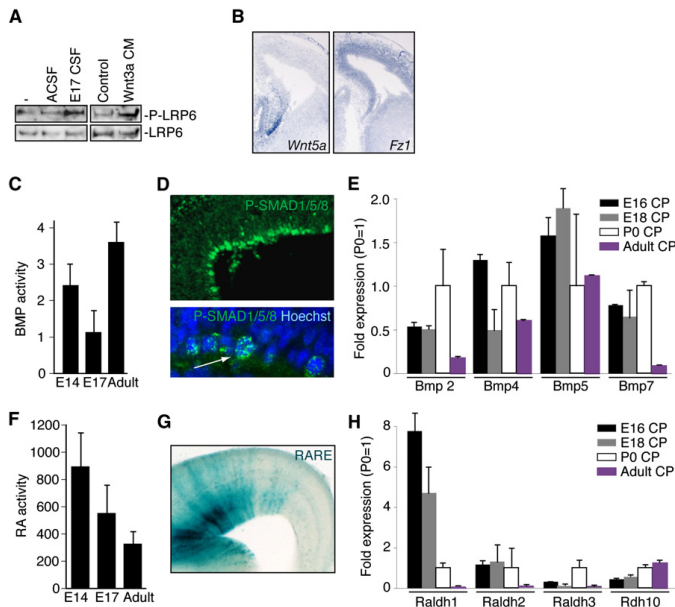


Figure 7. The CSF Proteome Coordinates Multiple Signaling Pathways that Regulate Brain Development

(A) Lysates of cortical cells were left untreated or treated with 20% ACSF or E17 CSF and 10% Wnt3a conditioned medium or its control medium for 2 hr and subjected to immunoblotting with the P-LRP6 or LRP6 antibodies.

(B) In situ hybridization for *Wnt5a* and *Fz1* in mouse E14.5 cortex.

(C) Bmp activity was measured in E14, E17, and adult rat CSF as luciferase signal in a clonally derived Bmp-sensitive cell line. Responses were compared to linear responses generated in the same cell line by pure ligand (Bmp4; data not shown). Bmp activity levels varied with age and were statistically significant between E17 and adult (ANOVA, $p < 0.001$; $n = 4$).

(D) Top panel: expression and nuclear localization of phospho-Smad (P-SMAD) 1/5/8 in E14 rat cortical ventricular cells. Bottom panel: arrow points to expression and nuclear localization of P-SMAD1/5/8 in E16.5 mouse cortical ventricular cells.

(E) qPCR measurement of Bmps 2, 4, 5, and 7 in the E16, E18, P0, and adult rat choroid plexus (CP). (F) Quantification of RA activity in E14, E17, and adult rat CSF. RA activity declined, based on comparison of CSF activation of an RA responsive, clonally derived cell line with response to RA at known concentrations, from midgestation through adulthood (ANOVA, $p = 0.07$; $n = 4$).

(G) RA responsive progenitor cells at the cortical ventricular zone from an E16.5 DR5-RARE transgenic mouse (LaMantia et al., 1993).

(H) qPCR of *Raldh1*, 2, 3, and *Rdh10*, in rat CP.

GFAP:Igf1Tg mice were obtained from heterozygous breedings, and *Pten^{loxP/loxP}/Pals1^{loxP/loxP}/Emx1Cre^{+/+}*, and *Pten^{loxP/loxP}/Pals1^{loxP/loxP}/Emx1Cre^{+/+}* mice were obtained from *Pten^{loxP/loxP}/Pals1^{loxP/loxP}/Emx1Cre^{+/+}* and *Pten^{loxP/loxP}/Emx1Cre^{-/-}* crosses (Groszer et al., 2001; Kim et al., 2010; Liu et al., 2009; Ye et al., 2004). *Igf2^{-/-}* and control CSF was collected from embryos obtained from homozygous breedings. *Igf2^{-/-}* and control P8 brains were obtained from homozygous crosses or paternal heterozygotes mated with homozygous knockouts (DeChiara et al., 1991). All animal experimentation was carried out under protocols approved by the IACUCs of Harvard Medical School, Children's Hospital Boston, and UNC-Chapel Hill.

Antibodies

The following antibodies were purchased: Ctip2, Igf2 (for EM), Tbr2 (Abcam); BrdU (AbD Serotec); Ki67 (Abnova); Vimentin 4A4 (Assay Designs); Pax6 (Developmental Studies Hybridoma Bank); β -catenin, Cdc42 (BD Biosciences); AKT, phospho-AKT, Igf1R, phospho-Igf1R, CC3, and phospho-S6rp (Cell Signaling); GLAST (Chemicon); Tuj1 (Covance); HRP conjugated anti-Transferrin (Immunology Consultants Laboratory, Inc.); Igf2 (NAb; Millipore); Cux1, Igf2 (for WB) (Santa Cruz Biotechnology); and phospho-Histone H3 (Upstate). Tbr1 was a kind gift of R. Hevner.

CSF Isolation

Embryonic rodent CSF, isolated as described (Zappaterra et al., 2007), was kept on ice during collection, centrifuged at $10,000 \times g$ at 4°C for 10 min., and stored at -80°C . Human GBM and disease-free CSF samples were collected by lumbar puncture from patients undergoing clinical evaluation. The 56 GBM samples tested were obtained from 21 individuals representing the full-range of disease progression. The samples used in analyses of highest and lowest CSF Igf2 concentration were obtained from distinct individuals. All research was approved by the IRBs at BIDMC and Children's Hospital Boston.

Cortical Explants

The telencephalic wall was dissected onto polycarbonate membranes (Whatman; 13 mm, $8.0 \mu\text{m}$) and cultured for 24 hr as described in text. Artificial (A)CSF (NaCl 119 mM, KCl 2.5 mM, NaHCO_3 26 mM, NaH_2PO_4 1 mM, glucose 11 mM, MgCl_2 2 mM, CaCl_2 2.8 mM) was supplemented with Igf2 (2 ng/ml; US Biologicals) as indicated. Igf2 NAb antibody was incubated with E17 CSF for 1 hr at 4°C . Explants were pulsed with BrdU for 30 min and fixed (60% methanol, 30% chloroform, and 10% acetic acid; 10 min). For in vivo BrdU labeling, pregnant dams were administered a 3 hr BrdU (60 mg/kg) pulse. Tissue was paraffin sectioned ($5 \mu\text{m}$).

SUPPLEMENTAL INFORMATION

Supplemental Information includes three figures, three tables, and Supplemental Experimental Procedures and can be found with this article online at doi:10.1016/j.neuron.2011.01.023.

ACKNOWLEDGMENTS

We thank A. Bonni, S. Gygi, R. Segal, and members of the Walsh laboratory for helpful discussions; H. Steen for assistance with mass spectrometry; D. Rubin and J. Sheng for pMSCVhyg-Igf2; U. Berger, J. Buchanan, M. Ericsson, Y. Lin, A. Peters, C. Kourkoulis, and S. White for technical assistance. This work was supported by a Sigrid Jusélius Fellowship, an Ellison/AFAR Postdoctoral Fellowship, and Award Number K99NS072192 from the NINDS (M.K.L.); a Stuart H.Q. & Victoria Quan Fellowship (M.W.Z.); a NIH MSTP grant (M.W.Z. and Y.J.Y.); the Child Neurology Foundation (X.C.); *A Reason To Ride* research fund (M.L. and E.T.W.), a NINDS grant (RO1 NS048868) (A.J.D. and P.Y.), a NICHD grant (RO1 HD008299) (A.J.D.), a NIH grant

(HD029178), and an UNC-CH Reynolds Faculty Fellowship (A.S.L.); a NINDS grant (3 RO1 NS032457), the Manton Center for Orphan Disease Research, and the Intellectual and Developmental Disabilities Research Centers (CHB DDR, P30 HD18655)(C.A.W.). C.A.W. is an Investigator of the Howard Hughes Medical Institute. The content is solely the responsibility of the authors and does not necessarily represent the official views of the NINDS or the NIH.

Accepted: December 7, 2010
 Published: March 9, 2011

REFERENCES

Ayer-le Lievre, C., Ståhlbom, P.A., and Sara, V.R. (1991). Expression of IGF-I and -II mRNA in the brain and craniofacial region of the rat fetus. *Development* 111, 105–115.

Baker, J., Liu, J.P., Robertson, E.J., and Efstratiadis, A. (1993). Role of insulin-like growth factors in embryonic and postnatal growth. *Cell* 75, 73–82.

Bendall, S.C., Stewart, M.H., Menendez, P., George, D., Vijayaragavan, K., Werbowetski-Ogilvie, T., Ramos-Mejia, V., Rouleau, A., Yang, J., Bossé, M., et al. (2007). IGF and FGF cooperatively establish the regulatory stem cell niche of pluripotent human cells in vitro. *Nature* 448, 1015–1021.

Binoux, M., Lassarre, C., and Gourmelin, M. (1986). Specific assay for insulin-like growth factor (IGF) II using the IGF binding proteins extracted from human cerebrospinal fluid. *J. Clin. Endocrinol. Metab.* 63, 1151–1155.

Bondy, C., Werner, H., Roberts, C.T., Jr., and LeRoith, D. (1992). Cellular pattern of type-I insulin-like growth factor receptor gene expression during maturation of the rat brain: Comparison with insulin-like growth factors I and II. *Neuroscience* 46, 909–923.

Bultje, R.S., Castaneda-Castellanos, D.R., Jan, L.Y., Jan, Y.N., Kriegstein, A.R., and Shi, S.H. (2009). Mammalian Par3 regulates progenitor cell asymmetric division via notch signaling in the developing neocortex. *Neuron* 63, 189–202.

Cappello, S., Attardo, A., Wu, X., Iwasato, T., Itohara, S., Wilsch-Bräuninger, M., Eilken, H.M., Rieger, M.A., Schroeder, T.T., Huttner, W.B., et al. (2006). The Rho-GTPase cdc42 regulates neural progenitor fate at the apical surface. *Nat. Neurosci.* 9, 1099–1107.

Chalhoub, N., Zhu, G., Zhu, X., and Baker, S.J. (2009). Cell type specificity of PI3K signaling in Pdk1- and Pten-deficient brains. *Genes Dev.* 23, 1619–1624.

Clemmons, D.R. (1997). Insulin-like growth factor binding proteins and their role in controlling IGF actions. *Cytokine Growth Factor Rev.* 8, 45–62.

Cohen, E., Binet, S., and Meininger, V. (1988). Ciliogenesis and centriole formation in the mouse embryonic nervous system. An ultrastructural analysis. *Biol. Cell* 62, 165–169.

DeChiara, T.M., Robertson, E.J., and Efstratiadis, A. (1991). Parental imprinting of the mouse insulin-like growth factor II gene. *Cell* 64, 849–859.

De Meyer, G., Shapiro, F., Vanderstichele, H., Vanmechelen, E., Engelborghs, S., De Deyn, P.P., Coart, E., Hansson, O., Minthon, L., Zetterberg, H., et al.; Alzheimer's Disease Neuroimaging Initiative. (2010). Diagnosis-independent Alzheimer disease biomarker signature in cognitively normal elderly people. *Arch. Neurol.* 67, 949–956.

Doetsch, F., Caillé, I., Lim, D.A., Garcia-Verdugo, J.M., and Alvarez-Buylla, A. (1999). Subventricular zone astrocytes are neural stem cells in the adult mammalian brain. *Cell* 97, 703–716.

Dugas, J.C., Mandemakers, W., Rogers, M., Ibrahim, A., Daneman, R., and Barres, B.A. (2008). A novel purification method for CNS projection neurons leads to the identification of brain vascular cells as a source of trophic support for corticospinal motor neurons. *J. Neurosci.* 28, 8294–8305.

Dziegielewska, K.M., Evans, C.A., Lai, P.C., Lorscheider, F.L., Malinowska, D.H., Møllgård, K., and Saunders, N.R. (1981). Proteins in cerebrospinal fluid and plasma of fetal rats during development. *Dev. Biol.* 83, 193–200.

Feng, W., Wu, H., Chan, L.N., and Zhang, M. (2008). Par-3-mediated junctional localization of the lipid phosphatase PTEN is required for cell polarity establishment. *J. Biol. Chem.* 283, 23440–23449.

Fishell, G., and Kriegstein, A.R. (2003). Neurons from radial glia: The consequences of asymmetric inheritance. *Curr. Opin. Neurobiol.* 13, 34–41.

Fuchs, J.L., and Schwark, H.D. (2004). Neuronal primary cilia: A review. *Cell Biol. Int.* 28, 111–118.

Gorski, J.A., Talley, T., Qiu, M., Puelles, L., Rubenstein, J.L., and Jones, K.R. (2002). Cortical excitatory neurons and glia, but not GABAergic neurons, are produced in the Emx1-expressing lineage. *J. Neurosci.* 22, 6309–6314.

Groszer, M., Erickson, R., Scripture-Adams, D.D., Lesche, R., Trumpp, A., Zack, J.A., Kornblum, H.I., Liu, X., and Wu, H. (2001). Negative regulation of neural stem/progenitor cell proliferation by the Pten tumor suppressor gene in vivo. *Science* 294, 2186–2189.

Grove, E.A., Tole, S., Limon, J., Yip, L., and Ragsdale, C.W. (1998). The hem of the embryonic cerebral cortex is defined by the expression of multiple Wnt genes and is compromised in Gli3-deficient mice. *Development* 125, 2315–2325.

Haskell, G.T., and LaMantia, A.S. (2005). Retinoic acid signaling identifies a distinct precursor population in the developing and adult forebrain. *J. Neurosci.* 25, 7636–7647.

Hébert, J.M., Mishina, Y., and McConnell, S.K. (2002). BMP signaling is required locally to pattern the dorsal telencephalic midline. *Neuron* 35, 1029–1041.

Hodge, R.D., D'Ercole, A.J., and O'Kusky, J.R. (2004). Insulin-like growth factor-I accelerates the cell cycle by decreasing G1 phase length and increases cell cycle reentry in the embryonic cerebral cortex. *J. Neurosci.* 24, 10201–10210.

Huang, X., Liu, J., Ketova, T., Fleming, J.T., Grover, V.K., Cooper, M.K., Litingtung, Y., and Chiang, C. (2010). Transventricular delivery of Sonic hedgehog is essential to cerebellar ventricular zone development. *Proc. Natl. Acad. Sci. USA* 107, 8422–8427.

Johansson, P.A., Cappello, S., and Gotz, M. (2010). Stem cell niches during development - lessons from the cerebral cortex. *Curr. Opin. Neurobiol.* 20, 1–8.

Kappeler, L., De Magalhaes Filho, C., Dupont, J., Leneuve, P., Cervera, P., Périn, L., Loudes, C., Blaise, A., Klein, R., Epelbaum, J., et al. (2008). Brain IGF-1 receptors control mammalian growth and lifespan through a neuroendocrine mechanism. *PLoS Biol.* 6, e254. 10.1371/journal.pbio.0060254.

Kemphues, K. (2000). PARs in embryonic polarity. *Cell* 101, 345–348.

Kim, S., Lehtinen, M.K., Sessa, A., Zappaterra, M.W., Cho, S.H., Gonzalez, D., Boggan, B., Austin, C.A., Wijnholds, J., Gambello, M.J., et al. (2010). The apical complex couples cell fate and cell survival to cerebral cortical development. *Neuron* 66, 69–84.

LaMantia, A.S., Colbert, M.C., and Linney, E. (1993). Retinoic acid induction and regional differentiation prefigure olfactory pathway formation in the mammalian forebrain. *Neuron* 10, 1035–1048.

Levine, A.J., and Brivanlou, A.H. (2006). GDF3 at the crossroads of TGF-beta signaling. *Cell Cycle* 5, 1069–1073.

Liu, W., Ye, P., O'Kusky, J.R., and D'Ercole, A.J. (2009). Type 1 insulin-like growth factor receptor signaling is essential for the development of the hippocampal formation and dentate gyrus. *J. Neurosci. Res.* 87, 2821–2832.

Llorens-Martín, M., Torres-Alemán, I., and Trejo, J.L. (2010). Exercise modulates insulin-like growth factor 1-dependent and -independent effects on adult hippocampal neurogenesis and behaviour. *Mol. Cell. Neurosci.* 44, 109–117.

Louis, D.N. (2006). Molecular pathology of malignant gliomas. *Annu. Rev. Pathol.* 7, 97–117.

Macdonald, D.R., Cascino, T.L., Schold, S.C., Jr., and Cairncross, J.G. (1990). Response criteria for phase II studies of supratentorial malignant glioma. *J. Clin. Oncol.* 8, 1277–1280.

Margolis, B., and Borg, J.P. (2005). Apical polarity complexes. *J. Cell Sci.* 118, 5157–5159.

Martín, C., Bueno, D., Alonso, M.I., Moro, J.A., Callejo, S., Parada, C., Martín, P., Camicero, E., and Gato, A. (2006). FGF2 plays a key role in embryonic cerebrospinal fluid trophic properties over chick embryo neuroepithelial stem cells. *Dev. Biol.* 297, 402–416.

Mirzadeh, Z., Han, Y.-G., Soriano-Navarro, M., García-Verdugo, J.M., and Alvarez-Buylla, A. (2010). Cilia organize ependymal planar polarity. *J. Neurosci.* 30, 2600–2610.

- Noctor, S.C., Flint, A.C., Weissman, T.A., Wong, W.S., Clinton, B.K., and Kriegstein, A.R. (2002). Dividing precursor cells of the embryonic cortical ventricular zone have morphological and molecular characteristics of radial glia. *J. Neurosci.* **22**, 3161–3173.
- Orkin, S.H., and Zon, L.I. (2008). Hematopoiesis: An evolving paradigm for stem cell biology. *Cell* **132**, 631–644.
- Palmer, T.D., Willhoite, A.R., and Gage, F.H. (2000). Vascular niche for adult hippocampal neurogenesis. *J. Comp. Neurol.* **425**, 479–494.
- Parada, C., Gato, A., and Bueno, D. (2005). Mammalian embryonic cerebrospinal fluid proteome has greater apolipoprotein and enzyme pattern complexity than the avian proteome. *J. Proteome Res.* **4**, 2420–2428.
- Pinal, N., Goberdhan, D.C., Collinson, L., Fujita, Y., Cox, I.M., Wilson, C., and Pichaud, F. (2006). Regulated and polarized PtdIns(3,4,5)P₃ accumulation is essential for apical membrane morphogenesis in photoreceptor epithelial cells. *Curr. Biol.* **16**, 140–149.
- Popken, G.J., Hodge, R.D., Ye, P., Zhang, J., Ng, W., O'Kusky, J.R., and D'Ercole, A.J. (2004). In vivo effects of insulin-like growth factor-I (IGF-I) on prenatal and early postnatal development of the central nervous system. *Eur. J. Neurosci.* **19**, 2056–2068.
- Purves, D. (1988). *Body and Brain. A Trophic Theory of Neural Connections* (Cambridge, MA: Harvard University Press).
- Randhawa, R., and Cohen, P. (2005). The role of the insulin-like growth factor system in prenatal growth. *Mol. Genet. Metab.* **86**, 84–90.
- Reynolds, B.A., and Weiss, S. (1996). Clonal and population analyses demonstrate that an EGF-responsive mammalian embryonic CNS precursor is a stem cell. *Dev. Biol.* **175**, 1–13.
- Sawamoto, K., Wichterle, H., Gonzalez-Perez, O., Chofin, J.A., Yamada, M., Spassky, N., Murcia, N.S., Garcia-Verdugo, J.M., Marin, O., Rubenstein, J.L., et al. (2006). New neurons follow the flow of cerebrospinal fluid in the adult brain. *Science* **317**, 629–632.
- Scadden, D.T. (2006). The stem-cell niche as an entity of action. *Nature* **441**, 1075–1079.
- Schubert, M., Brazil, D.P., Burks, D.J., Kushner, J.A., Ye, J., Flint, C.L., Farhang-Fallah, J., Dikkes, P., Warot, X.M., Rio, C., et al. (2003). Insulin receptor substrate-2 deficiency impairs brain growth and promotes tau phosphorylation. *J. Neurosci.* **23**, 7084–7092.
- Shen, Q., Goderie, S.K., Jin, L., Karanth, N., Sun, Y., Abramova, N., Vincent, P., Pumiglia, K., and Temple, S. (2004). Endothelial cells stimulate self-renewal and expand neurogenesis of neural stem cells. *Science* **304**, 1338–1340.
- Shen, Q., Wang, Y., Kokovay, E., Lin, G., Chuang, S.M., Goderie, S.K., Roysam, B., and Temple, S. (2008). Adult SVZ stem cells lie in a vascular niche: A quantitative analysis of niche cell-cell interactions. *Cell Stem Cell* **3**, 289–300.
- Shimogori, T., Banuchi, V., Ng, H.Y., Strauss, J.B., and Grove, E.A. (2004). Embryonic signaling centers expressing BMP, WNT and FGF proteins interact to pattern the cerebral cortex. *Development* **131**, 5639–5647.
- Siegenthaler, J.A., Ashique, A.M., Zarbalis, K., Patterson, K.P., Hecht, J.H., Kane, M.A., Follas, A.E., Choe, Y., May, S.R., Kume, T., et al. (2009). Retinoic acid from the meninges regulates cortical neuron generation. *Cell* **139**, 597–609.
- Siller, K.H., and Doe, C.Q. (2009). Spindle orientation during asymmetric cell division. *Nat. Cell Biol.* **11**, 365–374.
- Soroceanu, L., Kharbanda, S., Chen, R., Soriano, R.H., Aldape, K., Misra, A., Zha, J., Forrest, W.F., Nigro, J.M., Modrusan, Z., et al. (2007). Identification of IGF2 signaling through phosphoinositide-3-kinase regulatory subunit 3 as a growth-promoting axis in glioblastoma. *Proc. Natl. Acad. Sci. USA* **104**, 3466–3471.
- Stylianopoulou, F., Efstratiadis, A., Herbert, J., and Pintar, J. (1988). Pattern of the insulin-like growth factor II gene expression during rat embryogenesis. *Development* **103**, 497–506.
- Sun, Y., Goderie, S.K., and Temple, S. (2005). Asymmetric distribution of EGFR receptor during mitosis generates diverse CNS progenitor cells. *Neuron* **45**, 873–886.
- Tavazoie, M., Van der Veken, L., Silva-Vargas, V., Louissaint, M., Colonna, L., Zaidi, B., Garcia-Verdugo, J.M., and Doetsch, F. (2008). A specialized vascular niche for adult neural stem cells. *Cell Stem Cell* **3**, 279–288.
- Vasioukhin, V., Bauer, C., Degenstein, L., Wise, B., and Fuchs, E. (2001). Hyperproliferation and defects in epithelial polarity upon conditional ablation of alpha-catenin in skin. *Cell* **104**, 605–617.
- Vescovi, A.L., Reynolds, B.A., Fraser, D.D., and Weiss, S. (1993). bFGF regulates the proliferative fate of unipotent (neuronal) and bipotent (neuronal/astroglial) EGF-generated CNS progenitor cells. *Neuron* **11**, 951–966.
- von Stein, W., Ramrath, A., Grimm, A., Müller-Borg, M., and Wodarz, A. (2005). Direct association of Bazooka/PAR-3 with the lipid phosphatase PTEN reveals a link between the PAR/aPKC complex and phosphoinositide signaling. *Development* **132**, 1675–1686.
- Weber, M.M., Melmed, S., Rosenbloom, J., Yamasaki, H., and Prager, D. (1992). Rat somatotroph insulin-like growth factor-II (IGF-II) signaling: role of the IGF-I receptor. *Endocrinology* **131**, 2147–2153.
- Wodarz, A. (2005). Molecular control of cell polarity and asymmetric cell division in *Drosophila* neuroblasts. *Curr. Opin. Cell Biol.* **17**, 475–481.
- Wu, H., Feng, W., Chen, J., Chan, L.N., Huang, S., and Zhang, M. (2007). PDZ domains of Par-3 as potential phosphoinositide signaling integrators. *Mol. Cell* **28**, 886–898.
- Ye, P., Popken, G.J., Kemper, A., McCarthy, K., Popko, B., and D'Ercole, A.J. (2004). Astrocyte-specific overexpression of insulin-like growth factor-I promotes brain overgrowth and glial fibrillary acidic protein expression. *J. Neurosci. Res.* **78**, 472–484.
- Ye, P., Hu, Q., Liu, H., Yan, Y., and D'Ercole, A.J. (2010). β -catenin mediates insulin-like growth factor-I actions to promote cyclin D1 mRNA expression, cell proliferation and survival in oligodendroglial cultures. *Glia* **58**, 1031–1041.
- Zappaterra, M.D., Lisgo, S.N., Lindsay, S., Gygi, S.P., Walsh, C.A., and Ballif, B.A. (2007). A comparative proteomic analysis of human and rat embryonic cerebrospinal fluid. *J. Proteome Res.* **6**, 3537–3548.
- Zhang, C.C., and Lodish, H.F. (2004). Insulin-like growth factor 2 expressed in a novel fetal liver cell population is a growth factor for hematopoietic stem cells. *Blood* **103**, 2513–2521.
- Zhou, C.J., Borello, U., Rubenstein, J.L., and Pleasure, S.J. (2006). Neuronal production and precursor proliferation defects in the neocortex of mice with loss of function in the canonical Wnt signaling pathway. *Neuroscience* **142**, R1119–R1131.

Neuron, Volume 69

Supplemental Information

The Cerebrospinal Fluid Provides

a Proliferative Niche for Neural Progenitor Cells

Maria K. Lehtinen, Mauro W. Zappaterra, Xi Chen, Yawei J. Yang, Anthony Hill, Melody Lun, Thomas Maynard, Dilenny Gonzalez, Seonhee Kim, Ping Ye, A. Joseph D'Ercole, Eric T. Wong, Anthony S. LaMantia, and Christopher A. Walsh

Inventory of Supplemental figures and tables.

We present 3 Supplementary Figures and 3 Supplementary Tables as further support of the main Figures 1-7 and Table 1.

Supplemental Figure S1, related to Figure 1, presents data characterizing the *Pten*^{loxP/loxP}/*NestinCre*^{-/-} mouse and *Pten*^{loxP/loxP}/*Pals1*^{loxP/+}/*Emx1Cre*^{+/-} mice. The following data are presented in the figure panels:

- A. Brain sizes of *Pten*^{loxP/loxP}/*NestinCre*^{+/-} and control mice.
- B. H&E staining of samples presented in (A).
- C. Higher magnification images of H&E staining shown in (B).
- D. Analysis of progenitor exit from cell cycle using Ki67 and BrdU immunostaining in embryonic *Pten*^{loxP/loxP}/*NestinCre*^{+/-} and control mice.
- E. Analysis of ratio of apical to basal progenitors in *Pten*^{loxP/loxP}/*NestinCre*^{+/-} and control mice.
- F. Cdc42 staining in *Pten*^{loxP/loxP}/*NestinCre*^{+/-} and control mice at E17.
- G. Brain sizes of *Pten*^{loxP/loxP}/*Pals1*^{+/+}/*Emx1Cre*^{+/-}, *Pten*^{loxP/+}/*Pals1*^{loxP/+}/*Emx1Cre*^{+/-}, *Pten*^{loxP/loxP}/*Pals1*^{loxP/+}/*Emx1Cre*^{+/-}, and control mice at E14.5
- H. H&E staining of samples presented in (G).

Supplemental Figure S2, related to Figure 4, presents data characterizing the role of embryonic CSF in supporting cortical explant survival and proliferation of neurospheres, an in vitro model of neural stem cells. The following data are presented in the figure panels:

- A. Representative images of E16 rat explants cultured with artificial or 100% E17 CSF and immunostained with cleaved caspase 3.
- B. Quantification of embryonic CSF's support of cortical explant survival compared to adult CSF.
- C. Representative images of E16 explants cultured with E13, E17, P6, or adult CSF.
- D. Quantification of long-term neurospheres maintained by E17 CSF.
- E. Quantification of relative size of long-term neurospheres maintained by E17 CSF.
- F. Quantification of circularity of long-term neurospheres maintained by E17 CSF.
- G. Representative images of long-term neurospheres maintained by E17 CSF.

H. Neurospheres cultured with E17 CSF maintained responsiveness to Egf and Fgf.

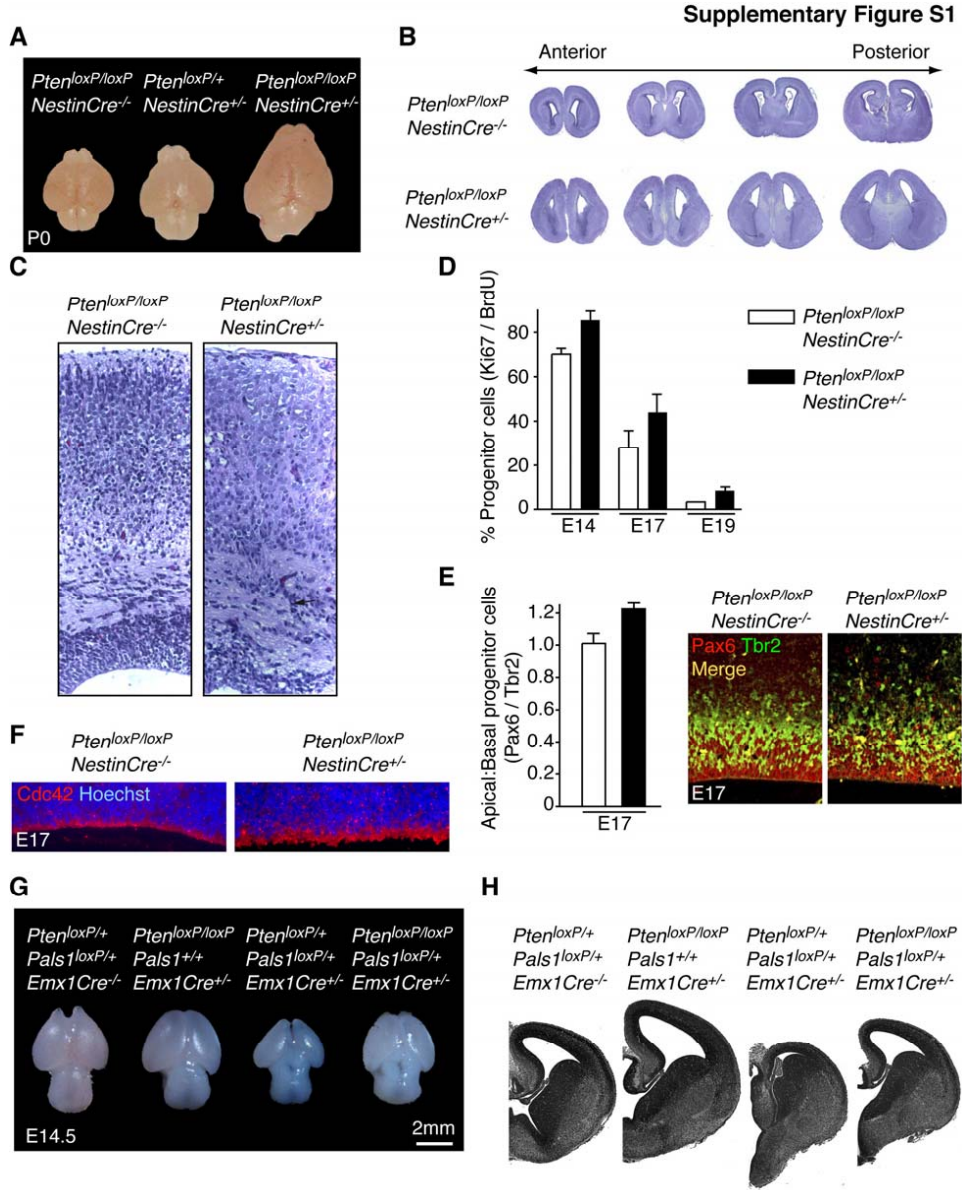
Supplemental Figure S3, related to Figure 5, presents Igf2 expression in mouse brain and CSF.

- A. *Igf2* in situ hybridization at E14.5.
- B. Mouse CSF Igf2 expression by immunoblotting.

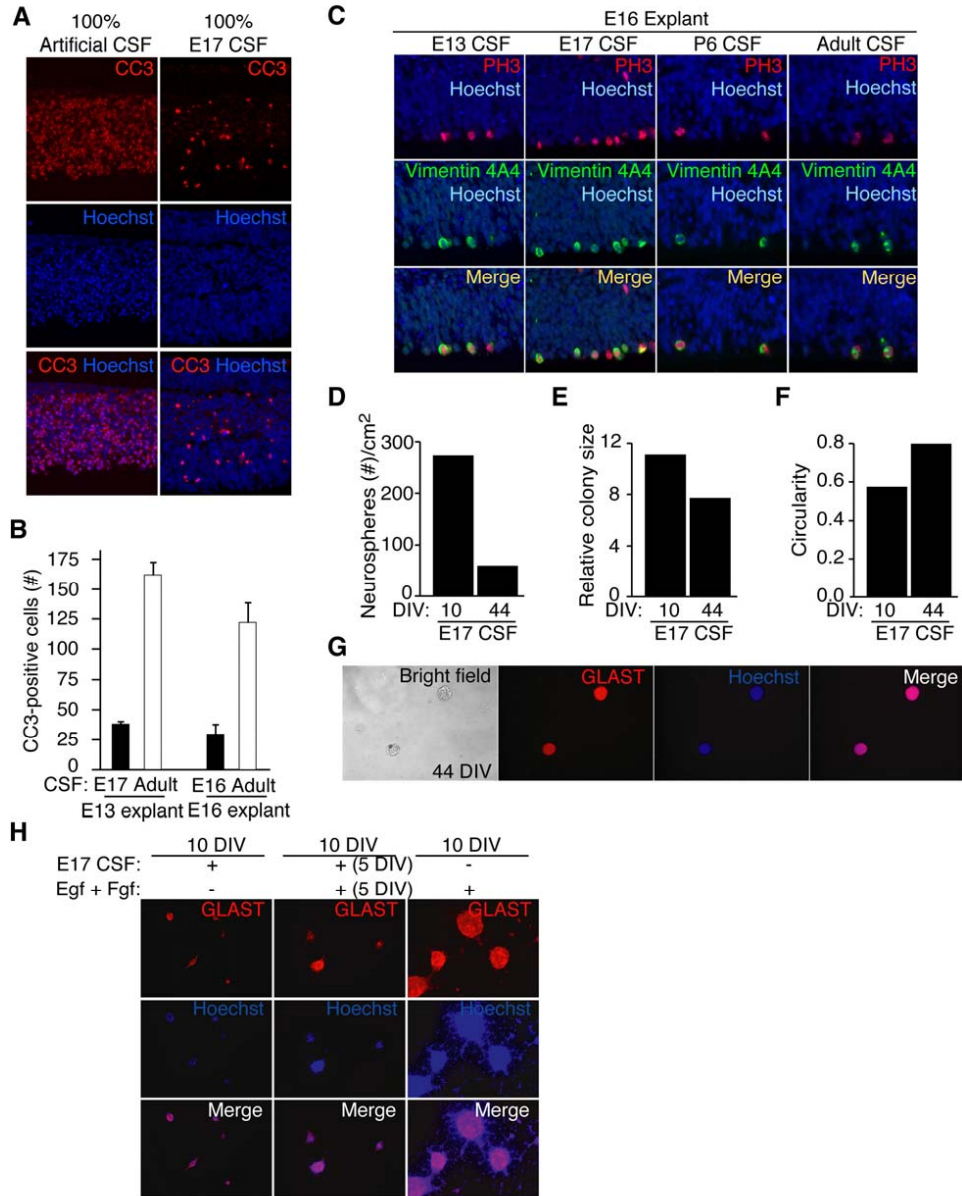
Supplemental Table S1, related to Figure 3, presents tandem mass spectrometry (LC-MS/MS) analyses of rat E17 CSF. See separate Excel spreadsheet.

Supplemental Table S2, related to Figure 4, presents data in which the CSF fraction containing proteins from 10-100kDa contained activities essential for neurosphere growth.

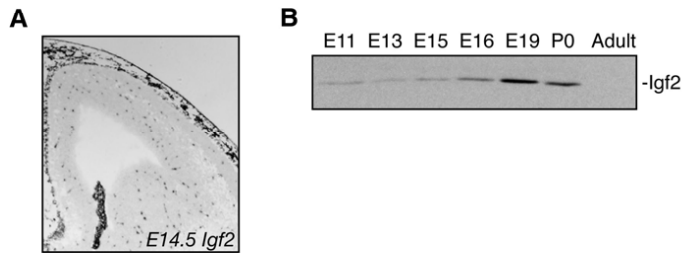
Supplemental Table S3, related to Figure 4, presents data in which media conditioned with E17 choroid plexus provided enhanced support for neurosphere formation compared to media conditioned with embryonic cortex, adult choroid plexus, or adult brain.



Supplementary Figure S2



Supplementary Figure S3



SUPPLEMENTAL FIGURE LEGENDS

Supplemental Figure S1, related to Figure 1. *Pten* deletion results in increased brain size, progenitor proliferation, and partially restores the *Pals1*-deficient brain phenotype. (A)

Representative brains from *Pten*^{loxP/+}/*NestinCre*^{+/-} and *Pten*^{loxP/loxP}/*Emx1Cre*^{+/-} mice at P0. Loss of *Pten* function in the developing neural tube increased brain size. **(B)** H&E stained serial sections of *Pten*^{loxP/+}/*NestinCre*^{+/-} (top) and *Pten*^{loxP/loxP}/*NestinCre*^{+/-} (bottom) brains. Sections separated by approximately 160µm showed that both the radial thickness and the tangential extent of the cerebral cortex were increased in brains lacking *Pten* expression. **(C)** Higher magnification images of sections from panel **(B)**. The cortical plate appears disorganized in *Pten*^{loxP/loxP}/*NestinCre*^{+/-} mice. **(D)** *Pten*^{loxP/+}/*NestinCre*^{+/-} and *Pten*^{loxP/loxP}/*NestinCre*^{+/-} pulsed with BrdU for 24 hours were analyzed at E14, E17, or E19 for proliferation. A greater percentage of BrdU positive cells remained in the cell cycle in *Pten*^{loxP/loxP}/*NestinCre*^{+/-} mutants compared to control littermates at all ages examined (E14: Control 70.1 ± 2.8%, *Pten*^{loxP/loxP}/*NestinCre*^{+/-} 85.5 ± 5.3%; E17: Control 28 ± 6.9%, *Pten*^{loxP/loxP}/*NestinCre*^{+/-} 44 ± 6.1%; E19: Control = 3.4%, *Pten*^{loxP/loxP}/*NestinCre*^{+/-} 8.4 ± 1.8%; t-test, p<0.05). **(E)** *Pten*^{loxP/+}/*NestinCre*^{+/-} and *Pten*^{loxP/loxP}/*NestinCre*^{+/-} mutants were analyzed for numbers of apical (Pax6) and intermediate progenitors (Tbr2) and revealed a relative increase in numbers of Pax6-positive apical progenitors in *Pten*^{loxP/loxP}/*NestinCre*^{+/-} mutants at E16 and E17 (Numbers of positive staining cells per section at E17: *Pten*^{loxP/+}/*NestinCre*^{+/-} Tbr2 = 424 ± 43, Pax6 = 432 ± 52, Tbr2/Pax6 = 99 ± 0.06; *Pten*^{loxP/loxP}/*Emx1Cre*^{+/-} Tbr2 = 529 ± 54, Pax6 = 651 ± 26, Tbr2/Pax6 = 0.80 ± 0.05. A similar trend was observed for Tbr2 positive progenitors labeled with BrdU 24 hours earlier at E16, where 36.0 ± 1.8% of BrdU positive cells were Tbr2 positive in *Pten*^{loxP/+}/*NestinCre*^{+/-} compared with 29.4 ± 1.3% in *Pten*^{loxP/loxP}/*NestinCre*^{+/-}. Collectively, these data demonstrate a

shift in *Pten*-deficient mutants from epithelial, Pax6-positive progenitors that divide asymmetrically to produce neurons or intermediate progenitors, towards symmetric divisions that produce two radial glia. Data are presented as mean \pm SD. **(F)** Apical marker expression including Cdc42 was disrupted in E17 *Pten*^{loxP/loxP}/*NestinCre*^{+/-} mice compared to littermate controls. **(G)** Conditional *Pten* deletion (*Pten*^{loxP/loxP}/*Emx1Cre*^{+/-}) resulted in an enlarged cerebral cortex already by 14.5. The small brain size of *Pals1* heterozygotes appeared more normal in the double mutants by E14.5. **(H)** H&E staining of brains shown in panel (G).

Supplemental Figure S2, related to Figure 4. Embryonic CSF supports cortical explant survival and proliferation. **(A)** E16 explants cultured for 24 hours in 100% E17 CSF or 100% artificial CSF were immunostained with the apoptotic cell death marker cleaved caspase 3 (CC3). Explants cultured in 100% embryonic CSF has decreased CC3 immunoreactivity compared to explants grown in ACSF. **(B)** CC3-positive dying cells were quantified in E13 explants cultured for 24 hours in 100% E17 CSF or 100% adult CSF and in E16 explants cultured for 24 hours in 100% E16 CSF or 100% adult CSF. Embryonic CSF supports embryonic tissue viability and survival (E13 explant + E17 CSF = 39.5 ± 3.9 ; adult CSF = 163.5 ± 10.4 ; Mann-Whitney, $p < 0.05$, $n = 3$; E16 explant + E16 CSF = 33.7 ± 4.4 ; adult CSF = 122.1 ± 19.4 ; Mann-Whitney, $p < 0.05$, $n = 3$ and $n = 4$, respectively). **(C)** Representative images of E16 explants cultured with E13, E17, P6, or adult CSF quantified in **Figure 4D-F**. **(D)** Dissociated cells from primary neurospheres cultured in E17 CSF for 44 DIV maintain GLAST-positive neural progenitors when cultured in embryonic CSF, $n = 2$. Quantification of number of spheres/cm² when cultured for 10 DIV vs. 44 DIV. **(E)** Quantification of relative colony size of spheres cultured for 10 DIV vs. 44 DIV. **(F)** Quantification of circularity of spheres cultured for

10 DIV vs. 44 DIV. **(G)** Representative images of neurospheres quantified in **D-F**. **(H)** Left and middle panels: Dissociated cells from primary neurospheres cultured in E17 CSF for 5 DIV and then supplemented with Egf and Fgf. GLAST-positive-staining cells cultured in E17 CSF maintain responsiveness to Egf and Fgf suggesting that stem cells cultured in CSF maintain undifferentiated and uncommitted state. Right panels: Dissociated cells from primary neurospheres cultured in Egf and Fgf for 10 DIV.

Supplemental Figure S3, related to Figure 5. Igf2 expression in mouse choroid plexus and CSF. **(A)** *Igf2* in situ hybridization at E14.5. *Igf2* levels are highest in the choroid plexus, leptomeninges, and vasculature. **(B)** *Igf2* is transiently expressed in mouse CSF.

Supplementary Table S2

Filtration analysis of E17 CSF	
Sample	Neurosphere formation
< 3 kDa	-
< 10kDa	-
< 30kDa	+
< 100kDa	+++
E17 CSF	+++

Supplementary Table S2. CSF factors that stimulate neurosphere formation are likely small proteins ranging from 10-100kDa. Neurospheres derived from E14 rat brain were dissociated and plated at clonal density in CSF fractions of various sizes and assayed for the presence of neurospheres after 10 DIV; n=3.

Supplementary Table S3

Tissue-conditioned media	
Sample	Neurosphere formation
E14 cortex	+
E17 cortex	+
E17 choroid plexus	+++
Adult cortex	-
Adult choroid plexus	++

Supplementary Table S3. Actively secreted factors from choroid plexus stimulate neurosphere formation. Neurospheres derived from E14 rat brain were dissociated and plated at clonal density in either cortex- or choroid plexus-conditioned medium. The presence of neurospheres was assayed after 10 DIV; n=3.

SUPPLEMENTAL EXPERIMENTAL PROCEDURES

Immunostaining

Paraffin sections (5µm) of brains or explants were dehydrated and subjected to antigen retrieval with Antigen Unmasking Solution (Vector), followed by blocking (PBS/5% serum), permeabilization, and antibody incubation. Alternately, cryosections (14-50µm) were blocked, permeabilized, and incubated with antibodies. Immunostained cells counted in serial explants are expressed as numbers of cells along the ventricular surface as detailed in figure legends. All samples were counterstained with Hoechst 33258 (Sigma). For quantification of cells in distinct cortical laminae, the radial extent of the cortex was either divided into six equally sized bins (Figure 1D) and quantified, or all positive staining cells were counted in an area of cortex of equal width across all samples (Figure 5H). All quantification was carried out using ImageJ software.

Neurospheres

E14, E17, or adult rat cortex was dissected in sterile HBSS and dissociated by the Papain Dissociation System (Worthington Biochem. Corp). Primary spheres were generated in either CSF or DMEM/F12 supplemented with heparin, N2, Fgf2 (10ng/ml), and Egf (20ng/ml), and collected after 7-9 DIV. In the latter case, primary spheres were then re-suspended in media without Egf or Fgf, dissociated, plated at a final density of 2,500 cells/cm², and cultured as described in text. Fresh media was supplemented at 4 DIV. Cells were fixed in 4% paraformaldehyde and stained for GLAST.

Cortical cell cultures

Rodent E13.5 cortices were isolated and dissociated by the Papain Dissociation System (Worthington Biochem. Corp). Cells were cultured in NBM supplemented with penicillin-streptomycin, glutamine, N2, and Fgf (10ng/ml) for 24 hours. For Igf signaling experiments, cells were deprived of growth factors for 6 hours, followed by a 5 minute pulse of 20% ACSF, 20% embryonic CSF, or Igf2 (20ng/ml). For P-LRP6 experiments, cells were left untreated, or treated with 20% CSF, 10% L-cell conditioned media, or 10% Wnt3a conditioned media (ATCC) for 2 hours.

Tissue-conditioned media

Rat tissue was dissected in approximately equal mass, washed in HBSS, and placed in 250 μ l of embryonic neurosphere media without Egf or Fgf at 37°C for 2-3 days. Dissociated primary neurospheres were added to the centrifuged conditioned media free of tissue content. The numbers of secondary neurospheres generated were assayed at 10 DIV.

Indicator cell experiments

Luciferase reporter constructs were generated using synthetic responsive elements (3xDR5-RARE (Balkan et al., 1992) or 2xBMP responsive element (Korchynskiy and ten Dijke, 2002)), fused to a thymidine kinase minimal promoter and inserted into the Luciferase reporter of pGL3 (Promega). Reporter cassettes were inserted into a vector containing a constitutive neomycin cassette, and electroporated into L-M^{tk-} (RA) or 3T3 (BMP) cell lines, and grown in DMEM containing 10% charcoal-stripped calf serum, antibiotic/antimycotic solution (Gibco/Invitrogen) and 750 μ g/ml of G418. Clonal cell lines were produced by dilution cloning. Samples were

screened by adding CSF (20%) to assay media (as above, but with 5% charcoal-stripped calf serum and 25mM HEPES, pH 7.4). Cells were treated for 48 hours, with the sample refreshed after 24 hours. Effective ligand concentration was calculated by assaying wells using a luciferase assay, and comparing activity to assays treated with a dilution series of known concentrations of all-trans RA (Sigma) or recombinant mouse BMP4 (R&D Systems) prepared in ACSF.

Electron microscopy

Scanning electron microscopy (SEM): E12.5 mouse cortex fixed in 2% glutaraldehyde was processed for SEM according to standard procedures. Samples were examined using a Carl Zeiss 1450 VP Scanning Electron Microscope. Transmission electron microscopy (TEM): Pre-embedding and immunogold labeling were carried out E17 rat embryos perfused with 0.5% glutaraldehyde / 2.5% paraformaldehyde and postfixed overnight. Briefly, 100µm vibratome sections were blocked with 5% BSA / 5% goat serum in PBS, immunostained with anti-Igf2 antibodies (Abcam) followed by incubation with a secondary antibody conjugated to colloidal gold, enhanced with silver, postfixed with 0.5% osmium tetroxide, and embedded. Ultrathin sections were stained on copper grids stained with lead citrate and examined in a JEOL 1200EX Transmission electron microscope.

In Situ hybridization

Non-radioactive in situ hybridization was performed as described (Berger and Hediger, 2001), using digoxigenin (DIG)-labeled cRNA probes generated from a TA vector (Invitrogen) clone of Igf2 and Igf1R.

Brain size measurements

Cortical perimeter was measured using ImageJ by tracing the edges of both hemispheres.

Cortical surface area was measured similarly using ImageJ.

Biochemical assays

Igf1 concentration in rat CSF was measured using the Active Mouse/Rat Igf-1 ELISA (Diagnostic Systems Laboratories) according to the manufacturer's instructions. Igf2 concentration in human CSF was measured using the Non-extraction Igf2 ELISA (Diagnostic Systems Laboratories) according to the manufacturer's instructions.

RNA quantification

Expression of Bmp and RA synthetic and catabolic enzymes relative to Gapdh was measured in embryonic rat choroid plexus by Sybr-green qPCR. The following primer sets were used: Bmp2 forward (F): CGGGACCCGCTGTCTTCTAGTGTTG, Bmp2 reverse (R): GGGCACCACGACGTCCTTGCTG; Bmp4 (F): GGAGGCGCGAGCCATGCTAGTTTG, Bmp4 (R): CCCGGTTCCTGGCTCTGCTCTTC; Bmp5 (F): GAAGACACGGGCCTCAGTCAAAGCAG, Bmp5 (R): CCATCCCAGATCGCGAAACTCAC; Bmp7 (F): GGCAGGGAGTCCGACCTTCTCTTG, Bmp7 (R): CTTGGAGCGTTCTGGCTGCGTTG; Raldh1 (F): TTCCTCCTGGCGTGGTGAACATTG, Raldh1 (R): ACGCAGCATTGGCCTTGATGGTAG; Raldh2 (F): GCAGGGGCAGCAATAGCGTCTCAC, Raldh2 (R): GCGCCTTGGCTCTTCCACAC; Raldh3 (F): GCGGCCTCCAGGGTGTGTTGTG, Raldh3 (R): CCGCCGTGAGCCCATAGTCAGTG; Raldh10 (F): GCTGGTGCGGCCCAAGGAGAAG,

Rdh10(R): CCAGCGTTATTGACCAGGACCGAGAC; Ttr (F):
GCCCTGGGGGTGCTGGAGAATC, Ttr (R): GAGCAGGGCTGCGATGGTGTAGTG; Gapdh
(F): GGCATGGCCTCCGTGTTCCCTAC, Gapdh (R): GCCAGCCCCAGCATCAAAGGTG.

Reactions were carried out 4 separate times in duplicate and mRNA expression levels were calculated by the comparative C_T method.

SUPPLEMENTAL REFERENCES

Balkan, W., Colbert, M., Bock, C., and Linney, E. (1992). Transgenic indicator mice for studying activated retinoic acid receptors during development. *Proc Natl Acad Sci U S A* 89, 3347-3351.

Berger, U. V., and Hediger, M. A. (2001). Differential distribution of the glutamate transporters GLT-1 and GLAST in tanyocytes of the third ventricle. *J Comp Neurol* 433, 101-114.

Korchynskyi, O., and ten Dijke, P. (2002). Identification and functional characterization of distinct critically important bone morphogenetic protein-specific response elements in the Id1 promoter. *J Biol Chem* 277, 4883-4891.